Philipps Universität Marburg

Singular Equivariant Spectral Asymptotics of Schrödinger Operators in $\mathbb{R}^n$ and Resonances of Schottky Surfaces

Dissertation

zur

Erlangung des Doktorgrades der Naturwissenschaften

(Dr. rer. nat.)

dem

Fachbereich Mathematik und Informatik

der Philipps-Universität Marburg

vorgelegt von

Tobias Weich

aus

Villingen-Schwenningen

Marburg/Lahn, 2014

Vom Fachbereich Mathematik und Informatik der Philipps-Universität als Dissertation angenommen am 04.06.2014
Erstgutachter: Prof. Dr. Pablo Ramacher
Zweitgutachter: Prof. Dr. Joachim Hilgert
Tag der mündlichen Prüfung: 13.06.2014
Hochschulkennziffer 1180

Abstract

This work consists of four self-containedly presented parts.

In the first part we prove equivariant spectral asymptotics for h-pseudo-differential operators for compact orthogonal group actions generalizing results of El-Houakmi and Helffer (1991) and Cassanas (2006). Using recent results for certain oscillatory integrals with singular critical sets (Ramacher 2010) we can deduce a weak equivariant Weyl law. Furthermore, we can prove a complete asymptotic expansion for the Gutzwiller trace formula without any additional condition on the group action by a suitable generalization of the dynamical assumptions on the Hamilton flow.

In the second and third part we study resonance chains which have been observed in many different physical and mathematical scattering problems.

In the second part we present a mathematical rigorous study of the resonance chains on three funneled Schottky surfaces. We prove the analyticity of the generalized zeta function which provide the central mathematical tool for understanding the resonance chains. Furthermore we prove for a fixed ratio between the funnel lengths and in the limit of large lengths that after a suitable rescaling the resonances in a bounded domain align equidistantly along certain lines. The position of these lines is given by the zeros of an explicit polynomial which only depends on the ratio of the funnel lengths.

In the third part we provide a unifying approach to these resonance chains by generalizing dynamical zeta functions. By means of a detailed numerical study we show that these generalized zeta functions explain the mechanism that creates the chains of quantum resonance and classical Ruelle resonances for 3-disk systems as well as geometric resonances on Schottky surfaces. We also present a direct system-intrinsic definition of the continuous lines on which the resonances are strung together as a projection of an analytic variety. Additionally, this approach shows that the existence of resonance chains is directly related to a clustering of the classical length spectrum on multiples of a base length. Finally, this link is used to construct new examples where several different structures of resonance chains coexist.

The fourth part deals with a symmetry factorization of dynamical zeta functions for holomorphic iterated function schemes. We introduce the notion of a finite symmetry group for these iterated function schemes and prove that the dynamical zeta function factorizes into entire symmetry reduced zeta functions that are parametrized by the irreducible characters of the symmetry group. Under an assumption on the group action on the symbols of the symbolic dynamics, we are able to simplify the formulas for the symmetry

reduced zeta functions considerably. As an application we apply the symmetry factorization to Selberg zeta functions of symmetric n-funneled Schottky surfaces and show that the symmetry reduction simplifies the numerical calculation of the resonances strongly.

Zusammenfassung

Diese Arbeit besteht aus vier eigenständigen Teilen.

Im ersten Teil beweisen wir äquivariante spektrale Asymptotiken für h-Pseudodifferentialoperatoren und für kompakte, orthogonale Gruppenwirkungen. Diese Ergebnisse verallgemeinern bisher bekannte Resultate von El-Houakmi und Helffer (1991) sowie Cassanas (2006). Indem wir neue Ergebnisse für oszillierende Integrale mit singulärer kritischer Menge (Ramacher 2010) nutzen, können wir eine schwache Form des Weyl-Gesetzes beweisen. Außerdem erhalten wir vollständige asymptotische Entwicklungen für die Gutzwiller-Spurformeln ohne eine zusätzliche Bedingung an die Gruppenwirkung zu stellen, indem wir die Annahmen an die Dynamik des Hammilton Flusses geeignet verallgemeinern.

Im zweiten und dritten Teil untersuchen wir Resonanzketten, die in vielen unterschiedlichen physikalischen und mathematischen Streuproblemen beobachte wurden.

Im zweiten Teil präsentieren wir eine mathematisch rigorose Untersuchung der Resonanzketten auf Schottky-Flächen mit drei hyperbolischen Trichtern. Wir zeigen die analytische Fortsetzbarkeit der verallgemeinerten Zetafunktionen, die das zentrale Werkzeug zum Verständnis der Resonanzketten liefern. Außerdem beweisen wir, dass die Resonanzen nach geeigneter Reskalierung, für ein festes, rationales Verhältnis zwischen den Trichterweiten und im Grenzwert großer Weiten äquidistant auf Geraden angeordnet sind. Die Position dieser Geraden ist vollständig durch ein explizites Polynom gegeben, das nur vom Verhältnis der Trichterweiten abhängt.

Im dritten Teil präsentieren wir einen vereinheitlichenden Ansatz zu den Resonanzketten durch eine Verallgemeinerung der dynamischen Zetafunktionen. Mittels einer detaillierten numerischen Untersuchung illustrieren wir, dass die verallgemeinerten Zetafunktionen den Mechanismus erklären, der diese Ketten erzeugt und der sich sowohl auf klassische Ruelle-Resonanzen und Quantenresonanzen in 3-Disk Systemen anwenden lässt, als auch auf geometrische Resonanzen auf Schottkyflächen. Desweiteren präsentieren wir eine System-inhärente Definition der kontinuierlichen Linien, auf denen die Resonanzen aufgereiht sind, indem wir sie als Projektionen analytischer Varietäten schreiben. Außerdem zeigt dieser Ansatz, dass die Ausbildung von

Resonanzketten direkt mit einer Clusterbildung im klassischen Längenspektrum um Vielfache einer Basislänge verknüpft ist. Schließlich nutzen wir diese Erkenntnis um neue Beispiele konstruieren, in denen sogar mehrere Kettenstrukturen koexistieren.

Der vierte Teil behandelt die Symmetriereduzierung dynamischer Zetafunktionen für holomorphe iterierte Funktionensysteme. Wir führen den Begriff einer endlichen Symmetriegruppe für ein solches iteriertes Funktionensystem ein und zeigen, dass die dynamische Zeta-Funktion in ganze symmetriereduzierte Zetafunktionen faktorisiert, welche durch die irreduziblen Charaktäre der Symmetriegruppe parametrisiert werden. Unter einer Annahme an die Gruppenwirkung auf den Symbolen der symbolischen Dynamik gelingt es uns, die Formeln für die symmetriereduzierten Zetafunktionen noch weiter zu vereinfachen. Als Anwendungsbeispiel wenden wir die Faktorisierung auf Selberg-Zetafunktionen von symmetrischen Schottkyflächen mit n Trichtern an und wir zeigen, dass durch die Faktorsierung die numerische Suche der Nullstellen enorm vereinfacht wird.

Contents

1 General introduction

This work consists of four parts that, however different they may look like, all deal with the following basic question: Given a partial differential equation, that one cannot hope to solve exactly, what rigorous results can one prove about the "structure" of its solutions? Two other principles that are common in all parts are, first the utilization of symmetries in order to simplify the problems and second the role of an asymptotic parameter. This means that instead of proving results for one partial differential equation, we consider a whole family of them and are able to prove asymptotic results in a certain limit of the parameter, parametrizing the family of equations.

The motivation for considering the studied partial differential equations as well as the kind of results that is proven differs, however, between the four parts.

In Part I Schrödinger operators in $\mathbb{R}^n$ are studied. These operators are important as they describe quantum mechanics and the asymptotic limit is the *semiclassical limit* which allows to prove a rigorous connection between quantum and semiclassical physics. In particular we are interested in Schrödinger operators that are invariant under a Lie-group symmetry. In this case one can use the Peter-Weyl theorem and study the symmetry reduced operator and we are interested in results on the asymptotic number of its eigenvalues (Weyl law) as well as in the correlation of them (Gutzwiller trace formula). The particular difficulty that arises in this part is that the symmetry group action can have different orbit types. In these cases the standard proof for the Weyl and Gutzwiller formula broke down up to now, due to a singular critical set in the stationary phase approximation. Using recent results of resolution of singularieties in this case, as well as a better understanding of the critical set in the Gutzwiller case, allowed to considerably extend the known results.

Part II and IV deal mainly with resonances of the Laplace operators on Schottky surfaces. These surfaces arise as concrete examples in a vast range of topics, such as differential and complex geometry, number theory, representation theory, partial differential equations and mathematical physics. The motivation for their study is similarly rich. In Part II and III the recently discovered phenomenon of resonance chains is treated, which are surprisingly strong structures in the resonance structure and which were up to now merely understood. In Part II we provide a rigorous treatment of these chains on three funneled Schottky surfaces. We prove the existence of these chains in a certain geometrical limit by giving a surprisingly easy asymptotic formula for the location of the resonances. Part III then provides a more applied approach to these resonance chains and builds a bridge to physics and quan-

tum chaos. There very similar chains have been observed since a long time and by numerical experiments an underlying mechanism for the resonance chains is revealed, that applies to resonance chains in many different settings. Additionally this approach allows to deduce a hypothesis for which systems resonance chains are in general observable and this hypothesis is verified numerically in a variety of different examples.

Finally Part IV deals again with a symmetry reduction, but this time for dynamical zeta functions. These zeta functions play a crucial role in the numerical calculation of resonances on Schottky surfaces. In presence of a finite symmetry group we obtain a factorization of the zeta function and very explicit formulas for the symmetry reduced factors. As an application of these formulas we show, that the symmetry reduction simplifies the calculation of resonances on Schottky surfaces by several orders of magnitudes and we use this gain in efficiency for some further tests of the hypothesis from Part III.

Even if there are common principles and links between all these four parts, the audience that could be interested in these different results differs strongly. I therefore decided to present the four parts as self-contained texts. Each part contains its own introduction providing a motivation and an overview over previous results. Also all the needed objects and notations are introduced in each part, separately. This has the obvious disadvantage, that there are many repetitions, e.g. the definition of Schottky surfaces appears three times in the text. However, this approach inhibits the advantage, that in different parts, different aspects can be emphasized. In Part II and IV for example the symbolic coding is a very important technical tool in the proof and the appearing zeta functions are mostly written as sums over closed symbolic words. In Part III, however, these technical details are less important so that zeta functions can be seen from a more global point of view as sums over closed geodesics. For readers that intend to read all or several parts I kept the notation between the parts as consistent as possible and added some remarks in footnotes, that illuminate connections between the different parts.

Part I
Equivariant spectral asymptotics for h-pseudodifferential operators

2 Introduction

Semiclassical analysis provides a rigorous way to establish a connection between quantum physics and classical mechanics. Mathematically, a non-relativistic quantum mechanical system is described by the spectrum of an h-pseudodifferential operator (h-PDO) $\hat{H}$ on $\mathbb{R}^n$ while the classical system is described by the Hamilton-flow of the associated symbol $H(x,\xi)$ on the symplectic vector space $T^*\mathbb{R}^n$. From a mathematical point of view the question of connecting quantum physics to classical mechanics thus consists in proving asymptotic formulae for the spectrum of $\hat{H}$ in terms of H in the limit $h \to 0$.

The two main theorems which have been established in this field are the Weyl law and the Gutzwiller trace formula. While the Weyl law gives an estimate for the number of eigenvalues below a certain energy in terms of the phase space volume of the corresponding classical energy shell, the Gutzwiller trace formula gives an asymptotic formula for the correlation of the eigenvalues in terms of periodic orbits of the classical flow.

The first version of Weyl's law was already proven in 1912 for special second order partial differential equations by Hermann Weyl [92], who wanted to give a rigorous foundation for the Rayleigh-Jeans law for black body radiation. This work has been generalized in various different works, among which we want to mention the work of Hörmander [51], who extended these results to elliptic pseudodifferential operators on compact manifolds, using the approach of Fourier integral operators (FIOs), and the work of Helffer and Robert [79] in the context of elliptic h-PDOs on $\mathbb{R}^n$.

The connection between spectral correlations and periodic orbits was first established in physics by the pioneering work of Gutzwiller [47] and Balian and Bloch [1] around 1970. Shortly later, between 1973 and 1975, similar results were rigorously proven for elliptic operators on compact manifolds by Colin de Verdière [19, 20, 22], Chazarain [18], and Duistermaat and Guillemin [28]. For h-PDOs, rigorous proofs have finally been given in the 90s by Paul and Uribe [73, 74] using a trick of Colin de Verdière [21] which allows to link

the semiclassical problem to homogeneous PDOs, and by Meinrenken using a direct FIO approach [62].

Symmetries of physical systems are known to simplify their study significantly. If for example the Hamiltonian $\hat{H}$ commutes with a compact Lie group G acting linearly on $\mathbb{R}^n$, then $\hat{H}$ leaves the Peter-Weyl decomposition $L^2(\mathbb{R}^n) = \bigoplus_{\chi\in\hat{G}} L^2_\chi$ of this group action invariant. Accordingly, one can restrict the Hamilton operator to one of the subspaces L^2_χ belonging to an irreducible representation χ of G. One can then study the spectral asymptotics of the symmetry-reduced Hamilton operator $\hat{H}_\chi := \hat{H}_{|L^2_\chi}$. This amounts to the question of counting the eigenvalues of this reduced Hamilton operator (equivariant Weyl law) and the question of correlations in the spectrum of $\hat{H}_\chi$ (equivariant Gutzwiller trace formula).

For elliptic operators on compact manifolds, the leading term of the equivariant Weyl law has been obtained for general group actions by Donnelly [27] and Brüning-Heintze [12] using heat kernel methods, which however do not allow to obtain remainder estimates. First remainder estimates were only obtained for actions with only one orbit type by Donnelly [27], Brüning-Heintze[12], Brüning [11] and Guillemin-Uribe [41] in the homogeneous setting, and by Helffer-Robert [49, 50] and El-Houakmi-Helffer for h-PDOs. When trying to obtain remainder estimates for general group actions, it turns out that singularities in the critical set of the appearing phase function cause serious problems. Recently it has been possible to obtain remainder estimates for the equivariant Weyl law for elliptic operators on compact manifolds which are invariant under general compact group actions [78] by partially resolving the singularities of the critical set (see also [17] for preliminary results).

In the derivation of equivariant Gutzwiller formulae, singularities in the critical set are a major obstruction in deriving the desired spectral asymptotics, too. There are two sources for these singularities: The group action and the Hamilton dynamics. Because of this, in all articles on equivariant Gutzwiller trace formulae (Guillemin-Uribe [41] for elliptic PDOs on compact manifolds and Cassanas [15, 16] for h-PDOs) the spectral asymptotics only hold under two conditions: The clean-flow or non-degenerate orbit condition, which are conditions on properties of the Hamilton flow (see e.g. [16, Definition 4.4]), and the condition of reduction, which is a condition on the group action (see e.g. [16, Definition 2.1]).

In the present work, equivariant spectral asymptotics of h-PDOs for general compact group actions are derived. Concerning the number of eigenvalues, we prove a weak equivariant Weyl law by reducing the problem to oscillatory integrals with singular critical sets which already appeared in [78].

Regarding the spectral correlations, we drop the condition on the group action on which the clean flow and non-degenerate orbit conditions are usually based. Instead we generalize the non-degenerate orbit condition for arbitrary group actions. Based on this new generalized condition on the Hamilton flow, we can derive a complete asymptotic expansion for the equivariant Gutzwiller trace formula without additional reduction assumptions. Furthermore we present a simple explicit example of a 3-dimensional Harmonic oscillator which illustrates that these new conditions are much less restrictive.

3 Definitions and notations

3.1 Classical Hamilton mechanics and quantization

We will consider Hamilton systems on the phase space $\mathbb{R}^{2n}$. Points in phase space will commonly be denoted by $z \in \mathbb{R}^{2n}$, respectively by $(x, \xi) \in \mathbb{R}^{2n}$, $x, \xi \in \mathbb{R}^n$, if we want to distinguish between the space variable x and momentum variable ξ. Even if the tangent space $T_z\mathbb{R}^{2n}$ is canonically isomorphic to $\mathbb{R}^{2n}$ we will emphasize the difference by denoting tangent vectors by Greek letters $\alpha, \beta \in T_z\mathbb{R}^{2n}$. The $2n \times 2n$ matrix $J = \begin{pmatrix} 0 & \mathbb{1} \\ -\mathbb{1} & 0 \end{pmatrix}$ defines a symplectic form by $\omega(\alpha, \beta) := \langle \alpha, J\beta \rangle$ where $\langle , \rangle$ is the standard scalar product on $\mathbb{R}^{2n}$.

A Hamiltonian on the symplectic manifold $(\mathbb{R}^{2n}, \omega)$ is a smooth function $H : \mathbb{R}^{2n} \to \mathbb{R}$. Via the symplectic structure we can associate a Hamilton vector field X_H to the Hamiltonian H by the condition $dH(\bullet) = \omega(X_H, \bullet)$. For the trivial symplectic manifold $(\mathbb{R}^{2n}, \omega)$ the Hamilton vector field is simply given by $J\nabla H(z)$, where ∇ denotes the gradient in $\mathbb{R}^{2n}$. This vector field generates the Hamilton flow $\Phi_t : \mathbb{R}^{2n} \to \mathbb{R}^{2n}$ by setting

$$\tfrac{d}{dt}\Phi_t(z) = J\nabla H(\Phi_t(z)). \tag{3.1}$$

In order to simplify notation we will sometimes write $(x_t, \xi_t) = z_t = \Phi_t(z)$.

For a given energy $E \in \mathbb{R}$, the energy shell is denoted by $\Sigma_E := H^{-1}(E)$. As ω is antisymmetric, we have $0 = \langle \nabla H(z_t), J\nabla H(z_t) \rangle = \frac{d}{dt} H(z_t)$. Thus, the energy is preserved along the flow, and the Hamilton flow leaves Σ_E invariant. Furthermore, $\nabla H(z) \perp J\nabla H(z)$, and if H is non-degenerate in z, i.e. if $\nabla H(z) \neq 0$, then Σ_E is locally smooth and $T_z\Sigma_E = (\nabla H(z))^\perp$.

Using a general formula for the Lie-derivative of a differential form we calculate

$$\frac{d}{dt}_{|t=0}(\Phi_t^*\omega) = \mathcal{L}_{X_H}\omega = d(X_H \lrcorner \omega) + X_H \lrcorner d\omega = ddH = 0$$

where we used the closeness of ω and the definition of X_H. Consequently the symplectic form is preserved under the Hamilton flow and the flow consists thus of symplectomorphisms.

In order to discuss the quantization of the classical Hamiltonian, we first introduce the notion of order functions and symbol classes (see e.g. [97, Chapter 4] for a more detailed introduction).

Definition 3.1 (Order function)**.** A measurable function $m : \mathbb{R}^{2n} \to \mathbb{R}^+$ is called *order function* if there exist constants $C > 0$ and $N \in \mathbb{R}$ such that

$$m(z) \leq C\langle z - z' \rangle^N m(z')$$

where $\langle z \rangle := \sqrt{1 + |z|^2}$.

A standard example for such an order function is e.g. $m(x, \xi) = \langle x \rangle^a \langle \xi \rangle^b$ with $a, b \in \mathbb{R}$.

Definition 3.2 (Symbol class)**.** Let m be an order function. Then the corresponding *symbol class* is defined by

$$S(m) := \{a \in C^\infty(\mathbb{R}^{2n}),\ \forall\, \gamma \in \mathbb{N}^{2n}\, \exists\, C_\gamma \text{ with } |\partial^\gamma a| \leq C_\gamma m\}.$$

Definition 3.3 (Quantization)**.** For a symbol $H \in S(m)$ and $t \in [0, 1]$, the *quantization* of H is defined on the Schwartz space $\mathcal{S}(\mathbb{R}^n)$ of rapidly decreasing functions as the operator

$$\Big(\mathrm{Op}_{h,t}(H)\Psi\Big)(x) := (2\pi h)^{-n} \int\limits_{\mathbb{R}^{2n}} H\left(tx + (1-t)y, \xi\right) \Psi(y) e^{\frac{i}{h}(x-y)\xi} dy d\xi.$$

Two particular important special cases are the standard quantization for $t = 1$

$$\Big(\mathrm{Op}_h(H)\Psi\Big)(x) := (2\pi h)^{-n} \int\limits_{\mathbb{R}^{2n}} H\left(x, \xi\right) \Psi(y) e^{\frac{i}{h}(x-y)\xi} dy d\xi$$

and the Weyl quantization for $t = \frac{1}{2}$

$$\Big(\mathrm{Op}^w_h(H)\Psi\Big)(x) := (2\pi h)^{-n} \int\limits_{\mathbb{R}^{2n}} H\left(\frac{x+y}{2}, \xi\right) \Psi(y) e^{\frac{i}{h}(x-y)\xi} dy d\xi.$$

The Weyl quantization has the particular advantage that real symbols give rise to L^2-symmetric operators. We will therefore mainly use the Weyl quantization, and in order to shorten the notation, we will denote the Weyl quantization of a symbol by $\hat{H} := \mathrm{Op}^w_h(H)$. In general, such a quantized pseudodifferential operator will, however, not have purely discrete spectrum. In order to obtain a Hamilton operator with satisfactory spectral properties we suppose

Hypothesis 3.1. $H : \mathbb{R}^{2n} \to \mathbb{R}$ is a smooth function bounded from below such that $\langle H \rangle$ is an order function and $H \in S(\langle H \rangle)$.

From these regularity conditions it follows with [48, Théorème 2.6] that $\hat{H}$ extends to a unique self-adjoint operator on the space of square integrable functions $L^2(\mathbb{R}^n)$. However, such an operator will not have discrete spectrum in an interval $[E_1, E_2]$ in general, and therefore we assume

Hypothesis 3.2. There are constants $E_1 < E_2$ and $\varepsilon > 0$ such that $H^{-1}([E_1 - \varepsilon, E_2 + \varepsilon]) \subset \mathbb{R}^{2n}$ is compact.

The physical interpretation of this condition is that the system is closed, and from [48, Proposition 5.1] we obtain that there is an $h_0 > 0$ such that for $h \in]0, h_0]$ the spectrum of $\hat{H}$ in the interval $[E_1, E_2]$ is purely discrete.

3.2 Group actions and symmetry reduction

We first recall some general facts about compact group actions. Let G be a compact Lie group acting on a smooth manifold M. For $g \in G$ and $m \in M$ we will simply denote the group action by gm. Given a point $m \in M$, we define its stabilizer subgroup as $G_m := \{g \in G,\ gm = m\} \subset G$. The orbit of m under the group action will be denoted by $Gm := \{gm, g \in G\} \subset M$, and it is always a smooth manifold diffeomorphic to the homogeneous space G/G_z. Furthermore, all the stabilizer subgroups $G_{m'}$ for arbitrary points on the orbit $m' \in Gm$ are conjugate to each other. In general, for points on different orbits this is not the case, which leads to

Definition 3.4 (Orbit types)**.** Let $m, m' \in M$ be two points. Their orbits G/G_m and $G/G_{m'}$ are said to be *of the same type* if the stabilizer subgroups G_m and $G_{m'}$ are conjugate in G. If two orbits G/H_1 and G/H_2 (H_1 and H_2 being closed subgroups of G) are given, then one can define a *partial order* on the orbit types by defining

$$\text{type}(G/H_1) \leq \text{type}(G/H_2) \Leftrightarrow H_2 \text{ is conjugate to a subgroup of } H_1. \quad (3.2)$$

One of the most important results in the theory of compact group actions is the existence of a principal orbit type.

Proposition 3.1. *Let G be a compact group acting smoothly on a manifold M. Then there exists a principal orbit type G/H such that the union of all points of this orbit type $M(H) := \{m \in M,\ G_m \text{ is conjugate to } H\}$ is open and dense in M. Furthermore, this orbit type is maximal with respect to the order relation (3.2).*

Proof. See e.g. [10, Theorem IV.3.1]. □

Symmetry groups of a Hamilton system are always required to preserve the symplectic structure. For a Hamilton system on $\mathbb{R}^{2n}$ a linear group G preserving the symplectic structure ω (i.e. fulfilling $\omega(g\alpha, g\beta) = \omega(\alpha, \beta)$ for all $\alpha, \beta \in \mathbb{R}^{2n}$ and $g \in G$) has thus to be a subgroup of the symplectic group $Sp(n)$. An important class of symplectic group actions arise from subgroups $G \subset Gl(n, \mathbb{R})$. For an element $g \in G$ acting linearly on $\mathbb{R}^n$, this action can be lifted to a symplectic action on $\mathbb{R}^{2n}$ by defining $g(x, \xi) := (gx, (g^t)^{-1}\xi)$. In the sequel, we will only consider compact subgroups $G \subset O(n)$, so that the symplectic action simplifies to $g(x, \xi) = (gx, g\xi)$. Studying orthogonal subgroups is in fact not more restrictive than studying compact subgroups $G \subset GL(n, \mathbb{R})$, because by a standard averaging argument each such group G is conjugate to an orthogonal subgroup $S_0 G S_0^{-1} \subset O(n)$ for a suitable $S_0 \in Gl(n, \mathbb{R})$ (see e.g. [15, Lemma 4.6] for more details). Through the smooth path $e^{At}z \subset \mathbb{R}^{2n}$, each element A of the Lie algebra $\mathfrak{g}$ of G defines a vector in $T_z\mathbb{R}^{2n}$. Identifying the tangent space with $\mathbb{R}^{2n}$, and considering $\mathfrak{g}$ as a matrix Lie algebra of $n \times n$ matrices, this vector is exactly given by the matrix action $(Ax, A\xi)$. We will generally denote it by Az and write the vector space spanned by this Lie algebra action as $\mathfrak{g}z := \{Az,\ A \in \mathfrak{g}\}$. It is straightforward to check that $\mathfrak{g}z = T_z(Gz)$.

A Hamiltonian is said to be G-invariant if $H(gz) = H(z)$ for all $g \in G, z \in \mathbb{R}^{2n}$. In this case the flow commutes with the G-action. Indeed, under certain assumptions such Hamilton systems can be reduced, i.e. one can construct a lower dimensional Hamilton system by using constants of motion and dividing out the group action. An important object for this symplectic reduction is the so called momentum map, which encodes the constants of motion. In our setting it is given by

$$\mu : \left\{ \begin{array}{ccc} \mathbb{R}^{2n} & \to & \mathfrak{g}^* \\ z & \mapsto & \mu(z) \end{array} \right. \quad \text{where } \mu(z)(A) := \langle z, JAz \rangle.$$

The zero level of the momentum map is given by

$$\Omega_0 := \mu^{-1}(0) := \{z \in \mathbb{R}^{2n}, \langle z, JAz \rangle = 0 \ \ \forall A \in \mathfrak{g}\}.$$

The regularity of Ω_0 strongly depends on the properties of the G-action. If $U \subset \mathbb{R}^{2n}$ is an open G-invariant subset intersecting Ω_0 such that all orbits in $\Omega_0 \cap U$ are of the same type, then it is known (see e.g. [17, Proposition 2]) that $\Omega_0 \cap U$ is a smooth manifold with tangent space

$$T_z(\Omega_0 \cap U) = (J\mathfrak{g}z)^{\perp}.$$

Furthermore, one has the following important

Theorem 3.2 (Symplectic reduction)**.** *If U is a set with the properties as above, then $G\backslash(\Omega_0 \cap U)$ carries a unique structure of a smooth symplectic manifold and the projection*

$$Pr : \left\{ \begin{array}{ccc} \Omega_0 \cap U & \to & G\backslash(\Omega_0 \cap U) \\ z & \mapsto & [z] \end{array} \right.$$

which associates to each point z the corresponding equivalence class $[z]$ in the quotient is a smooth submersion. If $H : U \to \mathbb{R}$ is a G-invariant Hamiltonian, then it reduces to a smooth Hamiltonian $\tilde{H} : G\backslash(\Omega_0 \cap U) \to \mathbb{R}$, and the Hamilton flow $\tilde{\Phi}_t$ of $\tilde{H}$ on $G\backslash(\Omega_0 \cap U)$ is compatible with the flow Φ_t of H on U, i.e.

$$\tilde{\Phi}_t \circ Pr = Pr \circ \Phi_t \tag{3.3}$$

Proof. see [69, Theorem 8.1.1, p.302] □

An important example for such an G-invariant open subset is the open and dense set of all principal orbits $M(H)$ described by Proposition 3.1. We will call the intersection of Ω_0 with this set the *regular part* of Ω_0 and write $\text{Reg } \Omega_0 := \Omega_0 \cap M(H)$.

If the condition of equal G-orbits on $\Omega_0 \cap U$ is not fulfilled, a reduction to a singular stratified space is possible [69, Theorem 8.1.1, p302]. The reduction is however much more complicated and uses results on the stratification of G-spaces in orbit types.

On the quantum mechanical side, the symmetry reduction appears via the Peter-Weyl theorem. The orthogonal action of G on $\mathbb{R}^n$ induces a unitary representation on $L^2(\mathbb{R}^n)$, which is the space on which we study the quantized Hamilton operator, by

$$(M(g)\Psi)(x) := \Psi(g^{-1}x) \quad \forall\ \Psi \in L^2(\mathbb{R}^n).$$

By the Peter-Weyl theorem, this unitary representation leads to the following decomposition of our Hilbert space $L^2(\mathbb{R}^n)$: Let $\chi \in \hat{G}$ be an equivalence class of unitary irreducible G-representations given by an irreducible character of the compact group G and $d_\chi = \chi(Id)$ the dimension of the irreducible representation. Then

$$P_\chi := d\chi \int_G \overline{\chi(g)} M(g) dg \quad (dg \text{ is the normalized Haar measure})$$

is a projector, and we denote its image by $L^2_\chi(\mathbb{R}^n)$. The space $L^2(\mathbb{R}^n)$ then decomposes into a direct sum

$$L^2(\mathbb{R}^n) = \bigoplus_{\chi \in \hat{G}} L^2_\chi(\mathbb{R}^n).$$

As a direct consequence of the G-invariance of the Hamiltonian H, we get that the quantized Hamilton operator $\hat{H}$ commutes with the G-action $M(g)$ so that

$$\hat{H} = M(g)\hat{H}M(g^{-1}). \tag{3.4}$$

Equation (3.4) implies that the Hamilton operator leaves $L^2_\chi(\mathbb{R}^n)$ invariant. We can therefore consider the restriction of $\hat{H}$ to $L^2_\chi(\mathbb{R}^n)$ and denote it by $\hat{H}_\chi$. This restricted operator is the symmetry-reduced Hamilton operator. Note that that in contrast to the symmetry reduction of the classical system, for the quantum reduction there are no additional complications if G acts with different orbit types.

4 Weak equivariant Weyl asymptotics

In this section we will prove a theorem for the asymptotic number of eigenvalues of the reduced Hamilton operator $\hat{H}_\chi$ for an arbitrary compact orthogonal group action. Suppose that $\hat{H}_\chi$ has purely discrete spectrum on $]E_1, E_2[$ and let $f \in C_0^\infty(]E_1, E_2[)$. Note that as $\hat{H} = \mathrm{Op}^w_h(H)$ is a family of operators parametrized by $h > 0$, its spectrum will equally depend on the semiclassical parameter h. We will give the leading term in the limit $h \to 0$, plus a remainder estimate, for the expression $\sum f(\lambda_i)$, where the sum is over all eigenvalues of $\hat{H}_\chi$ in $]E_1, E_2[$ repeated according to their multiplicity. By taking a smooth function approximating the characteristic function of an interval $[a, b] \subset]E_1, E_2[$, this expression immediately gives us approximate information on the asymptotic number of eigenvalues in the interval $[a, b]$. As we are restricted to smooth functions f, and cannot take f exactly to be a characteristic function, we call these asymptotics "weak Weyl asymptotics". The strong version of the equivariant Weyl's law i.e. asymptotics for f being a characteristic function, have been obtained by El-Houakmi and Robert [32] via FIOs in the case of one orbit type.

We will prove the "weak Weyl asymptotics" for an arbitrary orbit structure by reducing the problem via functional calculus to oscillatory integrals with singular critical sets, and use results of [78] for these integrals. A generalization of the strong version of Weyl's law to arbitrary orbit structures seems not possible by reducing the problem to the integrals studied in [78], but would require to resolve a much more complicated phase function.

We can now state and prove our first main result

Theorem 4.1. *Let G be a compact subgroup of $O(n)$ and $H : \mathbb{R}^{2n} \to \mathbb{R}$ a smooth G-invariant Hamiltonian which is bounded from below, and satisfies the regularity conditions of Hypothesis 3.1. Let $E_1 < E_2$ and $\epsilon > 0$ be such*

that $H^{-1}([E_1-\epsilon, E_2+\epsilon])$ *is compact, and let* $f:\mathbb{R}\to\mathbb{R}$ *be smooth and compactly supported in* $]E_1, E_2[$. *For a given character* $\chi\in\hat{G}$ *and small* h, $f(\hat{H}_\chi)$ *is of trace class, and its trace is asymptotically given by*

$$\mathrm{Tr}(f(\hat{H}_\chi)) = (2\pi h)^{-n+\kappa} d_\chi \mathcal{L}_0 + \mathcal{O}(h^{-n+\kappa+1}\log(h^{-1})^\Lambda) \tag{4.1}$$

where κ *is the dimension of a principal orbit in* $\mathbb{R}^n$, Λ *the maximal number of elements of a totally ordered subset of the set of orbit types, and*

$$\mathcal{L}_0 = [\pi_{\chi|H_{\mathrm{prin}}}:1] \int\limits_{\mathrm{Reg}\ \Omega_0} \frac{f(H(z))}{\mathrm{Vol}(Gz)} d(\mathrm{Reg}\ \Omega_0)(z). \tag{4.2}$$

Here $\mathrm{Vol}(Gz)$ *denotes the induced volume of the principal* G*-orbit through* z *as a submanifold of* $\mathbb{R}^n$, *and* $d(\mathrm{Reg}\ \Omega_0)$ *the induced measure on* $\mathrm{Reg}\ \Omega_0$. $[\pi_{\chi|H_{\mathrm{prin}}}:1]$ *is the Frobenius factor which is given by the multiplicity with which the trivial representation occurs in the restriction of the irreducible* G*-representation* π_χ *to the isotropy subgroup of the principal orbits* $H_{\mathrm{prin}}\subset G$.

Remark 4.1. As mentioned in Section 3.2, the case of a compact symmetry group $G\subset GL(n,\mathbb{R})$ can be reduced to the case of an orthogonal subgroup, treated in the theorem, by a standard averaging argument.

Remark 4.2. As G acts with only one orbit type G/H_{prin} on $\mathrm{Reg}\ \Omega_0$, the quotient $G\backslash\mathrm{Reg}\ \Omega_0$ has the structure of a symplectic manifold (see Theorem 3.2) and $\mathrm{Reg}\ \Omega_0$ is a fiber bundle over this quotient

$$Pr: \left\{ \begin{array}{ccc} \mathrm{Reg}\ \Omega_0 & \to & G\backslash\mathrm{Reg}\ \Omega_0 \\ z & \mapsto & [z] \end{array} \right.$$

with the principal orbit G/H_{prin} as the fiber. By its G-invariance, the Hamiltonian $H(z)$ takes constant values along the fibers equal to the value of the reduced Hamiltonian $\tilde{H}([z])$. Consequently, using a fiberwise integration we can rewrite (4.2) as

$$\mathcal{L}_0 = [\pi_{\chi|H_{\mathrm{prin}}}:1] \int\limits_{G\backslash\mathrm{Reg}\ \Omega_0} f(\tilde{H}([z]))\, d(G\backslash\mathrm{Reg}\ \Omega_0)([z]). \tag{4.3}$$

Proof. In a first step we show that $f(\hat{H}_\chi)$ is trace class, and express the trace as an oscillatory integral. Afterwards we will derive the asymptotic behavior for this integral from a result in [78].

From the compactness of $H^{-1}(E_1-\epsilon, E_2+\epsilon)$ we conclude that $\hat{H}$ has purely discrete spectrum on the interval $[E_1, E_2]$ with eigenvalues $\lambda_1,\ldots,\lambda_r$

and eigenstates $\Psi_1, \dots \Psi_r$ [48, Proposition 5.1]. The expression $f(\hat{H})$ is thus defined by

$$f(\hat{H})\Psi = \sum_{i=1}^{r} f(\lambda_i)\langle \Psi_i, \Psi\rangle \Psi_i, \text{ for } \Psi \in L^2(\mathbb{R}^n).$$

As $H(z)$ is G-invariant, each eigenstate Ψ_i belongs precisely to one G representation L^2_χ. Consequently, if we denote by σ_χ the set of all eigenvalues belonging to $\chi \in \hat{G}$ we can write

$$f(\hat{H})\Psi = \sum_{\chi\in\hat{G}} \sum_{\lambda_i\in\sigma_\chi} f(\lambda_i)\langle \Psi_i, \Psi\rangle \Psi_i = \left(\sum_{\chi\in\hat{G}} f(\hat{H}_\chi)\right)\Psi$$

with

$$f(\hat{H}_\chi)\Psi = \sum_{\lambda_i\in\sigma_\chi} f(\lambda_i)\langle \Psi_i, \Psi\rangle \Psi_i.$$

Thus we conclude

$$f(\hat{H}_\chi) = f(\hat{H})\hat{P}_\chi. \tag{4.4}$$

Now, for $f(\hat{H})$ we can use the Helffer-Robert functional calculus [48, Théorème 4.1] and get for each $N \in \mathbb{N}$ the expression

$$f(\hat{H}) = \sum_{j=0}^{N} h^j Op^w_h(a_j) + h^{N+1}\hat{R}_{N+1}(h), \tag{4.5}$$

where the a_j are symbols with $\mathrm{supp}(a_j) \subset H^{-1}(]E_1-\epsilon, E_2+\epsilon[)$ and $a_0 = f\circ H$. Furthermore, from the proof of Théorème 5.1 in [48] it follows that $\hat{R}_N$ is of trace class for h sufficiently small and that its trace norm is bounded by $\|\hat{R}_{N+1}\|_{\mathrm{Tr}} \leq Ch^{-n}$. As the a_j are compactly supported symbols, the operators $Op^w_h(a_j)$ are of trace class. Consequently also $f(\hat{H})$ and $f(\hat{H}_\chi)$ are trace class operators.

In order to express $f(\hat{H}_\chi)$ as an oscillatory integral we first prove the following

Lemma 4.2. *Let $Op_h(a_j)$ be the standard quantization. Then $Op_h(a_j)\hat{P}_\chi$ can be written as an integral operator with smooth kernel*

$$K(x,y) = (2\pi h)^{-n} d_\chi \int_G \int_{\mathbb{R}^n} a_j(x,\xi)\overline{\chi(g)} e^{\frac{i}{h}(x-g^{-1}y)\xi} d\xi dg.$$

Proof. For $\Psi \in C_0^\infty(\mathbb{R}^n)$, we calculate with Fubini

$$\begin{aligned}\int_{\mathbb{R}^n} K(x,y)\Psi(y)dy &= (2\pi h)^{-n} d_\chi \int_{\mathbb{R}^n} \left[\int_G \int_{\mathbb{R}^n} a_j(x,\xi)\overline{\chi(g)} e^{\frac{i}{h}(x-g^{-1}y)\xi} d\xi dg \right] \Psi(y)dy \\ &= (2\pi h)^{-n} \int_{\mathbb{R}^n}\int_{\mathbb{R}^n} a_j(x,\xi) e^{\frac{i}{h}(x-y)\xi} \left[\int_G d_\chi \overline{\chi(g)}\Psi(gy)dg \right] d\xi dy \\ &= [Op_h(a_j)P_\chi\Psi](x),\end{aligned}$$

where we used the fact that all integrands are compactly supported. □

In order to calculate the desired trace by the above lemma we need to change the quantization in (4.5).

Lemma 4.3. *If $b \in S(m)$ is a G-invariant, compactly supported symbol, then*

$$Op_h^w(b) = Op_h\left(\sum_{j=0}^N h^j b_j(x,\xi) + h^{N+1} R_N(x,\xi) \right) \tag{4.6}$$

for every $N \in \mathbb{N}$, where $b_j \in S(m)$ are compactly supported and G-invariant. Furthermore, $b_0 = b$ and $\|Op_h(R_N)\|_{Tr} < Ch^{-n}$.

Proof. By [97, Theorem 4.13] one has (4.6) with $b_j = \frac{(-ih\langle D_x, D_\xi\rangle)^j}{j!} b$, so that the compactness property follows immediately. From the G-invariance of b we conclude for arbitrary $g \in G$

$$\begin{aligned}\left(\tfrac{(-ih\langle D_x,D_\xi\rangle)^j}{j!} b\right)(x) &= \left(\tfrac{(-ih\langle D_x,D_\xi\rangle)^j}{j!}(b\circ g)\right)(x) \\ &= \left(\tfrac{(-ih\langle gD_x,gD_\xi\rangle)^j}{j!} b\right)(gx) \\ &= \left(\tfrac{(-ih\langle D_x,D_\xi\rangle)^j}{j!} b\right)(gx)\end{aligned}$$

which proves the G-invariance of the b_j. Finally, as b is compactly supported, b and consequently also R_N belong to $S(\langle z\rangle^{-k})$ for all k. Thus, R_N is a Schwartz function and $\mathrm{Tr}[Op_h(R_N)] = (2\pi h)^{-n} \iint R_N(x,\xi)dxd\xi$. □

Equation (4.4) and (4.5), together with Lemma 4.2 and Lemma 4.3 finally yield

Corrolary 4.4. *For each $N \in \mathbb{N}$ the trace of $f(\hat{H}_\chi)$ can be written as*

$$\mathrm{Tr}(f(\hat{H}_\chi)) = (2\pi h)^{-n} d_\chi \sum_{j=0}^N h^j \int_G \int_{\mathbb{R}^n}\int_{\mathbb{R}^n} \tilde{a}_j(x,\xi)\overline{\chi(g)} e^{\frac{i}{h}(x-gx)\xi} dxd\xi dg + \mathcal{O}(h^{-n+N}), \tag{4.7}$$

where the $\tilde{a}_j$ are compactly supported, G-invariant symbols and $\tilde{a}_0 = f \circ H$.

Each of the summands in (4.7) is thus an oscillatory integral with phase function $\Phi(x,\xi) = (x - gx)\xi$. The critical set of such an oscillatory integral is defined by $\mathcal{C} := \{(z,g) \in \mathbb{R}^{2n} \times G,\ d\Phi_{z,g} = 0\}$. For this phase function a straightforward computation yields

$$\mathcal{C} = \{(z,g) \in \Omega_0 \times G,\ gz = z\}.$$

If G acts with different orbit types, this set is not smooth and one cannot obtain the asymptotics directly by the stationary phase theorem. However, it has been shown [78] that by iteratively blowing up the critical set, the leading order term for integrals of this type can be obtained together with a remainder estimate. As all symbols of the oscillatory integral are compactly supported we can use [78, Theorem 11] and obtain in the limit $h \to 0$

$$\mathrm{Tr}(f(\hat{H}_\chi)) = (2\pi h)^{-n+\kappa} d_\chi \mathcal{L}_0 + \mathcal{O}(h^{-n+\kappa+1} \log(h^{-1})^\Lambda),$$

where κ is the dimension of a principal orbit in $\mathbb{R}^n$, Λ the maximal number of elements of a totally ordered subset of the set of orbit types, and

$$\mathcal{L}_0 = \int\limits_{\mathrm{Reg}\ \mathcal{C}} \frac{\overline{\chi(g)} f(H(x,\xi))}{\left|\det\left(\mathrm{Hess}\ \Phi(x,\xi,g)_{|N_{x,\xi,g}\mathrm{Reg}\ \mathcal{C}}\right)\right|^{1/2}} d(\mathrm{Reg}\ \mathcal{C})(x,\xi,g),$$

where the set $\mathrm{Reg}\ \mathcal{C} := \mathcal{C} \cap (\mathrm{Reg}\ \Omega_0 \times G)$ is a smooth submanifold of $\mathbb{R}^{2n} \times G$ and $\mathrm{Hess}\ \Phi(x,\xi,g)_{|N_{(x,\xi,g)}\mathrm{Reg}\ \mathcal{C}}$ the restriction of the Hessian to the normal-bundle of $\mathrm{Reg}\ \mathcal{C}$. Applying [17, Lemma 7] this expression can be simplified to

$$\mathcal{L}_0 = [\pi_{\chi|H_{\mathrm{prin}}} : 1] \int\limits_{\mathrm{Reg}\ \Omega_0} \frac{f(H(z))}{\mathrm{Vol}(Gz)} d(\mathrm{Reg}\ \Omega_0)(z).$$

This finally proves Theorem 4.1. □

5 Equivariant Gutzwiller formula

While the previous section treated a result on the number of eigenvalues of the symmetry-reduced operator $\hat{H}_\chi$, this section will be dedicated to the correlations in the spectrum of $\hat{H}_\chi$ which will be described by an equivariant Gutzwiller trace formula. In Section 5.1 we will introduce the equivariant spectral distribution which is the well known quantity to study asymptotic spectral correlations. This spectral distribution will be written as an oscillatory integral using results of Cassanas [16]. The phase analysis and a discussion of the possible singularities of the critical set will be the subject

of Section 5.2. We will see that, in general, the singularities can result from the group action as well as from the Hamilton dynamics, and we will review the assumptions which were imposed by Guillemin-Uribe [41] and Cassanas [16] in order to avoid these singularities. In Section 5.3 we introduce a generalization of the former assumptions which makes no special hypothesis on the group action anymore. Under these assumptions we finally prove the equivariant Gutzwiller trace formula in Section 5.4.

5.1 Spectral distribution and oscillatory integrals

Throughout this section we will assume that H is a Hamiltonian fulfilling Hypothesis 3.1 and 3.2 and that $G \subset O(n)$ is a compact Lie group acting on $\mathbb{R}^n$. Furthermore we assume that H is G-invariant. As discussed above, for an arbitrary equivalence class of irreducible unitary representation $\chi \in \hat{G}$ one can study the symmetry-reduced Hamilton operator $\hat{H}_\chi$ which has purely discrete spectrum in $[E_1, E_2]$ for $h \in]0, h_0]$. Let $\zeta \in C_0^\infty([E_1, E_2])$ be a smooth cut-off function and $h \in]0, h_0]$. We can then define for each $E \in]E_1, E_2[$ the spectral distribution $\rho^\chi_{E,h} \in \mathcal{S}'(\mathbb{R})$ by its action on $f \in \mathcal{S}(\mathbb{R})$ by setting

$$\rho^\chi_{E,h}(f) := \mathrm{Tr}\left(\zeta(\hat{H}_\chi) f\left(\frac{E - \hat{H}_\chi}{h}\right)\right). \tag{5.1}$$

This expression can be reformulated using the Fourier inversion formula, and one obtains

$$\rho^\chi_{E,h}(f) := \frac{1}{2\pi}\mathrm{Tr}\left(\zeta(\hat{H}_\chi) \int_{\mathbb{R}} e^{\frac{i}{h}Et} e^{-\frac{i}{h}\hat{H}_\chi t} \hat{f}(t) dt\right) \tag{5.2}$$

with $\hat{f}(t)$ being the Fourier transform $\hat{f}(t) := \int_{\mathbb{R}} e^{-iEt} f(E) dE$.

In order to understand the significance of this spectral distribution, consider the following heuristics: Assume, that $\hat{f}(t)$ is compactly supported and that this support is very close to $t_0 \neq 0$ such that it approximates the delta distribution at t_0. One then obtains

$$\rho^\chi_{E,h}(f) \approx \frac{1}{2\pi} e^{\frac{i}{h}Et_0} \sum_{E_j \in \sigma(\hat{H}_\chi) \cap [E_1, E_2]} \zeta(E_j) e^{-\frac{i}{h}E_j t_0}$$

where $\sigma(\hat{H}_\chi)$ denotes the spectrum of $\hat{H}_\chi$. From the Weyl law we know that the number of eigenvalues E_j of $\hat{H}_\chi$ in $[E_1, E_2]$ diverges as $h \to 0$. Therefore, if they are randomly distributed in $[E_1, E_2]$, the spectral distribution will be

very small for small h due to phase cancellation. The contrary extreme would be a totally correlated spectrum, respectively an equidistant spectrum

$$E_{j+1} = E_j + \frac{2\pi h}{t_0}$$

In this case the spectral distribution gives

$$\rho^{\chi}_{E,h}(f) \approx \frac{1}{2\pi} e^{\frac{i}{h}(E-E_0)t_0} \sum_{E_j \in \sigma(\hat{H}_\chi) \cap [E_1,E_2]} \zeta(E_j),$$

which constitutes for small h a large quantity according to the weak asymptotics. Of course such an equidistant spectrum is only possible for very special dimensions of phase space and G-orbits in order to be in accordance with the equivariant Weyl law, and also the approximation of the delta distribution by $\hat{f}$ strictly speaking does not hold anymore in the limit $h \to 0$. This heuristic discussion however shows that contributions of the spectral distribution at $t_0 \neq 0$ measure the correlation of the spectrum with a correlation length $\frac{2\pi h}{t_0}$, motivating its study. The equivariant Gutzwiller trace formula will be an asymptotic expansion of the spectral distribution $\rho^{\chi}_{E,h}$ evaluated at a Schwartz function f with $\hat{f}$ compactly supported away from zero.

The standard way to obtain the asymptotic expansion of the spectral distribution is to rewrite it as an oscillatory integral, and apply the stationary phase approximation. This transformation of the spectral distribution to an oscillatory integral can be performed in different ways. The most common way is to use Fourier integral operator theory in order to characterize the operator $e^{\frac{i}{h}\hat{H}}$ in (5.2). An alternative approach has been proposed by Combescure-Ralston-Robert [23] using their previous results on the propagation of coherent states [24]. This coherent state approach has been elaborated in detail by Cassanas [15, 16] in exactly the same setting which we study in this work, i.e. for symmetry-reduced h-PDOs. We will thus use the following result of those works:

Proposition 5.1. *Let $f \in \mathcal{S}(\mathbb{R})$ such that $\hat{f}$ is compactly supported. Then*

$$\rho^{\chi}_{E,h}(f) = d_\chi \int_{\mathbb{R}} dt \int_{\mathbb{R}^{2n}} dz \int_G dg \;\; a_g(z,h) \hat{f}(t) e^{\frac{i}{h}\phi_E(z,t,g)}, \tag{5.3}$$

where the complex phase function is given by $\phi_E = \phi^1_E + i\phi^2_E$ with

$$\begin{aligned} \phi^1_E(z,t,g) &= (E - H(z))t + \frac{1}{2}\langle g^{-1}z, Jz\rangle - \frac{1}{2}\int_0^t \langle (z_t - g^{-1}z), J\dot{z}_s\rangle ds, \\ \phi^2_E(z,t,g) &= \frac{1}{4}\langle (\mathbb{1} - \hat{W}_t)(gz_t - z), (gz_t - z)\rangle. \end{aligned}$$

Here $\hat{W}_t$ is a complex valued $2n\times 2n$-matrix such that $(\mathbb{1}-\hat{W}_t)$ defines a non-degenerate quadratic form. More precisely, $\hat{W}_t := \begin{pmatrix} W_t & -iW_t \\ -iW_t & -W_t \end{pmatrix}$ where the $n\times n$ matrice W_t is given by the equation

$$\tfrac{1}{2}(\mathbb{1}+W_t) := \left(\mathbb{1} - ig(C+iD)(A+iB)^{-1}g^{-1}\right)^{-1}$$

with A, B, C, D being the real t- and z-dependent $n\times n$ matrices such that the linearized flow is given by $(\Phi_t)_{*,z} = \begin{pmatrix} A & B \\ C & D \end{pmatrix}$. The integrand $a_g(\bullet, h) : \mathbb{R}^{2n}\to\mathbb{C}$ is supported in $H^{-1}([E-\delta E, E+\delta E])$ and is given by an asymptotic expansion in h with leading term

$$a_g(z,h) \sim_{h\to 0^+} \frac{(2\pi h)^{-d}}{2\pi}\overline{\chi(g)}\chi_2(z)\zeta(H(z))\mathrm{det}_*^{-1/2}\left(\frac{A+iB-i(C+iD)}{2}\right). \tag{5.4}$$

Here χ_2 is a smooth cut-off function compactly supported around Σ_E and equal to one in a neighborhood of $\Sigma_E = H^{-1}(E)$ and $\mathrm{det}_*^{-1/2}(M)$ is defined as the product of the reciprocal square roots of eigenvalues of the matrix M with real parts chosen to be positive.

Proof. See [16], Section 4, Equation (4.1). For the non degeneracy of $\mathbb{1}-\hat{W}_t$ see the discussion in [15] on page 10 (Section IV A). □

By this proposition we have thus written the spectral distribution as an oscillatory integral with complex phase function. The next section will be dedicated to its phase analysis.

5.2 The critical set

For a complex valued phase function $\Phi\in C^\infty(\mathbb{R}^n)$ with $\mathrm{Im}(\Phi)\geq 0$, the critical set is defined as (c.f. [52] Theorem 7.7.1)

$$\mathcal{C}_\Phi := \{x\in\mathbb{R}^n,\ \mathrm{Im}(\Phi(x)) = 0 \text{ and } \nabla\Phi(x) = 0\}.$$

Using the fact that $(\mathbb{1}-\hat{W}_t)$ is non-degenerate, a straightforward but slightly tedious calculation leads to

Proposition 5.2. *For the complex phase function ϕ_E of Proposition 5.1, the critical set is given by*

$$\mathcal{C}_{\phi_E} = \{(z,t,g)\in\mathbb{R}^{2n}\times\mathbb{R}\times G,\quad z\in\Omega_0\cap\Sigma_E,\ g\Phi_t(z) = z\} \tag{5.5}$$

Proof. See [16, Proposition 4.1]. □

This critical set $\mathcal{C}_{\phi_E}$ is in general a singular set. There are two different sources for these singularities: First of all, they can purely result from the Hamilton flow even if there is no symmetry group acting. For example, an isolated fixed point or a singular family of periodic orbits would lead to such singularities. A second source of singularities are, as in the case of the weak asymptotics, different orbit types of the group action. The same critical set with the same sources of singularities also appears in the work of Guillemin-Uribe [41]. In order to make sure that the critical set is smooth, and to prove the asymptotic expansion for the equivariant Gutzwiller trace formula, both works [41, 16] impose the following three conditions (H1)-(H3) which we now recall, using the notation of [16].

Hypothesis (H1). For $E \in \mathbb{R}$, the *hypothesis of reduction* is fulfilled if there exists some $\delta E > 0$ such that for $U = H^{-1}(]E - \delta E, E + \delta E[)$

- $\Omega_0 \cap U \neq \emptyset$,
- all G-orbits in $\Omega_0 \cap U$ are of the same type.

This hypothesis prevents the possible singularities coming from the group action. If it is fulfilled one can consider the reduced Hamiltonian $\tilde{H} : G\backslash(\Omega_0 \cap U) \to \mathbb{R}$ given by Theorem 3.2. In order to avoid the singularities coming from the Hamilton dynamics, one further needs the following two Hypothesis.

Hypothesis (H2). Assume that (H1) is fulfilled. Then E is a *non critical value* of $\tilde{H}$, i.e. $d\tilde{H} \neq 0$ on $\tilde{\Sigma}_E := \tilde{H}^{-1}(E)$.

Hypothesis (H3). Assume that (H1) and (H2) are fulfilled. Let $\gamma \subset \tilde{\Sigma}_E$ be an arbitrary closed orbit of the reduced Hamiltonian $\tilde{H}$, $[z] \in \gamma$ an arbitrary point on this orbit, and $T_\gamma > 0$ the period of the orbit so that $\tilde{\Phi}_{T_\gamma}([z]) = [z]$. Let furthermore $\tilde{F}_t := \partial_z \tilde{\Phi}_t$ be the linearized flow. Then we assume that γ is a *non-degenerate orbit* i.e. the eigenvalue 1 of $\tilde{F}_{T_\gamma}([z])$ has algebraic multiplicity 2.

More generally, the non-degenerate orbit condition can be weakened replacing it by the *clean-flow condition*. However, under this assumption, the resulting spectral asymptotics can not be written as a sum over periodic orbits anymore, and are much less explicit.

In the following we shall drop the Hypothesis (H1) and study the Gutzwiller trace formula for general compact group actions. As the formulation of (H2) and (H3) is usually based on (H1), these two conditions have to be replaced by appropriate generalizations which will be formulated in the next subsection.

5.3 The G-non-stationary and G-non-degenerate assumption

Let (H1) be fulfilled. Then assumption (H2) is equivalent to the fact that the Hamilton flow of $\tilde{H}$ on the reduced phase space has no stationary points at the given energy level E. Suppose that $[z] \in \tilde{\Sigma}_E$ is such a stationary point, i.e. $\tilde{\Phi}_t([z]) = [z]$ for all t, then we infer from (3.3), that $\Phi_t(z) \subset Pr^{-1}([z]) = Gz \subset \Omega_0 \cap \Sigma_E$ for all t. In particular we have $\frac{d}{dt}\Phi_t(z)_{|t=0} \in \mathfrak{g}z$. If, on the other hand, we have for some $z \in \Omega_0 \cap \Sigma_E$ that $\frac{d}{dt}\Phi_t(z)_{|t=0} = Az$ for some $A \in \mathfrak{g}$, then we obtain that $\Phi_t(z) = e^{At}z$ because we check that it fulfills the Hamilton equations of motions (3.1)

$$\begin{aligned} \frac{d}{dt}e^{At}z_{|t=t_0} &= e^{At_0}Az \\ &= e^{At_0}\frac{d}{dt}\Phi_t(z)_{|t=0} \\ &= e^{At_0}J\nabla H(z) \\ &= J\nabla H(e^{At_0}z). \end{aligned}$$

Here we used in the last equality that the group action is symplectic and that the Hamiltonian is G-invariant. Consequently a stationary point on the symmetry-reduced system in $\tilde{\Sigma}_E$ is equivalent to an orbit of the Hamilton flow of H which is tangent to a G-orbit in at least one point in $\Omega_0 \cap \Sigma_E$. Let now (H1) be dropped. Hypothesis (H2) can then be easily reformulated for general compact group actions and we arrive at

Hypothesis (H2′). The given Hamilton dynamics is called *G-non-stationary* for a given energy $E \in \mathbb{R}$ if and only if $J\nabla H(z) \notin \mathfrak{g}z$ for all $z \in \Sigma_E \cap \Omega_0$.

The generalization of (H3) requires a little bit more work. We assume that the Hamilton dynamics is G-non-stationary, so that in particular $\nabla H(z) \neq 0$ on $\Omega_0 \cap \Sigma_E$ and Σ_E is a smooth submanifold in some neighborhood of Ω_0. From the G-invariance of the Hamiltonian we obtain that the G-orbit Gz of a point $z \in \Omega_0 \cap \Sigma_E$ is completely contained in Σ_E thus the same inclusion holds for their tangent spaces $\mathfrak{g}z \subset T_z\Sigma_E$. Consequently $\nabla H(z) \perp Az$ for all $z \in \Omega_0 \cap \Sigma_E$ and $A \in \mathfrak{g}$. For $z \in \Omega_0 \cap \Sigma_E$, we obtain thus the decomposition

$$T_z\mathbb{R}^{2n} = (\mathbb{R}\nabla H(z) \oplus J\mathfrak{g}z) \bigoplus (\mathbb{R}J\nabla H(z) \oplus \mathfrak{g}z) \bigoplus \mathcal{R}, \tag{5.6}$$

where $\mathcal{R}$ is simply the orthogonal complement of $(\mathbb{R}\nabla H(z) \oplus J\mathfrak{g}z) \bigoplus (\mathbb{R}J\nabla H(z) \oplus \mathfrak{g}z)$ in $T_z\mathbb{R}^{2n}$. In order to obtain a clearer interpretation of (5.6) we introduce a notation which will turn out to be convenient at several other points in the

sequel. We define the Lie group $F := \mathbb{R} \times G$ and its action for $f = (t, g) \in F$ on $z \in \mathbb{R}^{2n}$ by

$$fz := g\Phi_t(z).$$

The fact that the G-action commutes with Φ_t assures that this is really a Lie group action. We will denote its Lie algebra by $\mathfrak{f} = \mathbb{R} \oplus \mathfrak{g}$ and an Lie-algebra element by (τ, A). Its infinitesimal Lie-algebra action is given by $(\tau, A)z = \tau J\nabla H(z) + Az$ and for the subspace of $T_z\mathbb{R}^{2n}$ spanned by the $\mathfrak{f}$-action we write

$$\mathfrak{f}z := \{\tau J\nabla H(z) + Az,\ (\tau, A) \in \mathfrak{f}\} = T_z(Fz).$$

With this notation (5.6) becomes

$$T_z\mathbb{R}^{2n} = J\mathfrak{f}z \oplus \mathfrak{f}z \oplus \mathcal{R}. \tag{5.7}$$

Consider now a point $z \in \Omega_0 \cap \Sigma_E$ which fulfills $fz = z$ for some $f \in F$. We can then study the differential $f_{*,z} = (g\Phi_T)_{*,z} : T_z\mathbb{R}^{2n} \to T_z\mathbb{R}^{2n}$.

Lemma 5.3. *Assume that (H2′) is fulfilled and consider for a fixed $f = (T, g) \in F$ a point $z \in \Omega_0 \cap \Sigma_E$ such that $fz = g\Phi_T(z) = z$. Then the differential of f has the form*

$$f_{*,z} = \begin{pmatrix} \boxed{\mathcal{A}} & 0 & 0 \\ * & \boxed{\mathcal{B}} & * \\ * & 0 & \boxed{\mathcal{P}} \end{pmatrix} \tag{5.8}$$

where the block form is with respect to the decomposition (5.7) of the tangent space, i.e. $\mathcal{A}$ acts on $J\mathfrak{f}z$, $\mathcal{B}$ on $\mathfrak{f}z$, and $\mathcal{P}$ on $\mathcal{R}$. Furthermore, $\mathcal{B}$ is given on $\mathfrak{f}z = \mathbb{R}J\nabla H(z) \oplus \mathfrak{g}z$ by

$$\mathcal{B} = \begin{pmatrix} 1 & 0 \\ 0 & \mathrm{Ad}(g) \end{pmatrix}$$

Proof. As the F-action leaves the corresponding F-orbits invariant, $\mathfrak{f}z$ is invariant under $f_{*,z}$ which explains the second column in (5.8). As the Hamilton flow and the G action are both symplectic, the F action is symplectic as well, which implies that the symplectic complement $(J\mathfrak{f}z)^\perp = \mathfrak{f}z \oplus \mathcal{R}$ of $\mathfrak{f}z$ is an invariant subspace under $f_{*,z}$ and consequently we obtain the first row in (5.8). For the refined form of $\mathcal{B}$ we consider the vector $J\nabla H(z) = \frac{d}{dt}\Phi_t(z)_{|t=0}$. Since

$$\frac{d}{dt}g\Phi_T(\Phi_t(z))_{|t=0} = \frac{d}{dt}g\Phi_t(\Phi_T(z))_{|t=0} = \frac{d}{dt}\Phi_t(g\Phi_T(z))_{|t=0} = J\nabla H(z),$$

$J\nabla H(z)$ is eigenvector of $(g\Phi_T)_{*,z}$ with eigenvalue 1. On the other hand, if $v \in \mathfrak{g}z$ i.e. $v = \frac{d}{dt}e^{At}z_{|t=0}$, one computes

$$(g\Phi_T)_{*,z}(v) = \frac{d}{dt}g\Phi_T(e^{At}z)_{|t=0} = \frac{d}{dt}ge^{At}g^{-1}g\Phi_T(z)_{|t=0} = (\mathrm{Ad}(g)A)z.$$

□

With this general form of the differential $(g\Phi_T)_*$ one can now reformulate (H3) to a new assumption (H3′) which we call *G-non-degenerate assumption*. In order to formulate it we first introduce some further notations.

Definition 5.1. By a *relative periodic point* $z \in \mathbb{R}^{2n}$ we will denote a point for which there are $T \neq 0$ and $g \in G$ such that $g\Phi_T(z) = z$. For a relative periodic point z_0 the set $\gamma = \{g\Phi_t(z_0),\ g \in G \text{ and } t \in \mathbb{R}\}$ is then called *relative periodic orbit*. For a given relative periodic orbit γ, its *primitive period length* T_γ is defined as the smallest $T > 0$ such that there exists $g \in G$ with $g\Phi_T(z) = z$ for some $z \in \gamma$.

Remark 5.1. Relative periodic points are thus simply fixed points under some element $f = (T, g) \in F$ with $T \neq 0$ and the relative periodic orbits are the F-orbits of a relative periodic point.

Definition 5.2. Let $z \in \Omega_0 \cap \Sigma_E$ be a relative periodic point with $g\Phi_T(z) = z$ for some $g \in G$ and $T > 0$. Then this point, as well as the corresponding relative periodic orbit γ, are called *G-non-degenerate* if $\mathcal{P}$ in (5.8) has no eigenvalue equal to 1.

Hypothesis (H3′). We assume that all relative periodic points in $\Omega_0 \cap \Sigma_E$ are *G-non-degenerate*.

This condition assumes assumption (H2′) but not assumption (H1). If however the condition of reduction (H1) is fulfilled the following equivalence holds.

Lemma 5.4. *If the hypothesis of reduction (H1) is fulfilled, then an orbit is G-non-degenerate if and only if this orbit is non-degenerate in the sense of (H3).*

Proof. If the condition of reduction is satisfied for $E \in \mathbb{R}$ we obtain a smooth symplectic manifold $\Omega_{\mathrm{red}} = G\backslash(\Omega_0 \cap U)$ with a reduced Hamiltonian $\tilde{H}([z]) = H(z)$ and the reduced Hamilton flow given by $\tilde{\Phi}_t([z]) := [\Phi_t(z)]$ for $[z] \in \Omega_{\mathrm{red}}$. The condition that $[z]$ is a periodic point under $\tilde{\Phi}_t$ is equivalent to the fact that z is a relative periodic point, i.e. that there is a $g \in G$ and $T > 0$ such that $g\Phi_T(z) = z$.

As all Hamilton flows preserve the energy, the Hamilton vector field $\tilde{H}$ of the reduced Hamiltonian is tangential to $\tilde{\Sigma}_E = \tilde{H}^{-1}(E)$. We therefore have

$$T_{[z]}(\Omega_{\mathrm{red}}) = X_{\tilde{H}}([z]) \oplus \nabla\tilde{H}([z]) \oplus \mathcal{R}', \ [z] \in \tilde{\Sigma}_E. \tag{5.9}$$

As the direction of the flow is always an eigenvector of the linearized flow with eigenvalue 1, we obtain for a relative periodic point $[z]$ the block form

$$(\tilde{\Phi}_T)_{*,[z]} = \begin{pmatrix} 1 & * & * \\ 0 & 1 & 0 \\ 0 & * & \boxed{P} \end{pmatrix} \tag{5.10}$$

with respect to the decomposition (5.9). This block form immediately implies that the characteristic polynomial of the linearized flow is

$$\det\left(\lambda\mathbb{1} - (\tilde{\Phi}_T)_{*,[z]}\right) = (\lambda - 1)^2 \det(\lambda\mathbb{1} - P).$$

The ordinary hypothesis of non-degenerate orbits (H3), demanding that the algebraic multiplicity of 1 is at most 2, is thus equivalent to the fact that P has no eigenvalue equal to 1.

We finally show, that P corresponds to $\mathcal{P}$ in (5.8). In order to see this we first consider the restriction of the reduced flow to the reduced energy shell $\tilde{\Sigma}_E = \tilde{H}^{-1}(0)$. As hypothesis (H2′) implies that $\nabla\tilde{H}([z]) \neq 0$ for all $[z] \in \tilde{\Sigma}_E$ the reduced energy shell is again a smooth manifold. Equation (5.10) then reduces to

$$((\tilde{\Phi}_T)_{|\tilde{\Sigma}_E})_{*,[z]} = \begin{pmatrix} 1 & * \\ 0 & \boxed{P} \end{pmatrix}$$

where the decomposition in block form is with respect to the decomposition

$$T_{[z]}(\tilde{\Sigma}_E) = X_{\tilde{H}}([z]) \oplus \mathcal{R}'. \tag{5.11}$$

As (H3′) implies (H2′) which is under (H1) equivalent to (H2) we conclude from [16, Lemma 4.5] that $\Omega_0 \cap \Sigma_E$ is again a smooth manifold. We can therefor consider a similar restriction of $g\Phi_T$to $\Omega_0 \cap \Sigma_E$. Using the fact that $T_z(\Omega_0 \cap \Sigma_E) = (J\mathfrak{f}z)^\perp$ we obtain from Lemma 5.3 the expression

$$((g\Phi_T)_{|\Omega_0\cap\Sigma_E})_{*,z} = \begin{pmatrix} 1 & 0 & * \\ 0 & \boxed{Ad(g)} & * \\ 0 & 0 & \boxed{P'} \end{pmatrix},$$

where the decomposition in block form is with respect to the decomposition

$$T_z(\Omega_0 \cap \Sigma_E) = (J\nabla H(z) \oplus \mathfrak{g}z) \oplus \mathcal{R}. \tag{5.12}$$

From the compatibility of the reduced flow with the projection

$$Pr : \Omega_0 \cap \Sigma_E \to G\backslash(\Omega_0 \cap \Sigma_E) = \tilde{\Sigma}_E$$

we get

$$Pr \circ ((g\Phi_T)_{|\Omega_0 \cap \Sigma_E}) = ((\tilde{\Phi}_T)_{|\tilde{\Sigma}_E}) \circ Pr$$

and consequently

$$Pr_{*,z} \circ ((g\Phi_T)_{|\Omega_0 \cap \Sigma_E})_{*,z} = ((\tilde{\Phi}_T)_{|\tilde{\Sigma}_E})_{*,[z]} \circ Pr_{*,z}. \tag{5.13}$$

With respect to the decomposition (5.11) and (5.12) the differential of the projection $Pr_{*,z} : T_z(\Omega_0 \cap \Sigma_E) \to T_{[z]}\tilde{\Sigma}_E$ can be written as

$$Pr_{*,z} = \begin{pmatrix} 1 & 0 & 0 \\ 0 & 0 & \mathbb{1} \end{pmatrix}.$$

Inserting this expression in (5.13) and comparing both sides finally yields $P = \mathcal{P}$ and finishes the proof of this Lemma. □

The following simple example shows that in systems with different orbit types it is quite likely that the G-non-degenerate assumption holds, and that there is a large class of systems where (H2′) and (H3′) hold, but not (H1), (H2) and (H3).

Example 5.1. Let us consider the Hamiltonian of a 3-dimensional harmonic oscillator with two different frequencies $\omega_1 = 2\pi$ and $\omega_2 = \frac{2\pi}{\sqrt{2}}$

$$H(x,\xi) = \frac{1}{2}\left((2\pi)^2 \cdot (x_1^2 + x_2^2) + \left(\frac{2\pi}{\sqrt{2}}\right)^2 x_3^2 + |\xi|^2\right), \quad x, \xi \in \mathbb{R}^3.$$

The group $SO(2)$ acts on the phase space $\mathbb{R}^6$ symplectically as a symmetry group by acting canonically on the variables x_1, x_2 and ξ_1, ξ_2, respectively. As this action stabilizes the points $(0, 0, x_3, 0, 0, \xi_3)$ it acts with different orbit types on Σ_E for any $E > 0$. In particular (H1) is not satisfied. The zero level of the momentum map consists of the set of points with zero angular momentum in x_3 direction

$$\Omega_0 = \{(x_1, x_2, x_3, \lambda \cdot x_1, \lambda \cdot x_2, \xi_3) : \ x_i, \xi_3, \lambda \in \mathbb{R}\}.$$

The general solutions $(x(t), \xi(t)) = \Phi_t(x_1, x_2, x_3, \xi_1, \xi_2, \xi_3)$ are explicitly given by

$$\begin{aligned} x(t) &= \left(x_1 \cos(2\pi t) + \frac{\xi_1}{2\pi} \sin(2\pi t),\ x_2 \cos(2\pi t) + \frac{\xi_2}{2\pi} \sin(2\pi t),\ x_3 \cos\left(\frac{2\pi}{\sqrt{2}} t\right) + \right. \\ &\quad \left. \frac{\sqrt{2}\xi_3}{2\pi} \sin\left(\frac{2\pi}{\sqrt{2}} t\right) \right), \\ \xi(t) &= \left(\xi_1 \cos(2\pi t) - 2\pi x_1 \sin(2\pi t),\ \xi_2 \cos(2\pi t) - 2\pi x_2 \sin(2\pi t),\ \xi_3 \cos\left(\frac{2\pi}{\sqrt{2}} t\right) - \right. \\ &\quad \left. \frac{2\pi}{\sqrt{2}} x_3 \sin\left(\frac{2\pi}{\sqrt{2}} t\right) \right). \end{aligned}$$

Thus, all points with $x_3 = \xi_3 = 0$ are periodic with primitive period length 1, whereas all points with $x_1 = x_2 = \xi_1 = \xi_2 = 0$ have primitive period length $\sqrt{2}$. All other points are not relative periodic at all, as the two frequencies have irrational ratio. Comparing

$$J\nabla H(z) = \left(\xi_1, \xi_2, \xi_3, -(2\pi)^2 x_1, -(2\pi)^2 x_2, -\frac{(2\pi)^2}{\sqrt{2}} \right)$$

and

$$\mathfrak{g}z = \mathbb{R}(x_2, -x_1, 0, \xi_2, -\xi_1, 0)$$

we see that all points in $\Sigma_E \cap \Omega_0$ with $E > 0$ are G-non-stationary thus condition (H2′) is fulfilled (note that there are however points $z \in \Sigma_E$ with $J\nabla H(z) \in \mathfrak{g}z$). Looking at the solutions $(x(t), \xi(t))$ one sees that the points $z \in \Omega_0 \cap \Sigma_E \cap \{x_3 = \xi_3 = 0\}$ have a smaller primitive period equal to $\frac{1}{2}$ as relative periodic orbits. Besides there is only one other relative periodic orbit, the periodic orbit with period $\sqrt{2}$ in $\Omega_0 \cap \Sigma_E \cap \{x_1 = x_2 = \xi_1 = \xi_2 = 0\}$.

Both relative periodic orbits are G-non-degenerate, which follows directly from the fact that the Hamilton flow $\Phi_t(x, \xi)$ is linear with respect to (x, ξ) and the ratio of the frequencies ω_1 and ω_2 are irrational. To illustrate this, we take the relative periodic point $z_0 = (1, 0, 0, 0, 0, 0) \in \Omega_0 \cap \Sigma_{2\pi^2}$ of the relative periodic orbit with primitive period $1/2$. It fulfills $g\Phi_{1/2}(z_0) = z_0$ for $g = -1 \in SL(2, \mathbb{R})$. The decomposition (5.6) is given by

$$T_{z_0}\mathbb{R}^3 = \operatorname{span}(e_1, e_5) \oplus \operatorname{span}(e_2, e_4) \oplus \mathcal{R}$$

with $\mathcal{R} = \operatorname{span}(e_3, e_6)$ and e_i being the canonical basis of $\mathbb{R}^6 \cong T_{z_0}\mathbb{R}^6$. Then the restriction of the differential $(g\Phi_{k/2})_{*,z_0}$ to $\mathcal{R} \cong \mathbb{R}^2$ for $k \in \mathbb{N}_{>0}$ is given

by

$$\mathcal{P} = ((g\Phi_{k/2})_{*,z_0})_{|\mathcal{R}} = \begin{pmatrix} \cos\left(\frac{2\pi k}{\sqrt{2}}\right) & \frac{\sqrt{2}}{2\pi}\sin\left(\frac{2\pi k}{\sqrt{2}}\right) \\ -\frac{2\pi}{\sqrt{2}}\sin\left(\frac{2\pi k}{\sqrt{2}}\right) & \cos\left(\frac{2\pi k}{\sqrt{2}}\right) \end{pmatrix}$$

This linear transformation has however no eigenvalue 1 for all $k \in \mathbb{N}_{>0}$. The arguments for the other relative periodic orbit are completely analogous.

Analogous to the case of non-degenerate orbits, the hypothesis of G-non-degenerate orbits implies that the relative periodic orbits are discrete. This will be an important property for the proof of the equivariant Gutzwiller trace formula.

Proposition 5.5. *Let $T > 0$ and denote by $(\Gamma_E^{\mathrm{rel}})_T$ the set of all relative periodic orbits γ in $\Omega_0 \cap \Sigma_E$ with $0 \leq |T_\gamma| \leq T$. If all $\gamma \in (\Gamma_E^{\mathrm{rel}})_T$ are non-degenerate, then they are discrete, i.e. for each $z \in \gamma$ there is $\epsilon > 0$ such that the only relative periodic points in $B_\epsilon(z) \cap \Omega_0 \cap \Sigma_E$ with primitive period length smaller than T are the points on the orbit γ.*

Proof. Suppose that $(\Gamma_E^{\mathrm{rel}})_T$ is not discrete, so that there exists a relative periodic point $z_0 \in \Omega_0 \cap \Sigma_E$ with $g_0\Phi_{T_0}(z_0) = z_0$ and a sequence $z_n \in \Omega_0 \cap \Sigma_E$, $z_n \to z_0$, of relative periodic points belonging to mutually disjoint relative periodic orbits which fulfill $g_n\Phi_{T_n}(z_n) = z_n$ with $|T_n| \leq T$. At the point $z = z_0$ we will now construct an eigenvector of the matrix $\mathcal{P}$ in (5.8) with eigenvalue 1 leading to a contradiction to the G-non-degenerate assumption.

Step 1: As $[-T, T] \times G$ is compact we can assure after going to a subsequence, that $f_n := (T_n, g_n) \in [-T, T] \times G \subset F$ converges to the element $f_\infty = (T_\infty, g_\infty) \in [-T, T] \times G$.

Step 2: From

$$z_0 = \lim_{n\to\infty} z_n = \lim_{n\to\infty} f_n z_n = f_\infty z_0 \tag{5.14}$$

we deduce that z_0 is relative periodic with period length T_∞.

Step 3: By definition of the vector space $\mathfrak{g}z_0$, for each normed vector $e_i \in \mathfrak{g}z_0$ there is $A \in \mathfrak{g}$ such that $\langle Az_0, e_i\rangle \neq 0$. From the continuity of the G-action it follows that there is a neighborhood $U \subset \mathbb{R}^{2n}$ of z_0 such that for all $z \in U$ we still have $\langle Az, e_i\rangle \neq 0$. From the continuity of $J\nabla H$ follows that U can be chosen such that additionally $\langle J\nabla H(z), J\nabla H(z_0)\rangle \neq 0$. We can thus choose a neighborhood of z_0 such that all relative periodic orbits (F-orbits) intersect the affine vector space tangent to $(\mathfrak{f}z_0)^\perp = (\mathbb{R}J\nabla H(z_0) \oplus \mathfrak{g}z_0)^\perp \subset T_{z_0}$ transversally. Thus, for sufficiently large n we can assume that z_n is in such a neighborhood, and consequently we can choose a different point $\tilde{z}_n$ on the same relative periodic orbit with $\tilde{z}_n - z_0 \in (\mathbb{R}J\nabla H(z_0) \oplus \mathfrak{g}z_0)^\perp$. Consequently

we can suppose without loss of generality that our sequence of points z_n fulfills $z_n - z_0 \in (\mathbb{R}J\nabla H(z_0) \oplus \mathfrak{g}z_0)^\perp$.

Step 4: Consider the sequence $\frac{z_n - z_0}{\|z_n - z_0\|} \in \mathcal{S}^{2n-1}$. After restricting once more to a subsequence, we can assume, that $\frac{z_n - z_0}{\|z_n - z_0\|} \to v$ with $\|v\| = 1$. As $z_n \in \Omega_0 \cap \Sigma_E$, we get $v \in (\mathbb{R}\nabla H(z_0) \oplus J\mathfrak{g}z_0)^\perp$. From Step 3 we furthermore obtain

$$v \in \Big((\mathbb{R}\nabla H(z_0) \oplus J\mathfrak{g}z_0) \oplus (\mathbb{R}J\nabla H(z_0) \oplus \mathfrak{g}z_0)\Big)^\perp.$$

So v belongs to the subspace $\mathcal{R}$ of (5.6) and the aim of the remaining steps in this proof is to show that it is an eigenvector of the matrix $\mathcal{P}$.

Step 5: Setting $t_n := \|z_n - z_0\|$ we can choose a smooth curve $\gamma \subset \Sigma_E$ such that $\gamma(0) = z_0$ and $\gamma(t_n) = z_n$. For this curve we calculate $\dot\gamma(0) = \lim\limits_{n\to\infty} \frac{\gamma(t_n)-\gamma(0)}{t_n} = v$.

Step 6: With this smooth path and (5.14) we calculate

$$\begin{aligned}
(f_\infty)_{*,z_0}(v) &= \frac{d}{dt} f_\infty \gamma(t)_{|t=0} \\
&= \lim_{n\to\infty} \frac{f_\infty\gamma(t_n) - f_\infty\gamma(0)}{t_n} \\
&= \lim_{n\to\infty} \frac{f_\infty z_n - f_n z_n + z_n - z_0}{t_n} \\
&= v + \lim_{n\to\infty} \frac{f_\infty z_n - f_n z_n}{t_n}.
\end{aligned}$$

Now, using the fact that the F-action is smooth, Taylor expansion yields for any $f \in F$

$$fz_n = fz_0 + f_{*,z_0}(z_n - z_0) + O(t_n^2).$$

Consequently we obtain

$$\begin{aligned}
(f_\infty)_{*,z_0}(v) &= v + \lim_{n\to\infty} \left[\frac{f_\infty z_0 - f_n z_0}{t_n} + ((f_\infty)_{*,z_0} - (f_n)_{*,z_0}) \left(\frac{z_n - z_0}{t_n} \right) \right] \\
&= v + \lim_{n\to\infty} \left[\frac{f_\infty z_0 - f_n z_0}{t_n} \right].
\end{aligned}$$

Since obviously

$$\lim_{n\to\infty} \left[\frac{f_\infty z_0 - f_n z_0}{t_n} \right] \in \mathfrak{f}z_0,$$

and $\mathcal{P}$ was the restriction of $(f_\infty)_{*,z_0}$ to $(J\mathfrak{f}z_0 \oplus \mathfrak{f}z_0)^\perp$, v is an eigenvector of $\mathcal{P}$ with eigenvalue 1 which finishes the proof. □

5.4 Proof of the equivariant Gutzwiller formula

We are now ready to prove the equivariant Gutzwiller formula under the assumption of G-non-degenerate orbits. According to Section 5.1 the Gutzwiller terms are given by the asymptotic expansion of the spectral distribution $\rho^{\chi}_{E,h}(f)$ for a Schwartz function f with $0 \notin \mathrm{supp}\hat{f}$. In order to apply Proposition 5.5 and to avoid problems concerning the Ehrenfest time, we will additionally need to assume that $\hat{f}$ is compactly supported.

As a first step we show that already under the new conditions (H2′) and (H3′) and without any conditions on the group action, the critical set in (5.3) is smooth.

Proposition 5.6. *Let f be a Schwartz function with $\mathrm{supp}\hat{f} \subset [-T,T]\setminus\{0\}$. If for $E \in \mathbb{R}$ the Hamilton dynamics is G-non-stationary, the energy shell $\Sigma_E \subset \mathbb{R}^{2n}$ is compact, and all relative periodic orbits in $\Omega_0 \cap \Sigma_E$ having a relative period contained in $\mathrm{supp}\hat{f}$ are G-non-degenerate, then the set $\mathcal{C}_{\phi_E} \cap \left(\mathbb{R}^{2n} \times \mathrm{supp}\hat{f} \times G\right)$ is a disjoint finite union of smooth submanifolds of dimension $\dim F$.*

To prove this proposition, recall from Proposition 5.2 that the critical set is given by

$$\mathcal{C}_{\phi_E} = \{(z,t,g) \in \mathbb{R}^{2n} \times \mathbb{R} \times G, \quad z \in \Omega_0 \cap \Sigma_E,\ g\Phi_t(z) = z\}$$

which can be written in terms of the F-action as

$$\mathcal{C}_{\phi_E} = \{(z,f) \in \mathbb{R}^{2n} \times F, \quad z \in \Omega_0 \cap \Sigma_E,\ f \in F_z\}$$

with F_z being the stabilizer group of z for the F-action. We are especially interested in the set of all t-values in this stabilizer group. In particular, we need the following

Lemma 5.7. $\mathcal{L}^{\mathrm{rel}}_z := \{t \in \mathbb{R},\ \exists g \in G \text{ such that } (t,g) \in F_z\} \subset \mathbb{R}$ *is a closed subgroup.*

Proof. The subgroup property is clear from the definition, so that it remains to prove the closeness. Suppose that there is a sequence $t_n \in \mathcal{L}^{\mathrm{rel}}_z$ such that $t_n \to t_\infty$. For each t_n there is a $g_n \in G$ such that $(t_n, g_n) \in F_z$. After restricting to a subsequence one can assume that g_n also converges since G is compact. Consequently (t_n, g_n) converges in F and from the closeness of F_z one concludes that $t_\infty \in \mathcal{L}^{\mathrm{rel}}_z$. □

Corrolary 5.8. *If z is a G-non-stationary, relative periodic point, then there is a $T_z > 0$ such that $\mathcal{L}^{\mathrm{rel}}_z = T_z \cdot \mathbb{Z}$.*

Proof. All closed subgroups of $\mathbb{R}$ are either empty, $\mathbb{R}$ or of the type $k\mathbb{Z}$ for some $k > 0$. As z is relative periodic, we can exclude the empty set. As z is G-non-stationary, the trajectory of the Hamilton flow cannot be contained in the G-orbit of z, so we can exclude $\mathbb{R}$. □

If z is an arbitrary relative periodic point, the corresponding relative periodic orbit γ_0 is exactly its orbit under the F-action and there is an injective immersion $i : F/F_z \to \gamma_0$. Note that in general an F-orbit does not have to be an embedded submanifold in $\mathbb{R}^{2n}$. However, if z is relative periodic, $\mathcal{L}_z^{\mathrm{rel}} = T_z \cdot \mathbb{Z}$ or $\mathcal{L}_z^{\mathrm{rel}} = \mathbb{R}$, and consequently F/F_z is compact. The immersion i is thus additionally closed, and γ_0 is diffeomorphic to F/F_z as an embedded submanifold.

Next, note that the critical set $\mathcal{C}_{\Phi_E}$ is essentially a union of the isotropy bundles of certain relative periodic orbits γ, which are defined as

$$\mathrm{Iso}(\gamma) := \{(z, f) \in \gamma \times F,\ f \in F_z\} \subset \mathbb{R}^{2n} \times F.$$

For those isotropy bundles we have the following

Proposition 5.9. *Let $z \in \mathbb{R}^{2n}$ be a G-non-stationary, relative periodic point and γ its relative orbit. Then* $\mathrm{Iso}(\gamma)$ *can be written as*

$$\mathrm{Iso}(\gamma) = \bigcup_{k \in \mathbb{Z}} M_{k,\gamma}, \tag{5.15}$$

where

$$M_{k,\gamma} := \{(z, kT_\gamma, g) \in \gamma \times \mathbb{R} \times G :\ g\Phi_{kT_\gamma}(z) = z\} \subset \mathbb{R}^{2n} \times F \tag{5.16}$$

are smooth disjoint submanifolds.

Proof. The disjoint decomposition (5.15) follows directly from Corollary 5.8. It only remains to prove the submanifold property of $M_{k,\gamma}$.

We will again construct a closed injective immersion, and first recall that for general homogeneous spaces, the isotropy bundle can be written as a quotient (see e.g. [29, Section 1.11 and 2.4]). Consider therefore F_z acting from the right on $F \times F_z$ by right multiplication on the first factor F and by conjugation on the second factor F_z. This action is proper and free as the action in the first component is the invertible right multiplication in F. Consequently, the quotient $(F \times F_z)/F_z$ carries the structure of a smooth manifold. Furthermore, there is an injective immersion on $\mathrm{Iso}(\gamma_0)$ which is explicitly given by

$$\mathcal{I} : \begin{cases} (F \times F_z)/F_z & \to & \mathrm{Iso}(\gamma_0) \subset \mathbb{R}^{2n} \times F \\ (f, f_z)F_z & \mapsto & (fz, ff_zf^{-1}). \end{cases}$$

For $k \in \mathbb{Z}$ we define the compact sets $F_z^{(k)} := \{(kT_\gamma, g) \in \mathbb{R} \times G : g\Phi_{kT_\gamma}(z) = z\} \subset F_z$. As $F = \mathbb{R} \times G$ is commutative in its $\mathbb{R}$ component, conjugation with F_z leaves $F_z^{(k)}$ invariant, and $(F \times F_z^{(k)})/F_z$ is a compact smooth manifold. It is now straightforward to check that $\mathcal{I}((F \times F_z^{(k)})/F_z) = M_{k,\gamma}$. So the sets $M_{k,\gamma}$ are images of a compact manifold under an injective immersion and consequently embedded submanifolds. □

We are now able to prove Proposition 5.6.

Proof of Proposition 5.6. Proposition 5.5 implies that the relative periodic orbits are discrete. Together with the assumption that Σ_E is compact, this implies that there are only finitely many relative periodic orbits in $(\Gamma_E^{\mathrm{rel}})_T$, so that

$$\mathcal{C}_{\phi_E} \cap \left(\mathbb{R}^{2n} \times \operatorname{supp}\hat{f} \times G\right) = \bigcup_{\gamma \in (\Gamma_E^{\mathrm{rel}})_T} \left(\bigcup_{k \in \mathbb{Z} : kT_\gamma \in \operatorname{supp}\hat{f}} M_k, \gamma \right).$$

Proposition 5.9 assures that the $M_{k,\gamma}$ are disjoint, smooth, submanifolds of dimension $\dim F$, and as $\operatorname{supp}\hat{f}$ is compact, for each $\gamma \in (\Gamma_E^{\mathrm{rel}})_T$ there are also only finitely many $k \in \mathbb{Z}$ with $kT_\gamma \in \operatorname{supp}\hat{f}$. □

In oder to apply the generalized stationary phase theorem to (5.3) it only remains to show the following proposition.

Proposition 5.10. *Let* $(z,t,g) \in \mathcal{C}_{\phi_E} \cap \left(\mathbb{R}^{2n} \times \operatorname{supp}\hat{f} \times G\right)$*, and assume that the dynamics is* G*-non-stationary and that all relative periodic orbits having relative period contained in* $\operatorname{supp}\hat{f}$ *are* G*-non-degenerate. Then* $(\mathrm{Hess}\ \phi_E)_{|N_{(z,t,g)}\mathcal{C}_E}$ *is a non-degenerate bilinear form.*

Proof. Recall that on a d-dimensional Riemannian manifold (M, g) the Hessian of a complex valued function ϕ on its critical set is a complex valued symmetric 2-form given by

$$\mathrm{Hess}\ \phi := \nabla d\phi.$$

The Hessian is said be non-degenerate on a subspace $V \subset T_xM$ if for $v \in V$ and $\mathrm{Hess}\ \phi(v, w) = 0$ for all $w \in V$ we have $v = 0$. By the metric g we can identify Hess ϕ with a complex valued $d \times d$ matrix $B = \Re(B) + i\Im(B)$. We denote the real kernel of the Hessian by $\ker_{\mathbb{R}} \mathrm{Hess}\ \phi(x) := \ker \Re(B) \cap \ker \Im(B)$, and recall that by [14, Lemma 4.3.5] we have for $(z,t,g) \in \mathcal{C}_{\phi_E}$ the equivalence

$$(\mathrm{Hess}\ \phi_E)_{|N_{(z,t,g)}\mathcal{C}_E} \text{ is non-degenerate } \Leftrightarrow \ker_{\mathbb{R}}(\mathrm{Hess}\ \phi_E(z,t,g)) = T_{(z,t,g)}\mathcal{C}_{\phi_E}.$$

By the definition of the critical set, $d\phi_E$ vanishes on $\mathcal{C}_{\phi_E}$. Consequently for $v \in T_{(z,t,g)}\mathcal{C}_{\phi_E}$ the one form $\nabla_v d\phi_E$ equals zero, which implies that $\ker_{\mathbb{R}}(\text{Hess } \phi_E) \supset T_{(z,t,g)}\mathcal{C}_{\phi_E}$. Thus, it suffices to show that in each point (z,t,g) the dimensions of these two linear subspaces of $T_{(z,t,g)}(\mathbb{R}^{2n} \times F)$ coincide. Furthermore, we can directly use the calculations in [16, Prop 4.3] by which

$$\begin{aligned} \ker_{\mathbb{R}}(\text{Hess } \phi_E) &= \{(\alpha,\tau,A) \in \mathbb{R}^{2n} \times \mathbb{R} \times \mathfrak{g} : \ \alpha \perp \nabla H(z), \alpha \perp J\mathfrak{g}z, \\ &\quad \tau J\nabla H(z) + Az + ((g\Phi_t)_{*,z} - Id))\,\alpha = 0\}. \end{aligned} \tag{5.17}$$

Recall that under the G-non-stationary hypothesis we have from (5.6) the decomposition

$$T_z\mathbb{R}^{2n} = J\mathfrak{f}z \oplus \mathfrak{f}z \oplus \mathcal{R},$$

where $J\mathfrak{f}z$ and $\mathfrak{f}z$ both have dimensions equal to $\dim F - \dim F_z$. According to this decomposition we write $\alpha = (\alpha_1, \alpha_2, \alpha_R)$. The first two conditions $\alpha \perp \nabla H(z), \alpha \perp J\mathfrak{g}z$ in (5.17) immediately imply $\alpha_1 = 0$. As $\tau J\nabla H(z) + Az \in \mathfrak{f}z$, the third condition in (5.17) implies, after using the general form (5.8) of $(g\Phi_t)_{*,z}$, that

$$(\mathcal{P} - \mathbb{1})\alpha_R = 0,$$

and from the G-non-degenerate orbit property we directly conclude that $\alpha_R = 0$. The third condition therefore reduces to

$$\tau J\nabla H(z) + Az + (\mathcal{B} - 1)\alpha_2 = 0.$$

It forms a system of $\dim F - \dim F_z$ linear equations with $2\dim F - \dim F_z$ variables. From the G-non-stationary condition it follows that this system of equations has full rank. Consequently we obtain $\dim \ker_{\mathbb{R}}(\text{Hess } \phi_E) = \dim F = \dim \mathcal{C}_{\phi_E}$ which finishes the proof of Proposition 5.10. □

Taking everything together we finally arrive at

Theorem 5.11. *Let H be a Hamiltonian fulfilling Hypothesis 3.1 and 3.2 which is invariant under the compact symmetry group $G \subset O(n)$. Let furthermore $f \in \mathcal{S}(\mathbb{R})$ be such that* $\text{supp}\hat{f} \subset [-T,T] \setminus \{0\}$ *for some $T > 0$. If the Hamilton dynamics is G-non-stationary (Hypothesis (H2′)) for a given energy $E \in [E_1, E_2]$ and all relative periodic orbits in $\Omega_0 \cap \Sigma_E$ having a relative period contained in* $\text{supp}\hat{f}$ *are G-non-degenerate (Hypothesis (H3′)),*

then $\rho^{\chi}_{E,h}(f)$ has a complete asymptotic expansion in powers of h given by

$$\rho^{\chi}_{E,h}(f) = \frac{d_\chi}{2\pi} \sum_{\gamma \in (\Gamma_E^{\mathrm{rel}})_T} \left[\sum_{k\in\mathbb{Z}} e^{\phi_{k,\gamma}} \hat{f}(kT_\gamma) \left(\int_{M_{k,\gamma}} \overline{\chi(g)} d(z,t,g) d\sigma_{M_{k,\gamma}}(z,t,g) \right) + \sum_j h^j a_{j,\gamma,k} \right].$$

Here $M_{k,\gamma}$ was defined in (5.16), $d\sigma_{M_{k,\gamma}}$ is the induced measure on this smooth submanifold, $\phi_{k,\gamma} = \int_0^{kT_\gamma} p_s \dot{q}_s ds$ is the constant value the phase function takes on $M_{k,\gamma}$, and the density which has to be integrated is given by

$$d(z,t,g) = \det{}_*^{-1/2} \left(\frac{\mathrm{Hess}\ (\phi_E)_{|N\mathcal{C}_{\phi_E}}}{i} \right) \det{}_*^{-1/2} \left(\frac{A + iB - i(C+iD)}{i} \right)$$

where the matrices A, B, C, D are as in Proposition 5.1.

All the lower order coefficients $a_{j,\gamma,k}$ are tempered distributions with support in kT_γ applied to $\hat{f}$, which can in principle be calculated from the stationary phase approximation.

Remark 5.2. Again, the case of a compact symmetry group $G \subset GL(n,\mathbb{R})$ can be treated by conjugating to an orthogonal subgroup (see the discussion in Section 3.2).

Proof. Proposition 5.1 allows us to write the spectral distribution as an oscillating integral. Proposition 5.6 together with Proposition 5.10 assure that the critical set is smooth and that the transversal Hessian is non-degenerate. We can therefore apply the generalized stationary phase theorem (see e.g. [23, Theorem 3.3]) to (5.3) finishing the proof of Theorem 5.11. □

Part II
Resonance chains and geometric limits on Schottky surfaces

6 Introduction

Let $X = \Gamma\backslash\mathbb{H}$ be a convex co-compact hyperbolic surface, then this surface has infinite volume, finite genus and a finite number of funnels. The resolvent of the positive Laplacian Δ_X is usually defined as

$$R(s) = (\Delta_X - s(s-1))^{-1},$$

and on $L^2(X)$ it is analytic in s for $\mathrm{Re}(s) > 1$. Changing the function spaces this resolvent can be meromorphically extended to $s \in \mathbb{C}$ with poles of finite rank. The poles of this meromorphic continuation are called the resonances of X and the multiplicity of a resonance is defined by the rank of the associated pole. The set of all resonances on X repeated according to multiplicity will be called $\mathrm{Res}(X)$.

The study of the distribution of resonances on infinite volume hyperbolic surfaces is of interest in number theory (see e.g. the recent work of Bourgain-Gamburd-Sarnak [9] on the affine sieve) as well as in the study of quantum chaos, because these surfaces provide an important model of open, classically chaotic systems (see [65] for a recent review).

Since the seminal work of Patterson it is known that there is alway one resonance at $s = \delta$, where δ is the Hausdorff dimension of the limit set $\Lambda(\Gamma)$(see [70] for $\delta > 1/2$ and [71] for $\delta \leq 1/2$). For the hyperbolic cylinder even the complete resonance spectrum can be computed, but apart from this special example there are no other explicit formulas for the location of individual resonances.

However, it has been a very fruitful approach to prove coarser results on the distribution of resonances in the complex plane. For example Guillopé-Lin-Zworski [43] proved a fractal Weyl upper bound on the number of resonances near the critical line

$$\#\{s \in \mathrm{Res}(X),\ r \leq |\mathrm{Im}(s)| \leq r+1 \text{ and } \mathrm{Re}(s) > -C\} = O(r^\delta)$$

and Naud [63] the existence of a spectral gap, i.e. of a constant $\varepsilon > 0$ such that

$$\{s \in \mathrm{Res}(X),\ \mathrm{Re}(s) > \delta - \epsilon\} = \{\delta\}.$$

Such asymptotic results on the resonance distribution have important analogons in theoretical physics [39, 59, 84] and are even observable experimentally [4, 77]. Despite the big progress in recent years there are still many open questions and conjectures. For example it has been conjectured that the fractal Weyl upper bound is sharp and that, in the semiclassical limit, i.e. for $\mathrm{Im}(s) \to \infty$ the spectral gap can be extended to $\delta/2$. For a more thorough discussion on recent progress on the distribution of resonances and open questions we refer to [65] and references therein.

The existence of these open conjectures motivated Borthwick to study the resonance spectrum on infinite volume hyperbolic surfaces numerically [7] and to a great surprise he observed that the resonances on 3-funneled Schottky surfaces are often highly ordered and form resonance chains. It will be shown in Part III that these resonance chains can be understood by a generalized zeta function and are related to a clustering of the length spectrum on X and that the same kind of resonance chains also appear in various other physical systems (for details on the significance of resonance chains in physics we refer to [91] and references therein).

Statement of the results: In this part we will show the existence of resonance chains for 3-funneled surfaces by proving explicit formulas for individual resonances in a certain geometrical limit in the Teichmüller space. A 3-funneled Schottky surface of genus zero is up to isometry uniquely defined by three positive real numbers l_1, l_2, l_3 which correspond to the funnel widths i.e. the lengths of the primitive closed geodesics that turns once around one funnel. The numbers l_1, l_2, l_3 are also called Fenchel-Nielsen coordinates of the Teichmüller space of 3-funneled surfaces (cf. [5, Section 13.3]) and we will denote these surfaces by X_{l_1,l_2,l_3}. Let $n_1, n_2, n_3 \in \mathbb{N}$ be positive integers, then we consider for $\ell > 0$ the family of Schottky surfaces

$$X_{n_1,n_2,n_3}(\ell) := X_{n_1\ell,n_2\ell,n_3\ell}$$

with a fixed rational ratio of the funnel widths. In the limit $\ell \to \infty$ the system becomes more and more open and the dimension of the limit set tends to zero $\delta \to 0$. One observes that in this limit not only the leading resonance at δ tends to zero but all other resonances do as well. In order to study a meaningful, nontrivial limit of the resonance spectrum, the spectrum has to be rescaled with ℓ and we define the set of rescaled resonances as

$$\widetilde{\mathrm{Res}}_{n_1,n_2,n_3}(\ell) := \{s \in \mathbb{C},\ s/\ell \in \mathrm{Res}(X_{n_1,n_2,n_3}(\ell))\}.$$

Then we obtain the following theorem for the rescaled resonances in the limit $\ell \to \infty$.

Theorem 6.1. *Let n_1, n_2, n_3 be positive integers that fulfill a triangle condition i.e. they fulfill the inequality $n_i + n_j > n_k$ for any permutation of $1, 2, 3$. Let furthermore be*

$$\begin{aligned} P_{n_1,n_2,n_3}(x) &:= 1 - 2(x^{n_1} + x^{n_2} + x^{n_3}) + x^{2n_1} + x^{2n_2} + x^{2n_3} \\ &\quad +2(x^{n_1+n_2} + x^{n_2+n_3} + x^{n_1+n_3}) - 4x^{n_1+n_2+n_3} \end{aligned} \tag{6.1}$$

and

$$\mathcal{N}_{n_1,n_2,n_3} := \{s \in \mathbb{C},\ P_{n_1,n_2,n_3}(e^{-s}) = 0\}$$

where the zeros are repeated according to the multiplicities. Then for any bounded domain $U \subset \mathbb{C}$ with $\partial U \cap \mathcal{N}_{n_1,n_2,n_3} = \emptyset$ we have

$$\lim_{\ell\to\infty} \#\Big(U \cap \widetilde{\mathrm{Res}}_{n_1,n_2,n_3}(\ell)\Big) = \#\Big(U \cap \mathcal{N}_{n_1,n_2,n_3}\Big).$$

Note that U can be chosen arbitrarily small, so Theorem 6.1 states that a finite number of resonances is determined by P_{n_1,n_2,n_3} at an arbitrary precision for large enough ℓ. As $\mathcal{N}_{n_1,n_2,n_3}$ is the zero set of a polynomial in e^{-s}, this set naturally forms straight chains in the sense that

$$s_0 \in \mathcal{N}_{n_1,n_2,n_3} \Rightarrow s_k = s_0 + 2\pi i k \in \mathcal{N}_{n_1,n_2,n_3},\quad \forall\ k \in \mathbb{Z}.$$

Theorem 6.1 then says that the rescaled resonance spectrum converges against straight resonance chains which are explicitly described by the polynomial P_{n_1,n_2,n_3}. Note that this convergence however only holds for an arbitrarily large but finite number of resonances and one can not suspect Theorem 6.1 to hold uniformly for all resonances because this would contradict the fractal Weyl conjecture on the number of resonances in the semiclassical limit. The limit $\ell \to \infty$ thus can be understood as a limit complementary to the semiclassical limit which holds in the low frequency regime i.e. for a finite number of resonances. And in fact we will see in Section 11 that P_{n_1,n_2,n_3} describes the first 50-100 resonances already for relatively small values of $\ell \approx 4$.

In the proof of Theorem 6.1 a generalized dynamical zeta function will play an important role and we will show that such generalized zeta functions always have an analytic extension [1]. Therefore we introduce $\mathcal{P}_{X_{l_1,l_2,l_3}}$ as the set of all primitive closed geodesics on X_{l_1,l_2,l_3}, where primitive means that the geodesic is not a repetition of a shorter closed geodesic. If we additionally denote for a closed geodesic γ its length by $l(\gamma)$ then we can state the following result.

[1] More motivation for the study of this generalized zeta function can be fund in Part III

Theorem 6.2. *Let X_{l_1,l_2,l_3} be a Schottky surface with three funnels of widths l_1, l_2, l_3 and let $n_1, n_2, n_3 \in \mathbb{N}$. We define*

$$\mathbf{n} : \begin{cases} \mathcal{P}_{X_{l_1,l_2,l_3}} & \to & \mathbb{N} \\ \gamma & \mapsto & \sum_{i=1}^{3} n_i w_i(\gamma) \end{cases} \tag{6.2}$$

where $w_i(\gamma)$ denotes the winding number around the funnel of width l_i. Then the generalized zeta function

$$d_{\mathbf{n}}(s,z) = \prod_{\gamma \in \mathcal{P}_{X_{l_1,l_2,l_3}}} \prod_{k \geq 0} \left(1 - z^{\mathbf{n}(\gamma)} e^{-(k+s)l(\gamma)}\right). \tag{6.3}$$

extends to an analytic function on $\mathbb{C}^2$.

Similar to an ordinary dynamical zeta function, obtained by a Bowen-Series transfer operator, this generalized zeta function is equal to the Selberg zeta function of X_{l_1,l_2,l_3} for $z = 1$. Beside its appearance in the proof of Theorem 6.1 this result is also of independent interest as in Part III it will be numerically shown that for the understanding of the resonance chains for finite ℓ these generalized zeta functions are the central object. The numerical algorithms used in Part III and the interpretation of the results were also heavily based on the assumption that the generalized zeta function is analytic.

The particularly simple structure of the resonance spectrum in the limit $\ell \to \infty$ as stated in Theorem 6.1 can finally be understood by the following result which states the in the limit $\ell \to \infty$ the generalized zeta function of Theorem 6.2 is given by the polynomial P_{n_1,n_2,n_3}.

Theorem 6.3. *Let n_1, n_2, n_3 be positive integers fulfilling the triangle condition. Consider for $\ell > 0$ the family of Schottky surfaces $X_{n_1,n_2,n_3}(\ell)$ then the generalized zeta function of this family of surfaces, as defined in Theorem 6.2, also depends on the parameter ℓ and we denote it by $d_{\mathbf{n}}(s,z;\ell)$. If P_{n_1,n_2,n_3} is the polynomial defined in (6.1), then on any bounded set $B \subset \mathbb{C}^2$ the rescaled generalized zeta function $d_{\mathbf{n}}(z, s/\ell; \ell)$ converges to the polynomial in the sense that*

$$\lim_{\ell \to \infty} \left\| d_{\mathbf{n}}(z, s/\ell; \ell) - P_{n_1,n_2,n_3}(ze^{-s}) \right\|_{\infty,B}. \tag{6.4}$$

This part is organized as follows: First we will recall some basic facts on the definition of Schottky surfaces, their resonances and Selberg zeta functions in Section 7. Then, in Section 8, we recall the definition of the dynamical zeta function the way they are usually obtained using Bowen-Series

maps and iterated function schemes (IFS). While this traditional approach is very natural from an algebraic point of view, we will see that it is not natural from the geodesic flow point of view. Section 9 will then be dedicated to an iterated function scheme whose dynamical zeta function also contains the Selberg zeta function of the Schottky surface but that is much better adapted to the geodesic flow. These *flow-adapted IFS* are then used to prove Theorem 6.2 on the analyticity of the generalized zeta functions. The flow-adapted IFS in addition turn out to be the central ingredient in treating the limit $\ell \to \infty$ in Section 10. The idea in proving Theorem 6.1 and Theorem 6.3 is to write the generalized zeta function as a Fredholm determinant of a transfer operator defined by the flow-adapted IFS. We will then consider the Taylor expansion of this Fredholm determinant and apply techniques from Jenkinson-Pollicott [56] on these Taylor coefficients. We will however use them in a different way: while they used them for a fixed IFS to bound the high Taylor coefficients in order to obtain rigorous dimension estimates we will use them to show, that in the limit $\ell \to \infty$ only the first view terms survive. Furthermore all remaining terms become particularly simple and cancel each other to a great extend. From a physical point of view the proof strategy is to show that the ideas which Cvitanovic-Eckhardt [25] introduced under the name "cycle expansion" in physics become rigorous in the limit $\ell \to \infty$ on Schottky surfaces. Finally, in Section 11 we will compare the results with numerical calculations and we will observe that the resonances in the low-frequency regime are already surprisingly well described by P_{n_1,n_2,n_3} for relatively small values of ℓ ($\ell \approx 4$) which illustrates the practical value of Theorem 6.1.

7 Resonances and zeta functions for Schottky surfaces

All hyperbolic surfaces can be written as a quotient of the hyperbolic half plane $\mathbb{H}$ by a discrete subgroup of its orientation preserving isometry group $\Gamma \subset \mathrm{Isom}^+(\mathbb{H}) = PSL(2,\mathbb{R})$. We will be particularly interested in Schottky surfaces which are quotients by certain freely generated groups, called Schottky groups. These groups can be defined as follows.

Definition 7.1. Let $D_1, \ldots, D_{2r}$ be disjoint open disks in $\mathbb{C}$ with centers on the real line and mutually disjoint closures. Then there exists for each pair D_i, D_{i+r} a hyperbolic element $S_i \in PSL(2,\mathbb{R})$ that maps ∂D_i to ∂D_{i+r} and that maps the interior of D_i to the exterior of D_{i+r}. A *Schottky group* is then the free group generated by $S_1, \ldots, S_r$.

With this definition Schottky surfaces are always surfaces of infinite volume without cusps and with a finite number of funnels. The simplest nontrivial example of Schottky surfaces are those surfaces with three funnels of genus zero (see upper part or Figure 9.1). Given three positive real numbers l_1, l_2, l_3 a Schottky group of such a surface is freely generated by the two hyperbolic elements

$$S_1 = \begin{pmatrix} \cosh(l_1/2) & \sinh(l_1/2) \\ \sinh(l_1/2) & \cosh(l_1/2) \end{pmatrix}, \quad S_2 = \begin{pmatrix} \cosh(l_2/2) & a\sinh(l_2/2) \\ a^{-1}\sinh(l_2/2) & \cosh(l_2/2) \end{pmatrix}, \tag{7.1}$$

where the parameter a is chosen such that $\mathrm{Tr}(S_1 S_2^{-1}) = -2\cosh(l_3/2)$. We write

$$\Gamma_{l_1,l_2,l_3} := \langle S_1, S_2 \rangle \text{ and } X_{l_1,l_2,l_3} := \Gamma_{l_1,l_2,l_3} \backslash \mathbb{H}.$$

The parameters l_1, l_2, l_3 coincide with the lengths of the three primitive closed geodesics around the three funnels of the surface X_{l_1,l_2,l_3} (see the geodesics γ_1, γ_2 and γ_3 in Figure 9.1) and parametrize uniquely all hyperbolic surfaces of this type. They are also called Fenchel-Nielsen coordinates because they are global coordinates on the Teichmüller space for 3-funneled surfaces of genus zero, i.e. the space of all isometry classes of hyperbolic metrics on this surface (cf. [5, Section 13.3]).

The study of the Laplacian Δ_X allows to study the spectral properties of a Schottky surface X. As the surface has infinite volume it is known that it has at most finitely many L^2-eigenvalues in $(0, 1/4)$ and absolutely continuous spectrum on $[1/4, \infty)$ with no embedded eigenvalues. The L^2-spectrum thus is not a good spectral quantity and it is well known that instead one has to study the resonances of the Laplace operator. These resonances can be defined by the meromorphic continuation of the resolvent which has been shown by Mazzeo-Melrose [60] and Guillope-Zworski [44]

Theorem 7.1. *The resolvent*

$$R_X(s) := (\Delta_X - s(1-s))^{-1} : L^2(X) \to H^2(X)$$

which is defined for $\mathrm{Re}(s) \geq 1/2$ *and* $s(1-s) \notin \mathrm{spec}(\Delta_X)$ *extends to a meromorphic family of operators*

$$R_X(s) : L^2_{\mathrm{comp}}(X) \to H^2_{\mathrm{loc}}(X)$$

with poles of finite rank.

By this meromorphic continuation we can define the set of resonances as

$$\mathrm{Res}(X) := \{s \in \mathbb{C},\ s \text{ is pole of } R_X(s),\ \text{repeated according to multiplicity}\}. \tag{7.2}$$

Surfaces with constant negative curvature have the remarkable property that their resonance spectrum is related to the zeros of their Selberg zeta function which we introduce now. If γ is a closed geodesic on a hyperbolic surface surface X we can create longer closed geodesics by simply repeating it. We call a geodesic *primitive* if it cannot be obtained as a repetition of a shorter geodesic and we denote the *set of primitive closed geodesics* on X by

$$\mathcal{P}_X := \{\gamma, \text{ closed primitive godesic on } X\}.$$

If $l(\gamma)$ denotes the length of a geodesic γ, then the *Selberg zeta* function of X is defined as

$$Z_X(s) := \prod_{\gamma\in\mathcal{P}_X}\prod_{k\geq 0}\left(1-e^{-(s+k)l(\gamma)}\right). \tag{7.3}$$

This product is absolutely convergent for $\mathrm{Re}(s)$ sufficiently large and for Schottky surfaces it extends to an analytic function on $\mathbb{C}$ [42]. The result of Patterson-Perry [72] which was later generalized to surfaces with cusps by Borthwick-Judge-Perry [8] (see also Bunke-Olbrich [13]) relates the resonances to the zeros of the Selberg zeta function.

Theorem 7.2. *For a Schottky surface $X = \Gamma\backslash\mathbb{H}$ the zero set of the zeta function $Z_X(s)$ is the union of the resonances* $\mathrm{Res}(X)$ *and the negative integers $s = -k$, $k \in \mathbb{N}_0$.*

8 Dynamical zeta functions for iterated function schemes

The correspondence between the zeros of the Selberg zeta function and the resonances as stated in Theorem 7.2 is a central ingredient for understanding the resonance chains. However we first have to develop a different point of view on the Selberg zeta function by the so called dynamical zeta function, which we introduce in this section for holomorphic iterated function schemes (see e.g. [56]).

Definition 8.1 (Holomorphic iterated function scheme)**.** For $N \in \mathbb{N}$ let $D_1, \ldots, D_N \subset \mathbb{C}$ be N open disks such that their closures $\overline{D}_i$ are pairwise disjoint. Let $A \in \{0,1\}^{N\times N}$ be the *adjacency matrix* and denote $i \rightsquigarrow j$ if $A_{i,j} = 1$. Furthermore for each pair $(i,j) \in \{1,\ldots,N\}^2$ with $i \rightsquigarrow j$ we have a biholomorphic map $\phi_{i,j} : D_i \mapsto \phi_{i,j}(D_i)$ such that $\phi_{i,j}(D_i) \Subset D_j$ and such that different images are pairwise disjoint, i.e.

$$\phi_{i,j}(D_i) \cap \phi_{k,l}(D_k) \neq \emptyset \Leftrightarrow i = k \text{ and } j = l. \tag{8.1}$$

For convenience we denote the union of all the disjoint disks by

$$D := \bigcup_i D_i$$

and the union of all their images by

$$\phi(D) := \bigcup_{i \rightsquigarrow j} \phi_{i,j}(D_i).$$

From (8.1) it follows directly that for $u \in \phi(D)$ there is exactly one pair $i \rightsquigarrow j$ and $u' \in D_i$ such that $u = \phi_{i,j}(u')$. We have thus a well defined holomorphic inverse function

$$\phi^{-1} : \phi(D) \to D.$$

Example 8.1. The disks D_i and generators S_i in the construction of a Schottky group (see Definition 7.1) give a natural construction of a holomorphic IFS. For convenience we denote for $i = 1, \ldots, r$ $S_{i+r} := S_i^{-1}$ and use a cyclic notation of the indices i.e. $S_{i+2r} = S_i$ and $D_{i+2r} = D_i$. Then for $i = 1, \ldots, r$ all elements S_i map all disks, except D_i, holomorphically into the interior of D_{i+r}. Thus the adjacency matrix of this IFS is given by a $2r \times 2r$ matrix with $A_{i,j} = 0$ if $|i - j| = r$ and $A_{i,j} = 1$ else. For any $i \rightsquigarrow j$ the maps are given by

$$\phi_{i,j}(u) := S_{j+r}u = S_j^{-1}u.$$

They clearly fulfill (8.1) and are also known to be eventually contracting (see e.g. [5, Proposition 15.4]). Note that the inverse map ϕ^{-1} restricted to $D_j \cap \phi(D)$ is exactly given by S_j. The IFS which we defined is consequently the inverse of the usual *Bowen-Series map* for Schottky groups (see e.g. [5, Section 15.2]).

It will turn out to be useful for the notation to introduce the following symbolic coding. The *symbols* are given by the integers $1, \ldots, N$ and the set of words of length n by the tuples of symbols

$$\mathcal{W}_n := \{(w_0, \ldots, w_n), w_i \rightsquigarrow w_{i+1} \text{ for all } i = 0, \ldots, n-1\}.$$

Note that our notation of *word length* does not refer to the number of symbols, but to the number of transitions $w_i \rightsquigarrow w_{i+1}$ which they indicate. For $w \in \mathcal{W}_n$ and $0 < k \leq n$ we define the *truncated word* by

$$w_{0,k} := (w_0, \ldots, w_k) \in \mathcal{W}_k.$$

Finally we define the iteration of the maps $\phi_{i,j}$ along a word $w \in \mathcal{W}_n$ as

$$\phi_w := \phi_{w_{n-1},w_n} \circ \ldots \circ \phi_{w_0,w_1} : D_{w_0} \mapsto D_{w_n}$$

and their images as

$$D_w := \phi_w(D_{w_0}).$$

Note that $D_w \Subset D_{w_n}$ and that from the separation condition (8.1) one obtains inductively for $w, w' \in \mathcal{W}_n$

$$D_w \cap D_{w'} \neq \emptyset \Leftrightarrow w = w'.$$

We call a word $w \in \mathcal{W}_n$ of length n *closed* if $w_0 = w_n$ and we denote the set of all closed words of length n by $\mathcal{W}_n^{cl}$. We call a holomorphic IFS *eventually contracting*, if there is a N_0 and $\theta < 1$ such that for $n \geq N_0$

$$|\phi'_w(u)| \leq \theta \text{ for all } w \in \mathcal{W}_n \text{ and } u \in D_{w_0}.$$

Given a closed word $w \in \mathcal{W}_n^{cl}$, the map

$$\phi_w : D_{w_0} \to D_w \Subset D_{w_0}$$

of an eventually contracting IFS has a unique fixed point (see Lemma 18.1) which we denote by u_w. If a closed word $w \in \mathcal{W}_n^{cl}$ of length n is concatenated k-times with itself, we obtain a closed word of length $k \cdot n$

$$w^k = (w_0, w_1, \ldots, w_{n-1}, w_0, \ldots, \ldots w_{n-1}, w_0, \ldots, w_{n-1}, w_0) \in \mathcal{W}_{nk}^{cl}.$$

In analogy to the primitive closed geodesics, we call a word w *prime* if it can not be obtained by the repetition of a shorter word and we write

$$\mathcal{W}_n^{\text{prime}} := \{w \in \mathcal{W}_n^{cl},\ w \text{ is prime}\}.$$

Note that as well the set of closed words as the set of prime words is invariant under the left-shift

$$\sigma_L : \left\{ \begin{array}{ccc} \mathcal{W}_n^{cl/\text{prime}} & \to & \mathcal{W}_n^{cl/\text{prime}} \\ (w_0, \ldots, w_{n-1}, w_0) & \mapsto & (w_1, \ldots, w_{n-1}, w_0, w_1) \end{array} \right. .$$

and the right-shift

$$\sigma_R : \left\{ \begin{array}{ccc} \mathcal{W}_n^{cl/\text{prime}} & \to & \mathcal{W}_n^{cl/\text{prime}} \\ (w_0, \ldots, w_{n-1}, w_0) & \mapsto & (w_{n-1}, w_0 \ldots, w_{n-1}, w_{n-1}) \end{array} \right. .$$

obviously $\sigma_L^{-1} = \sigma_R$ and iterative application of these operators induce a $\mathbb{Z}$-action on the set of words. The importance of this shift action arises from the fact that on the periodic orbits, the dynamics of the IFS is conjugated to the dynamics of the shift operator on the closed words in the following sense

$$\forall w \in \mathcal{W}_n^{cl}, 0 < k < n : \quad \phi_{w_0,k}(u_w) = u_{\sigma_L^k w}. \tag{8.2}$$

We will denote by $[w]$ the orbit of a word w by this $\mathbb{Z}$-action on $\mathcal{W}_n^{cl/\text{prime}}$ and write the space of these orbits, i.e. the quotient by the group action as

$$\left[\mathcal{W}_n^{cl/\text{prime}}\right] := \mathbb{Z}\backslash\mathcal{W}_n^{cl/\text{prime}}.$$

Next we define the transfer operators associated to the iterated function schemes (c.f.[56]).

Definition 8.2. Let $\mathcal{A}_\infty(D)$ be the Banach space of holomorphic functions on D that are bounded on $\overline{D}$ with the supremum norm. If we have a function $V \in A_\infty(\phi(D))$ then we define the *transfer operator* $\mathcal{L}_V : \mathcal{A}_\infty(D) \to \mathcal{A}_\infty(D)$ associated to the IFS by

$$(\mathcal{L}_V h)(u) := \sum_{i=1}^{N} (\mathcal{L}_V^{(i)} h)(u) \tag{8.3}$$

where

$$\mathcal{L}_V^{(i)} : \left\{ \begin{array}{ccc} \mathcal{A}_\infty(D) & \to & \mathcal{A}_\infty(D_i) \\ h(u) & \mapsto & (\mathcal{L}_V^{(i)} h)(u) := \sum\limits_{j \text{s.t.} i \rightsquigarrow j} V(\phi_{i,j}(u)) h(\phi_{i,j}(u)) \end{array} \right. . \tag{8.4}$$

The sum in (8.3) is then understood in the sense that $\mathcal{A}_\infty(D) = \bigoplus_{i=1}^N \mathcal{A}_\infty(D_i)$.

Given such a potential V, a word $w \in \mathcal{W}_n$ and a point $u \in D_{w_0}$, we can define the iterated product

$$V_w(u) := \prod_{k=1}^{n} V(\phi_{w_{0,k}}(u)). \tag{8.5}$$

A straight forward calculation of powers of the transfer operator $\mathcal{L}_V$ leads to

$$\left(\mathcal{L}_V^n h\right)(u) = \sum_{w \in \mathcal{W}_n, \text{s.t.} u \in D_{w_0}} V_w(u) h(\phi_w(u)),$$

thus these iterated products naturally occur in powers of $\mathcal{L}_V$.

Definition 8.3. An operator $\mathcal{L} : \mathcal{B} \to \mathcal{B}$ on a Banach space $\mathcal{B}$ is called *nuclear*, if there exist $v_n \in \mathcal{B}$, $\alpha_n \in \mathcal{B}^*$ with $\|v_n\| = \|\alpha_n\| = 1$ and $\lambda_n \in \mathbb{C}$ with $\sum\limits_{n=0}^{\infty} |\lambda_n| < \infty$ such that

$$\mathcal{L}h = \sum_{n=0}^{\infty} \lambda_n \alpha_n(h) v_n \tag{8.6}$$

for any $h \in \mathcal{B}$. The representation (8.6) is then called *nuclear representation* of $\mathcal{L}$.

It is a well known fact that these transfer operators of holomorphic IFS are nuclear operators (see [80] or [56, Proposition 2], respectively) and that for eventually contracting IFS the trace can be expressed in terms of the points u_w. Accordingly one can define the *dynamical zeta function* by the Fredholm determinant

$$d_V(z) := \det(1 - z\mathcal{L}_V) = \exp\left(\sum_{n>0} \frac{z^n}{n} \mathrm{Tr}(\mathcal{L}_V^n)\right) \tag{8.7}$$

which is an entire function on $\mathbb{C}$ and which can be written for $|z|$ sufficiently small as (see e.g. [56, (3.26)])

$$d_V(z) = \exp\left(-\sum_{n>0} \frac{z^n}{n} \sum_{w \in \mathcal{W}_n^{cl}} V_w(u_w) \frac{1}{1 - \phi'_w(u_w)}\right). \tag{8.8}$$

One has the following important connection between the dynamical and Selberg zeta function:

Theorem 8.1. *Let $X = \Gamma\backslash\mathbb{H}$ be a Schottky surface and take the iterated function scheme associated to the Bowen-Series maps as defined in Example 8.1. For $s \in \mathbb{C}$ define the potential $V_s(z) = [(\phi^{-1})'(z)]^{-s}$ which depends holomorphically on s as $(\phi^{-1})'(z) \neq 0$ and consider the holomorphic family of nuclear operators $\mathcal{L}_{V_s}$. Then the dynamical zeta function*

$$d(s, z) := \det(1 - z\mathcal{L}_{V_s})$$

is holomorphic in both variables and

$$Z_X(s) = d(s, 1).$$

Proof. We will only give a sketch of the proof here, considering those steps which will be of further importance in this part of the thesis. For a detailed proof see e.g. [5, Theorem 15.8].

The proof heavily relies on a product form of the general dynamical zeta function which we will derive now. Expanding the last quotient in (8.8) as a geometric series one obtains

$$d_V(z) = \exp\left(-\sum_{k\geq 0}\sum_{n>0}\sum_{w \in \mathcal{W}_n^{cl}} \frac{z^n}{n} V_w(u_w) \left(\phi'_w(u_w)\right)^k\right).$$

Next one checks that for a given class of words $[w] \in \left[\mathcal{W}_n^{cl}\right]$ neither $V_w(u_w)$ nor $\phi'_w(u_w)$ depend on the choice of the representative w. Furthermore one easily calculates that

$$V_{w^k}(u_{w^k}) = (V_w(u_w))^k \text{ and } \phi'_{w^k}(u_{w^k}) = (\phi'_w(u_w))^k.$$

Consequently the sum over all closed words represented by the double sum $\sum_{n>0}\sum_{w\in\mathcal{W}_n^{cl}}$ can be transformed into a sum over all classes of prime words and their repetitions and one obtains

$$d_V(z) = \exp\left(-\sum_{k\geq 0}\sum_{r>0}\sum_{[w]\in[\mathcal{W}^{\text{prime}}]}\frac{\left(z^{n_w}V_w(u_w)\left(\phi_w'(u_w)\right)^k\right)^r}{r}\right).$$

where $\left[\mathcal{W}^{\text{prime}}\right] = \bigcup_n \left[\mathcal{W}_n^{\text{prime}}\right]$ is the set of the prime word-classes of arbitrary length and n_w denotes the length of the word w. Finally using the Taylor expansion $\log(1-x) = -\sum_{r>0} x^r/r$ one obtains

$$d_V(z) = \prod_{[w]\in[\mathcal{W}^{\text{prime}}]}\prod_{k\geq 0}\left(1 - z^{n_w}V_w(u_w)\left(\phi_w'(u_w)\right)^k\right). \tag{8.9}$$

With the special choice of the potential $V_s(u) = ((\phi^{-1})'(u))^{-s}$ one then obtains

$$d(s,z) = \prod_{[w]\in[\mathcal{W}^{\text{prime}}]}\prod_{k\geq 0}\left(1 - z^{n_w}\left(\phi_w'(u_w)\right)^{s+k}\right).$$

The equivalence to the Selberg zeta function then follows from a one-to-one correspondence between the classes of prime words of the Bowen-Series IFS and the primitive geodesics on the Schottky surfaces (see e.g. [5, Proposition 15.5]) and from the fact that the stabilities of the fixed points $\phi_w'(u_w)$ are related to the lengths of these geodesics. □

As explained in Section 7 we are especially interested in zeros of the zeta function. The fixed point formula (8.8) for the dynamical zeta function can however not vanish if the series are absolutely convergent. But the fixed point formula (8.8) is only valid in the region of absolute convergence, in the rest of the complex plane the zeta function is only defined by analytic continuation. Equation (8.8) is thus only valid in a region where the zeta function has no zeros. The same is true for the product formula (7.3) of the Selberg zeta functions. Both formulas are thus not at all useful for determining the zeros numerically. One can however use the following clever trick which has been introduced in physics by Cvitanovic-Eckhardt [25] under the name *cycle expansion* and that has been rigorously applied to Schottky surfaces by Jenkinson-Pollicott [56] in mathematics: As for any bounded potential V the series in (8.8) converges in a neighborhood of zero, one can derive a general formula for the Taylor coefficients of the Taylor expansion of $d_V(z)$ in z around zero. This expansion is given by [56, Proposition 8]:

$$d_V(z) = 1 + \sum_{N=1}^{\infty} z^N d_V^{(N)} \tag{8.10}$$

with

$$d_V^{(N)} = \sum_{m=1}^{N} \left(\sum_{(n_1,\ldots,n_m)\in P(N,m)} \frac{(-1)^m}{m!} \prod_{l=1}^{m} \frac{1}{n_l} \sum_{w\in\mathcal{W}_{n_l}^{cl}} \frac{V_w(u_w)}{1-\phi_w'(u_w)} \right) \tag{8.11}$$

where $P(N,m)$ is the set of all m-partitions of N, i.e. the set of all integer m-tuples that sum up to N. As $d_V(z)$ is known to be analytic on all $\mathbb{C}$ its Taylor expansion (8.10) converges absolutely on $\mathbb{C}$ and is well suited for numerical calculations of its zeros (c.f. [7]).

9 Flow-adapted iterated function schemes and generalized zeta functions

As mentioned in the proof of Theorem 8.1 the key ingredient for the equivalence between the dynamical zeta function of the standard Bowen-Series IFS and the Selberg zeta function is an equivalence between periodic geodesics on the surface and periodic orbits of the IFS. This equivalence is usually proven in a purely algebraic way by arguing with conjugacy classes in the Schottky group Γ. This equivalence can however also be understood from a geometric or dynamical point of view by interpreting the Bowen-Series maps as some kind of Poincaré section of the geodesic flow. The 3-funneled Schottky surface can be obtained from its fundamental domain by gluing together the circles of the same color (see Figure 9.1). Each closed geodesic on the surface crosses the blue and red cut lines a finite number of times and can be represented by one or several arcs in the fundamental domain. The fixed points of the Bowen-Series map are then exactly the end-points of these arcs. We do not want to go any further into details, as we will need no rigorous statement of this correspondence in the sequel (in all proofs it is more convenient to do the calculations from the algebraic point of view). It is however important to realize that the standard Bowen-Series IFS seems to be very natural from the algebraic point of view (it is directly constructed from the two generators S_1, S_2 of the freely generated Schottky group) but not from the point of view of the geodesic flow: Geodesics that turn one time around one of the funnels and which are topologically similar are treated differently depending on the choice of the funnel. For example the geodesics γ_1 and γ_2 in Figure 9.1 only cross one cut line, while the geodesic γ_3 crosses two of them. This implies that γ_3 corresponds to a periodic orbit of word length two while γ_1 and γ_2 only correspond to a word length one. From a purely dynamical point of view it would thus be more natural to take a Poincaré

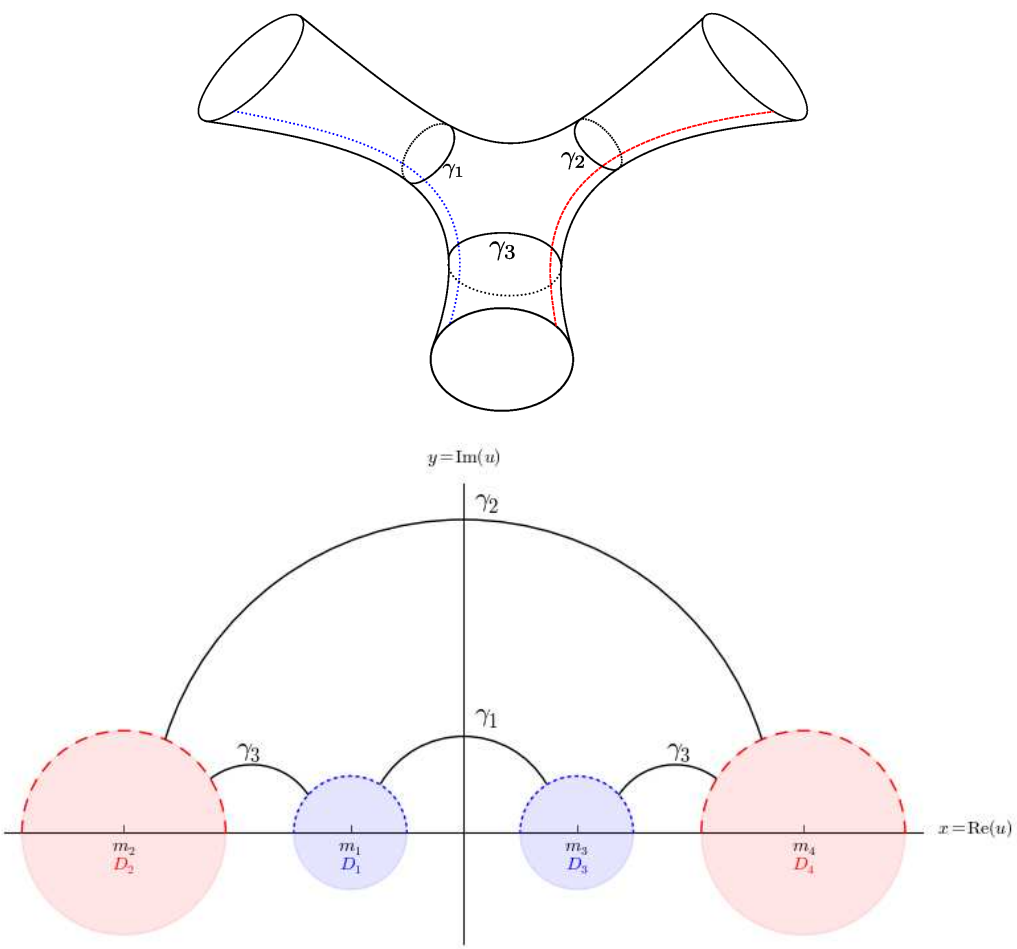

Figure 9.1: Upper part: Schematic sketch of a 3-funneled Schottky surface. The dashed red and dotted blue line indicate the cut lines which would correspond to the Poincaré section of the standard Bowen-Series IFS. The black lines represent the three fundamental geodesics that wind one time around one of the funnels. Lower part: Configuration of 4 disks that give rise to the construction of a 3-funneled Schottky surface. The upper half plane without the disks represents a fundamental domain and the surface can be obtained by gluing together the two red dashed lines and the two blue dotted lines. In black the three fundamental closed geodesics $\gamma_1, \gamma_2, \gamma_3$ from the upper part of the figure are shown. While γ_1 and γ_2 are only represented by one arc each, the geodesic γ_3 appears as two arcs in the fundamental domain.

section with three cut lines as presented on the lower part of Figure 9.2. The Schottky surface can then be thought of being obtained by gluing together two identical domains (see Figure 9.2). We will see below that these domains correspond to fundamental domains of a McMullen reflection group .

The aim of this section is thus to construct a holomorphic IFS leading to a dynamical zeta function that also equals the Selberg zeta function but which is constructed in the spirit of Figure 9.2. This *flow-adapted* IFS will turn out to be the natural choice for proving the analyticity of the generalized zeta function (Theorem 6.2) and a crucial ingredient for proving the geometric limits (Theorem 6.3). [2]

The flow-adapted IFS will be obtained by doubling a McMullen reflection IFS [61] (see also [56, Section 6]) and we will first recall the definition of a McMullen reflection group. Those groups are best visualized in the Poincaré disk model. Let c_1, c_2, c_3 denote three geodesics that do not intersect. Geometrically these geodesics are circles that are perpendicular to the disk boundary $\partial\mathbb{D}$ (see upper part of Figure 9.2). The reflection at the geodesic c_i is then an antiholomorphic isometry

$$\rho_{c_i}(u) : \mathbb{D} \to \mathbb{D}$$

and the Kleinian group Γ generated by the reflections ρ_{c_i} is called a McMullen reflection group. Note that it contains as well orientation preserving (i.e. holomorphic) as orientation inverting (i.e. antiholomorphic) isometries. The subgroup Γ^+ of orientation preserving isometries is then a Schottky group of a 3-funneled surface containing only hyperbolic transformations. If we introduce the displacement length of an hyperbolic positive isometry T as

$$l(T) := \min_{u\in\mathbb{D}} \mathrm{dist}_{\mathbb{D}}(u, Tu),$$

then we can always construct a McMullen reflection group with the following properties.

Lemma 9.1. *Let $l_1, l_2, l_3 > 0$ be real positive numbers, then there exist non-intersecting geodesics c_A, c_B, c_C such that $\rho_{c_A}, \rho_{c_B}, \rho_{c_C}$ generate a McMullen reflection group and the displacement length of the composition of two different generators is given by*

$$l(\rho_{c_B}\rho_{c_C}) = l_1,\ l(\rho_{c_A}\rho_{c_C}) = l_2,\ l(\rho_{c_A}\rho_{c_B}) = l_3. \tag{9.1}$$

[2] The flow adapted IFS weil also play an important role in Part IV. Therre we use a slightly different version for symmetric n-funneled surface to obtain a symmetry factorization of the Selberg zeta functions.

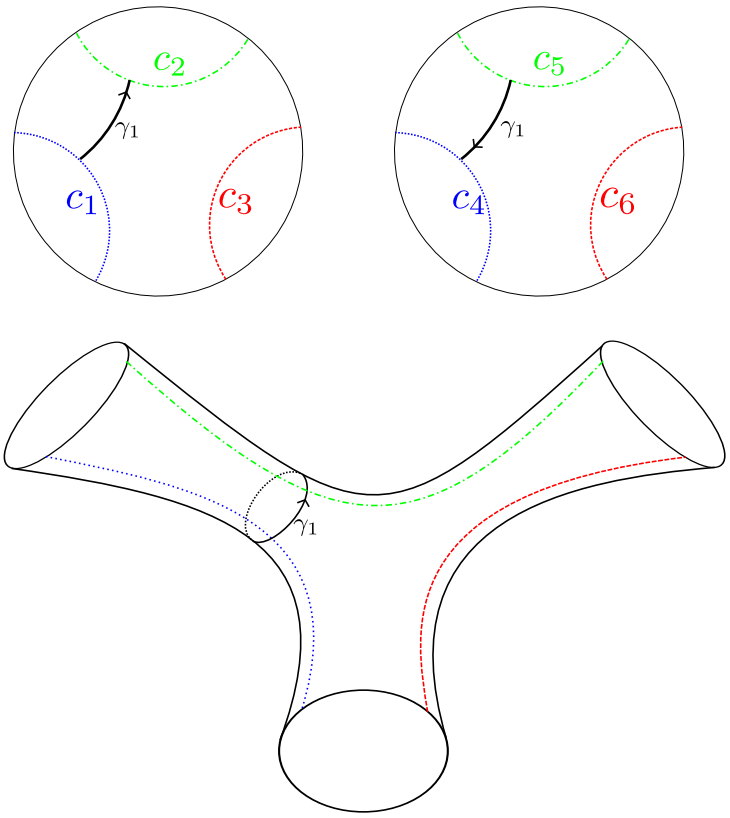

Figure 9.2: Lower part: Schematic sketch of a 3-funneled Schottky surface. The red, green and blue lines indicate the cut lines which would correspond to the Poincaré section of the flow-adapted IFS. The black line γ_1 represents a geodesic which winds once around one of the funnels. Upper part: Fundamental domain of two McMullen IFS represented in the Poincaré disk $\mathbb{D}$. The Schottky surface below can be obtained by gluing those two fundamental domains together along the cycles such that the colors match each other. In black the two arcs of the geodesic γ_1 are sketched.

Proof. First we use the fact from hyperbolic trigonometry (see e.g. [5, Lemma 13.2]) that given three positive numbers α, β, γ there exist positive numbers A, B, C and a right-angled hexagon with side lengths $\alpha, C, \beta, A, \gamma, B$ (see Figure 9.3). Note that the geodesic lines c_A, c_B, c_C obtained as the prolongation of A, B, C do not intersect as they are perpendicular to a common geodesic. Thus the reflections along these three geodesics generate a McMullen reflection group. If we choose $\alpha = l_1/2, \beta = l_2/2, \gamma = l_3/2$ we also have (9.1) which can be seen as follows. Let c_α be the geodesic prolongation of the side of length α. As it is perpendicular to c_B and c_C it is preserved under the reflection along both circles and is thus also preserved under the hyperbolic element $\rho_{c_B}\rho_{c_A}$. Such an invariant geodesic of an hyperbolic element is also called *axis* and it is known that the displacement length is given for any $u \in c_\alpha$ by (see e.g. [5, Section 2.1])

$$l(\rho_{c_B}\rho_{c_C}) = d_{\mathbb{D}}(u, \rho_{c_B}\rho_{c_C}u).$$

Choosing u to be the intersection point of c_C and c_α one immediately sees that

$$d_{\mathbb{D}}(u, \rho_{c_B}\rho_{c_C}u) = d_{\mathbb{D}}(u, \rho_{c_B}u) = 2\alpha = l_1.$$

□

The flow-adapted IFS of a Schottky surface X_{l_1,l_2,l_3} will be constructed from the generators $\rho_{c_A}, \rho_{c_B}, \rho_{c_C}$. It is however convenient to transform them by the isometry

$$C : \begin{cases} \mathbb{D} & \to & \mathbb{H} \\ u & \mapsto & -i\frac{u-1}{u+1} \end{cases} \tag{9.2}$$

to the upper half plane. Without loss of generality we can assume that the boundary point $-1 \in \partial\mathbb{D}$ is not contained in any of the disks bounded by c_A, c_B, c_C. The transformation thus gives us 6 points $a_1 < b_1 < a_2 < b_2 < a_3 < b_3 \in \mathbb{R} = \partial\mathbb{H}$ and three geodesic circles c_i with start- and end-points a_i and b_i (see Figure 9.4 for an illustration) . If we denote by m_i the center and by r_i the radius of the circle c_i then the reflection at this geodesic is given by

$$\rho_{c_i}(u) = \frac{r}{\overline{u} - m_i} + m_i$$

which is an antiholomorphic map on $\mathbb{H}$. For holomorphic IFS we however need holomorphic maps on $\mathbb{C}$, so we extend the map antiholomorphically to $\mathbb{C}$ and compose it with a complex conjugation which gives a holomorphic transformation on $\mathbb{C}$ given by

$$R_i(u) = \frac{r_i}{u - m_i} + m_i. \tag{9.3}$$

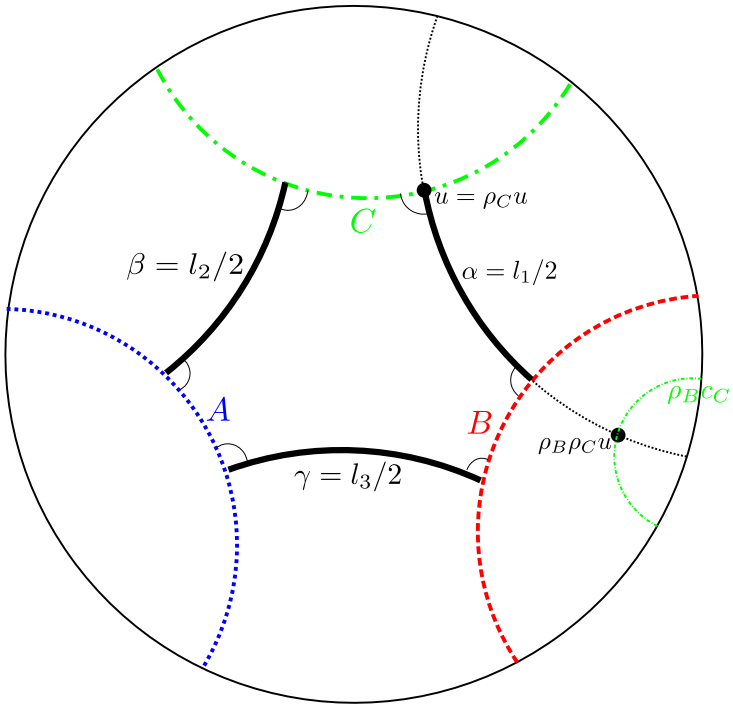

Figure 9.3: Sketch of the orthogonal hexagon in the Poincaré disk $\mathbb{D}$ together with the notations from the proof of Lemma 9.1.

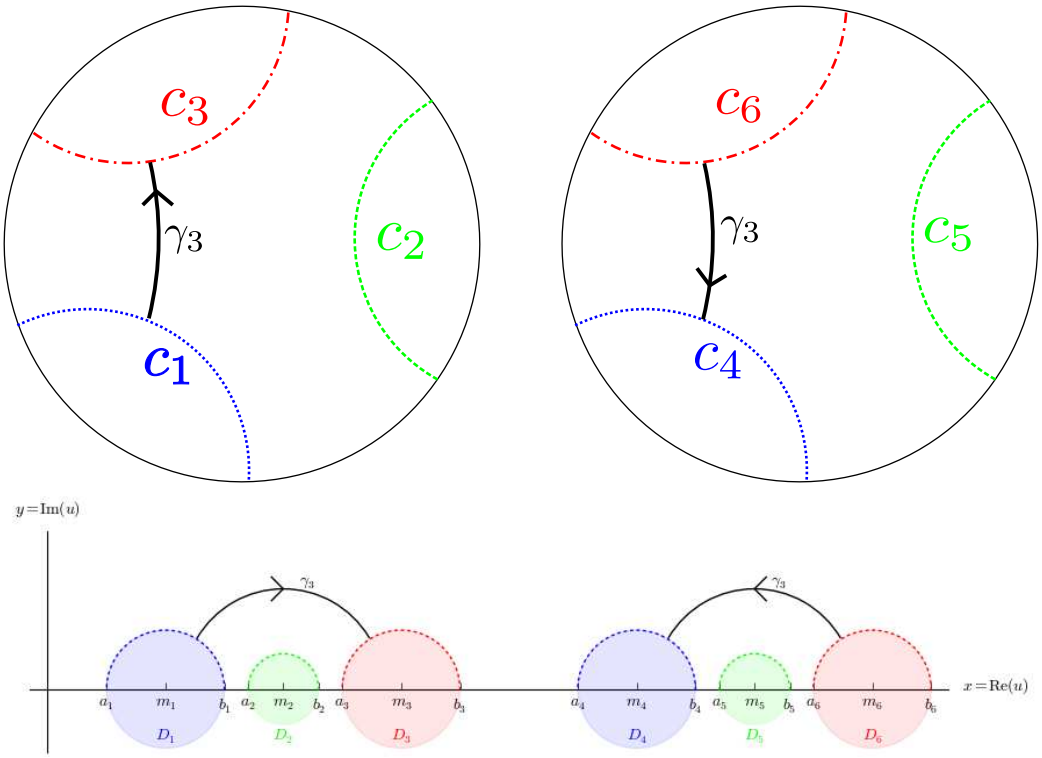

Figure 9.4: Upper part: The two copies of the fundamental domain of the McMullen reflection group from Figure 9.2. Lower part: Disk of the associated flow-adapted IFS with the notations as in Definition 9.1.

which can also by expressed as a Moebius transformation with the matrix

$$R_i = \frac{1}{\sqrt{r_i}} \begin{pmatrix} m_i & r_i - m_i^2 \\ 1 & m_i \end{pmatrix}, \tag{9.4}$$

Note that $\det R_i = -1$ thus the matrices R_i are not in $SL(2,\mathbb{R})$ but any product of an even number of R_i is. Finally, by choosing the indices appropriately, equation (9.1) transforms to

$$l(R_1R_2) = l_1,\ l(R_2R_3) = l_2,\ l(R_1R_3) = l_3. \tag{9.5}$$

We can now define the flow-adapted IFS.

Definition 9.1 (Flow-adapted IFS)**.** Let l_1, l_2, l_3 be real positive numbers and let c_i, a_i, b_i, m_i, r_i and R_i be constructed as above from Lemma 9.1. We define the offset variable

$$\delta_{\text{offset}} := b_3 - a_1 + 1.$$

The *flow-adapted IFS* then is a holomorphic IFS with $N = 6$ where the disks D_i are the Euclidean disks in $\mathbb{C}$ with centers m_i and radii r_i for $1 \leq i \leq 3$ and with centers $m_{i-3} + \delta_{\text{offset}}$ and radii r_{i-3} for $4 \leq i \leq 6$. The adjacency matrix A is given by $A_{i,j+3} = A_{j+3,i} = 1$ for all $1 \leq i, j \leq 3$ with $i \neq j$ and $A_{i,j} = 0$ else. Finally for $i \rightsquigarrow j$ the maps $\phi_{i,j}$ are given by

$$\phi_{i,j}(u) := \begin{cases} R_{j-3}(u) + \delta_{\text{offset}} & \text{for } i \leq 3 \\ R_j(u - \delta_{\text{offset}}) & \text{for } i > 3. \end{cases}$$

Remark 9.1. Note that the concrete form of the flow-adapted IFS is far from being uniquely defined by the lengths l_i. The three lengths only determine uniquely the side lengths of the orthogonal hexagon in the proof of Lemma 9.1 but not its orientation and position inside $\mathbb{D}$. So every other realization of this pentagon where the point -1 is not contained in any of the disks leads to an equivalent IFS. Additionally the offset variable is completely arbitrary, provided it assures that the disks D_i are mutually disjoint.

As indicated in the discussion above, we want to show that the dynamical zeta function of the flow-adapted IFS with a suitable potential also equals the Selberg zeta function. The key ingredient for this equality is, as in the case of the ordinary Bowen-Series map, a one-to-one correspondence between the classes of prime closed words of the IFS and the primitive closed geodesics which we want to state and prove next.

Proposition 9.2. *Let l_1, l_2, l_3 be positive, real numbers and consider the corresponding flow-adapted IFS from Definition 9.1. Then there exists a bijection between the classes of prime words in $\left[\mathcal{W}^{\text{prime}}\right]$ and the primitive closed geodesics on X_{l_1,l_2,l_3}. Additionally the length of the geodesic associated to $[w]$ is given by*

$$-\log(\phi_w'(u_w)). \tag{9.6}$$

Proof. Let R_1, R_2, R_3 be as in Definition 9.1 and $\Gamma = \langle R_1, R_2, R_3 \rangle^+$ the subgroup of orientation preserving isometries of the McMullen reflection group. Then Γ is generated by the two hyperbolic isometries $S_1 = R_1 R_2$ and $S_2 = R_2 R_3$ and it is straightforward to check that S_1, S_2 generate the Schottky group Γ_{l_1,l_2,l_3}. Thus it is known (see e.g. [5, Proposition 2.16]) that the set of primitive closed geodesics on X_{l_1,l_2,l_3} is in bijection to the set of primitive conjugacy classes $[T] \in \Gamma$ where primitive means that there is no $S \in [T]$ such that $S = R^k$ for some $R \in \Gamma$ and $k > 1$. Consequently our aim is to construct a bijection

$$T : \left[\mathcal{W}^{\text{prime}}\right] \to \{\text{primitive conjugacy classes of } \Gamma\}.$$

In order to do so, we note that for $w \in \mathcal{W}_k$ from the form of the adjacency matrix in Definition 9.1 we have $w_i \leq 3 \Rightarrow w_{i+1} > 3$. Thus, if w is a closed word, k has to be even. We first define the map

$$T : \left[\mathcal{W}^{\mathrm{cl}}\right] \to \{\text{conjugacy classes of } \Gamma\}\,.$$

on the closed words and will later show that we can easily restrict it to the prime words. For a closed word $w = (w_0, \ldots, w_{2r})$ we define the map T by

$$T(w) := \begin{cases} R_{w_{2r}} R_{w_{2r-1}-3} \ldots R_{w_2} R_{w_1-3} & \text{if } w_0 \leq 3 \\ R_{w_{2r-1}} R_{w_{2r-2}-3} \ldots R_{w_1} R_{w_0-3} & \text{if } w_0 > 3 \end{cases}.$$

As closed words have to be of even length, $T(w)$ consists of an even number of reflections and is thus a positive isometry. We first show that T is well defined on $\left[\mathcal{W}^{\mathrm{prime}}\right]$, i.e. that it doesn't depend on the choice of the representative of $[w]$. So let $v \in [w]$. Without loss of generality we can assume that $w_0 \leq 3$ and $v_0 \leq 3$ because otherwise we could simply apply the right-shift σ_R to obtain such an element in the same equivalence class that fulfills this condition and that is mapped to the identical element in Γ. Consequently there exists an integer $0 \leq t \leq r$ such that $v = (w_{2t}, \ldots, w_{2r}, w_1 \ldots, w_{2t})$ and we obtain

$$T(v) = R_{w_{2t}} \ldots R_{w_1-3} R_{w_{2r}} \ldots R_{w_{2t+2}} R_{w_{2t+1}-3} = S^{-1} T(w) S$$

for $S = R_{w_{2r}} \ldots R_{w_{2t+1}-3}$. Thus $T(v)$ is in the same conjugacy class as $T(w)$.

In order to see the injectivity we take two words v and w that are mapped to the same conjugacy class. We assume first that

$$T(v) = R_a R_b T(w) R_b R_a.$$

However from the form of the adjacency matrix, it is not possible that an element in the image of T starts and ends with the same generator. Thus we have either

$$R_b R_a = R_{w_1-3} R_{w_2}$$

or

$$R_a R_b = R_{w_{2r-1}-3} R_{w_{2r}}.$$

In the first case we have $v = \sigma_L^2 w$ in the latter case $v = \sigma_R^2 w$. By iterating this argument for arbitrary conjugations of $T(w)$ and $T(v)$ we have shown the injectivity of the map T.

In order to see the surjectivity, let $S \in \Gamma$ be an arbitrary element. By definition of Γ we can write $S = R_{s_{2r}} \ldots R_{s_1}$ with $1 \leq s_i \leq 3$. As two consecutive identical reflections cancel each other we can assume that $s_i \neq s_{i+1}$. Finally while $s_1 = s_{2r}$ we can conjugate S by $R_{s_2} R_{s_1}$ which leads to an

element composed from $2r-2$ reflections. By iterative conjugation we can thus reduce the element to $\tilde{S} = R_{\tilde{s}_{2\tilde{r}}} \dots R_{\tilde{s}_1}$ with $\tilde{s}_1 \neq \tilde{s}_{2\tilde{r}}$ and we obtain

$$\tilde{S} = T((s_{2\tilde{r}}, s_1 + 3, s_2, \dots, s_{2\tilde{r}-1} + 3, s_{2\tilde{r}})).$$

We have thus constructed a bijective map between the classes of closed words and the conjugacy classes in Γ. We will now prove that this map can be restricted to a bijection between the classes of prime words and the primitive conjugacy classes. As T is a bijectiona and on both sides an element can either be primitive or composite it suffices to show that T maps composite closed words to composite conjugacy classes. This is, however, straight forward from the definition of T as obviously $T([w^k]) = T([w])^k$.

With this restriction we have constructed a bijection between the classes of closed, prime words and primitive conjugacy classes. Using the above mentioned result on the one-to-one correspondence between oriented primitive geodesics and primitive conjugacy classes, this is equivalently a bijection to the set of primitive, oriented, closed geodesics and it only remains to prove (9.6).

In order to achieve this, we first recall that the length of the primitive geodesic associated to a conjugacy class of an hyperbolic element $T \in \Gamma$ is equal to the displacement length of T (see e.g. [5, Proposition 2.16]) and it is also a well known fact that if $u_T \in \partial\mathbb{H}$ is the stable fixed point of T then $l(T) = -\log((T)'(u_T))$ (see e.g. [5, (15.2)]). Next we recall from the proof of Theorem 8.1 that $\phi'_w(u_w)$ is independent of the representative in $[w]$. Assuming once more, that $w_0 \leq 3$ we calculate that

$$\phi_w(u_w) = R_{w_{2r}} \dots R_{w_1 - 3} u_w.$$

Thus u_w is the stable fixed point of the hyperbolic element $T(w)$ and for the displacement length of T we obtain $l(T(w)) = -\log((T(w))'(u_w))$. As however the displacement length coincides with the length of the associated closed geodesic (see e.g. [5, Proposition 2.16]) we established (9.6) and finished the proof of Proposition 9.2. □

Corrolary 9.3. *Let l_1, l_2, l_3 be real positive numbers, and $\mathcal{L}_s$ the Ruelle transfer operator of the flow-adapted IFS as defined in Definition 9.1 with potential $V_s(u) = [(\phi^{-1})'(u)]^{-s}$, then the dynamical zeta function coincides with the Selberg zeta function of X_{l_1,l_2,l_3}*

$$Z_{X_{l_1,l_2,l_3}}(s) = \det(1 - \mathcal{L}_s)$$

Proof. As (8.9) did not depend on the choice of the IFS we obtain also for the flow-adapted IFS

$$\det(1 - \mathcal{L}_s) = \prod_{[w] \in [\mathcal{W}^{\text{prime}}]} \prod_{k \geq 0} \left(1 - \phi'_w(u_w)^{k+s}\right).$$

Using Proposition 9.2 this can be written as

$$\det(1-\mathcal{L}_s) = \prod_{\gamma\in\mathcal{P}_{X_{l_1,l_2,l_3}}} \prod_{k\geq 0} \left(1-e^{-(k+s)l(\gamma)}\right).$$

which is exactly the Selberg zeta function of X_{l_1,l_2,l_3}. □

With help of the flow-adapted IFS we can now prove the analyticity of the generalized zeta functions which was stated in the introduction as Theorem 6.2.

Theorem 6.2. *Let X_{l_1,l_2,l_3} be a Schottky surface with three funnels of widths l_1, l_2, l_3 and let $n_1, n_2, n_3 \in \mathbb{N}$. We define*

$$\mathbf{n} : \begin{cases} \mathcal{P}_{X_{l_1,l_2,l_3}} & \to & \mathbb{N} \\ \gamma & \mapsto & \sum_{i=1}^{3} n_i w_i(\gamma) \end{cases}$$

where $w_i(\gamma)$ denotes the winding number around the funnel of width l_i. Then the generalized zeta function

$$d_{\mathbf{n}}(s,z) = \prod_{\gamma\in\mathcal{P}_{X_{l_1,l_2,l_3}}} \prod_{k\geq 0} \left(1-z^{\mathbf{n}(\gamma)}e^{-(k+s)l(\gamma)}\right).$$

extends to an analytic function on $\mathbb{C}^2$.

Proof. First we note that for $|z|<1$ and $\mathrm{Re}(s)>1$ the products in (6.3) expand to an absolutely convergent series. In the region of absolute convergence we can Taylor expand $d_{\mathbf{n}}$ in z around zero and obtain

$$d_{\mathbf{n}}(s,z) = \sum_{k=0}^{\infty} b_k(s) z^k. \tag{9.7}$$

In order to show the analytic continuation we construct an appropriate s- and z-dependent trace class operator. We take the flow-adapted IFS and define a potential V which depends analytically on two complex parameters $s, z \in \mathbb{C}$ by setting for $i \rightsquigarrow j$ and $u \in \phi_{i,j}(D)$

$$V(u;s,z) := z^{n_{i,j}}[-(\phi^{-1})'(u)]^{-s}$$

where

$$\begin{aligned} n_{1,5} = n_{5,1} = n_{4,2} = n_{2,4} &:= n_1 \\ n_{2,6} = n_{6,2} = n_{5,3} = n_{3,5} &:= n_2 \\ n_{3,4} = n_{4,3} = n_{6,1} = n_{1,6} &:= n_3 \end{aligned}$$

Note that $-(\phi^{-1})'$ is non-vanishing on $\phi(D)$ and real and positive on $\Phi(D) \cap \mathbb{R}$, so we can extend for each $s \in \mathbb{C}$ the function $[-(\phi^{-1})']^{-s}$ from the real line to each of the disks $\phi_{i,j}(D_i)$ and obtain this way a family of holomorphic and bounded potentials on $\phi(D)$ that depends analytically on s and z. Following [56, Proposition 2] the family of transfer operators

$$\mathcal{L}_{s,z} := \mathcal{L}_{V(\bullet;s,z)} \tag{9.8}$$

with this potential is nuclear on $\mathcal{A}_\infty(D)$ and as a consequence of the analytic dependence of V on the parameters s, z the Fredholm determinant $\det(1 - \mathcal{L}_{s,z})$ also is an analytic function of s, z. The choice of the factors z^{n_i} is exactly such that each half winding around one of the i-th funnel contributes with a factor z^{n_i}. Thus each winding around the i-th funnel contributes with $2n_i$ and the total dynamical zeta function is in the region of absolute convergence given by

$$\tilde{d}_{\mathbf{n}}(s,z) := \det(1 - \mathcal{L}_{s,z}) = \prod_{\gamma \in \mathcal{P}_{X_{l_1,l_2,l_3}}} \prod_{k \geq 0} \left(1 - z^{2\mathbf{n}(\gamma)} e^{-(k+s)l(\gamma)}\right). \tag{9.9}$$

As we know that the function is analytic we can Taylor expand it in z around 0 and obtain

$$d_{\mathbf{n}}(s,z) = \sum_{k=0}^{\infty} b_k(s) z^k. \tag{9.10}$$

with analytic coefficients $b_k(s)$. As in (9.9) only even powers of z appear we immediately can conclude $b_{2k+1}(s) = 0$. Comparing furthermore the product expressions (6.3) with (9.9) and the Taylor expansions (9.7) with (9.10) in the region of absolute convergence we obtain

$$b_k(s) = \tilde{b}_{2k}(s).$$

By this identification we obtain an analytic continuation of the Taylor coefficients $b_k(s)$. As for each $s \in \mathbb{C}$ the power series (9.10) has a radius of convergence equal to infinity, i.e. $\limsup_k |\tilde{b}_k(s)|^{1/k} = 0$ we also obtain that (9.7) converges for all $z \in \mathbb{C}$ and the generalized zeta function is thus analytic. □

10 Geometric limits

In this section we will prove Theorem 6.3 and then show that Theorem 6.1 is a consequence of this result. The proof of Theorem 6.3 will be performed in three steps: First we will derive a form of the flow-adapted IFS that is

especially suited to treat the family of Schottky surfaces in the limit $\ell \to \infty$. In a next step (Lemma 10.2) we will derive explicit bounds for the coefficients of the cycle expansion of the generalized zeta function using techniques from [56]. Finally we will be able to prove the convergence using these bounds and the special form of the flow-adapted IFS (See Lemma 10.5 and 10.6 as well as the rest of this section).

We start with the construction of the special form of flow-adapted IFS.

Lemma 10.1. *Let n_1, n_2, n_3 be positive integers fulfilling the triangle condition. Then there exists ℓ_0 such that for any $\ell > \ell_0$ there exists a family of flow-adapted IFS associated to $X_{n_1,n_2,n_3}(\ell)$ in the sense of Definition 9.1 such that the lower boundaries a_j of the disks D_j are given by $a_j = 2(j-1)$ independently of ℓ and $r_j < 0.5$. Furthermore the radii fulfill the asymptotics*

$$\lim_{\ell \to \infty} r_j(\ell) e^{\kappa_j \ell} = C_j \tag{10.1}$$

where

$$\kappa_1 = \frac{n_1 + n_3 - n_2}{2},\ \kappa_2 = \frac{n_1 + n_2 - n_3}{2},\ \kappa_3 = \frac{n_2 + n_3 - n_1}{2}$$

and $\kappa_4 = \kappa_1,\ \kappa_5 = \kappa_2,\ \kappa_6 = \kappa_3$ are constants strictly larger then zero and

$$C_1 = C_3 = C_4 = C_6 = 8,\ C_2 = C_5 = \frac{1}{2}.$$

Proof. We will first use the freedom of choosing the position and orientation of the hexagon as already mentioned in Remark 9.1. Instead of constructing the reflection group on $\mathbb{D}$ we can also directly work on the upper half plane (see Figure 10.1). So we can consider again an orthogonal hexagon with side lengths $A, n_1\ell/2, B, n_2\ell/2, C, n_3\ell/2$ and we call c_1 to be the geodesic prolongation of the side A, c_2 the one of B and c_3 the one of C. Now there exists an isometry such that for the starting points $a_j \in \mathbb{R} = \partial\mathbb{H}$ of c_j we have $a_j = 2j$. This isometry can be constructed in three steps: First translate parallel to the real axis until $a_1 = 0$, then apply the dilation $z \to \lambda z$ which fixes a_1 until $a_2 = 2$ and finally apply the one parameter group of hyperbolic transformation that fixes a_1, a_2 until $a_3 = 6$ is fulfilled. Setting the offset parameter $\delta_{\text{offset}} = 6$ we then obtain the condition $a_j = 2(j-1)$ for all $1 \leq j \leq 6$. Note however that the flow-adapted IFS might be ill defined with this offset parameter, because we could in principle have $r_3 > 1$. In the next step we will show however that in the limit $\ell \to \infty$ all radii r_j will tend to zero. Thus for sufficiently large ℓ everything is well defined.

In order to show the convergence of the radii to zero we first note that even without the triangle condition at least two of the radii have to converge

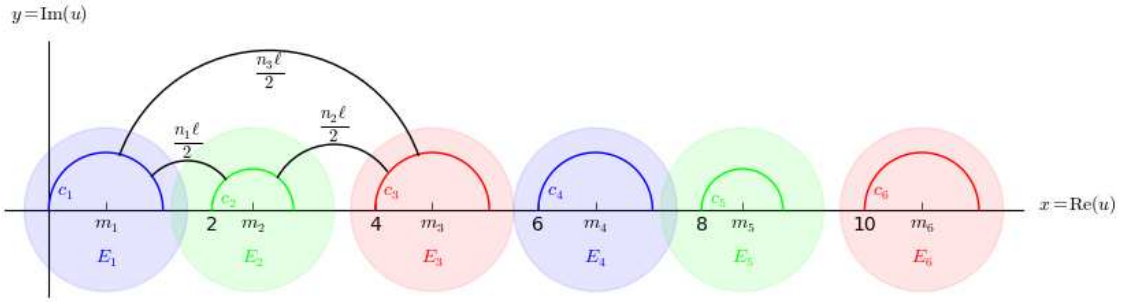

Figure 10.1: Illustration of the construction of the family of flow-adapted IFS in Lemma 10.1. The start points of the circles c_j are now fixed to $2(j-1)$. The light colored disks indicate the extended disks E_j which are crucial for obtaining the estimates in Lemma 10.2.

towards zero. Otherwise the perpendicular distance between those two circles can never tend towards infinity as already the distance between their start points a_i is fixed. We can thus assume, after possibly permuting the l_i that r_1 and r_3 converge to zero. For a proof by contradiction we now assume that r_2 is bounded away from zero by $r_{\min}$. We will first show that then also the side length B is bounded away from zero: For $x \in \partial\mathbb{H}$ and $r > 0$ we consider the unique geodesic that starts in x and is orthogonal to the circle of radius r that starts at a_2. We denote the intersection point of these two geodesics with $p(x, r)$. Then for two different points $x_1 \neq x_2$ the points $p(x_1, r)$ and $p(x_2, r)$ are different. Recall that B is exactly the hyperbolic distance between $p(r_2, x_1)$ and $p(r_2, x_2)$ where $x_1 \in [a_1, a_1+2r_1]$ and $x_2 \in [a_3, a_3+2r_3]$ such that the geodesics are also orthogonal to c_1 and c_3, respectively (see Figure 10.2 for an illustration of these points). From the fact that the disks D_i are mutually disjoint we conclude, that $[a_1, a_1 + 2r_1] \cap [a_3, a_3 + 2r_3] = \emptyset$ so $d_{\mathbb{H}}(p(x_1, r_2), p(x_2, r_2)) > 0$ for all ℓ. Furthermore the disjoint disk and the lower bound on r_2 together imply that $r_2 \in [r_{\min}, 1]$. The fact that r_1 and r_2 converge to zero finally means that there exist $r_{1,\max}, r_{3,\max}$ such that $r_1 \leq r_{1,\max}$ and $r_3 \leq r_{3,\max}$ for all ℓ. We can thus bound

$$B = d_{\mathbb{H}}(p(x_1, r_2), p(x_2, r_2)) \geq \min_{\substack{y_1 \in [a_1, a_1 + 2r_{1,\max}], \\ y_2 \in [a_3, a_3 + 2r_{3,\max}], \\ r \in [r_{\min}, 1]}} d_{\mathbb{H}}(p(y_1, r), p(y_2, r)) =: B_0.$$

As $d_{\mathbb{H}}(p(y_1, r), p(y_2, r))$ is a positive quantity that depends continuously on the parameters r, y_1, y_2 which vary in a compact set, $B_0 > 0$ and B is bounded away from zero. This is however in contradiction to the triangle condition.

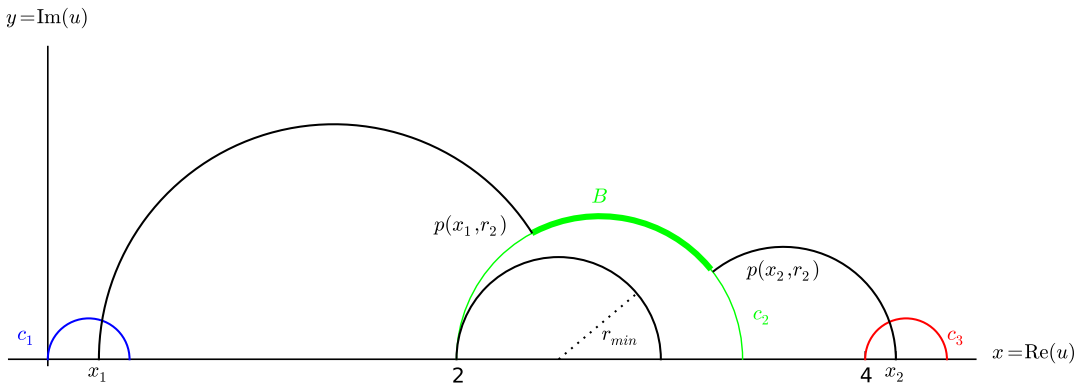

Figure 10.2: Illustration of the notation for the lower bound on B in the proof of Lemma 10.1.

From [88, (2.6.10)] we have the formula for orthogonal hexagons

$$\cosh B = \frac{\cosh(n_1\ell/2)\cosh(n_2\ell/2) + \cosh(n_3\ell/2)}{\sinh(n_1\ell/2)\sinh(n_2\ell/3)}.$$

In the limit $\ell \to \infty$ the right side becomes

$$1 + \frac{e^{n_3\ell}}{e^{(n_1+n_2)\ell}}$$

which converges to 1 if the triangle condition is fulfilled and consequently $\lim_{\ell\to\infty} B = 0$. We have thus shown that under the triangle condition all three radii have to converge to zero.

In order to prove the concrete form of the asymptotics (10.1) we use the following general formula for the displacement length of an hyperbolic element $T \in SL(2,\mathbb{R})$ ([5])

$$\cosh(l(T)/2) = |\mathrm{Tr}(T)/2|.$$

So using (9.5) together with the explicit form (9.4) for the R_i one obtains the set of equations.

$$\begin{aligned}
\cosh(n_1\ell/2) = \cosh(l(R_1R_2)/2) &= \left|\frac{\mathrm{Tr}(R_1R_2)}{2}\right| &= \frac{(m_1-m_2)^2 - r_1 - r_2}{2\sqrt{r_1r_2}} \\
\cosh(n_2\ell/2) = \cosh(l(R_2R_3)/2) &= \left|\frac{\mathrm{Tr}(R_2R_3)}{2}\right| &= \frac{(m_2-m_3)^2 - r_2 - r_3}{2\sqrt{r_2r_3}} \\
\cosh(n_3\ell/2) = \cosh(l(R_1R_3)/2) &= \left|\frac{\mathrm{Tr}(R_1R_3)}{2}\right| &= \frac{(m_1-m_3)^2 - r_1 - r_3}{2\sqrt{r_1r_3}}.
\end{aligned}$$

Dividing both sides by $e^{n_i\ell/2}$ and taking the limit $\ell \to \infty$ one obtains

$$\begin{aligned}
1 = \lim_{\ell\to\infty} \frac{\cosh n_1\ell/2}{e^{n_1\ell/2}} &= \lim_{\ell\to\infty} \frac{(m_1-m_2)^2 - r_1 - r_2}{2\sqrt{r_1r_2}e^{n_1\ell/2}} \\
1 = \lim_{\ell\to\infty} \frac{\cosh n_2\ell/2}{e^{n_1\ell/2}} &= \lim_{\ell\to\infty} \frac{(m_2-m_3)^2 - r_2 - r_3}{2\sqrt{r_2r_3}e^{n_2\ell/2}} \\
1 = \lim_{\ell\to\infty} \frac{\cosh n_3\ell/2}{e^{n_3\ell/2}} &= \lim_{\ell\to\infty} \frac{(m_1-m_3)^2 - r_1 - r_3}{2\sqrt{r_1r_3}e^{n_3\ell/2}}.
\end{aligned}$$

From the fact that the a_i do not depend on ℓ and that the radii all converge to zero we explicitly know $\lim_{\ell\to\infty}(m_i-m_j)^2 - r_i - r_j$ and obtain

$$\begin{aligned}
\lim_{\ell\to\infty} \sqrt{r_1r_2}e^{n_1\ell/2} &= 2 \\
\lim_{\ell\to\infty} \sqrt{r_2r_3}e^{n_2\ell/2} &= 2 \\
\lim_{\ell\to\infty} \sqrt{r_1r_3}e^{n_3\ell/2} &= 8.
\end{aligned}$$

We now multiply two of these equations and divide by the third one and obtain

$$\begin{aligned}
\lim_{\ell\to\infty} r_1 e^{(n_1+n_3-n_2)\ell/2} &= 8 \\
\lim_{\ell\to\infty} r_2 e^{(n_1+n_2-n_3)\ell/2} &= \frac{1}{2} \\
\lim_{\ell\to\infty} r_3 e^{(n_2+n_3-n_1)\ell/2} &= 8
\end{aligned}$$

which finishes the proof of Lemma 10.1. □

From the property $r_j < 0.5$ of these flow-adapted IFS it directly follows that for any $\ell > \ell_0$ and any $1 \le j \le 6$ there exists extended disks E_j which are concentric with D_j, have a radius $r_{E_j} > 1$ and do not intersect any of the other disks D_i (see Figure 10.1) for an illustration).

Lemma 10.2. *Let n_1, n_2, n_3 be positive integers fulfilling the triangle condition and $\ell > \ell_0$ as in Lemma 10.1. Let $d_{\mathbf{n}}(s,z)$ be the generalized zeta function of the family of Schottky surfaces $X_{n_1,n_2,n_3}(\ell)$. Let furthermore $\mathcal{L}_{s,z;\ell}$ be the transfer operator as defined in (9.8) of the flow-adapted IFS from Lemma 10.1 and let its cycle expansion be given by*

$$\det(1 - y\mathcal{L}_{s,z;\ell}) = 1 + \sum_{k=1}^{\infty} y^k \tilde{d}^{(k)}_{\mathbf{n}}(s,z;\ell). \tag{10.2}$$

With this definition of $\tilde{d}^{(k)}_{\mathbf{n}}(s,z;\ell)$ *we can express the generalized zeta function as*

$$d_{\mathbf{n}}(s,z;\ell) = 1 + \sum_{k=1}^{\infty} \tilde{d}^{(k)}_{\mathbf{n}}(s,\sqrt{z};\ell). \tag{10.3}$$

If we furthermore fix six disks E_j *with radius* $r_{E_j} > 1$ *and center* m_j *such that for* $i \neq j$ $E_i \cap D_j = \emptyset$ *then we have the explicit bounds*

$$|\tilde{d}^{(k)}_{\mathbf{n}}(s,z;\ell)| \leq k^{k/2} K(s,z;\ell)^k \sum_{m_1<\cdots<m_k} r(\ell)^{\lfloor m_1/6\rfloor+\ldots+\lfloor m_k/6\rfloor}, \tag{10.4}$$

where $\lfloor x \rfloor$ *denotes the integer part of a real number* x *and*

$$r(\ell) := \max_{1\leq j\leq 6} r_j \quad \text{and} \quad K(s,z;\ell) := \frac{1}{2\pi} \max_{j\rightsquigarrow i} \|V(\phi_{j,i}(\bullet);s,z)\|_{\infty,E_j}. \tag{10.5}$$

Remark 10.1. We will follow closely the techniques of Jenkinson-Pollicott [56] which they used to obtain rigorous dimension estimates, but in a different spirit. While they were interested in the question how fast the cycle expansion coefficients $d^{(k)}$ for a fixed IFS vanish if the order k becomes large, we consider the coefficients for a family of IFS at a fixed order k and we want to determine which coefficients vanish in the limit $\ell \to \infty$. The estimate (10.4) then says that only the first six coefficients survive in this limit.

Proof. We know that the transfer operator $\mathcal{L}_{s,z;\ell}$ of the flow-adapted IFS is a nuclear operator, so using the following result of Grothendieck we obtain a direct formula for the coefficients of the cycle expansion in terms of the nuclear representation.

Proposition 10.3 (Grothendieck 1956 [40])**.** *If* $\mathcal{B}$ *is a Banach space and* $\mathcal{L} : \mathcal{B} \to \mathcal{B}$ *is a nuclear operator with the nuclear representation* $\mathcal{L}h = \sum_{n=1}^{\infty} \lambda_n \alpha_n(h) v_n$ *as defined in Definition 8.3, then the Fredholm determinant of* $\mathcal{L}$ *can be expanded in a power series* $\det(1 - z\mathcal{L}) = 1 + \sum_{k=1}^{\infty} z^k d^{(k)}$ *with*

$$d^{(k)} = (-1)^k \sum_{m_1<\cdots<m_k} \lambda_{m_1} \ldots \lambda_{m_k} \det\left[(\alpha_{m_p}(v_{m_q}))_{p,q=1}^{k}\right] \tag{10.6}$$

where

$$(\alpha_{m_p}(v_{m_q}))_{p,q=1}^{k} = \begin{pmatrix} \alpha_{m_1}(v_{m_1}) & \ldots & \alpha_{m_k}(v_{m_1}) \\ \vdots & \ddots & \vdots \\ \alpha_{m_1}(v_{m_k}) & \ldots & \alpha_{m_k}(v_{m_k}) \end{pmatrix}$$

is a $k \times k$ *matrix.*

Thus (10.6) allows us to obtain estimates on the coefficients $\tilde{d}^{(k)}_{\mathbf{n}}(s,z;l)$ in terms of the nuclear representation of $\mathcal{L}_{s,z;\ell}$. We therefore want to derive its nuclear decomposition now and obtain explicit estimates on the λ_n.

Recall from (8.3) that $\mathcal{L}_{s,z;l}$ can be decomposed into a sum of the following six operators

$$\left(\mathcal{L}^{(j)}h\right)(u) = \sum_{i \text{ s.t.} j \rightsquigarrow i} V(\phi_{j,i}(u))h(\phi_{j,i}(u)).$$

with $1 \leq j \leq 6$.

It is now an important remark that the function $\mathcal{L}^{(j)}_{s,z;\ell}h$ is not only holomorphic on D_j but can be extended holomorphically to a much larger disk with the same center. We illustrate the mechanism for $\mathcal{L}^{(1)}_{s,z;\ell}h$ which is given by

$$\begin{aligned}(\mathcal{L}^{(1)}_{s,z;\ell}h)(u) &= V(\phi_{1,5}(u);s,z)h(\phi_{1,5}(u)) + V(\phi_{1,6}(u);s,z)h(\phi_{1,6}(u)) \\ &= z^{n_1}\left[-R_2'(u)\right]^s h(R_2(u)+\delta_{\text{offset}}) + z^{n_3}\left[-R_3'(u)\right]^s h(R_3(u)+\delta_{\text{offset}}).\end{aligned}$$

The factor $h(R_2(\bullet)+\delta_{\text{offset}})$ is just the pullback of h with a reflection at the boundary of disk D_2 plus complex conjugation and a final translation. Thus from the fact that h is holomorphic on D_5 follows that $h(R_2(\bullet)+\delta_{\text{offset}})$ is holomorphic on $\mathbb{C}\setminus D_2$. For the same reason the term $h(R_3(\bullet)+\delta_{\text{offset}})$ is holomorphic on $\mathbb{C}\setminus D_3$. Let us next consider the term $[-R_2'(u)]^s$. From the form (9.3) one deduces directly that $-R_2'(\bullet)$ is a nonzero holomorphic function on $\mathbb{C}\setminus\{m_2\}$, consequently $[-R_2'(u)]^s$ can be extended to every split plane $\mathbb{C}\setminus l$ where l is a half line starting at the center m_2 and going to infinity. Analogously $[-R_3']^s$ can be extended to every split plane without a line starting at m_3. We can therefore extend $\mathcal{L}^{(1)}_{s,z;\ell}h$ to any disk centered around m_1 that does not intersect D_2 nor D_3 and in particular to the disk E_1 as defined above. Analogously any of the other functions $\mathcal{L}^{(j)}_{s,z;\ell}h$ can be extended from D_j to E_j. This extension will now allow us to construct a nuclear representation of the operators $\mathcal{L}^{(j)}_{s,z;\ell}$ and control the appearing terms.

Let us denote by C_j the circle of radius 1 around m_j. As C_j is strictly contained in E_j we can write with the holomorphic extension to E_j and Cauchy's integral formula for any $\ell > \ell_0$ and any $u \in D_j$

$$(\mathcal{L}^{(j)}_{s,z;\ell}h)(u) = \frac{1}{2\pi i}\int_{C_j}\frac{(\mathcal{L}^{(j)}_{s,z;\ell}h)(\xi)}{\xi-u}d\xi.$$

As we know for any $\xi \in C_j$ and $u \in D_j$ that $|u-m_j| < |\xi-m_j|$ we can use

the geometric series to write

$$\begin{aligned}(\mathcal{L}^{(j)}_{s,z;\ell}h)(u) &= \frac{1}{2\pi i}\int\limits_{C_j}\frac{(\mathcal{L}^{(j)}_{s,z;\ell}h)(\xi)}{\xi-m_j}\left(1-\frac{u-m_j}{\xi-m_j}\right)^{-1}d\xi\\ &= \sum_{n=0}^{\infty}\frac{1}{2\pi i}\int\limits_{C_j}\frac{(\mathcal{L}^{(j)}_{s,z;\ell}h)(\xi)}{\xi-m_j}\left(\frac{u-m_j}{\xi-m_j}\right)^{n}d\xi\\ &= \sum_{n=0}^{\infty}\tilde{\alpha}^{(j)}_n(h)\tilde{v}^{(j)}_n(u),\end{aligned}$$

where

$$\tilde{\alpha}^{(j)}_n(h) := \frac{1}{2\pi i}\int\limits_{C_j}\frac{(\mathcal{L}^{(j)}_{s,z;\ell}h)(\xi)}{(\xi-m_j)^{n+1}}d\xi \quad\text{and}\quad \tilde{v}^{(j)}_n(u) = (u-m_j)^n. \tag{10.7}$$

We can finally normalize the elements $\tilde{v}^{(j)}_n$ with respect to the supremum norm and $\tilde{\alpha}^{(j)}_n$ with respect to the operator norm as a linear operator $\mathcal{A}(D)\to\mathbb{C}$ and we obtain the nuclear representation

$$(\mathcal{L}^{(j)}_{s,z;\ell}h)(u) = \sum_{n=0}^{\infty}\lambda^{(j)}_n\alpha^{(j)}_n(h)v^{(j)}_n(u)$$

with $\lambda^{(j)}_n = \|\tilde{\alpha}^{(j)}_n\|\|\tilde{v}^{(j)}_n\|$.

Equation (10.7) also allows us to obtain estimates on $\lambda^{(j)}_n$. Recall that r_j was the radius of disk D_j so we have

$$\|\tilde{v}^{(j)}_n\|_{\infty,D_j} = r_j^n.$$

In order to bound $\|\tilde{\alpha}^{(j)}_n\|$ first calculate for any $h\in\mathcal{A}_\infty$ that

$$|\tilde{\alpha}^{(j)}_n(h)| \le \frac{1}{2\pi}\|\mathcal{L}^{(j)}_{s,z;\ell}h\|_{\infty,E_j} \le \frac{1}{2\pi}\max_{i:\,j\rightsquigarrow i}\|V(\phi_{j,i}(\bullet);s,z)\|_{\infty,E_j}\|h\|_{\infty,D}$$

so putting the two bounds together we get

$$\begin{aligned}\lambda^{(j)}_n &= \|\alpha^{(j)}_n\|\|v^{(j)}_n\|\\ &\le r_j^n\frac{1}{2\pi}\max_{i:\,j\rightsquigarrow i}\|V(\phi_{j,i}(\bullet);s,z)\|_{\infty,E_j}.\end{aligned}\tag{10.8}$$

We have thus derived the nuclear representation of $\mathcal{L}^{(j)}_{s,z;\ell}$ and also obtained explicit bounds on the $\lambda^{(j)}_n$. In order to control the nuclear representation

of the full operator $\mathcal{L}_{s,z;\ell}$ we have to sum up the six operators $\mathcal{L}^{(j)}_{s,z;\ell}$ with $1 \le j \le 6$. We arrange the different summands such that

$$\mathcal{L}_{s,z;\ell} h = \sum_{n=0}^{\infty} \lambda_n \alpha_n(h) v_n$$

with

$$\lambda_{6n+j} = \lambda_n^{(j)}, \quad \alpha_{6n+j} = \alpha_n^{(j)} \text{ and } v_{6n+j} = v_n^{(j)}.$$

If we define

$$r(\ell) := \max_j(r_j) \quad \text{and} \quad K(s,z;\ell) := \frac{1}{2\pi} \max_{j \rightsquigarrow i} \|V(\phi_{j,i}(\bullet); s, z)\|_{\infty, E_j}$$

then we have the explicit bound

$$\lambda_n \le K(s,z;\ell) r(\ell)^{\lfloor n/6 \rfloor}. \tag{10.9}$$

We can now use the Grothendieck formula (10.6) as well as the Hadamard bound on the $k \times k$ matrices with entries lower or equal to one and obtain

$$\begin{aligned} |\tilde{d}^{(k)}_{\mathbf{n}}(s,z,\ell)| &= \sum_{m_1 < \cdots < m_k} \lambda_{m_1} \dots \lambda_{m_k} \det\left[(\alpha_{m_p}(v_{m_q}))_{p,q=1}^k\right] \\ &\le k^{k/2} K(s,z;\ell)^k \sum_{m_1 < \cdots < m_k} r(\ell)^{\lfloor m_1/6 \rfloor + \ldots + \lfloor m_k/6 \rfloor} \end{aligned}$$

which finishes the proof of Lemma 10.2. □

For the rest of the proof of Theorem 6.3 there remain two steps to be done: First we will show that the bounds in Lemma 10.2 allow to uniformly truncate the cycle expansion after the sixth order and secondly we will show that the finitely many remaining terms converge against the polynomial. For both steps, the following lemma will be useful.

Lemma 10.4. *For any $j \rightsquigarrow i$ and any bounded domain $B \subset \mathbb{C}^2$ we have*

$$\lim_{\ell \to \infty} V(\phi_{j,i}(u), s/\ell, \sqrt{z}) = z^{n_{j,i}/2} e^{-\kappa_i s}$$

uniformly for $u \in E_i$ and $(s,z) \in B$.

Proof. Recall that

$$V(\phi_{j,i}(u); s/\ell, \sqrt{z}) = z^{n_{j,i}/2} \left[-(\phi_{j,i}^{-1})'(\phi_{j,i}(u))\right]^{s/\ell} = z^{n_{j,i}/2} \left[-\phi'_{j,i}(u)\right]^{s/\ell}$$

and calculate that for $1 \leq i \leq 3$

$$-\phi'_{j,i}(u) = \frac{r_i}{(u - \delta_{\text{offset}} - m_i)^2}$$

while for $4 \leq i \leq 6$

$$-\phi'_{j,i}(u) = \frac{r_{i-3}}{(u - m_{i-3})^2}.$$

By the definition of the family of flow-adapted IFS in Lemma 10.1 and the extended disks E_i we know that there exist two constants $0 < c < C$ such that for any $j \rightsquigarrow i$, any $u \in E_j$ we have $c < |u - \delta_{\text{offset}} - m_i| < C$ if $i \leq 3$ and $c < |u - m_{i-3}| < C$ if $i > 3$. Furthermore the asymptotics (10.1) for r_i gives us another pair of constants $0 < c < C$ with $c < r_i e^{\kappa_i \ell} < C$. Together with the fact that s can vary only in a bounded set $\text{Pr}_s B$, which is the projection of B to the s variable, this gives the existence of constants $0 < c < C$ with

$$c < \left(-\phi'_{j,i}(u) e^{\kappa_i \ell}\right)^s < C \quad \forall\ u \in E_j, \ell > \ell_0 \text{ and } s \in \text{Pr}_s B. \tag{10.10}$$

In order to use this inequality we calculate

$$\begin{aligned} \left\| V(\phi_{j,i}(u), s/\ell, \sqrt{z}) - z^{n_{j,i}/2} e^{-\kappa_i s} \right\|_{\infty, E_j \times B} &= \left\| z^{n_{j,i}/2} \left(\left(-\phi'_{j,i}(u)\right)^{s/\ell} - e^{-\kappa_i s} \right) \right\|_{\infty, E_j \times B} \\ &\leq \left\| z^{n_{j,i}/2} e^{-\kappa_i s} \right\|_{\infty, B} \left\| \left(\left(-\phi'_{j,i}(u) e^{\kappa_i \ell}\right)^{s/\ell} - 1 \right) \right\|_{\infty, E_j \times B}. \end{aligned}$$

While the first term $\left\| z^{n_{j,i}/2} e^{-\kappa_i s} \right\|_{\infty, B}$ is bounded and independent of ℓ, the uniform bounds (10.10) imply that the second term converges to zero. □

Lemma 10.5. *Let $B \subset \mathbb{C}^2$ be any bounded domain, and*

$$d_{\mathbf{n}}(s, z; \ell) = 1 + \sum_{k=1}^{\infty} \tilde{d}^{(k)}_{\mathbf{n}}(s, \sqrt{z}; \ell).$$

the series expansion (10.3) of the generalized zeta function from Lemma 10.2. Then

$$\lim_{\ell \to \infty} \left\| \sum_{k>6} \tilde{d}^{(k)}_{\mathbf{n}}(s/\ell, \sqrt{z}; \ell) \right\|_{\infty, B} = 0, \tag{10.11}$$

i.e. the rescaled generalized zeta function $d_{\mathbf{n}}(s/\ell, z; \ell)$ converges uniformly to the finitely truncated sum $1 + \sum_{k=1}^{6} \tilde{d}^{(k)}_{\mathbf{n}}(s/\ell, \sqrt{z}; \ell)$.

Proof. In a first step we show that Lemma 10.4 implies a bound for $\|K(s/\ell,\sqrt{z},\ell)\|_{\infty,B}$. Recall from the definition (10.5) that

$$\|K(s/\ell,\sqrt{z},\ell)\|_{\infty,B} = \max_{j\rightsquigarrow i} \left\|V(\phi_{j,i}(u);s/\ell,\sqrt{z})\right\|_{\infty,B\times E_j}.$$

Now Lemma 10.4 implies that

$$\left\|V(\phi_{j,i}(u);s/\ell,\sqrt{z}) - z^{n_{j,i}/2}e^{-\kappa_i s}\right\|_{\infty,B\times E_j} < C_{j,i}$$

for all $\ell > \ell_0$ and thus

$$\|K(s/\ell,\sqrt{z},\ell)\|_{\infty,B} \le \max_{j\rightsquigarrow i}\left(\left\|z^{n_{j,i}/2}e^{-\kappa_i s}\right\|_{\infty,B} + C_{j,i}\right) =: K_B.$$

As a second step we use that $\lfloor n/6\rfloor \ge (n-5)/6$ and obtain

$$\|\tilde{d}^{(k)}_{\mathbf{n}}(s/\ell,z,\ell)\|_{\infty,B} \;\le\; k^{k/2}K_B^k r(\ell)^{-5k/6}\sum_{m_1<\cdots<m_k}\left(r(\ell)^{1/6}\right)^{m_1+\ldots+m_k}.$$

Setting $\tilde{r}(\ell) = r(\ell)^{1/6}$ and using the Euler formula this gives

$$\|\tilde{d}^{(k)}_{\mathbf{n}}(s/\ell,z,\ell)\|_{\infty,B} \le k^{k/2}K_B^k\tilde{r}(\ell)^{-5k}\frac{\tilde{r}(\ell)^{k(k-1)/2}}{(1-\tilde{r}(\ell))\ldots(1-\tilde{r}(\ell)^k)}$$

which allows us to obtain an estimate for $k \ge 12$

$$\left\|\sum_{k=12}^{\infty}\tilde{d}^{(k)}_{\mathbf{n}}(s/\ell,z,\ell)\right\|_{\infty,B} \le \tilde{r}(\ell)\sum_{k=12}^{\infty}k^{k/2}K_B^k\;\frac{\tilde{r}(\ell)^{k\left(\frac{k-1}{2}-5-\frac{1}{k}\right)}}{(1-\tilde{r}(\ell))\ldots(1-\tilde{r}(\ell)^k)}.$$

If $k \ge 12$ then we have $\left(\frac{k-1}{2}-5-\frac{1}{k}\right) > 0$ and every term in the sum is uniformly bounded for all $\ell \ge \ell_0$. Furthermore since the terms in the series decay super-exponentially in k thanks to the term $\tilde{r}(\ell)^{k^2}$ the series converges with a uniform bound and the factor $\tilde{r}(\ell)$ in front assures the convergence to zero.

It remains thus to prove that the coefficients for $7 \le k \le 11$ vanish. This can be seen as follows. Note that we can estimate

$$\sum_{m_1<\cdots<m_k} r(\ell)^{\lfloor m_1/6\rfloor+\ldots+\lfloor m_k/6\rfloor} \le \left(\sum_{m>0} r(\ell)^{\lfloor m/6\rfloor}\right)^k \le C_k$$

for all $\ell > \ell_0$ with $C_k := \max_{\ell>\ell_0}(6/(1-r(\ell))^k)$ independent of ℓ. We can thus write for $k > 6$

$$\begin{aligned}\sum_{m_1<\cdots<m_k} r(\ell)^{\lfloor m_1/6\rfloor+\ldots+\lfloor m_k/6\rfloor} &= \sum_{m_1<\cdots<m_{k-1}} r(\ell)^{\lfloor m_1/6\rfloor+\ldots+\lfloor m_{k-1}/6\rfloor} \sum_{m_k>m_{k-1}} r(\ell)^{\lfloor m_k/6\rfloor} \\ &\leq C_{k-1}\sum_{m_k\geq 6} r(\ell)^{\lfloor m_k/6\rfloor} \\ &= C_{k-1}\frac{6\tilde{r}(\ell)}{1-\tilde{r}(\ell)}.\end{aligned}$$

Here we used crucially that from $k \geq 7$ we have $m_k \geq 6$ and thus can obtain the bound on the sum over m_k. We have finally shown (10.11) and finished the proof of Lemma 10.5. □

In order to prove Theorem 6.3 it finally remains to prove that

$$\lim_{\ell\to\infty}\left\|1+\sum_{k=1}^{6}\tilde{d}_{\mathbf{n}}^{(k)}(s/\ell,\sqrt{z};\ell)-P_{n_1,n_2,n_3}(ze^{-s})\right\|_{\infty,B}=0.$$

Recall that from (8.11) we have

$$\tilde{d}_{\mathbf{n}}^{(k)}(s/\ell,\sqrt{z};\ell)=\sum_{m=1}^{k}\left(\sum_{(n_1,\ldots,n_m)\in P(k,m)}\frac{(-1)^m}{m!}\prod_{l=1}^{m}\frac{1}{n_l}\sum_{w\in\mathcal{W}_{n_l}^{cl}}\frac{V_w(u_w;s/\ell,\sqrt{z})}{1-\phi_w'(u_w)}\right), \tag{10.12}$$

so we can explicitly calculate the cycle expansion coefficients in terms of dynamical quantities of the holomorphic IFS. As the symbolic dynamics of the flow-adapted IFS directly implies that the set of closed words is empty for uneven word length this drastically reduces the complexity of the calculations: First of all only coefficients $\tilde{d}_{\mathbf{n}}^{(k)}$ with $k = 2, 4, 6$ can be nonzero, because otherwise at least one summand n_l is uneven and consequently one factor in the product $\prod_{l=1}^{m}$ is zero. Additionally this condition reduces the number or possible tuples $(n_1, \ldots, n_m)$ which lead to nonzero contributions drastically: For $k = 2$ it remains only the one tuple (2), for $k = 4$ there are two possibilities (4) and (2, 2) and for $k = 6$ there are four possible tuples, namely (6), (4, 2), (2, 4) and (2, 2, 2). Even if each coefficient is only given by an explicit finite sum and even if the complexity of this sums is tremendously reduced by the above discussion it remains still very complex as the number of closed words increases exponentially. As $\#\mathcal{W}_2^{cl} = 12$, $\#\mathcal{W}_4^{cl} = 36$ and $\#\mathcal{W}_6^{cl} = 132$, the coefficient $d_{\mathbf{n}}^{(6)}$ would a priori be given by $132+12\cdot 36+36\cdot 12+12^3 = 2724$ summands. The following Lemma however allows to reduce the complexity in the limit $\ell \to \infty$ strongly.

Lemma 10.6. *Let us define for any $n \in \mathbb{N}$*

$$\mathbf{n} : \left\{ \begin{array}{ccc} \mathcal{W}_n^{cl} & \to & \mathbb{N} \\ (w_0, \dots, w_n) & \mapsto & \frac{1}{2}\sum_{r=0}^{n-1} n_{w_r, w_{r+1}} \end{array} \right. . \tag{10.13}$$

Then for any finite closed word $w \in \mathcal{W}_n^{cl}$ for the symbolic dynamics of the flow-adapted IFS and any $B \subset \mathbb{C}^2$ we have

$$\lim_{\ell \to \infty} \left\| \frac{V_w(u_w; s/\ell, \sqrt{z})}{1 - \phi_w'(u_w)} - \left(z e^{-s}\right)^{\mathbf{n}(w)} \right\|_{\infty, B} = 0. \tag{10.14}$$

Remark 10.2. The notation of the application $\mathbf{n} : \mathcal{W}_k^{cl} \to \mathbb{N}$ does not only coincide by chance with the notation of the order function on the closed geodesic which was defined in (6.2). In fact if w is a prime word, then Proposition 9.2 associates this word to a primitive geodesic in $\mathcal{P}_{X_{n_1,n_2,n_3}}(\ell)$. The definition (10.13) of the order function restricted to the subset of prime words $\mathcal{W}_k^{\text{prime}}$ is then equal to the order function (6.2) on primitive geodesics with respect to this identification.

Proof. Let us first note that from the fact that $r_i \to 0$ we conclude for any $w \in \mathcal{W}_n^{cl}$ that $\lim_{\ell \to \infty} \phi_w'(u_w) = 0$. It thus only remains to handle the term $V_w(u_w; s/\ell, \sqrt{z})$ and as a first step we note that as $u_w \in D_{w_0} \subset E_{w_0}$, Lemma 10.4 implies that

$$\lim_{\ell \to \infty} \left\| V(\phi_{w_0,w_1}(u_w), s/\ell, \sqrt{z}) - z^{n_{w_0,w_1}/2} e^{-\kappa_{w_1} s} \right\|_{\infty, B} = 0. \tag{10.15}$$

From the definition (8.5) of the iterated product we obtain

$$\begin{aligned} V_w(u_w; s/\ell, \sqrt{z}) &:= \prod_{k=1}^{n} V(\phi_{w_{0,k}}(u_w); s/\ell, \sqrt{z}) \\ &= \prod_{k=1}^{n} V(\phi_{w_{k-1},w_k}(u_{\sigma_L^{(k-1)} w}); s/\ell, \sqrt{z}). \end{aligned}$$

Here we used that the dynamics on the fixed points is conjugated to the shift operation (see (8.2)). Plugging in (10.15) we obtain

$$\lim_{\ell \to \infty} \left\| V_w(u_w; s/\ell, \sqrt{z})) - z^{\frac{1}{2}\left(\sum_{k=1}^{n} n_{w_{k-1},w_k}\right)} e^{-s\left(\sum_{k=1}^{n} \kappa_{w_k}\right)} \right\|_{\infty, B} = 0.$$

Thus it only remains to show that $\sum_{k=1}^{n} \kappa_{w_k} = \mathbf{n}(w)$ in order to finish the proof. This can finally be seen as follows. First one checks that for any $i \rightsquigarrow j$ we have $\kappa_i + \kappa_j = n_{i,j}$. Secondly as $w_0 = w_n$ we can write

$$\sum_{k=1}^{n} \kappa_{w_k} = \frac{1}{2} \sum_{k=1}^{n} \kappa_{w_{k-1}} + \kappa_{w_k} = \frac{1}{2} \sum_{k=1}^{n} n_{w_{k-1},w_k} = \mathbf{n}(w).$$

□

Remark 10.3. The identity $\sum_{k=1}^{n} \kappa_{w_k} = \mathbf{n}(w)$ shows that we could also have taken another definition of the potential functions for the generalized zeta functions namely $V(u) = z^{2\kappa_j}[-(\phi^{-1})'(u)]^{-s}$ for $u \in \phi_{i,j}(D_i)$. Note that however the κ_i are only positive if the n_i fulfill the triangle condition as defined in Lemma 10.1. In those cases where it is not satisfied the analyticity of the generalized zeta function would have been much harder to proof, so we chose the definition by the $n_{i,j}$.

We are now ready to proof Theorem 6.3.

Proof of Theorem 6.3. Lemma 10.6 implies that the w dependent terms in (10.12) depend only on $\mathbf{n}(w)$ in the limit $\ell \to \infty$. We thus introduce for any $k, n \in N$ the sets

$$\mathcal{W}_k^{cl}(n) := \left\{ w \in \mathcal{W}_k^{cl},\ \mathbf{n}(w) = n \right\}.$$

and observe that the relevant set of words split into

$$\begin{aligned}
\mathcal{W}_2^{cl} &= \mathcal{W}_2^{cl}(n_1) \cup \mathcal{W}_2^{cl}(n_2) \cup \mathcal{W}_2^{cl}(n_3) && (10.16)\\
\mathcal{W}_4^{cl} &= \mathcal{W}_4^{cl}(2n_1) \cup \mathcal{W}_4^{cl}(2n_2) \cup \mathcal{W}_4^{cl}(2n_3) \cup \\
&\quad \mathcal{W}_4^{cl}(n_1+n_2) \cup \mathcal{W}_4^{cl}(n_2+n_3) \cup \mathcal{W}_4^{cl}(n_1+n_3) && (10.17)\\
\mathcal{W}_6^{cl} &= \mathcal{W}_6^{cl}(3n_1) \cup \mathcal{W}_6^{cl}(3n_2) \cup \mathcal{W}_6^{cl}(3n_3) \cup \\
&\quad \mathcal{W}_6^{cl}(2n_1+n_2) \cup \mathcal{W}_6^{cl}(n_1+2n_2) \cup \mathcal{W}_6^{cl}(2n_2+n_3) \cup \mathcal{W}_6^{cl}(n_2+2n_3) \cup \\
&\quad \mathcal{W}_6^{cl}(2n_1+n_3) \cup \mathcal{W}_6^{cl}(n_1+2n_3) \cup \mathcal{W}_6^{cl}(n_1+n_2+n_3) && (10.18)
\end{aligned}$$

where the number of elements per set is given by

$$\begin{aligned}
\#\mathcal{W}_2(n_j) = \#\mathcal{W}_4(2n_j) = \#\mathcal{W}_6(3n_j) &= 4 \quad \forall 1 \le j \le 3\\
\#\mathcal{W}_4(n_i+n_j) &= 8 \quad \forall 1 \le i,j \le 3 \text{ with } i \ne j\\
\#\mathcal{W}_6(2n_i+n_j) &= 12 \quad \forall 1 \le i,j \le 3 \text{ with } i \ne j\\
\#\mathcal{W}_6(n_1+n_2+n_3) &= 48
\end{aligned} \qquad (10.19)$$

One can convince oneself of the validity of these formulas by geometric arguments. For example the only closed geodesics, that intersect only two of the blue lines in Figure 10.3 are those who make one circle around one of the three funnels. As the closed words correspond to closed geodesics, the closed words of order two split according to (10.16). Around each funnel there are two different geodesics (one in each sense of orientation) and each geodesic is encoded by two different words which leads to $\mathcal{W}_2^{cl}(n_i) = 4$. All other results can be understood by similar arguments, the easiest way to calculate (10.16)-(10.19) is however to solve the finite combinatorial problem exactly with a computer.

With this data it is a straight forward task to calculate that

$$\begin{aligned}
\left\| \tilde{d}^{(2)}_{\mathbf{n}}(s/\ell, \sqrt{z}; \ell) + 2\left[(ze^{-s})^{n_1} + (ze^{-s})^{n_2} + (ze^{-s})^{n_3}\right] \right\|_{\infty,B} &= 0 \quad (10.20) \\
\Bigg\| \tilde{d}^{(4)}_{\mathbf{n}}(s/\ell, \sqrt{z}; \ell) - \Big[(ze^{-s})^{2n_1} + (ze^{-s})^{2n_2} + (ze^{-s})^{2n_3} + \\
2\left((ze^{-s})^{n_1+n_2} + (ze^{-s})^{n_1+n_3} + (ze^{-s})^{n_2+n_3}\right)\Big] \Bigg\|_{\infty,B} &= 0 \quad (10.21) \\
\left\| \tilde{d}^{(6)}_{\mathbf{n}}(s/\ell, \sqrt{z}; \ell) + 4(ze^{-s})^{n_1+n_2+n_3} \right\|_{\infty,B} &= 0 \quad (10.22)
\end{aligned}$$

Equation (10.20) is seen immediately because as discussed above the only possible tuple $(n_1, \ldots, n_m)$ is the one-tuple (2). The next equation (10.21) can be seen as follows: First we split (10.12) according to the two possible tuples (4) and $(2, 2)$

$$\tilde{d}^{(4)}_{\mathbf{n}}(s/\ell, \sqrt{z}; \ell) = \underbrace{-\frac{1}{4}\left(\sum_{w \in \mathcal{W}_4^{cl}} \frac{V_w(u_w; s/\ell, \sqrt{z})}{1 - \phi'_w(u_w)}\right)}_{(A)} + \underbrace{\frac{1}{2!}\left(\frac{1}{2}\sum_{w \in \mathcal{W}_2^{cl}} \frac{V_w(u_w; s/\ell, \sqrt{z})}{1 - \phi'_w(u_w)}\right)^2}_{(B)}.$$

Next we treat the parts (A) and (B) separately. For (A) we use (10.17) and

obtain

$$
\begin{aligned}
(A) \;=\; & -\frac{1}{4}\Bigg(\sum_{w\in\mathcal{W}_4^{cl}(2n_1)} \left[\frac{V_w(u_w;s/\ell,\sqrt{z})}{1-\phi_w'(u_w)} - (ze^{-s})^{2n_1}\right] + \\
& \sum_{w\in\mathcal{W}_4^{cl}(2n_2)} \left[\frac{V_w(u_w;s/\ell,\sqrt{z})}{1-\phi_w'(u_w)} - (ze^{-s})^{2n_2}\right] + \\
& \sum_{w\in\mathcal{W}_4^{cl}(2n_3)} \left[\frac{V_w(u_w;s/\ell,\sqrt{z})}{1-\phi_w'(u_w)} - (ze^{-s})^{2n_3}\right] + \\
& \sum_{w\in\mathcal{W}_4^{cl}(n_1+n_2)} \left[\frac{V_w(u_w;s/\ell,\sqrt{z})}{1-\phi_w'(u_w)} - (ze^{-s})^{n_1+n_2}\right] + \\
& \sum_{w\in\mathcal{W}_4^{cl}(n_2+n_3)} \left[\frac{V_w(u_w;s/\ell,\sqrt{z})}{1-\phi_w'(u_w)} - (ze^{-s})^{n_2+n_3}\right] + \\
& \sum_{w\in\mathcal{W}_4^{cl}(n_1+n_3)} \left[\frac{V_w(u_w;s/\ell,\sqrt{z})}{1-\phi_w'(u_w)} - (ze^{-s})^{n_1+n_3}\right] - \\
& \Big[4(ze^{-s})^{2n_1} + 4(ze^{-s})^{2n_2} + 4(ze^{-s})^{2n_3} + 8(ze^{-s})^{n_1+n_2} + 8(ze^{-s})^{n_2+n_3} \\
& +8(ze^{-s})^{n_1+n_3}\Big]\Bigg).
\end{aligned}
$$

In order to treat (B) we use (10.16) and calculate

$$
\begin{aligned}
(B) \;=\; & +\frac{1}{2}\Bigg(\frac{1}{2}\sum_{w\in\mathcal{W}_2^{cl}(n_1)} \left[\frac{V_w(u_w;s/\ell,\sqrt{z})}{1-\phi_w'(u_w)} - (ze^{-s})^{n_1}\right] + \\
& \frac{1}{2}\sum_{w\in\mathcal{W}_2^{cl}(n_2)} \left[\frac{V_w(u_w;s/\ell,\sqrt{z})}{1-\phi_w'(u_w)} - (ze^{-s})^{n_2}\right] + \\
& \frac{1}{2}\sum_{w\in\mathcal{W}_2^{cl}(n_3)} \left[\frac{V_w(u_w;s/\ell,\sqrt{z})}{1-\phi_w'(u_w)} - (ze^{-s})^{n_3}\right] + \\
& \Big[2(ze^{-s})^{n_1} + 2(ze^{-s})^{n_2} + 2(ze^{-s})^{n_3}\Big]\Bigg)^2.
\end{aligned}
$$

Note that in both equations of (A) and (B), respectively, all terms except the last line converge uniformly to 0 on the set $B \subset \mathbb{C}^2$. So the limit $\ell \to \infty$

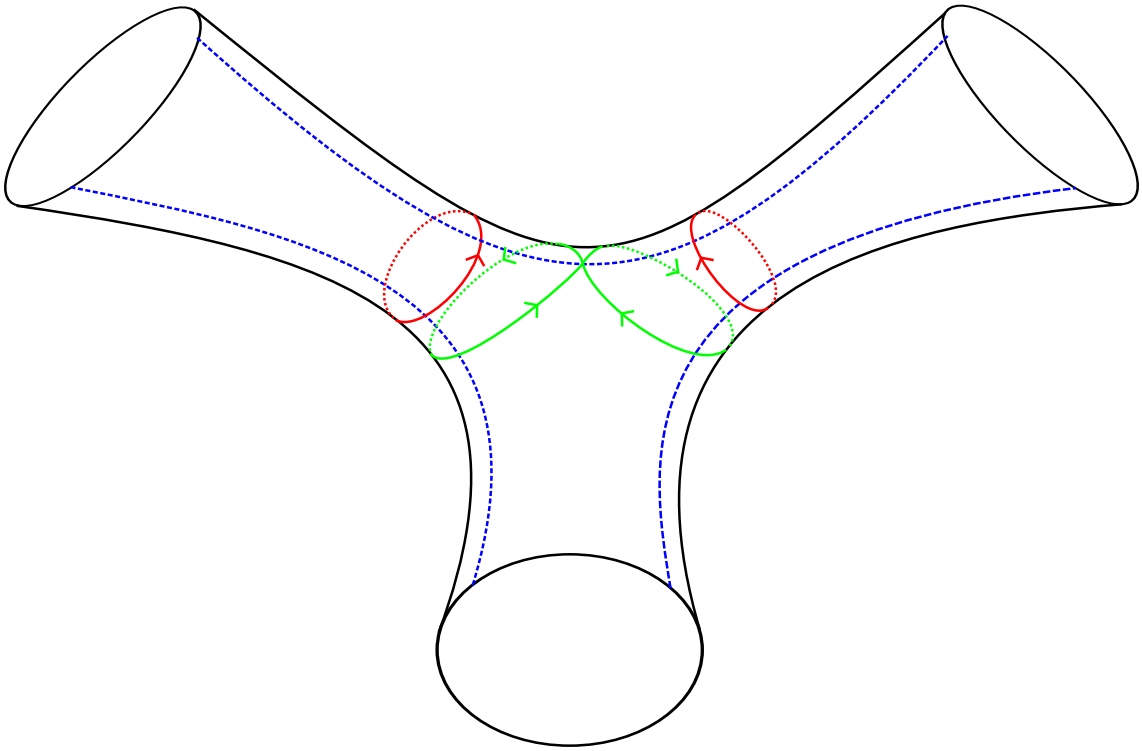

Figure 10.3: Schematic sketch of a 3-funneled Schottky surface. The blue, dashed lines indicate the cut lines of the Poincaré section which would correspond to the flow-adapted IFS. In red we see two geodesics which make one turn around one funnel each. They correspond to the closed words of length 2 $w^{(a)} = (1, 5, 1)$ and $w^{(a)} = (3, 5, 3)$. In green we see a geodesic which winds around both funnels in an eight-like shape. It corresponds to the closed word $w^{(c)} = (1, 5, 3, 5, 1)$ of length 4. Note that $\mathbf{n}(w^{(a)}) + \mathbf{n}(w^{(b)}) = \mathbf{n}(w^{(c)})$.

the coefficient $\tilde{d}^{(4)}_{\mathbf{n}}(s/\ell, \sqrt{z}; \ell)$ converges uniformly to

$$
\begin{aligned}
&-\frac{1}{4}\Big[4(ze^{-s})^{2n_1} + 4(ze^{-s})^{2n_2} + 4(ze^{-s})^{2n_3} + 8(ze^{-s})^{n_1+n_2} + 8(ze^{-s})^{n_2+n_3} + \\
&8(ze^{-s})^{n_1+n_3}\Big] + \frac{1}{2}\left[2(ze^{-s})^{n_1} + 2(ze^{-s})^{n_2} + 2(ze^{-s})^{n_3}\right]^2 \\
&= (ze^{-s})^{2n_1} + (ze^{-s})^{2n_2} + (ze^{-s})^{2n_3} + 2(ze^{-s})^{n_1+n_2} + 2(ze^{-s})^{n_2+n_3} + 2(ze^{-s})^{n_1+n_3}
\end{aligned}
$$

which proves (10.21). By a completely analogous but more tedious calculation we can show (10.22).

Finally we can put (10.20), (10.21) and (10.22) together and obtain (6.4) which finishes the proof of Theorem 6.3. □

Remark 10.4. Note that the limit form of $\frac{V_w(u_w;s/\ell,\sqrt{z})}{1-\phi'_w(u_w)}$ in (10.14) of Lemma 10.6 not only allows to group many terms together but also allows to take advantage of a systematic canceling. For example in the calculation of $\tilde{d}^{(4)}_{\mathbf{n}}(s/\ell,\sqrt{z};\ell)$ the terms $(ze^{-s})^{(n_1+n_2)}$ appears as limits of two different geodesics. First they appear in the term (A) as limits of the eight-shaped geodesics which turn around the funnels of width n_1 and n_2 (see green geodesic in Figure 10.3). Secondly they appear in (B) as the product of the geodesic which turns once around the funnel of width n_1 with another geodesic which turns once around the funnel of width n_2 (see the two red geodesics in Figure 10.3). As both terms appear with different signs they cancel each other to a big extend. Note that this cancellation is not exactly true for finite ℓ. In the setting of the physical quantum 3-disk system it has however been argued that this cancellation is approximately true. The mechanism that the contribution of longer orbits is approximately canceled by a combination of shorter orbits which Cvitanovic and Eckhardt call *shadowing orbits* has been identified in physics literature as the key mechanism for the fast convergence of the cycle expansion. Lemma 10.6 can thus also be seen as a proof that in the limit $\ell \to \infty$ this approximation becomes exact on Schottky surfaces.

Theorem 6.1 on the location of the rescaled resonances now follows directly from Theorem 6.3.

Proof of Theorem 6.1. Recall that

$$\mathcal{N}_{n_1,n_2,n_3} = \{s \in \mathbb{C},\ P_{n_1,n_2,n_3}(e^{-s}) = 0\}$$

and

$$\widetilde{\mathrm{Res}}_{n_1,n_2,n_3}(\ell) := \{s \in \mathbb{C},\ s/\ell \in \mathrm{Res}(X_{n_1,n_2,n_3}(\ell))\}.$$

If $U \subset \mathbb{C}$ is a domain whose boundary ∂U is disjoint with $\mathcal{N}_{n_1,n_2,n_3}$ then the argument principle implies that

$$\#\Big(U \cap \mathcal{N}_{n_1,n_2,n_3}\Big) = \frac{1}{2\pi i}\int\limits_{\partial U} \frac{f'(s)}{f(s)} ds$$

with $f(s) = P_{n_1,n_2,n_3}(e^{-s})$. On the other hand

$$\#\Big(U \cap \widetilde{\mathrm{Res}}_{n_1,n_2,n_3}(\ell)\Big) = \int\limits_{\partial U} \frac{\frac{d}{ds} Z_{X_{n_1,n_2,n_3}(\ell)}(s/\ell)}{Z_{X_{n_1,n_2,n_3}(\ell)}(s/\ell)} ds$$

and Theorem 6.3 implies that

$$Z_{X_{n_1,n_2,n_3}(\ell)}(s/\ell) = d_{\mathbf{n}}(s/\ell, 1) \to f(s)$$

uniformly on ∂U. This in turn immediately implies Theorem 6.1. □

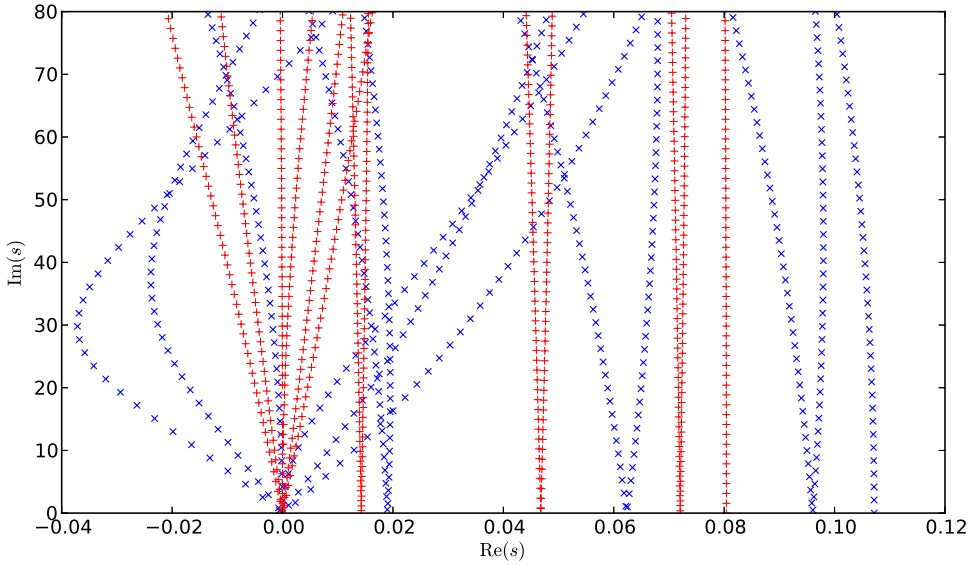

Figure 11.1: Resonance spectrum for the surfaces $X_{4,4,5}(\ell)$ for $\ell = 3$ (blue crosses) and $\ell = 4$ (red plus signs).

11 Numerical Illustration

In this section we will test the convergence of the rescaled spectrum towards the zeros of the polynomials P_{n_1,n_2,n_3}. The resonances are calculated by finding the zeros of the Selberg zeta function with the same algorithm as used by Borthwick [7] (see also [56, 43]) [3].

In Figure 11.1 we see the resonance spectrum of the surface $X_{4,4,5}(\ell)$ for two different ℓ-values ($\ell = 3$ as blue crosses, and $\ell = 4$ in red plus signs). Both plots show significant resonance chains. However, without rescaling, these chains are clearly different.The chains for $\ell = 4$ are denser and are positioned at significantly smaller real part and are much less curved than the chains for $\ell = 3$. Their rough structure is however very similar. From higher to lower real parts, both surfaces first have a single chain, then three pairs of chains that diverge from each other and finally six resonance chains that emerge from $s = 0$. This common structure can be completely understood by the zeros of the polynomial

$$P_{4,4,5}(z) = -4\,z^{13} + z^{10} + 4\,z^9 + 4\,z^8 - 2\,z^5 - 4\,z^4 + 1.$$

[3] In Appendix B it is explained how this algorithm has to be adapted for the gerealized zeta function

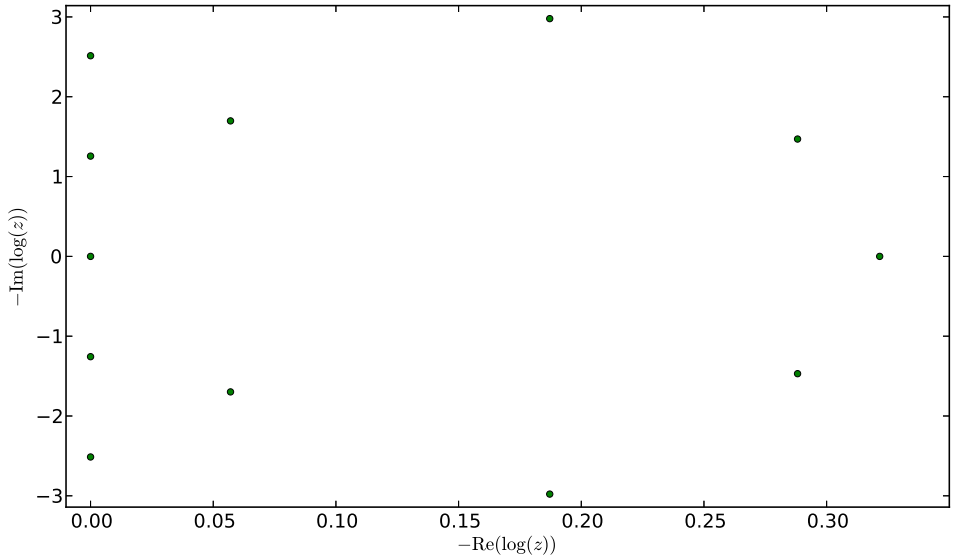

Figure 11.2: Solutions of the equation $P_{4,4,5}(z) = 0$ plotted on a negative logarithmic scale. The zero at $\log(z) = 0$ is of order two.

Figure 11.2 shows the solutions of $P_{4,4,5}(z) = 0$. As Theorem 6.1 provides a connection between the resonances and the zeros of $P(e^{-s})$ we have plotted $-\log(z)$ in order to compare the structure of the zeros directly with the resonances. And indeed the structure of the zeros of $P_{4,4,5}$ is exactly the same as the resonance chain structure. From higher to lower real parts (in the negative logarithmic plot of Figure 11.2) there is one leading zero, then three pairs of zeros which have the same real part and finally 5 zeros with real part equal to zero of which the zero with $\log(z) = 0$ is of order two. But not only the rough resonance structure is described by the zeros of $P_{4,4,5}$, also a large part of the rescaled spectrum is quantitatively well described by the zeros of $P_{4,4,5}(e^{-s})$. Figure 11.3 shows the rescaled spectrum for $\ell = 3$ and $\ell = 4$. Additionally the zeros of $P_{4,4,5}(e^{-s})$ are plotted in green circles. One sees that in the plot range already for $\ell = 4$ the first 7 rescaled chains do very well coincide with their limit values given by $P_{4,4,5}$. Only the chains emerging from zero are still very unstable and show a visible difference. Overall however more then 70 resonances in the plot range are quantitatively well described by $P_{4,4,5}$. For $\ell = 3$ the discrepancy is, as expected, higher however all resonances on the first chain are also very well approximated.

As a second example we show the same plots for the surfaces $X_{4,5,6}(\ell)$, this

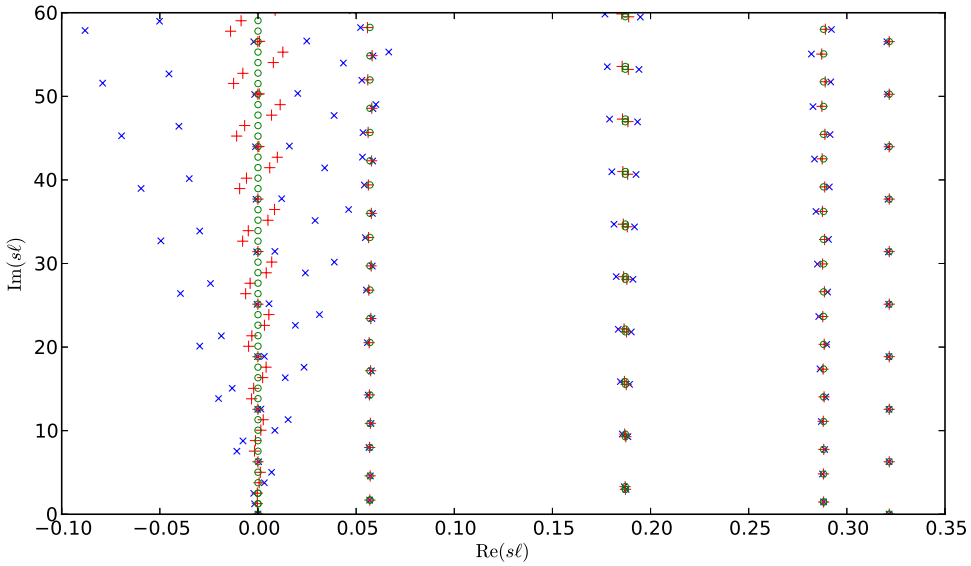

Figure 11.3: Rescaled resonances for the surface $X_{4,4,5}(\ell)$ for $\ell = 3$ (blue crosses) and $\ell = 4$ (red plus signs). Additionally the green circles indicate the zeros of the polynomial $P_{4,4,5}(e^{-s})$ in the plot range. One observes that the resonances of the different surfaces really lie on approximately the same points after rescaling and that the zeros of the polynomial $P_{4,4,5}(e^{-s})$ predict the position of most of the resonances for $\ell = 4$ already very well.

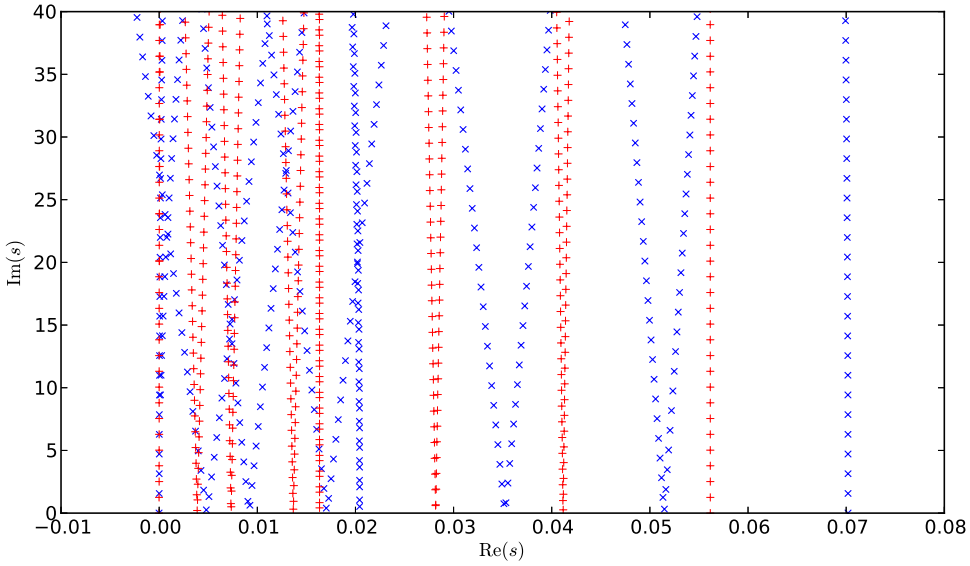

Figure 11.4: Resonance spectrum for the surfaces $X_{4,5,6}(\ell)$ for $\ell = 4$ (blue crosses) and $\ell = 5$ (red plus signs).

time for $\ell = 4$ and $\ell = 5$ (see Figure 11.4, 11.5 and 11.6). The corresponding polynomial is now given by

$$P_{4,5,6}(z) = -4\,z^{15} + z^{12} + 2\,z^{11} + 3\,z^{10} + 2\,z^9 + z^8 - 2\,z^6 - 2\,z^5 - 2\,z^4 + 1.$$

As this surface is even less symmetric, the zeros of the polynomial has an even more complex structure (Figure 11.5). Now there is one leading zero, then 6 pairs of zeros and finally a zero of order two at $\log(z) = 0$. This corresponds exactly to the more complex chain structure with one leading chain and 7 further pairs of chains (Figure 11.4). Finally, after rescaling, the position of a large part part of the plotted resonances agrees with the zeros of $P_{4,5,6}(e^{-s})$ (see Figure 11.6).

Increasing the parameter ℓ even further yields a better and better coincidence between the numerically calculated resonances and those predicted by the polynomial. For the surface $X_{12,12,12}$ we checked for example that the position of more then 150 individual resonances can be determined at a precision of 10^{-3} by calculating the zeros of the polynomial

$$P_{1,1,1}(z) = -4\,z^3 + 9\,z^2 - 6\,z + 1 = -(z-1)^2(4\,z-1)$$

which can in this case even be factorized by hand.

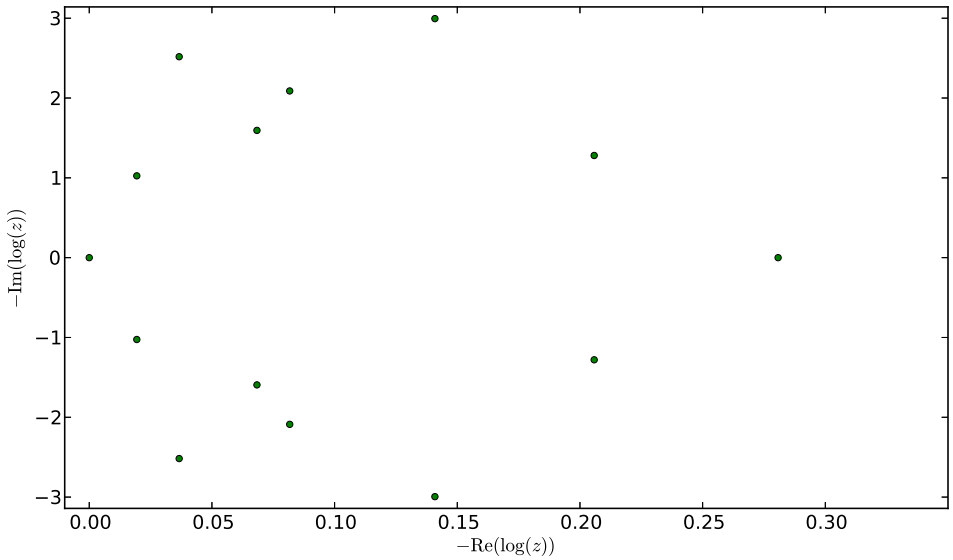

Figure 11.5: Solutions of the equation $P_{4,5,6}(z) = 0$ plotted on a negative logarithmic scale. The zero at $\log(z) = 0$ is of order two.

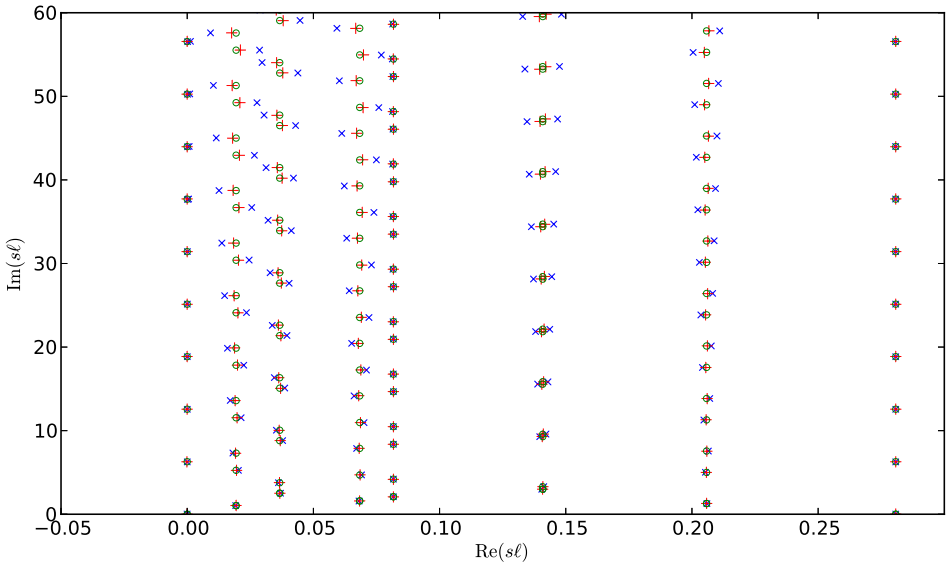

Figure 11.6: Rescaled resonances for the surface $X_{4,5,6}(\ell)$ for $\ell = 4$ (blue crosses) and $\ell = 5$ (red plus signs). Additionally the green circles indicate the zeros of the polynomial $P_{4,5,6}(e^{-s})$ in the plot range. One observes that the resonances of the different surfaces lie on approximately the same points after rescaling and that the zeros of the polynomial $P_{4,5,6}(e^{-s})$ predict the position of most of the resonances for $\ell = 5$ already very well.

Part III
Resonance chains in open systems and zeta functions

12 Introduction

The study of resonances in scattering systems with chaotic classical dynamics is an active field of research. It is at the same time driven by physicists being interested in the quantum properties of open chaotic systems as well as by mathematicians being interested in geometric analysis and partial differential equations (PDE) on non-compact manifolds. While in scattering theory, resonances are poles of the scattering matrix and correspond to quasi-stationary quantum states with purely in- or outgoing boundary conditions, from the PDE point of view resonances are often seen as the spectral invariants defined as the poles of a meromorphic continuation of the resolvent operator.

Aside from some very special exceptions (e.g. the Walsh quantized Baker map [67]) the position of the resonances of such complex systems cannot be determined exactly. It has, however, been a very successful approach to gain coarser information on general properties of the resonance distribution in terms of the underlying classical dynamics and geometry, respectively. For example results on spectral gaps [53, 68, 76] predict resonance free regions and the fractal Weyl law [85, 59, 84] gives an upper bound on the growth of the number of the so called "long living" resonances in the high frequency limit. Despite the large progress that has been made in obtaining rigorous results on the distribution of the resonances, there are still many open questions (we refer to [65] for an overview over recent results and open questions). For example the upper bound on the exponential growth of the resonance density which has been proven in the fractal Weyl law [66, 43, 85] is only conjectured to be sharp and there exists also a conjecture on the improvement of the spectral gap estimates [54]. It has thus been a very important approach to study the resonance structure numerically and by physical experiments in order to test the present conjectures and to show that the results on resonance distributions can be observed in real physical systems. There have been established two paradigmatic scattering systems for these kind of tests: the n-disk systems and Schottky surfaces.

A n-disk system describes the scattering of one particle at n-circular obstacles in the Euclidean plane (see Figure 13.1). It has been introduced by Gaspard-Rice [38, 39, 37] and Cvitanović-Eckhardt [25] in physics and by

Ikawa [53] in mathematics. In physics especially the completely symmetric 3-disk system, where 3 disks of the same size are arranged on a regular triangle, enjoys great popularity. It is already complex enough to have a classical dynamic with a non-trivial, fractal repeller and is still simple enough to be treated efficiently by numerics. There exist very efficient approaches to calculate the quantum resonances based on a direct scattering matrix ansatz [37] as well as by a semiclassical approach using zeta functions [25]. Consequently it has been among the first systems to numerically observe the fractal Weyl law [59]. Further importance arises from its experimental realizability [58] and in recent microwave experiments the spectral gap [4] and first hints of the fractal Weyl law [77] have been found. From a mathematical point of view the disadvantage of the n-disk system is that many of the numerical algorithms are not based on mathematical rigorous results. For example the conjecture that the zeros of the semiclassical zeta function are related to the quantum resonances, which has been thoroughly tested in physics [25, 94], is mathematically open (cf. [34, Section 1.6-1.8] for recent results into this direction).

This is the reason for the popularity of Schottky surfaces as an explicit model system in mathematics. Schottky surfaces are two-dimensional non-compact surfaces with constant negative curvature which are convex co-compact (see Figure 14.1 for a sketch of a 3-funneled Schottky surface). The constant negative curvature allows to prove that the zeros of the Selberg zeta function are related to the resonances of the Laplacian [72] and not only approximately as conjectured for the 3-disk system in physics. Furthermore Jenkinson-Pollicott [56] derived, analogously to the cycle expansion of the 3-disk system, efficient formulas to numerically compute the zeros of the Selberg zeta functions. The big drawback of these surfaces from the physical point of view is that there is no known experimental realization (see [83, 87] for attempts to realize the wave equation on negatively curved surfaces with water waves). As the curvature of these surfaces is, however, strictly negative, the geodesic flow is hyperbolic and these surfaces are an interesting model for open chaotic systems. Additionally the study of the resonances on constant negative curvature surfaces and the relation to their geometry is a mathematically interesting question itself (see e.g. [96]) thus we will call these resonances *geometric resonances*. The most simple example of Schottky surfaces which already has a non-trivial fractal repeller are the 3-funneled surfaces as shown in the upper part of Figure 14.1. For these surfaces Borthwick recently presented a thorough numerical study of their resonances structure [7].

One of the most surprising features of this resonance structure is an observation which has before already been made for the 3-disk system [37,

94]: Even though the underlying classical dynamic is completely hyperbolic, i.e. strongly chaotic, the distribution of the resonances is highly ordered and the resonances form a striking chain structure in the complex plane (see Figure 12.1). The 3-disk system and the Schottky surfaces are, however, not the only systems to embody these chain structures. Very similar chains have for example also been observed in higher dimensional systems, as the 4-sphere billiard [31], and even in microdisk resonators which are important models for physical applications such as microdisk lasers [93]. Furthermore the phenomenon of resonance chains is not only restricted to resonances of the Laplace operator and quantum resonances, respectively. Also the spectrum of the classical Ruelle resonances which describe the decay of correlations in classical dynamical systems has been reported to reveal these clear resonance chains [36].

Though these chains are eye-catching, little is known about these structures. For the completely symmetric 3-disk system and the completely symmetric 3-funneled Schottky surface, the distance between the resonances on one chain has been observed to be related to the length of the shortest periodic orbit [7, 94]. Additionally the oscillation length of the chains have been found to be to the length difference between two fundamental periodic orbits. Recently a numerical study of the 3-disk system [91] showed that the resonance chains are not only a visual effect, but that the resonances on one chain share common physical properties which are reflected in their scattering states, more precisely in their correlation behavior.

Two fundamental questions are, however, still open and will be addressed in this part of the thesis. First of all the resonance chains, are a visual impression, i.e. our brain groups the resonances to different chains and we have the impression that they are strung along different continuous lines. In this part we will give a system intrinsic definition of these continuous lines. Secondly, resonance chains have been observed in many, quite different systems. We will give a unifying condition on the classical length spectrum that is able to explain and predict the existence of resonance chains.

This part of the thesis is organized as follows: In Section 13 we treat the resonance chains of the symmetric 3-disk system. After a general introduction of 3-disk systems (Section 13.1) we will numerically illustrate that the resonance chains of the symmetric 3-disk system are created by fast rotating eigenvalues of a suitable transfer operator on the canonical Poincaré section. This idea applies for the semiclassical as well as for the classical resonances (Section 13.2). Then we give an introduction to Schottky surfaces (Section 14.1) and show in Section 14.2 that a straight forward application of this idea on the resonance spectrum of completely symmetric Schottky surfaces fails to explain the resonance chains. However, the ideas can be

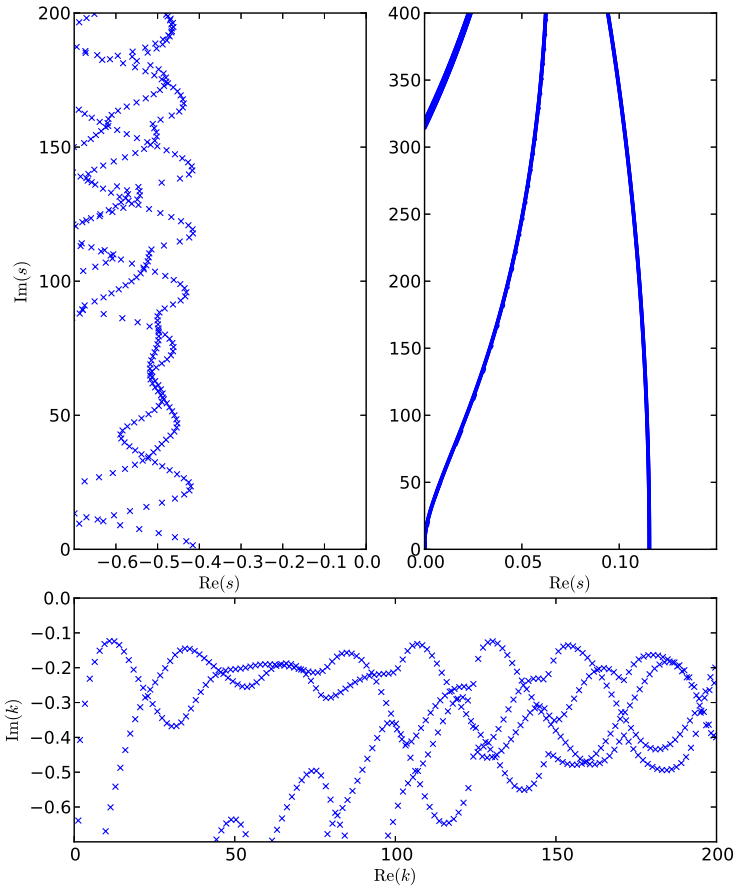

Figure 12.1: Resonance structure of the classical Ruelle resonances of the 3-disk system (upper left), the Schottky surface $X_{12,12,12}$ (upper right) and the quantum 3-disk system with $R/a = 6$ (lower). Note: the resonances for the Schottky surfaces are so dense that they appear as continuous lines in the plot above, however they are discrete. (Data for the 3-disk system provided by S. Barkhofen)

abstracted. This leads us to the introduction of a generalized zeta function and the generalized spectrum which are shown to be the right objects to describe and understand the resonance chains. These objects immediately also allow to deal with non-symmetric Schottky surfaces and 3-disk systems and also gives a condition for the existence of resonance chains (Section 14.3). In Section 15 we will finally test this condition in different cases and use its predictive power to identify systems incorporating different coexistent chain structures[4].

As this part of the thesis addresses a physical as well as a mathematical readership we decided to always state clearly which results and relations are known to be true by mathematically rigorous proofs and which results are achieved by physical arguments or experiments. This will help to keep an overview which parts of the argumentation are based on rigorous arguments and where further mathematical work remains to be done.

This part itself does not claim to derive any rigorous statements neither. Instead our aim is to gain a universal understanding of the appearance of the resonance chains and to identify the mathematical quantities, which are crucial for their understanding, via numerical investigations. As the question, whether a chain structure is visible or not, is mathematically not well posed but depends on the observer of the resonance structure, our condition cannot be an *if and only if* condition neither. The condition established in Section 14.2 is thus an approximate condition and our hypothesis is that the better this condition is fulfilled the clearer the chains will be visible. This hypothesis is tested and supported by various numerical results presented in Section 15. A rigorous proof of the existance of resonance chains is given in Part II, where the ideas and insights presented in this part are an essential ingredient.

13 3-disk systems and rotating resonances

13.1 Introduction to 3-disk systems

A 3-disk system describes one free particle in an Euclidean 2-dimensional space that scatters at three non-overlapping hard disks D_1, D_2 and D_3. For further use we will call the union of the disks by $D = \bigcup_i D_i$. Classically its trajectories are given by straight lines and hard wall reflections at the disk boundaries ∂D (see left panel of Figure 13.1). Its quantum dynamics

[4]While the importance of the generalized zeta function was first discovered during these numerical studies, it also turned out to be a central ingredient for the rigorous treatment in Part II

is described by the Laplacian Δ with Dirichlet boundary conditions at the disk boundaries and its quantum resonances can rigorously be defined as the poles of the resolvent

$$R(k) := (-\Delta - k^2)^{-1} : L^2_{\text{comp}}(\mathbb{R}^2 \setminus D) \to L^2_{\text{loc}}(\mathbb{R}^2 \setminus D). \tag{13.1}$$

This resolvent, as a map between compactly supported L^2 functions and locally L^2-integrable functions, is known to extend meromorphically to $\mathbb{C} \setminus l$ where l is any line connecting zero with infinity [89]. These poles do indeed coincide with the physical scattering resonances i.e. if k_n is a pole with multiplicity m, then there exist m solutions of

$$(-\Delta - k_n^2)\Psi = 0$$

with Dirichlet and purely outgoing boundary conditions. The latter condition means that the solution $\Psi(r, \phi)$ in polar coordinates (r, ϕ) can be written asymptotically in the limit $r \to \infty$ as [37]

$$\Psi(r, \phi) \sim \sum_{l=-\infty}^{\infty} C_l \frac{\exp(i(k_n r - l\pi/2 - \pi/4))}{\sqrt{2\pi k_n r}} \exp(il\phi).$$

Here C_l are constant coefficients and for fixed l the asymptotic r, ϕ dependence equals the asymptotic dependence of a free particle state with angular momentum l.

An important class of 3-disk systems are those which are completely symmetric. In those systems all three disks have the same size and the disks are arranged on an equilateral triangle (see left part of Figure 13.1). Historically the side length of the triangle is denoted by R and the disk radius by a [39]. These systems are then completely characterized, up to a scaling, by the ratio R/a. As the system is highly symmetric and possesses the symmetry group D_3 of the equilateral triangle often the symmetry reduced system is studied in physics. This system consists of an open billiard representing the fundamental domain of the 3-disk system (see light shaded region in left part of Figure 13.1).

As already mentioned before the classical time evolution of a particle between two disk reflections is just a linear propagation and thereafter hard wall reflections. The trajectory of a particle therefore does not depend on the absolute value of its momentum and we can always scale it to 1. It is furthermore convenient to get rid of the parts of linear propagation where no complex dynamic takes place and consider only the Poincaré section of disk reflections. A particle at the boundary of a disk D_i of radius a_i whose momentum is scaled to one, is completely described by its Birkhoff coordinates (q, p). They are defined as the arc length $q \in [-\pi a_i, \pi a_i]$ on the disk

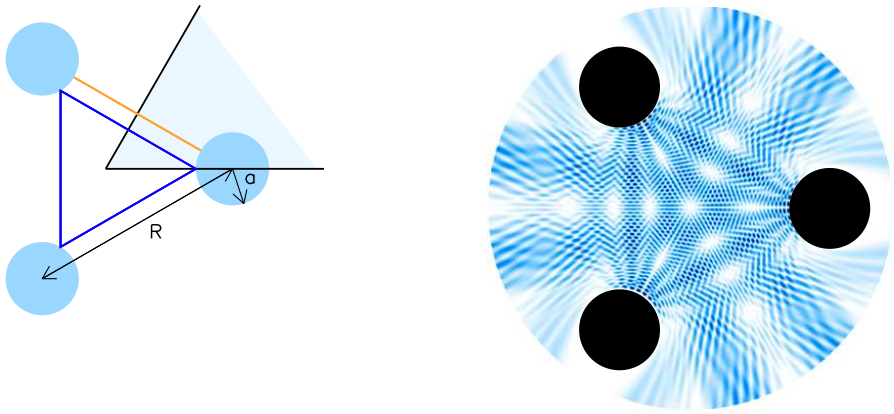

Figure 13.1: Left: Sketch of a symmetric 3-disk system and two classical closed trajectories (yellow and blue lines). The fundamental domain is shaded in light blue. The symmetry reduced billiard is then a billiard consisting of the fundamental domain with two additional hard walls along the symmetry axes. Right: Quantum mechanical scattering state with Dirichlet boundary conditions and purely outgoing boundary conditions calculated by the algorithm as described in [91]. Note that this scattering state is additionally vanishing along the symmetry axes and is thus also a scattering state of the symmetry reduced billiard with Dirichlet boundary conditions.

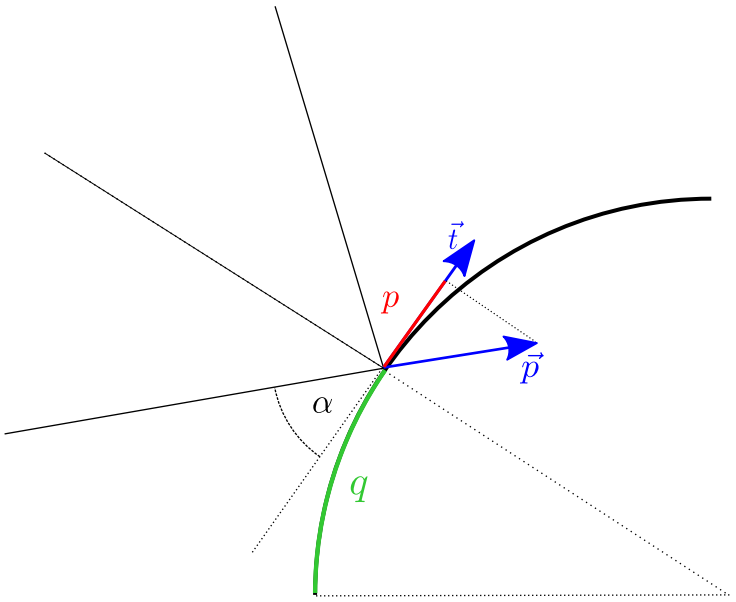

Figure 13.2: Sketch illustrating the Birkhoff coordinates. The Birkhoff coordinates of a trajectory being reflected at the disk boundaries are given by the position of the reflection on the boundary, measured by the arc length of the impact point with respect to a fixed reference point (denoted by q in the figure) and by the projection of the unit momentum vector on the unit tangent vector.

boundary as well as the projection of the normalized incoming momentum to the unit tangent vector at the disk boundary $p = \vec{p} \cdot \vec{t} = \cos(\alpha) \in [-1, 1]$ (see Figure 13.2). The complete space $\mathcal{P}$ of the Poincaré section consists of three copies of $[-\pi a_i, \pi a_i] \times [-1, 1]$. As the system is open the dynamics is not defined on all $\mathcal{P}$, because in many cases a particle with Birkhoff coordinates (q, p) will just escape to infinity after the reflection and will not hit any of the other disks in the future. We therefore introduce the forward trapped set $\mathcal{T}_+^{(n)}$ of order n as the set of all points in $\mathcal{P}$ which will hit at least n disks on their future trajectories. Analogously we define the backward trapped set $\mathcal{T}_-^{(n)}$ for the time inverted dynamics. The discrete time dynamics on the Poincaré section is then a diffeomorphism

$$\phi : \mathcal{T}_+^{(1)} \to \mathcal{T}_-^{(1)}.$$

Note that this diffeomorphism only leaves the trapped set

$$\mathcal{T} = \bigcap_{n=1}^{\infty} \mathcal{T}_+^{(n)} \cap \mathcal{T}_-^{(n)}$$

invariant which is known to be a fractal subset of $\mathcal{P}$ if the 3 disks are sufficiently far away from each other [38]. Using this discrete time dynamics we can define for any smooth function $V : \mathcal{T}_+^{(1)} \to \mathbb{C}$ the transfer operator $\mathcal{L}_V : C_0^\infty(\mathcal{T}_+^{(1)}) \to C^\infty(\mathcal{P})$ by setting

$$(\mathcal{L}_V f)(x) = V(\phi^{-1}(x)) f(\phi^{-1}(x))$$

which is an operator with integral kernel

$$K(x, y) = V(y)\delta(\phi^{-1}(x) - y). \tag{13.2}$$

In the theory of dynamical systems this function V is commonly called *potential function* even if V does not at all play the role of a potential in the sense of classical mechanics. With this transfer operator we can now introduce the zeta function. If we suppose that $\mathcal{L}_V$ can be extended to a Banach space $\mathcal{B}$ such that $\mathcal{L}_V$ is trace class then we can study the Fredholm determinant[5], also called dynamical zeta function

$$d_{\text{Fred}}(z) := \det(1 - z\mathcal{L}_V) = \exp\left(-\sum_{n>0} \frac{z^n}{n} \text{Tr}(\mathcal{L}_V^n)\right). \tag{13.3}$$

Under the trace class assumption, this function is then known to be analytic in z and the discrete spectrum $\sigma(\mathcal{L}_V)$ of the transfer operator is related to the zeros of the dynamical zeta function by

$$\sigma(\mathcal{L}_V) = \{z \in \mathbb{C} \setminus \{0\},\ d_{\text{Fred}}(1/z) = 0\}.$$

By the explicit form (13.2) of the kernel $K(x, y)$ we can on the other hand formally define the so called flat trace

$$\text{Tr}^\flat(\mathcal{L}_V^n) := \sum_{x \in \text{Fix}(\phi^n)} \frac{V_n(x)}{|\det(1 - (D\phi^n)(x))|},$$

where $(D\phi^n)(x) \in \mathbb{R}^{2\times 2}$ is the Jacobian of ϕ^n, $V_n(x) = \prod_{k=1}^n V(\phi^k(x))$ the iterated product and $\text{Fix}(\phi^n)$ the set of all fixed points of ϕ^n. By the flat trace we can define in complete analogy to (13.3) another zeta function by

$$d^\flat(z) := \exp\left(-\sum_{n>0} \frac{z^n}{n} \sum_{x \in \text{Fix}(\phi^n)} \frac{V_n(x)}{|\det(1 - (D\phi^n)(x))|}\right). \tag{13.4}$$

[5]To our knowledge such a function space is not known. In physics literature such an assumption is however often implicitly made.

By a standard calculation for zeta functions (see Appendix A) this expression can be brought to the form

$$d^\flat(z) := \prod_{p\in P}\prod_{k=0}^{\infty}\left(1 - z^{n_p}\frac{V_p}{|\Lambda_p|\Lambda_p^k}\right)^{k+1}. \tag{13.5}$$

Here P is the set of all *primitive periodic orbits* of the map ϕ, i.e. the set of all periodic orbits $\{x, \phi(x), \dots \phi^m(x) = x\}$ for which there is no $1 < k < m$ which also fulfills $\phi^k(x) = x$. Furthermore n_p is the discrete time length of this orbit, V_p is the iterated product of the potential V along the primitive orbit p and Λ_p is the eigenvalue of $D\phi^{n_p}(x_p)$ whose absolute value is larger than one.

It is important to note that the expressions (13.4) and (13.5) only converge absolutely for $|z|$ sufficiently small. Furthermore (13.4) directly implies that the zeta function has no zeros in the region of absolute convergence. Equations (13.4) and (13.5) are thus of no direct use for a calculation of the zeros of the dynamical zeta function. If one knows, however, that $d^\flat(z)$ can be extended analytically beyond the region of absolute convergence, its Taylor expansion in z around zero

$$d^\flat(z) = \sum_{n=0}^{\infty} C_n z^n$$

automatically converges absolutely on any disk contained in the region of analytic continuation. This trick has been introduced in physics by Cvitanović and Eckhardt [25] under the name cycle expansion.

From a mathematical point of view, the biggest challenge is to prove the analytic continuation of the zeta function defined by (13.4) and to show that its zeros correspond to the spectrum of $\mathcal{L}_V$. This is for example possible if one finds function spaces such that $\mathcal{L}_V$ is trace class and that its trace in this space equals the flat trace. Then one obtains by the analyticity of the Fredholm determinant automatically an analytic continuation of the zeta function. Such results are known for several classes of systems (for example for real analytic expanding or hyperbolic maps [80, 81, 33]) but to our knowledge not in any setting in which the 3-disk system fits.

Physicists usually skip this difficulty and test for concrete examples in which regions the cycle expansion numerically converges. It is then assumed that this region coincides with the region of analytic continuation. Furthermore it is usually assumed that the zeros of the zeta function defined by the flat trace (13.4) are eigenvalues of the transfer operator. As there is not yet a satisfying mathematical theory in the case of the 3-disk system we will also make these assumptions from now on.

For the 3-disk system two particular choices for the potential are of special interest as they lead to the classical zeta function and to the semiclassical or Gutzwiller-Vorros zeta function, respectively. The return time or return length of a particle at the disk boundary with Birkhoff coordinates $x \in \mathcal{T}_+^{(1)}$ is defined as the length of the trajectory until the next disk reflection. This defines a smooth bounded function

$$\tau : \mathcal{T}_+^{(1)} \to \mathbb{R}^+$$

and we first can consider for $s \in \mathbb{C}$ the analytic family of potentials

$$V_s^{cl}(x) = e^{-s\tau(x)}. \tag{13.6}$$

Plugging this potential into (13.5) we obtain a dynamical zeta function depending on two variables s, z

$$d^{cl}(s,z) := \prod_{p\in P}\prod_{k=0}^{\infty}\left(1 - z^{n_p}\frac{e^{-s\tau_p}}{|\Lambda_p|\Lambda_p^k}\right)^{k+1},$$

where τ_p is the Birkhoff sum along this orbit defined by

$$\tau_p = \sum_{k=1}^{n_p}\tau(\phi^k(x))$$

for x beeing an arbitrary point on the orbit p. It is related to the classical Selberg-Smale zeta function by [36]

$$Z(s) = d^{cl}(s,1).$$

This zeta function is of special interest because its zeros, the so-called Ruelle resonances, determine the decay of correlations of the classical dynamical system (at least for systems where the theory of Ruelle resonances is established, for the 3-disk system this is again conjectured to be true, c.f. [36]). This is why these zeta functions have been studied numerically by Gaspard and Ramirez [36] for the symmetric 3-disk system where they observed the resonance chains presented in Figure 12.1.

Using the ideas of [35] we can also express the Gutzwiller-Vorros zeta function by transfer operators. More precisely, we define the function $\Lambda(x)$ on $\mathcal{T}_+^{(1)}$ to be the restriction of the Jacobian $D\phi(x)$ to the unstable direction which is simply given by the multiplication with a nonzero number. If x is a fixed point of an iteration of the Poincaré map $\phi^n(x) = x$, then the iterated product of $\Lambda(x)$ is exactly the unstable eigenvalue Λ_n of $D\phi^n$.

With this function we define

$$V_s^{(a)}(x) = -|\Lambda(x)|^{1/2} e^{-s\tau(x)} \text{ and } V_s^{(b)}(x) = |\Lambda(x)|^{-1/2} e^{-s\tau(x)}$$

as well as the corresponding Fredholm determinants

$$d^{(a)}(s,z) = \det(1 - z\mathcal{L}_{V_s^{(a)}}) \text{ and } d^{(b)}(s,z) = \det(1 - z\mathcal{L}_{V_s^{(b)}}).$$

We can then study the quotient

$$\begin{aligned} \frac{d^{(a)}(s,z)}{d^{(b)}(s,z)} &= \exp\left(-\sum_{n>0} \frac{z^n}{n} \sum_{x\in \mathrm{Fix}(\phi^n)} \frac{e^{-s\tau_n(x)-in\pi} \left(|\Lambda_n(x)|^{1/2} - (-1)^n |\Lambda_n(x)|^{-1/2} \right)}{|\det(1 - (D\phi^n)(x))|} \right) \\ &= \exp\left(-\sum_{n>0} \frac{z^n}{n} \sum_{x\in \mathrm{Fix}(\phi^n)} \frac{e^{-s\tau_n(x)-in\pi}}{\sqrt{|\det(1 - (D\phi^n)(x))|}} \right). \end{aligned}$$

For the last equality we used that the Poincaré map is orientation inverting and consequently $\Lambda(x) < 0$ which implies that

$$\sqrt{|\det(1 - (D\phi^n)(x))|} = |\Lambda_n(x)|^{1/2} - (-1)^n |\Lambda_n(x)|^{-1/2}.$$

The final expression is related to the so called Gutzwiller-Vorros zeta function [90] by

$$Z_{GV}(k) = \frac{d^{(a)}(-ik,1)}{d^{(b)}(-ik,1)}. \tag{13.7}$$

It has been numerically thoroughly checked [25, 94] that the zeros of $Z_{GV}(k)$ coincide to a high precision to the quantum resonance which have numerically been obtained by a quantum scattering approach. It is conjectured that the zeros of the Gutzwiller-Vorros zeta function converge towards the quantum resonances in the semiclassical limit. This relation [39] is, however, based on the Gutzwiller-trace formula for the quantum propagator beyond the Ehrenfest time, and from the mathematical point of view the relation to the quantum spectrum is completely open [6]. For practical purpose this relation between the zeros of the zeta function and the quantum resonances has, however, a huge advantage because especially in the regime of high energies the calculations of the zeros of $Z_{GV}(k)$ via the cycle expansion is much faster than the calculation based on the quantum scattering matrix and it has been exploited in many numerical works on the quantum spectrum [59, 31, 93].

[6] For closed systems there has recently been derived a relation between the quantum and the so called prequantum operator which is an important step into this direction [34].

13.2 Rotating resonances

We now want to understand the resonance chains for the symmetric 3-disk system via the zeta functions introduced above. The zeta functions allow to handle the resonance chains for classical Ruelle resonances and quantum resonances by the same approach, even though the physical nature of these resonances is completely different.

In both cases one has a zeta function $Z(s,z)$ which depends on two complex variables and the resonances are defined by [7]

$$\text{Res} = \{s \in \mathbb{C},\ Z(s,1) = 0\}.$$

Note that for the quantum case we use the hypothesis that the semiclassical resonances (i.e. the zeros of the Gutzwiller-Vorros zeta function) and quantum resonances (i.e. the poles of the resolvent) coincide. We will, however, only use this correspondence for the symmetric 3-disk system in an energy regime, where this correspondence is known to hold with a very high precision [25, 94]. Beside the set of resonances which we have defined to be the zeros in s of $Z(s,z)$ for fixed $z = 1$ it seems also natural to consider for a fixed $s \in \mathbb{C}$ the zero set in z. In order to have a direct physical interpretation of this set we consider the inverses of these zeros and define for a fixed $s \in \mathbb{C}$

$$\sigma_s := \{z \in \mathbb{C} \setminus \{0\},\ Z(s,1/z) = 0\}\,. \tag{13.8}$$

Using the Fredholm determinant representation of the classical zeta function

$$Z_{cl}(s,z) = \det(1 - z\mathcal{L}_{V_s^{cl}})$$

one directly identifies $\sigma_s = \sigma(\mathcal{L}_{V_s^{cl}})$ which is the spectrum of $\mathcal{L}_{V_s^{cl}}$. For the semiclassical resonances this identification is slightly more subtle as Z_{GV} has been defined as the quotient of two zeta functions. If we assume, however, that $d^{(b)}(s,z)$ is analytic in a neighborhood of $z \in \sigma_s$, then the Gutzwiller-Vorros zeta function can only vanish if the nominator of the quotient vanishes, i.e. if

$$0 = d^{(a)}(s, z^{-1}) = \det(1 - z^{-1}\mathcal{L}_{V_s^{(a)}})$$

and $z \in \sigma(\mathcal{L}_{V_s^{(a)}})$. Note that the analyticity assumption of $d^{(b)}(s,z)$ is not very strong and and in the s-range which we will consider in the sequel it is always fulfilled (see Appendix C)

[7] In the case of quantum resonances the resonance set is usually the set $\text{Res} = \{k \in \mathbb{C},\ Z(-ik,1) = 0\}$ (see (13.7)). In order to emphasize the uniform approach to quantum and classical resonances as well as the geometric resonances on Schottky surfaces, we will, however, from now on consider the quantum resonances to be parametrized by $s = -ik$ which simply leads to a clockwise rotation by 90° of the quantum resonances in the plots.

Summarizing we have the following two objects in the classical as well as in the semiclassical or quantum case: On the one hand we have the resonance spectrum which equals the zeros of the zeta function in s for $z = 1$ and on the other hand we have for any $s \in \mathbb{C}$ the discrete set σ_s which can be interpreted as the eigenvalues of a transfer operator $\mathcal{L}_s$ which is parametrized by a complex number s. Obviously s_n is a resonance if and only if the operator $\mathcal{L}_{s_n}$ has 1 as an eigenvalue i.e.

$$s_n \in \text{Res} \Leftrightarrow 1 \in \sigma_{s_n}.$$

The simple but important observation is now the following: If we start with a resonance $s_0 \in \text{Res}$ of multiplicity one and continuously vary the parameter s then we can trace the eigenvalue which was equal to 1 for $s = s_0$ and which continuously depends on s. We will call this eigenvalue $\lambda_{s_0}(s)$. A closer look in the concrete form of our transfer operators $\mathcal{L}_s$ allows us to predict how the eigenvalues will approximately depend on s. In the quantum case for $\mathcal{L}_s = \mathcal{L}_{V_s^{(a)}}$ as well as in the classical case with $\mathcal{L}_s = \mathcal{L}_{V_s^{cl}}$ we have

$$\mathcal{L}_s = \mathcal{L}_0 e^{-s\tau(x)}$$

where $e^{-s\tau(x)}$ is simply the multiplication operator. In the case of the symmetric 3-disk system the return time is a smooth function which becomes more and more homogeneous the bigger R/a becomes. Assuming as a first order approximation that $\tau(x) \approx \tau_0 = R - 2a$ then

$$\lambda_{s_0}(s) = e^{-s\tau_0}.$$

If this approximation was exactly true and if we moved with s parallel to the imaginary axis, then the eigenvalue $\lambda_{s_0}(s)$ would simply rotate around zero on the unit circle. Note that by the definition of the resonance set, every s value for which $\lambda_{s_0}(s)$ crosses the value point 1 on the unit circle is itself a resonance. By this argument a single eigenvalue of $\mathcal{L}_{s_0}$ would create a whole chain of resonances, parallel to the imaginary axis.The resonances would be equally distributed along this chain with a distance of $2\pi/\tau_0$. As the return time is in reality not exactly constant one would expect that slight variations deform the chains and also lead to a distance variation between the extremal values of the return time.

It can be checked numerically that it is exactly this mechanism of a rotating eigenvalue of the operator $\mathcal{L}_s$ which creates the resonance chains. In Figure 13.3 this is visualized for the quantum resonances of the symmetric 3-disk system with $R/a = 6$. On the left we see can see a plot of the quantum

resonances s_n in the complex plane[8]. On the right we can see the spectrum of the transfer operator $\mathcal{L}_{V_s^{(a)}}$ The blue crosses indicate the eigenvalues with $|z| > 0.3$ for a s-value which equals the resonance $s_1 = -0.206 - 18.51i$. As expected we find an eigenvalue which is equal to 1. There is also another eigenvalue plotted which corresponds to the second chain which is nearby the chain to which s_1 belongs. There are further eigenvalues of the transfer operator near zero which we did not plot as the convergence of the zeta function becomes more and more complicated for small absolute values of z. The colored points show how the eigenvalue at 1 moves, if the s values varies between two resonances s_1 and $s_2 = -0.178 - 17.02i$. As suggested by the heuristic arguments above the eigenvalue moves along the unit circle in a clockwise orientation and creates the next resonances on the chain. Exactly the same can be observed for the classical Ruelle resonances of the 3-disk system with $R/a = 6$ (see Figure 13.4).

These numerical results do however not only confirm that the hypothesis that each resonance chain is created by a rotating $\mathcal{L}_s$-eigenvalue is true. They also indicate what the continuous mathematical object is, where the resonances are distributed on. Note that taking two neighboring resonances of one chain there are multiple paths to connect these two resonances. While each path will effectively lead to one rotation of $\lambda_{s_0}(s)$ around zero, there is only one such path, for which $\lambda_{s_0}(s)$ stays on the unit circle. As it can be seen in Figure 13.3 such a rotation on the unit circle is obtained if the two resonances are connected along the path which is suggested by the structure of the resonance chains. If one, however, takes a different path between the two resonances, then the corresponding eigenvalue of $\mathcal{L}_s$ will turn on a deformed circle around zero (see Figure 13.5 for an arbitrary path between the two resonances). We can thus define

$$\mathcal{C} := \{(s, z) \in \mathbb{C}^2, Z(s, z) = 0, |z| = 1\} \subset \mathbb{C}^2$$

and from the numerics above we conclude that the continuous object on which the resonances are distributed is given by $\mathrm{Pr}_s(\mathcal{C})$ where $\mathrm{Pr}_s : \mathbb{C}^2 \to \mathbb{C}$ is the projection on the s-component.

We have thus seen in this section that the resonance chains of the classical and the quantum resonances are generated by the same mechanism. As in both cases the resonances can be seen as the zero set in s of a zeta function, which can be represented as a Fredholm determinant of a s-dependent family of operators, the resonance chains are generated by single eigenvalues of $\mathcal{L}_s$ which circle around zero while s moves along the chains. Furthermore this

[8]Note that as discussed above the usual parametrization of quantum resonances is $k_n = is_n$.

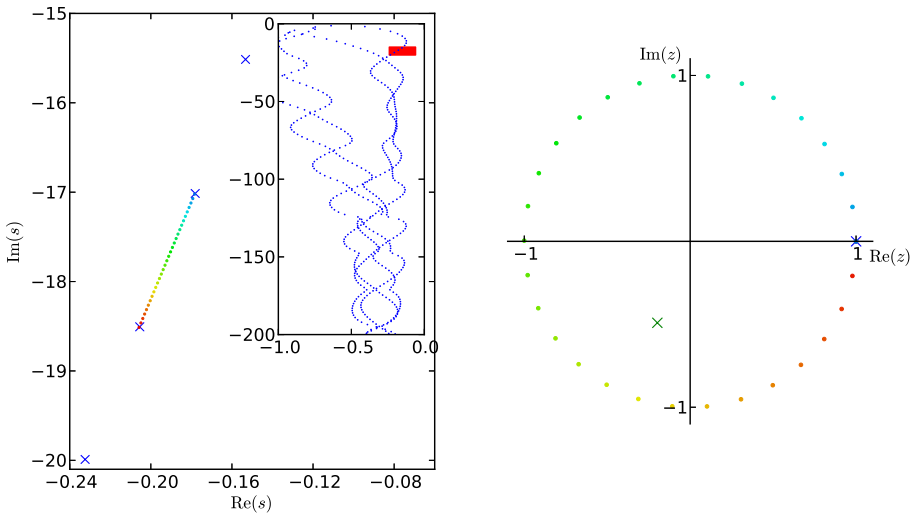

Figure 13.3: Left: Plot of the quantum resonances of the 3-disk system with $R/a = 6$. The inset shows the chain structure of the resonances on a large domain in the complex plane. The main plot shows a strong zoom into one chain, such that only few individual resonances are in the plot region (blue crosses). The region of the zoom is indicated in the inset by a red rectangle. The colored dots between the two resonances $s_1 = -0.206 - 18.51i$ and $s_2 = -0.178 - 17.02i$ represent a discrete interpolation between the two resonances. The interpolation follows the line suggested by the resonance chains. Right: Spectrum of the transfer operator on the Poincaré section. The blue crosses represent the spectrum of $\mathcal{L}_{s_1}$ with $|z| > 0.3$. By the colored dots we follow the evolution of the eigenvalue starting at 1 for s_1 while s varies as indicated by the colored points in the left panel. The evolution of the second eigenvalue is not plotted for more clarity. (Data provided by S. Barkhofen)

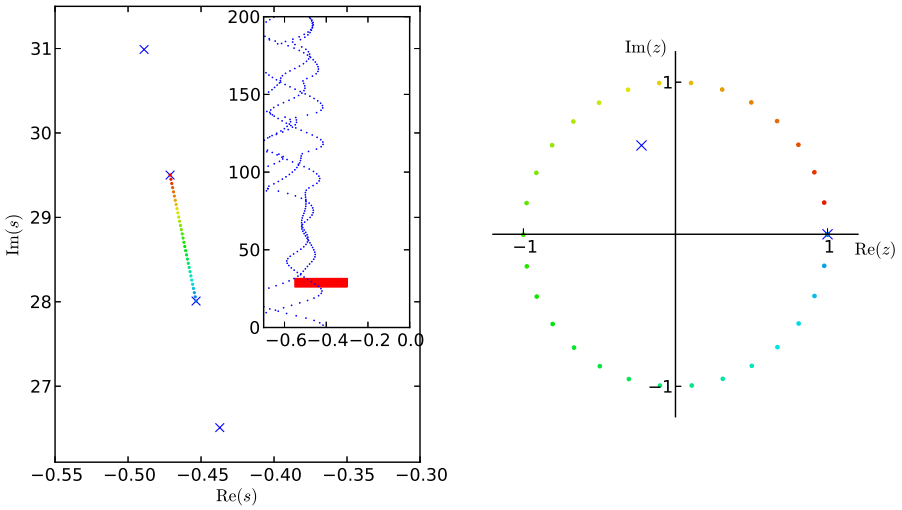

Figure 13.4: Left: Plot of the classical Ruelle resonances of the 3-disk system with $R/a = 6$. The inset shows the chain structure of the resonances on a large domaine in the complex plane. The main plot shows a strong zoom into one chain, such that only few individual resonances are in the plot region (blue crosses). The region of the zoom is indicated in the inset by a red rectangle. The colored dots between the two resonances $s_1 = -28.0 - 0.453i$ and $s_2 = 29.5 - 0.471i$ represent a discrete interpolation between the two resonances following the line suggested by the resonance chains. Right: Spectrum of the transfer operator on the Poincaré section. The blue crosses represent the spectrum of $\mathcal{L}_{s_1}$ with $|z| > 0.3$. By the colored dots we follow the evolution of the eigenvalue starting at 1 for s_1. (Data provided by S. Barkhofen)

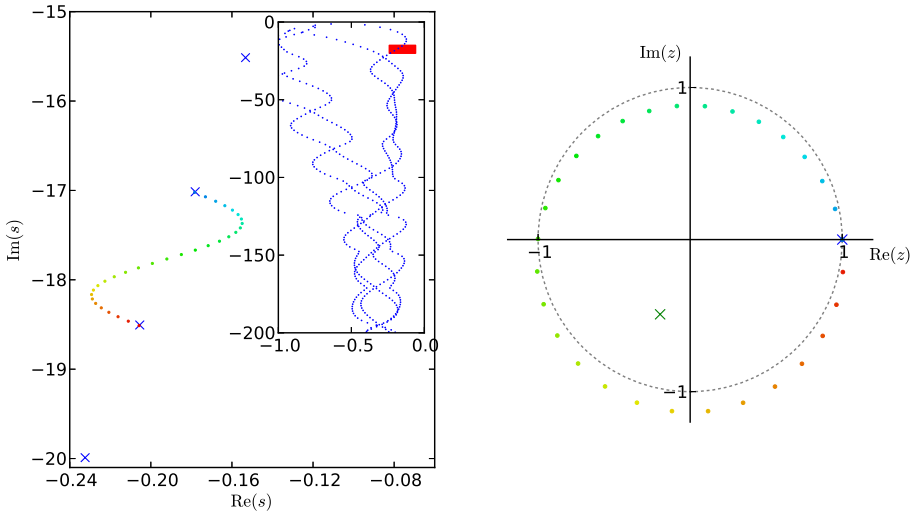

Figure 13.5: Same as in Figure 13.3. However the colored dots between the two resonances $s_1 = -0.206 - 18.51i$ and $s_2 = -0.178 - 17.02i$ now do not follow the line which is suggested by the resonance chains but a deformed path. As a consequence the eigenvalue of $\mathcal{L}_{s_1}$ starting at 1 for s_1 now turns one time around zero on a path which is not on the unit circle. (Data provided by S. Barkhofen)

approach allows a system-intrinsic definition of a continuous object that coincides with the visually suggested curves on which the resonances are strung together. In the next section we will see how this idea can be extended to the resonance chains on Schottky surfaces and examine in detail the question in which systems resonance chains will occur and in which not.

14 Schottky surfaces and generalized zeta functions

14.1 Introduction to Schottky surfaces

Schottky surfaces are a special class of infinite volume Riemann surfaces. In this section we will give a brief introduction to its most important properties. For a detailed introduction we refer to [5].[9]

The easiest way to define Schottky surfaces is as a quotient of the upper half plane by a so called Schottky group. The upper half plane $\mathbb{H} = \{u = x + iy \in \mathbb{C},\ y > 0\}$ together with the Riemannian metric $(dx^2 + dy^2)/y^2$ has a constant negative Gauss curvature $\kappa = -1$ and is a standard model of hyperbolic geometry. The group $SL(2,\mathbb{R})$ of real invertible matrices with determinant one acts on $\mathbb{H}$ via Moebius transformations

$$\begin{pmatrix} a & b \\ c & d \end{pmatrix} u := \frac{au+b}{cu+d}. \tag{14.1}$$

In fact for every $A \in SL(2,\mathbb{R})$ the Moebius transformation is an orientation preserving isometry and all orientation preserving isometries of the upper half-plane can be expressed as an $SL(2,\mathbb{R})$-action. A Schottky group is then a discrete subgroup $\Gamma \subset SL(2,\mathbb{R})$ which is constructed in the following way: Let $D_1, \ldots, D_{2r}$ be disks with centers on the real line and mutually disjoint closure. Then for every $1 \leq i \leq r$ there exists an element $S_i \in SL(2,\mathbb{R})$ that maps the boundary ∂D_i to the boundary of ∂D_{i+r} and the interior of D_i to the exterior of D_{i+r}. From the disjointness of the disks follows that the elements $S_1, \ldots, S_r$ are the generators of a free discrete subgroup

$$\Gamma = \langle S_1, \ldots, S_r \rangle \subset SL(2,\mathbb{R})$$

and such groups are called *Schottky groups*. The quotient

$$X = \Gamma \backslash \mathbb{H}$$

[9] Schottky surfaces play also a central role in Part II and IV. Section 7 contains also an introduction To these surfaces that is written in a slightly more rigorous style

is then again a surface with constant negative curvature and is called *Schottky surface*.

The 3-funneled surfaces, which we are interested in, are from the dynamical point of view the simplest nontrivial example and they are constructed from four disks arranged as in Figure 14.1. The surface can be thought as the set $\mathbb{H} \setminus \cup D_i$ glued together along the two dotted blue half circles as well as along the two dashed red half circles (see Figure 14.1). It is known that such 3-funneled Schottky surfaces are uniquely determined by the three lengths l_1, l_2, l_3 of the geodesics $\gamma_1, \gamma_2, \gamma_3$ that wind once around one of the 3-funnels (see upper part of Figure 14.1). Furthermore for any triple of positive numbers l_1, l_2, l_3 there exists a 3-funneled Schottky surface which has fundamental geodesics of this length and we will call this surface X_{l_1,l_2,l_3}.

In order to define the geometric resonances on a Schottky surface X we consider the positive Laplacian which is defined by the metric and which we call Δ_X and we define the resolvent

$$R_X(s) := (\Delta_X - s(s-1))^{-1}.$$

By Mazzeo-Melrose [60] and Guillope-Zworski [45] we know that the resolvent admits a meromorphic continuation and we define the resonance set Res_X again as the set of its poles. Note that the resolvent's parametrization is different from the parametrization via k in the 3-disk case, which leads to the fact that the resonance chains do not oscillate along the real axis but along the imaginary axis. This parametrization is, however, very useful as it admits the following exact relation between the resonances of the Laplacian and a zeta function.

Let P_X be the set of all primitive closed geodesics on X, i.e. those closed geodesics that cannot be obtained by repeting a shorter closed geodesic. If for $\gamma \in P_X$, $l(\gamma)$ denotes the length of the periodic geodesic, then the Selberg zeta function is defined as

$$Z_X(s) = \prod_{\gamma \in P_X} \prod_{m=0}^{\infty} \left(1 - e^{-(s+m)l(\gamma)}\right). \tag{14.2}$$

This product is known to converge uniformly on any compact set with $\mathrm{Re}(s) > 1$ and for X being a Schottky surface the Selberg zeta function is known to extend analytically to the whole complex plane $\mathbb{C}$ and there is the following relation between its zeros and the resonances of Δ_X: If $Z_X(s) = 0$ then s is either a topological zero with $s = 0, -1, -2, \ldots$ or a resonance i.e. $s \in \mathrm{Res}_X$ [72].

For Schottky surfaces we can express the Selberg zeta function as a Fredholm determinant of a transfer operator. We therefore define the *Bowen-*

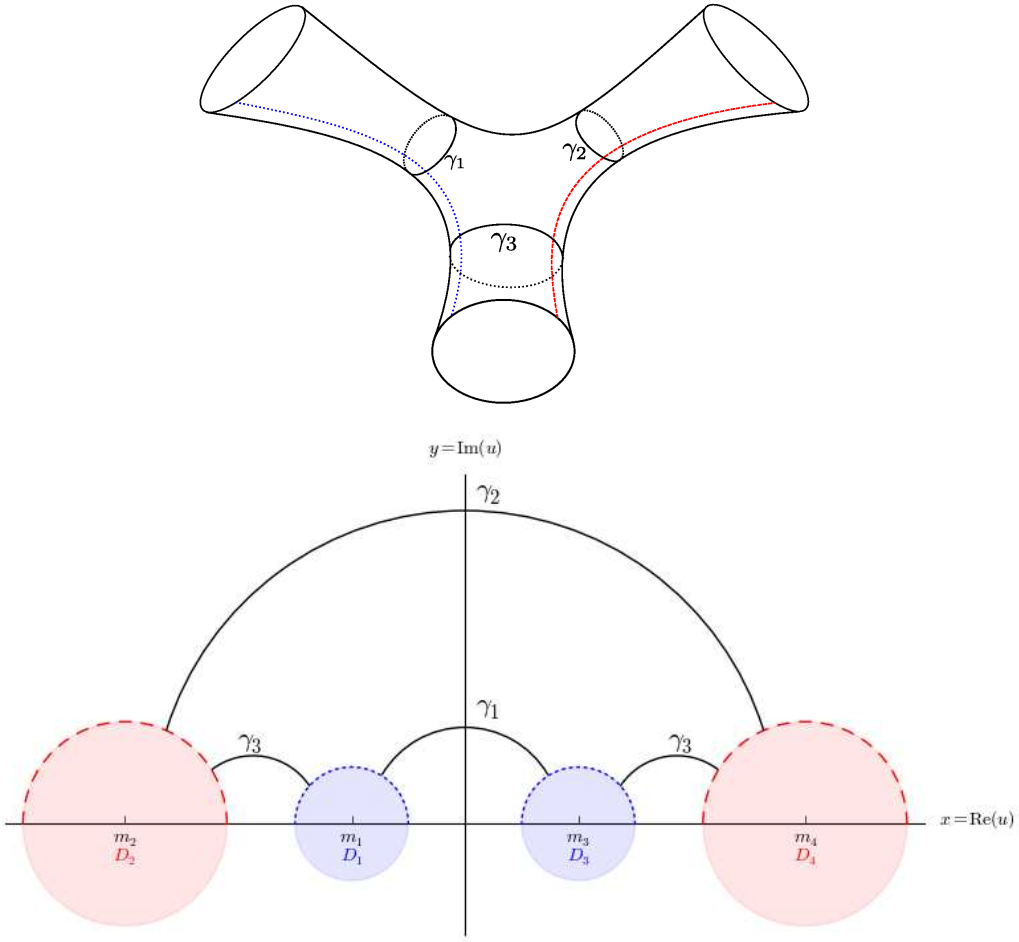

Figure 14.1: Upper part: Sketch of a Schottky surface with three funnels and the three fundamental closed geodesics $\gamma_1, \gamma_2, \gamma_3$. The dotted blue and dashed red lines indicate the lines along which the fundamental domain is glued together in order to obtain the surfaces. Lower part: Configuration of 4 disks that give rise to the construction of the Schottky group for a 3-funneled surface. The upper half plane without the disks represents a fundamental domain and the surface can be obtained by gluing together the red dashed lines with the blue dotted lines. In black the three fundamental closed geodesics $\gamma_1, \gamma_2, \gamma_3$ from the upper part of the figure are shown. While γ_1 and γ_2 are only represented by one arc each, the geodesic γ_3 appears as two arcs in the fundamental domain.

Series map [10] Schottky group $\Gamma = \langle S_1, \ldots, S_r \rangle$ by

$$B : \begin{cases} \bigcup_{i=1}^{2r} D_i & \to & \mathbb{C} \\ u & \mapsto & S_i u \text{ if } u \in D_i. \end{cases}$$

Here we used the convention that for $r < i \leq 2r$, $S_i := S_{i-r}^{-1}$. We can then define a family of transfer operators parametrized by $s \in \mathbb{C}$ via its action

$$(\mathcal{L}_s f)(u) := \sum_{v \in B^{-1}(u)} B'(v)^{-s} f(v),$$

where B' is the complex derivative of the Bowen-Series map and $u \in \cup_i D_i$. These transfer operators are known to be trace class on the space of holomorphic L^2-functions on $\cup_i D_i$ (see [80] for the original proof in slightly different functions spaces or [5, Lemma 15.6]) and one therefore knows that its dynamical zeta function

$$d_{BS}(s, z) := \det(1 - z\mathcal{L}_s)$$

is analytic. We will give a short sketch of the idea how to relate the dynamical zeta function to the Selberg zeta function. For more details we refer to [5, Section 15.3]. One first can proof that the trace of $\mathcal{L}_s$ equals its flat trace and obtains

$$d_{BS}(s, z) = \exp\left(- \sum_{n>0} \frac{z^n}{n} \sum_{u \in \mathrm{Fix}(B^n)} \frac{(B^n)'(u)^{-s}}{|1 - (B^{-n})'(u)|} \right). \tag{14.3}$$

As in the case of the 3-disk system (cf. equation (13.5) and Appendix A) one can transform the dynamical zeta function into a product over prime orbits of the Bowen-Series map B. In a second step one can prove that the set of primitive periodic geodesics is in one-to-one correspondence to the primitive periodic orbits of the Bowen-Series maps, i.e. for each $\gamma \in P_X$ there exists a unique $n \in \mathbb{N}$ and a periodic orbit $\{u, B(u), \ldots, B^n(u) = u\}$ and the length of the geodesic is related to the stability of the fixed point by

$$e^{l(\gamma)} = (B^n)'(u).$$

[10] Note that in Part II and IV we study the Bowen-Series IFS. They are obtained by inverting the Bowen-Series maps and technically more complicated because they are not univalued. As we do not need the notion of a general IFS in this part of the thesis I decided to work with the Bowen-Series maps instead of the of an IFS.

If we denote this n as the *Bowen-Series order* $n_{BS}(\gamma)$ of the geodesic γ, then we obtain, combining all arguments

$$d_{BS}(s,z) = \prod_{\gamma \in P_X} \prod_{m=0}^{\infty} \left(1 - z^{n_{BS}(\gamma)} e^{-(s+m)l(\gamma)}\right). \tag{14.4}$$

In particular this yields $d_{BS}(s,1) = Z_X(s)$ and we deduce that $s \in \mathrm{Res}_X$ implies that $\mathcal{L}_s$ has an eigenvalue equal to 1.

14.2 Generalized zeta function and spectra

The previous discussion on the relation between the spectrum of $\mathcal{L}_s$ and the resonances of the Laplacian, together with the observations from Section 13.2 that for 3-disk systems rotating eigenvalues of a transfer operator create the resonance chains would suggest that the resonance chains for the 3-funneled Schottky surfaces are generated by rotating eigenvalues of the Bowen-Series transfer operator $\mathcal{L}_s$. However, this idea fails completely to explain the resonance chains for the 3-funneled symmetric surfaces: In Figure 14.2 we have plotted for $X_{12,12,12}$ the spectrum of $\mathcal{L}_s$ for different s-values interpolating between two resonances s_1 and s_2. We observe that the eigenvalues start to turn while we move along the chain. However, the eigenvalue which was equal to 1 for $s = s_1$ is drawn towards zero and when we approach $s = s_2$ it is another eigenvalue of $\mathcal{L}_s$ which has been coming out from the interior, that creates the next resonance. In order to understand, why a direct application of the idea of rotating eigenvalues to the spectrum of the Bowen-Series transfer operator $\mathcal{L}_s$ fails, we recall that for the 3-disk system it has been an important argument that the return time of the Poincaré section is very homogeneous. This assumption is however not at all fulfilled for the standard Bowen-Series map, which corresponds morally to a Poincaré section[11] indicated by the blue and red lines in Figure 14.1. The return time or return length respectively is thus very inhomogeneous: While for the closed geodesics γ_1 and γ_2 it is equal to 12, it equals only 6 for the geodesic γ_3 as this geodesic crosses the Poincaré section twice.

In order to fix this issue we could try to construct another transfer operator which still has the property that its dynamical zeta function is related to the Selberg Zeta function but which has a homogeneous return time for the completely symmetric 3-funneled Schottky surface. Such a construction is in

[11] To be more precise, a Poincaré section along these two lines would by a bijective hyperbolic map on a two dimensional space. The Bowen-Series map can then be obtained as the restriction of this Poincaré map to the instable direction, which makes it expanding but not invertible anymore.

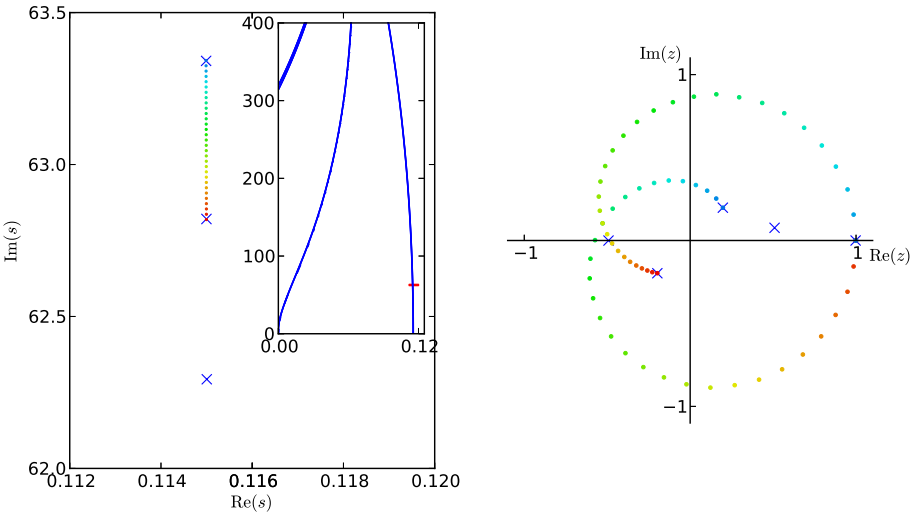

Figure 14.2: Left: Plot of the resonances of $X_{12,12,12}$. The inset shows the chain structure of the resonances on a large domain in the complex plane. The main plot shows a strong zoom into one chain, such that the individual resonances become visible (blue crosses). The region of the zoom is indicated in the inset by a red rectangle. The colored dots between the two resonances $s_1 = 0.1150{+}62.82i$ and $s_2 = 0.1150{+}63.34i$ represent a discrete interpolation between the two resonances, following the line suggested by the resonance chains. Right: Spectrum of the Bowen-Series transfer operator with $|z| > 0.2$. The blue crosses represent the spectrum of $\mathcal{L}_{s_1}$. By the colored dots we follow the evolution of two particular eigenvalues, as the s-values evolve as indicated by the colored points in the left panel. We only follow the evolution of the eigenvalue starting at 1 for s_1 and the one ending at 1 for s_2. The evolution of the other eigenvalues is not shown for more clarity.

principle possible (see Part II, Section 9), this solution would then, however, be restricted to completely symmetric Schottky surfaces. Non-symmetric surfaces, for which resonance chains have also been observed, would then need a construction of more and more complicated transfer operators. We will thus choose a different approach and work directly with the zeta functions which turns out to be much more flexible. Looking at equation (14.4) the choice of the Poincaré section appears only in the order function n_{BS}. This order function has been defined as the length of the prime B-orbit which is associated to the primitive geodesic γ and it is exactly given by the number of times the geodesic passes one of the cut lines in Figure 14.1. Instead of construction another Poincaré section we can also directly modify the zeta function and we can introduce for each map

$$\mathbf{n} : P_X \to \mathbb{N}$$

the *generalized zeta function*

$$d_{\mathbf{n}}(s,z) := \prod_{\gamma \in P_X} \prod_{m=0}^{\infty} \left(1 - z^{\mathbf{n}(\gamma)} e^{-(s+m)l(\gamma)}\right). \tag{14.5}$$

Of course for a general order function $\mathbf{n}$ it is not directly clear where this product converges and whether it has an analytic extension. For all order functions that will appear in the sequel, one can however show, that such an analytic extension exists and we refer to Part II, Theorem 6.2 for a rigorous proof. The important observation is now that changing the order function only changes the values of the dynamical zeta functions for $z \neq 1$ and one has still the important relation

$$d_{\mathbf{n}}(s,1) = Z_X(s). \tag{14.6}$$

We can therefore define in analogy to the spectrum of the transfer operator (13.8), the *generalized spectrum*

$$\sigma_s^{(\mathbf{n})} := \{z \in \mathbb{C} \setminus \{0\},\ d_{\mathbf{n}}(s, 1/z) = 0\}. \tag{14.7}$$

From (14.6) we conclude that also for this generalized spectrum we have the important relation

$$s \in \mathrm{Res}_X \Rightarrow 1 \in \sigma_s^{(\mathbf{n})}.$$

Thus instead of tracing the eigenvalues of a transfer operator we can follow the generalized spectral values while interpolating between different resonances on one chain. The order function which would correspond to a Poincaré section of the symmetric surface $X_{12,12,12}$ with a homogeneous return

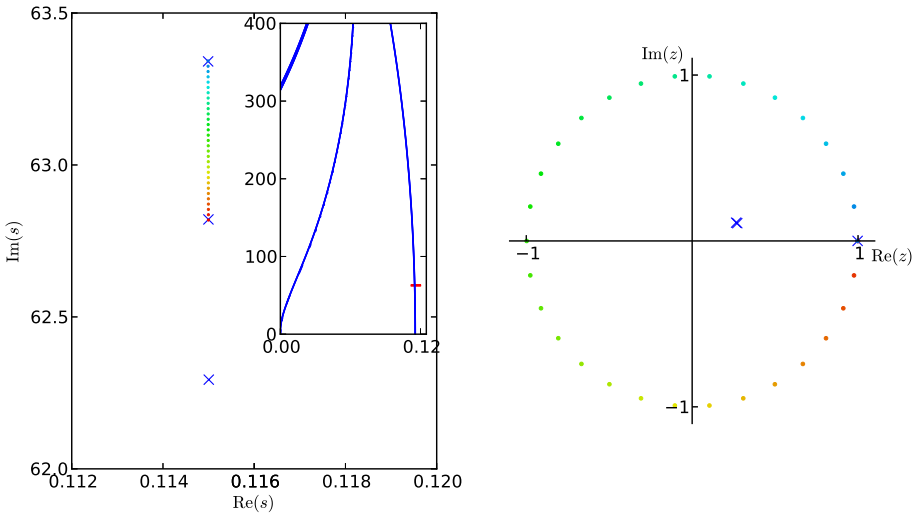

Figure 14.3: Left: Same as in Figure 14.2. Right: Plot of the generalized spectrum $\sigma_s^{(\mathbf{n})}$ with $|z| > 0.2$ for an order function that counts the number of windings around the funnels. The blue crosses represent the spectrum $\sigma_{s_1}^{(\mathbf{n})}$. By the colored dots we follow the evolution of the spectral value which equals 1 for $s = s_1$. The evolution of the other spectral values is not shown for more clarity.

time would just be an order function which counts for each closed geodesic how often it winds around one of the funnels. In Figure 14.3 we traced the generalized spectrum while we interpolate between the same two resonances as in Figure 14.2 and indeed we observe that the generalized spectral value which equals 1 for $s = s_1$ starts to turn around zero and creates all the other resonances on this chains by passing through 1. Additionally we see in Figure 14.3 that if the s-values follow the path which is suggested by the resonance chains, then the generalized spectral value stays on the unit circle. The continuous lines on which the resonances lie can thus be understood by the real analytic variety

$$\mathcal{C}_{\mathbf{n}} = \{(s, z) \in \mathbb{C}^2, d_{\mathbf{n}}(s, z) = 0, |z| = 1\}. \tag{14.8}$$

Precisely they are again given by $\mathrm{Pr}_s(\mathcal{C}_{\mathbf{n}})$, the projection of this variety on the s-component.

This approach of working with a generalized zeta function immediately allows us also to understand resonance chains for non-symmetric surfaces, too. These chains have first been observed by Borthwick, for example for

the surface $X_{12,13,14}$ (cf. [7, Figure 7]). A homogeneous return time would here require to cut one turn around the first funnel into 12 pieces, one turn around the second funnel into 13 and a turn around the third funnel into 14 pieces. We therefore define for $n_1 = 12, n_2 = 13, n_3 = 14$ the order function

$$\mathbf{n} : \begin{cases} P_X & \to & \mathbb{N} \\ \gamma & \mapsto & \sum_{i=1}^{3} n_i w_i(\gamma) \end{cases} \tag{14.9}$$

where $w_i(\gamma)$ counts the windings of the geodesic around the i-th funnel. Figure 14.4 shows the generalized spectrum for this order function and in fact it perfectly explains the resonance chains. Again the spectral value turns exactly once around the unit circle and creates the next resonance on the chains when the s value moves along the chains. Note that the two other spectral values in $\sigma_{s_1}^{(\mathbf{n})}$ (blue crosses in the left part of Figure 14.4) seem also to lie on the unit circle, which is not the case. Their absolute values are 1.0056 and 1.0032 and they belong to nearby chains, which are visible in the left part of Figure 14.4. There are also further spectral values with absolute value slightly smaller then one. We however decided to not plot them in Figure 14.4 for more clarity and as a reliable calculation of the generalized spectrum becomes more and more complicated for small absolute values of z as the order function $\mathbf{n}$ appears with high exponents (cf. Appendix B).

14.3 The length spectrum and existence of resonance chains

From the examples in the previous section we have learned that the resonance chains for symmetric as well as for asymmetric Schottky surfaces are best understood in terms of the generalized zeta function for a suitable choice of an order function. Up to now we have only presented two examples in (Figure 14.3 and Figure 14.4) together with a good choice of an order function but we have not yet clearly worked out under which circumstances it is possible to construct a "good" order function. We will see that this question automatically leads us to a condition on the observability of resonance chains.

The primitive length spectrum, which contains the lengths of all primitive closed geodesics, repeated by multiplicity, can be seen for $X_{12,12,12}$ in Figure 14.5 and for $X_{12,13,14}$ in Figure 14.6. We see that the length spectra of both surfaces form a clear clustering on multiples of a base length ℓ.

The big difference between these two cases is that the common base length to all clusters is $\ell = 12$ for $X_{12,12,12}$ and $\ell = 1$ for $X_{12,13,14}$. Analyzing the two order functions which we have used in these examples, we observe that they

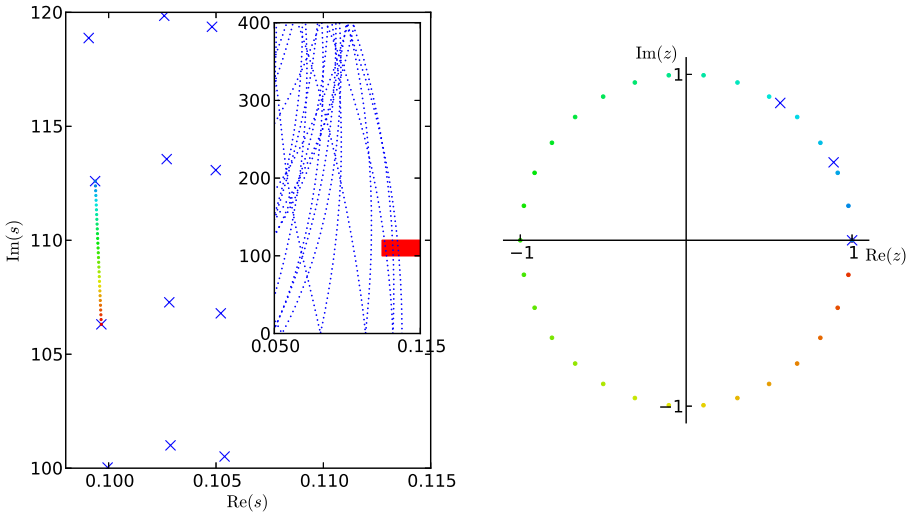

Figure 14.4: Left: Plot of the resonances of $X_{12,13,14}$. The inset shows the chain structure of the resonances on a large domain in the complex plane. The main plot shows a zoom into one chain, such that the individual resonances become better distinguishable (blue crosses). For orientation the region of the zoom is indicated in the inset by a red rectangle. The colored dots between the two resonances $s_1 = 0.09966+106.31i$ and $s_2 = 0.09938+112.59i$ represent a discrete interpolation between the two resonances following the line suggested by the resonance chains. Right: generalized spectrum for the order function as defined in (14.9) with $n_1 = 12, n_2 = 13, n_3 = 14$ for spectral values with $|z| > 0.995$. The blue crosses represent the spectrum $\sigma_{s_1}^{(\mathbf{n})}$. By the colored dots we follow the evolution of one spectral value as the s-values evolve as indicated by the colored points in the right panel. We only follow the evolution of the spectral value starting at 1 for $s = s_1$ for more clarity.

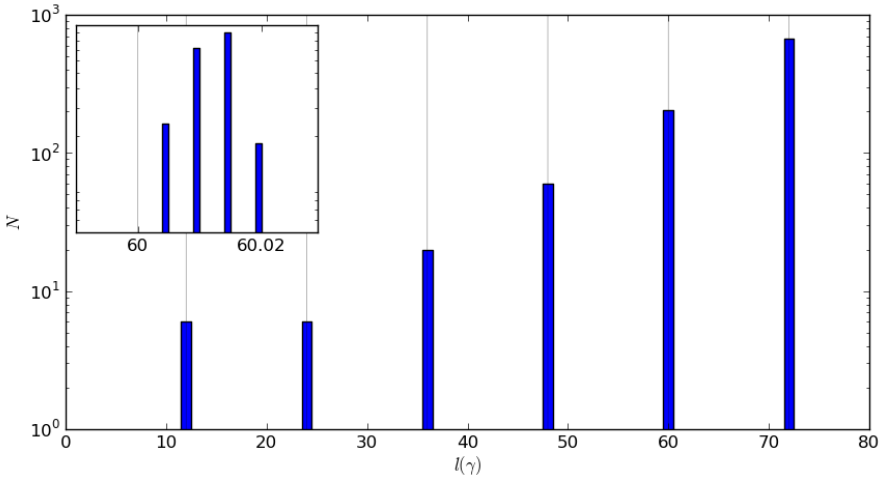

Figure 14.5: Histogram of the primitive length spectrum for the surface $X_{12,12,12}$. The thin light lines indicate the integer multiples of the base length 12 and one observes that the lengths form clear clusters around these values. This clustering is however not perfect as can be seen in the inset where a histogram with a much smaller binsize resolves the peak at a length equal to 60.

exactly respect this clustering: All geodesics of one cluster are mapped to the same integer which is given by the multiple of the base length ℓ on which the cluster is located. All geodesics that are necessary to be taken into account for the calculation of the resonances fulfill very well the approximation

$$l(\gamma) \approx \mathbf{n}(\gamma) \cdot \ell. \tag{14.10}$$

If this condition would be exactly fulfilled, then this would lead, similar to the case of a constant return time in Section 13.2, to the existence of straight resonance chains. In fact under this assumption the generalized zeta function could be written as

$$d_{\mathbf{n}}(s,z) := \prod_{\gamma \in P_X} \prod_{m=0}^{\infty} \left(1 - (ze^{-s\ell}e^{-m\ell})^{\mathbf{n}(\gamma)}\right),$$

and if $s_0 \in \mathrm{Res}_X$, i.e. $d_{\mathbf{n}}(s_0, 1) = 0$ then for all $b \in \mathbb{R}$ also $d_{\mathbf{n}}(s_0 + ib, e^{ib\ell}) = 0$. This condition, however, directly implies that $s_0 + 2\pi ki/\ell \in \mathrm{Res}_X$ for each $k \in \mathbb{Z}$, so all resonances would equidistribute on straight lines with a distance of $2\pi/\ell$. If (14.10) holds only approximately, then we expect that this straight chains start to bend and that the spacing of the resonances along the chains becomes more irregular.

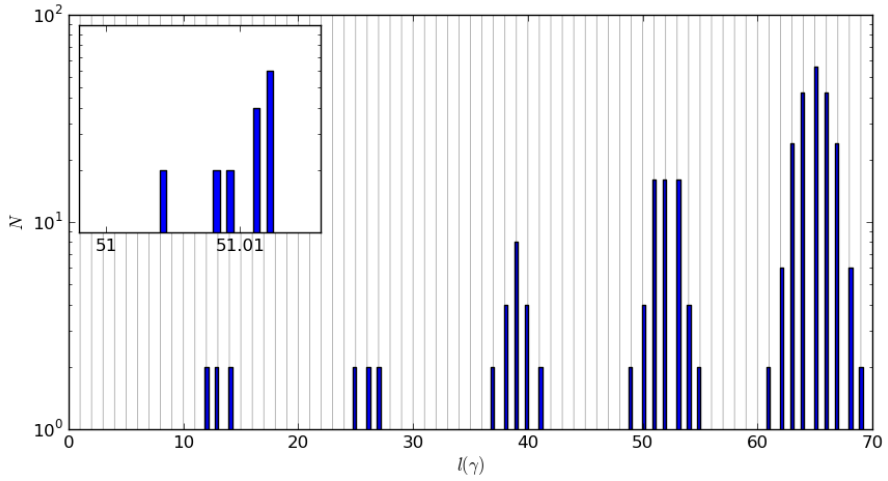

Figure 14.6: Histogram of the primitive length spectrum for the surface $X_{12,13,14}$. The thin light lines indicate the integer multiples of the base length 1 and one observes that the lengths form clear clusters around these values. Again this clustering is not perfect as can be seen in the inset where a histogram with a much smaller binsize resolves the peak at a length equal to 51.

We therefore can formulate the following hypothesis:

If the primitive length spectrum of an infinite volume Riemannian surface (or an open Euclidean billiard) forms clusters at integer multiples of a base length, i.e. if there is a length ℓ and an order function $\mathbf{n} : P_X \to \mathbb{N}$ such that (14.10) holds, then one will observe resonance chains. These chains will be described by the projection $\mathrm{Pr}_s(\mathcal{C}_\mathbf{n})$ of the analytic variety $\mathcal{C}_\mathbf{n} := \{d_\mathbf{n} = 0\} \cap \{|z| = 1\}$ to the s-component and the resonances will be approximately spaced by a distance of $2\pi/\ell$ on these lines. The worse the approximation (14.10) is fulfilled, the stronger the chains will bend and the more irregular the resonance distribution on the chains will become.

Of course (14.10) cannot hold on the whole length spectrum, but recall that for the calculation of the resonances in a bounded subset of a complex plane, one only needs finitely many geodesics. We thus suppose that the chains will be observable in this bounded domain, if (14.10) is fulfilled on the geodesics which are necessary for their calculation.

15 Further tests of the hypothesis

We already saw several examples in Section 13.2 and 14.2 which support our hypothesis on the existence of resonance chains. We will now test its validity against some more examples. First of all our condition should be able to explain the non-observability of resonance chains in some systems which are structurally similar to systems which show resonance chains.

For example one observes that symmetric 3-disk billiards only show resonance chains if the disks are sufficiently far away from each other. The resonance spectrum of the symmetric 3-disk billiard with $R/a = 3$ shows no chain structure contrary to the more open case with $R/a = 6$ (see Figure 15.1). This is easily understood by looking at the primitive length spectrum. While for $R/a = 6$ one sees a clear clustering of the lengths, the length spectrum for $R/a = 3$ equidistributes very quickly and it is impossible to choose an order function which fulfills (14.10). Our hypothesis also explains why symmetric 4-disk systems show in general no chain structure (see e.g. FIG. 13 in [36] for the Ruelle resonances of a 4-disk system) whereas the 3-dimensional 4-sphere billiard shows them: If 4 disks are distributed on a square, the lengths between two neighboring disks and the length between diagonal disks are in general not multiples of each others but form two incommensurable base lengths, so it will not be possible to construct a good order function. For the 4-sphere billiard where the spheres are placed on a regular tetrahedron, the distance between an arbitrary pair of spheres is equal and, if the spheres are sufficiently far away from each other, one expects a clustering of the length spectrum on multiples of this base length. Exactly in this case of sufficiently open 4-sphere billiards the chain structure has been observed (cf. Figure 5.2-5.9 in [30]).

We will end this section by using the predictive power of our hypothesis in order to identify a new interesting system which shows the coexistence of two chains. As we only demand (14.10) to hold approximately there should be examples for which there are different compatible base lengths and order functions, e.g. the surface $X_{12,12,13}$. As can be seen in Figure 15.2 the length spectrum can be either interpreted as forming clusters at multiples of the base length $\ell = 12$ or at multiples of the base length $\ell = 1$. The hypothesis thus predicts two different chain structures, one where the resonances are spaced by a distance of $2\pi/12$ and another one with a larger spacing of 2π. As for $\ell = 12$ the approximation (14.10) holds much worse then for $\ell = 1$ our hypothesis predicts that the resonance chains belonging to $\ell = 12$ are much more twisted then the chains belonging to $\ell = 1$. As Figures 15.3 and 15.4 show, all these predictions are fulfilled in the resonance structure. Choosing the order function (14.9) with $n_1 = n_2 = n_3 = 1$ which corresponds

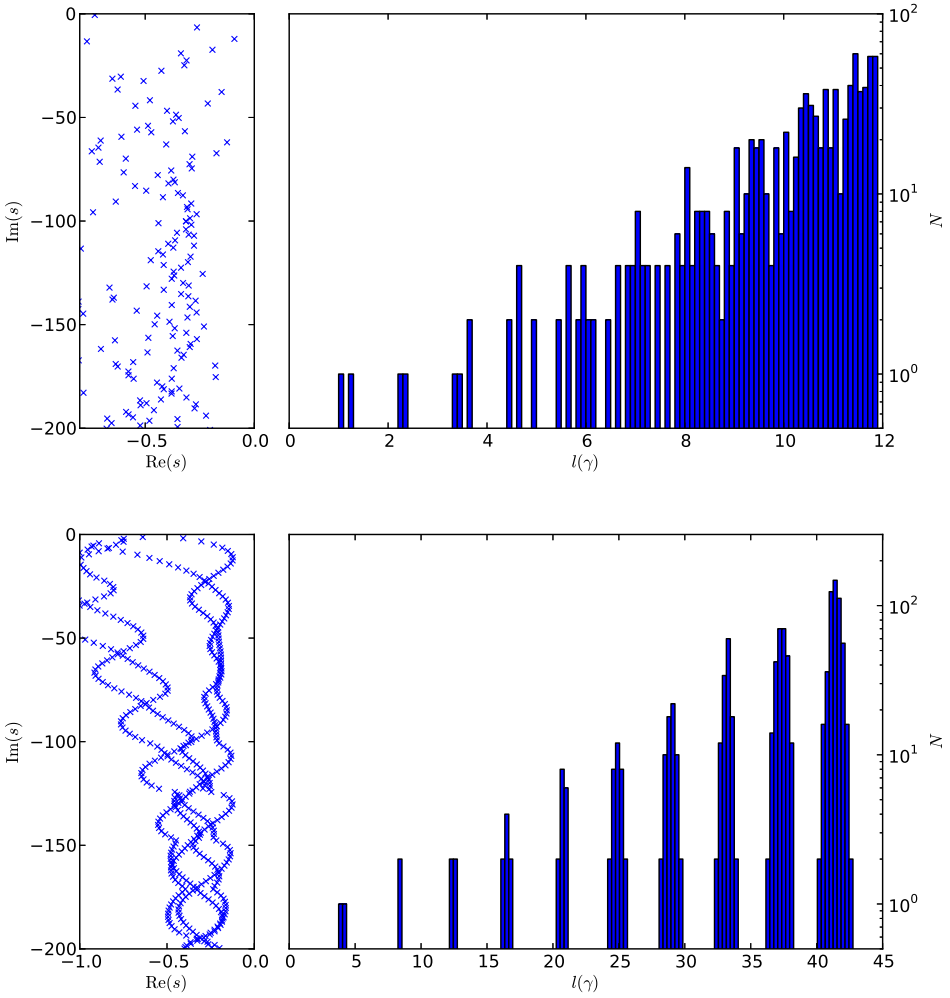

Figure 15.1: Comparison of the resonance structure (left) with the primitive length spectrum (right) of the symmetry reduced 3-disk system for $R/a = 3$ (upper plot) and $R/a = 6$ (lower plot). While for $R/a = 6$ one observes a clear clustering of the lengths and an obvious chain structure in the resonances, the lengths equidistribute very quickly and their are no visible chains in the resonance spectrum.

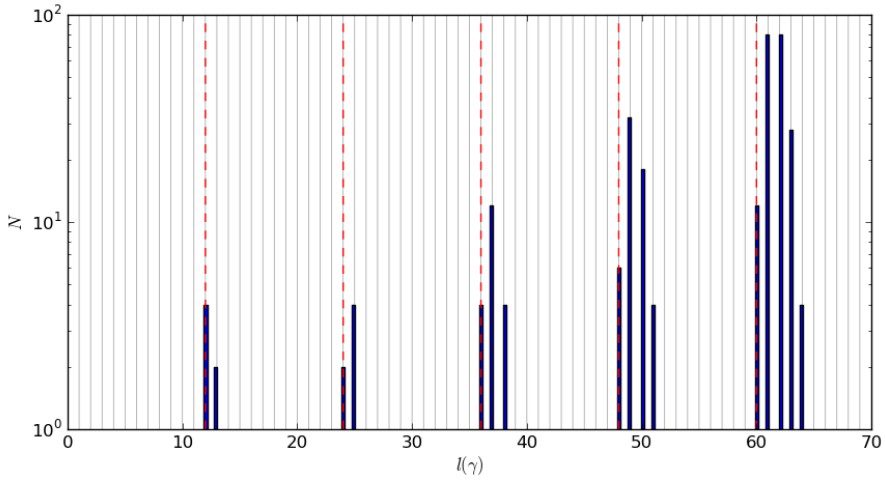

Figure 15.2: Histogram of the primitive length spectrum for the Schottky surface $X_{12,12,13}$. The thin light lines indicate the integer multiples of the base length $\ell = 1$ and red dashed lines the multiples of a second base length $\ell = 12$. One can observe two types of clustering, one very coarse clustering around the multiples of $\ell = 12$ and a much finer clustering around the multiples of $\ell = 1$.

to the base length $\ell = 12$ we observe strongly twisted resonance chains as indicated by the red circles in the left part of Figure 15.3. The generalized spectrum $\sigma_s^{(\mathbf{n})}$ of this order function creates this kind of chains by the rotating spectral values and if one connects neighboring resonances on this chain by the continuous line which is suggested by the chain structure, the generalized spectral value moves along the unit circle. This verifies that the chains are described by $\mathrm{Pr}_s(\mathcal{C}_\mathbf{n})$. Choosing, however, the order function (14.9) with $n_1 = n_2 = 12, n_3 = 13$ which is the corresponding choice for the base length $\ell = 1$ we obtain a generalized zeta function which describes a second structure of resonance chains, on which the resonance distances are much larger and which are much straighter (see Figure 15.4).

16 Conclusion

In this part of the thesis we presented a unifying approach to the chain structure of quantum resonances, classical Ruelle resonances and geometric resonances. We showed at the example of 3-disk systems and Schottky surfaces that the resonance chains can be understood in all three cases by

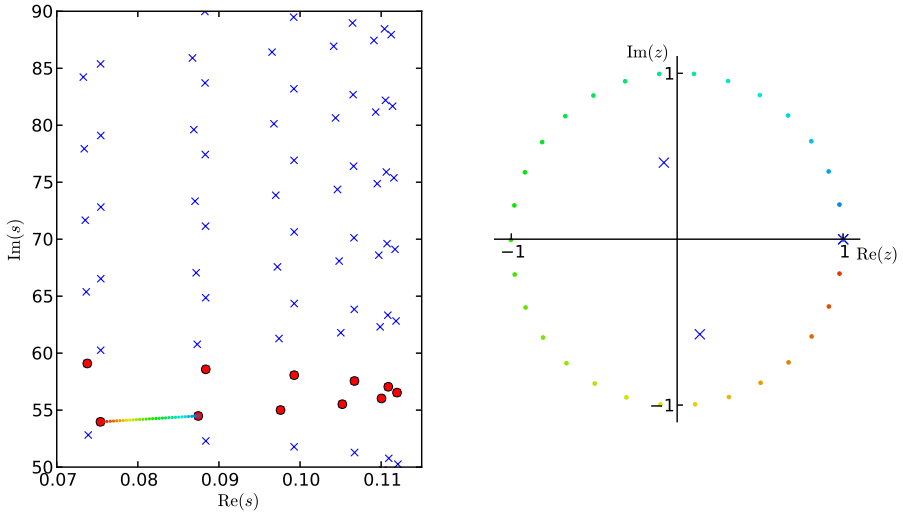

Figure 15.3: Left: The resonances of $X_{12,12,13}$ in the complex plane are marked by crosses. The red circles highlight the resonances on the chain, which belongs to the base length $\ell = 12$. The colored dots between the two resonances $s_1 = 0.07539 + 53.97i$ and $s_2 = 0.08746 + 54.49i$ represent a discrete interpolation between the two resonances following the line suggested by the resonance chains. Right: generalized spectrum for the order function as defined in (14.9) with $n_1 = n_2 = n_3 = 1$. The blue crosses represent the spectrum $\sigma_{s_1}^{(\mathbf{n})}$ for $|z| > 0.2$. By the colored dots we follow the evolution of the spectral value which equals one while interpolating the s-values between s_1 and s_2 as indicated by the colored points on the left.

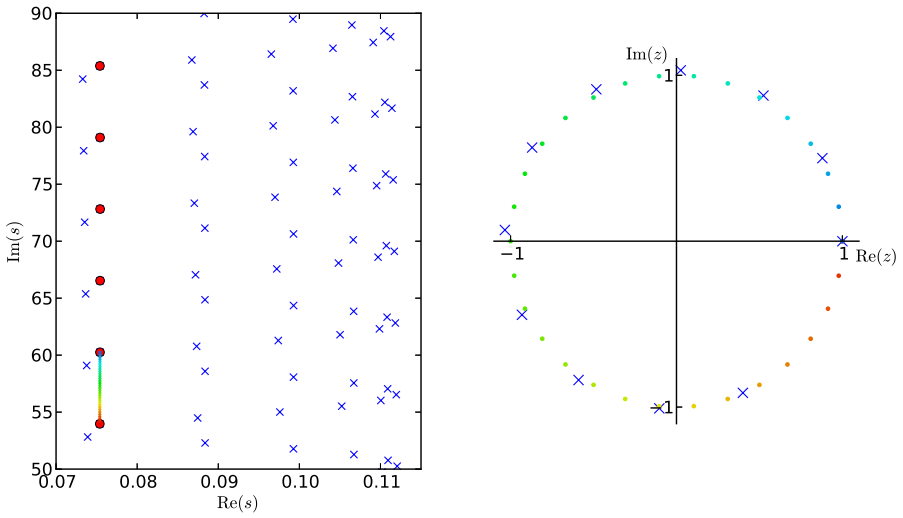

Figure 15.4: Left: The resonances of $X_{12,12,13}$ in the complex plane are marked by crosses. The red circles highlight the resonances on the chain, which belongs to the base length $\ell = 1$. The colored dots between the two resonances $s_1 = 0.07539 + 53.97i$ and $s_2 = 0.07542 + 60.25i$ represent a discrete interpolation between the two resonances following the line suggested by the resonance chains. Right: generalized spectrum for the order function as defined in (14.9) with $n_1 = n_2 = n_3 = 1$. The blue crosses represent the spectrum $\sigma_{s_1}^{(\mathbf{n})}$ for $|z| > 0.99$. By the colored dots we follow the evolution of the spectral value which equals one while interpolating the s-values between s_1 and s_2 as indicated by the colored points on the left.

means of a generalized zeta function $d_{\mathbf{n}}(s,z)$ which depends on the choice of an order function $\mathbf{n} : P \to \mathbb{N}$ on the set of primitive closed classical orbits P. The central property of this generalized zeta function is that independent of the choice of the order function the resonances are given by the zeros of the zeta function $Z(s) = d_{\mathbf{n}}(s,1)$. We showed that if the order function is chosen such that

$$l(\gamma) \approx \mathbf{n}(\gamma)\ell \tag{16.1}$$

for an arbitrary base length ℓ then the second complex variable allows to interpolate between the resonances of one chain. Furthermore we demonstrated that the continuous lines where the resonances are found on are given by the projection onto the s-component of the real analytic variety

$$\mathcal{C}_{\mathbf{n}} = \{d_{\mathbf{n}}(s,z) = 0\} \cap \{|z| = 1\}.$$

The existence of an order function that fulfills the condition (16.1) does of course depends on the structure of the length spectrum of the classical system. This led us to the hypothesis that the existence of resonance chains is directly linked to a clustering of the classical length spectrum that allows us to choose an order function according to (16.1). We finally validated this hypothesis by presenting several examples of systems with and without resonance chains. In all cases the resonance chains were found to be linked to a clustering of the length spectrum. Furthermore we showed that this new understanding allows to construct scattering systems with a customized resonance chain structure. This control of the resonance chains could be of importance in microdisk cavities where similar resonance chains have already been observed [93] and where a precise control of the resonance position in the complex plane is of great interest for their application as microdisk lasers.

Additionally this understanding is important for fundamental questions in quantum chaos. In chaotic systems the clear clusters in the length spectrum will only exist for short lengths. For larger lengths the clusters become broader and broader and will finally overlap. However, we required the condition (16.1) only to hold in the length range which is necessary for the calculation of the resonances in the studied frequency regime. In other words for the existence of resonance chains in a given frequency range, condition (16.1) only has to hold for the lengths which can be resolved by the Planck cells at this frequency. If one still observes resonance chains, then one has to keep in mind that one is not yet at high enough frequencies to resolve the length spectrum in a regime, where the clusters dissolve. This could be especially important for the test of results that are obtained by arguing with phase cancellation such as the conjectures on the improved spectral gaps [54].

Finally the study of resonance chains opens a variety of mathematical questions. We numerically observed that the chain structure becomes the

more clear the better condition (16.1) is fulfilled. By studying not a single system but a whole family of scattering systems, where (16.1) is better and better fulfilled in a certain limit one can then try to prove the existence of resonance chains asymptotically in this limit. Furthermore one can try to give precise, simple formulas for the location of these chains. For symmetric 3-disk systems this limit would correspond to large R/a-values and for Schottky surfaces to large funnel widths. For the latter case, first results into this direction are be presented in Part II.

Part IV
Symmetry reduction of holomorphic iterated function schemes and factorization of Selberg zeta functions

17 Introduction

Let $X = \Gamma\backslash\mathbb{H}$ be a convex co-compact hyperbolic surface, and Δ_X the positive Laplacian on this surface. Then its resolvent

$$R(s) = (\Delta_X - s(s-1))^{-1}$$

on $L^2(X)$ is analytic for $s \in \mathbb{C}$ with $\mathrm{Re}(s) > 1$. By changing the function spaces it can be continued meromorphically to $s \in \mathbb{C}$ with poles of finite rank [60]. The poles of this meromorphic continuation are called the resonances of X and the multiplicity of a resonance is defined to be the rank of the associated pole. The set of all resonances on X repeated according to multiplicity will be called $\mathrm{Res}(X)$ and they are the spectral invariant of the surface X which generalizes the discrete eigenvalue spectrum of the Laplacian on compact manifolds.

Interest in the distribution of the resonances arises from different areas of research. First it is a natural mathematical question, how strong the geometry of the surface X determines the distribution of resonances and vice versa. Secondly the distribution of resonances on infinite volume hyperbolic surfaces has been found to have implications in arithmetics [9]. And third the Laplace operator on convex co-compact surfaces is an important model for quantum-chaotic scattering and the resonance distribution has been intensively studied in theoretical [84, 59] and experimental [4, 77] physics during recent years.[12]

Driven by the interest from these different directions, there have been derived various results on the distribution of resonances on convex co-compact surfaces, for example results on the asymptotic number of resonances in a disk in the complex plane [44, 45, 6], results on upper and lower bounds

[12]Resonances on cnovex co-compact surfaces were also the object of central interest in Part II and III.

of resonances in a strip near the critical line [95, 43, 75, 46, 64] and about asymptotic spectral gaps [63, 55] in the limit of large $\mathrm{Im}(s)$. Despite these big advances, there are still many open conjectures on the distribution of the resonances, for example the fractal Weyl upper bound is conjectured to be sharp [43] and the asymptotic spectral gap is conjectured to be much bigger then what is actually known [54]. We refer to [65] for a more detailed overview on recent results and open questions.

In order to test these conjectures numerically, Borthwick recently presented a detailed numerical study of the resonance structure on convex co-compact surfaces [7]. For the calculation he used the fact that the resonances appear as zeros of the Selberg zeta function. This zeta function is defined for $\mathrm{Re}(s) > 1$ by

$$Z_X(s) := \prod_{\gamma \in \mathcal{P}_X} \prod_{k \geq 0} \left(1 - e^{-(s+k)l(\gamma)}\right) \tag{17.1}$$

where $\mathcal{P}_X$ is the set of primitive closed geodesics on X, i.e. those geodesics, that cannot be obtained by a repetition of a shorter closed geodesic, and $l(\gamma)$ denotes their lengths. For convex co-compact surfaces the Selberg zeta function is known to extend analytically to the complex plane and the relation to the resonances of Δ_X is given by

Theorem 17.1 ([72] Patterson-Perry 2001)**.** *For a convex co-compact surface $X = \Gamma\backslash\mathbb{H}$ the zero set of the zeta function $Z_X(s)$ is the union of the resonances* $\mathrm{Res}(X)$ *and the negative integers $s = -k$, $k \in \mathbb{N}_0$.*

For an tractable numerical calculation of the Selberg zeta function the correspondence of the Selberg zeta function and the dynamical zeta function of an iterated function scheme, the so called Bowen-Series maps, has been used. The problem of the analytic continuation can be circumvented by a trick which was introduced under the name cycle expansion in physics [25] by Cvitanovic-Eckhardt and which has later been rigorously applied to Selberg zeta functions by Jenkinson-Pollicott [56]. These techniques allow to calculated several thousand resonances on an ordinary personal computer and study their distribution in the complex plane. With these techniques Borthwick was not only able to compare the resonance distribution to the existent conjectures, but he also discovered the surprising formation of resonance chains, which triggered further numerical and mathematical studies (See Part II and III as well as [91]).

The problem with the numerical techniques, used so far, is that the due to the exponential growth of number of closed geodesic, the convergence of the algorithm was restricted to rather small resonance strips near the critical line. Additionally only surfaces whose Schottky group is generated by two

generators and whose fractal dimension of the limit set δ is rather small ($0 \leq \delta \lesssim 0.1$) could be treated [7, Section 4.1]. For a more thorough tests of the conjectures a larger δ-range would be desirable. Furthermore, recent predictions that the resonance chains, observed for 3-funneled surface should not or merely be observable for 4-funneled surfaces [3] can not be tested at all with the current techniques.

These shortcomings of the existent techniques motivated us to take advantage of the symmetry of the convex co-compact surfaces and prove a symmetry factorization for the dynamical zeta functions. Such factorizations have been calculated in physics in the very related setting of 3- and 4-disk systems by Cvitanovic and Eckhardt [26]. The aim of this part of the thesis is to establish rigorous version of their results and apply them to the calculation of resonances on convex co-compact surfaces.

If a convex co-compact surface $X = \Gamma\backslash\mathbb{H}$ has a finite symmetry group G, then the natural approach for a symmetry reduced calculation of the resonances would be, to apply the symmetry reduction on the level of the Laplacian Δ_X and to study the meromorphic continuation of the symmetry reduced resolvent. For the numerical calculation of the resonance we need, however, the Patterson-Perry correspondence (Theorem 17.1). The proof of a factorization of the Selberg zeta function thus would require to reprove this correspondence for the symmetry reduced resolvent, which seems rather technical. Therefore we have chosen to prove the factorization on the level of the dynamical zeta functions of iterated function schemes. This has the advantage that the results do not only apply to Bowen-Series maps and convex co-compact surfaces but immediately apply also to other cases where iterated function schemes appear, e.g. in the calculation of Hausdorff dimensions [56]. Additionally one automatically obtains the analyticity of the symmetry reduced zeta functions for free. The drawback of this approach is that the symmetry group of the commonly used Bowen-Series maps might be smaller than the symmetry group of the associated surface. This problem can be circumvented for a large class of interesting surfaces as we will show in Section 21.1.

This part of the thesis is organized as follows. In Section 18 we will first introduce the holomorphic iterated function schemes (IFS), their transfer operators and the dynamical zeta functions. In Section 19 we will introduce the notion of a symmetry group of a holomorphic IFS and derive a symmetry reduced trace formula for the transfer operator (Proposition 19.1). This symmetry reduced trace formula is then used in Section 20 to prove, as a first main result, the factorization of the dynamical zeta function (Theorem 20.5). The rest of the section is devoted to a simplification of the symmetry reduced zeta functions (Theorem 20.5 and Corollary 20.7) which hold under the as-

sumption that the symmetry group acts freely on the set of G-closed words. Section 21 is then devoted to the application of the results to the resonances on convex co-compact surfaces. In Section 21.1 we first introduce a family of symmetric n-funneled surfaces for which we construct iterated function schemes that incorporate the whole symmetry group of the surfaces. Using Theorem 20.1 this allows to prove a factorization of the Selberg zeta function into analytic symmetry reduced zeta functions (see equation (21.9)). In Section 21.2 we finally perform the numerical calculations, using these new symmetry reduced formulas. We show, that the symmetry reduction is not only interesting for fundamental reasons as it allows to associate the calculated resonances to certain unitary irreducible representations but also for practical purpose as it simplifies the numerical calculations tremendously: For a 3-funneled surface we show that we can increase the width of the numerically accessible resonance strip by a factor of three and at the same time reduce the number or required periodic orbits from over 170000 without symmetry reduction to only 41 with symmetry reduction. We are sure that this gain of efficiency will allow to perform much more thorough numerical investigations of the resonance structure on convex co-compact surfaces and as a first example we confirm the prediction from [3] that the resonance structure of symmetric 4-funneled surfaces show no clearly visible resonance chains.

18 Holomorphic iterated function schemes and their transfer operators

Definition 18.1 (Holomorphic iterated function scheme)**.** For $N \in \mathbb{N}$ let $D_1, \ldots, D_N \subset \mathbb{C}$ be N open disks such that their closures $\overline{D}_i$ are pairwise disjoint. Let $A \in \{0,1\}^{N\times N}$ be the *adjacency matrix* and write $i \rightsquigarrow j$ if $A_{i,j} = 1$. Furthermore for each pair $(i,j) \in \{1,\ldots,N\}^2$ with $i \rightsquigarrow j$ we have a biholomorphic map $\phi_{i,j} : D_i \mapsto \phi_{i,j}(D_i)$ such that $\phi_{i,j}(D_i) \Subset D_j$ and such that different images are pairwise disjoint, i.e.

$$\phi_{i,j}(D_i) \cap \phi_{k,l}(D_k) \neq \emptyset \Leftrightarrow i = k \text{ and } j = l. \tag{18.1}$$

For convenience we denote the union of all the disjoint disks by

$$D := \bigcup_i D_i$$

and the union of all their images by

$$\phi(D) := \bigcup_{i\rightsquigarrow j} \phi_{i,j}(D_i).$$

From (18.1) it follows directly that for $u \in \phi(D)$ there is exactly one pair $i \rightsquigarrow j$ and $u' \in D_i$ such that $u = \phi_{i,j}(u')$. We have thus a well defined holomorphic inverse function

$$\phi^{-1} : \phi(D) \to D.$$

Remark 18.1. Instead of disks D_i one could have also taken simply connected domains $U_i \subset C$. Using the Riemann mapping theorem such an IFS is biholomorphically conjugated to an IFS with disks, so one can always simplify such IFS to the above situation defined on disks D_i.

Example 18.1. Let $D_1, \ldots, D_{2r}$ be disjoint open disks in $\mathbb{C}$ with centers on the real line and mutually disjoint closures. Then there exists for each pair D_i, D_{i+r} an element $S_i \in PSL(2,\mathbb{R})$ that maps via its Moebius transformation ∂D_i to ∂D_{i+r} and that maps the interior of D_i to the exterior of D_{i+r}. The *Schottky group* is then the free subgroup $\Gamma \subset PSL(2,\mathbb{R})$, generated by $S_1, \ldots, S_r$ (for an illustration see Figure 18.1).

The generators and disks in the construction of a Schottky group give also a natural construction of a holomorphic IFS. For convenience we write for $i = 1, \ldots, r$ $S_{i+r} := S_i^{-1}$ and use a cyclic notation of the indices s.t. $S_{i+2r} = S_i$ and $D_{i+2r} = D_i$. Then for all $i = 1, \ldots, 2r$ the element S_i maps all disks except D_i holomorphically into the interior of D_{i+r}. Thus we define the adjacency matrix of this IFS as a $2r \times 2r$ matrix with $A_{i,j} = 0$ if $|i-j| = r$ and $A_{i,j} = 1$ else. Furthermore for any $i \rightsquigarrow j$ we define the maps for $u \in D_i$ by

$$\phi_{i,j}(u) := S_{j+r}u = S_j^{-1}u,$$

and from this definition it is clear that (18.1) is automatically fulfilled.

Note that the inverse map restricted to $D_j \cap \phi(D)$ is exactly given by S_j. The IFS which we defined is consequently the inverse of the usual *Bowen-Series map* for Schottky groups (see e.g. [5, Section 15.2]).

It will turn out to be useful for the notation to introduce the following symbolic coding. The *symbols* are given by the integers $1, \ldots, N$ and the set of words of length n is given by the tuples of symbols

$$\mathcal{W}_n := \{(w_0, \ldots, w_n), w_i \rightsquigarrow w_{i+1} \text{ for all } i = 0, \ldots, n-1\}.$$

Note that our notation of *word length* does not refer to the number of symbols, but to the number of transitions which they indicate. For $w \in \mathcal{W}_n$ and $0 < k \leq n$ we define the *truncated word* by

$$w_{0,k} := (w_0, \ldots, w_k) \in \mathcal{W}_k.$$

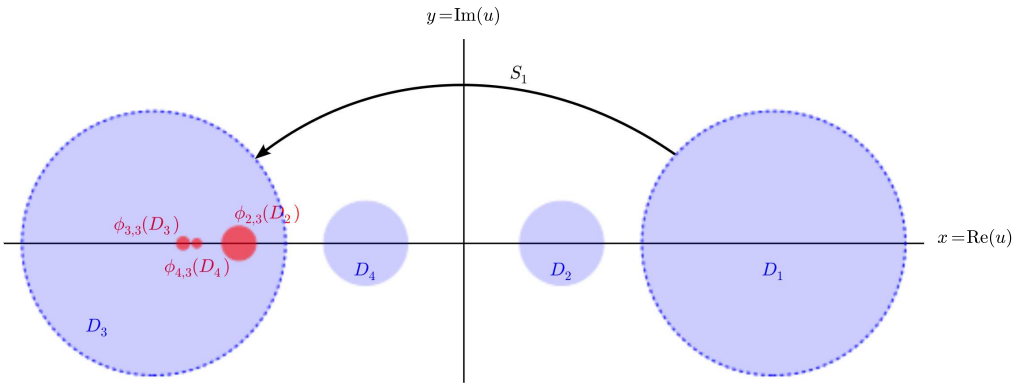

Figure 18.1: Illustration of the construction of a Schottky group and the corresponding IFS. The blue disks show the four disk from which the generators of the Schottky group are generated. For example the group element S_1 maps ∂D_1 to ∂D_3 and the exterior of D_1 into the interior of D_3. The red circles illustrate the images of the other three disks under the Moebius transformation S_1 which coincide with the images of the disks under the associates holomorphic IFS.

Finally we define the iteration of the maps $\phi_{i,j}$ along a word $w \in \mathcal{W}_n$ as

$$\phi_w := \phi_{w_{n-1},w_n} \circ \ldots \circ \phi_{w_0,w_1} : D_{w_0} \mapsto D_{w_n}$$

and their images as

$$D_w := \phi_w(D_{w_0}).$$

Note that $D_w \Subset D_{w_n}$ and that from the separation condition (18.1) one obtains inductively for $w, w' \in \mathcal{W}_n$

$$D_w \cap D_{w'} \neq \emptyset \Leftrightarrow w = w'.$$

Definition 18.2. We call a holomorphic IFS *eventually contracting*, if there is N_0 and $\theta < 1$ such that for $n \geq N_0$

$$|\phi'_w(u)| \leq \theta \text{ for all } w \in \mathcal{W}_n \text{ and } u \in D_{w_0}.$$

Remark 18.2. The Bowen-Series IFS as introduced in Example 18.1 are known to be eventually contracting (see e.g. [5, Proposition 15.4]).

We call a word $w \in \mathcal{W}_n$ of length n *closed* if $w_0 = w_n$ and we denote the set of all closed words of length n by $\mathcal{W}_n^{cl}$.

Lemma 18.1. *If a holomorphic IFS is eventually contracting, then for each $w \in \mathcal{W}_n^{cl}$ there exists a unique fixed point $\phi_w(u_w) = u_w$.*

Proof. If $w \in \mathcal{W}_n^{cl}$ is closed, then $\phi_w(D_{w_0}) = D_w \Subset D_{w_0}$ and we write $D_k := (\phi_w)^k(D_{w_0})$. Then $D_{k+1} \Subset D_k$ and if $k_0 n \geq N$ then from the eventually contracting property $\mathrm{diam}(D_{k_0 m}) \leq \theta^m \mathrm{diam} D_{w_0}$. So $D_1, D_2, \ldots$ is a nested sequence of disks whose diameter converges to zero so there is a unique $u_w := \bigcap_{k>0} D_k$ which has to be a fixed point of ϕ_w. □

Next we define the transfer operators associated to the iterated function schemes.

Definition 18.3. Let $\mathcal{B}(D) := \{f : D \to \mathbb{C} \text{ holomorphic, and } f \in L^2(D)\}$ be the Bergmann space on D. Let furthermore $V : \phi(D) \to \mathbb{C}$ be a bounded holomorphic function, and define the *transfer operator* $\mathcal{L}_V : \mathcal{B}(D) \to \mathcal{B}(D)$ associated to an IFS by

$$(\mathcal{L}_V f)(u) := \sum_{i \rightsquigarrow j \text{s.t.} u \in D_i} V(\phi_{i,j}(u)) f(\phi_{i,j}(u)) \text{ for } u \in D_i. \tag{18.2}$$

Given such a potential V, a word $w \in \mathcal{W}_n$ and a point $u \in D_{w_0}$ we can define the iterated product

$$V_w(u) := \prod_{k=1}^{n} V(\phi_{w_{0,k}}(u)).$$

A straight forward calculation of powers of the transfer operator $\mathcal{L}_V$ leads to

$$\left(\mathcal{L}_V^n f\right)(u) = \sum_{w \in \mathcal{W}_n \text{ s.t. } u \in D_{w_0}} V_w(u) f(\phi_w(u));$$

thus these iterated products naturally occur in powers of $\mathcal{L}_V$.

It is a well known fact that these transfer operators are trace class (see [80] for the original proof in slightly different function spaces respectively [5, Lemma 15.7] for a proof in our setting) and that the trace can be expressed in terms of periodic orbits. Accordingly one can define the *dynamical zeta function* by the Fredholm determinant

$$d_V(z) := \det(1 - z\mathcal{L}_V) \tag{18.3}$$

which is an entire function on $\mathbb{C}$. If furthermore the IFS is eventually contracting the dynamical zeta function can be written for $|z|$ sufficiently small as (see e.g. [5, proof of Thm 15.8]):

$$d_V(z) = \exp\left(-\sum_{n>0} \frac{z^n}{n} \sum_{w \in \mathcal{W}_n^{cl}} V_w(u_w) \frac{1}{1 - (\phi_w)'(u_w)} \right). \tag{18.4}$$

Example 18.2. An important class of transfer operators arises from the IFS associated to Bowen-Series maps of Schottky surfaces (see Example 18.1). If we choose the potential function $V_s(u) = [(\phi^{-1})'(u)]^s$ that depends analytically on $s \in \mathbb{C}$, then one obtains an analytic family of trace class operators $\mathcal{L}_s$.The dynamical zeta function

$$d(s, z) := \det(1 - z\mathcal{L}_s)$$

is then analytic in $(s, z) \in \mathbb{C}^2$ and one has the important relation to the Selberg zeta Z_X function on the Schottky surface X which is defined via the closed geodesics as follows. If γ is a closed geodesic on X, then it is called primitive if it cannot be obtained by a repetition of a shorter closed geodesic. If P_X is the set of oriented primitive geodesics and $l(\gamma)$ denotes the length of the geodesic, then the Selberg zeta function is defined as

$$Z_X(s) := \prod_{\gamma \in P_X} \prod_{k \geq 0} e^{-(s+m)l(\gamma)}.$$

These products are convergent for $\mathrm{Re}(s)$ sufficiently large and for X being a Schottky surface, it is known that the Z_X has an analytic extension to $\mathbb{C}$ [42]. Furthermore the relation to the dynamical zeta function is given by (see e.g. [5, Theorem 15.8] for a proof)

$$Z_X(s) = d(s, 1).$$

19 Trace formula for the symmetry reduced transfer operator

Definition 19.1 (Symmetry group of a holomorphic IFS)**.** By a *symmetry group of a holomorphic IFS* we denote a finite group G which acts holomorphically on D and commutes with the IFS, i.e. for each $g \in G$, $u \in D_i$ and $i \rightsquigarrow j$, there exists a pair $k \rightsquigarrow l$ such that $g\phi_{i,j}(u) = \phi_{k,l}(gu)$.

As an immediate consequence of the definition we obtain that $\phi(D) \subset D$ is a G-invariant subset. Furthermore, as the disks D_i are disjoint and connected, we have

$$g(D_i) = D_j. \tag{19.1}$$

for suitable j. Thus we can reduce the G-action to the set of symbols $\{1, \ldots, N\}$ by setting $gi := j$ for i, j such that (19.1) holds. With this notation the indices k, l in Definition 19.1 are uniquely defined by $k = gi$

and $l = gj$. Accordingly we conclude that $i \rightsquigarrow j$ implies $gi \rightsquigarrow gj$ and consequently we can extend the G-action on the symbols to an action on the words of length n by setting for $w \in \mathcal{W}_n$

$$gw := (gw_0, \ldots, gw_n) \in \mathcal{W}_n.$$

Considering iterations ϕ_w of the IFS, the commutation formula reads

$$g\phi_w(z) = \phi_{gw}(gz). \tag{19.2}$$

For further use we can also introduce for $g \in G$ the set of *g-closed words* of length n

$$\mathcal{W}_n^g := \{w \in \mathcal{W}_n, gw_n = w_0\}. \tag{19.3}$$

Example 19.1. We have seen in Example 18.1 that Schottky groups naturally give rise to holomorphic IFS. We will now consider the special case of 3-funneled surfaces (see Figure 19.1). These surfaces are known to be uniquely parametrized by their Fenchel-Nielsen coordinates l_1, l_2, l_3 which determine the lengths of the three fundamental geodesics $\gamma_1, \gamma_2, \gamma_3$ (see Figure 19.1).

Given three lengths l_1, l_2, l_3 we denote the associated Schottky surface by $X_{l_1,l_2,l_3} = \Gamma_{l_1,l_2,l_3} \backslash \mathbb{H}$, and the two generators of the Schottky group can be written in the form

$$S_1 = \begin{pmatrix} \cosh(l_1/2) & \sinh(l_1/2) \\ \sinh(l_1/2) & \cosh(l_1/2) \end{pmatrix}, \quad S_2 = \begin{pmatrix} \cosh(l_2/2) & a\sinh(l_2/2) \\ a^{-1}\sinh(l_2/2) & \cosh(l_2/2) \end{pmatrix},$$

where the parameter $a > 0$ is chosen such that $\mathrm{Tr}(S_1 S_2^{-1}) = -2\cosh(l_3/2)$.

Depending on the choice of l_1, l_2, l_3 the associated Bowen-Series IFS have different symmetry groups. In any case the IFS has a $\mathbb{Z}_2$ symmetry generated by the Moebius transformation of the matrix

$$\sigma_1 = \begin{pmatrix} -1 & 0 \\ 0 & 1 \end{pmatrix}.$$

This transformation corresponds to a reflection at the imaginary axis followed by a complex conjugation[13] and it is related to the fact that all 3-funneled Schottky surfaces are symmetric with respect to reflections on the plane spanned by the three funnels.

The action of σ_1 interchanges disk D_1 with D_3 and D_2 which D_4, thus we get the following action on the symbols

$$\sigma_1(1) = 3, \sigma_1(2) = 4, \sigma_1(3) = 1, \sigma_1(4) = 2$$

[13]This complex conjugation is necessary to make the symmetry holomorphic.

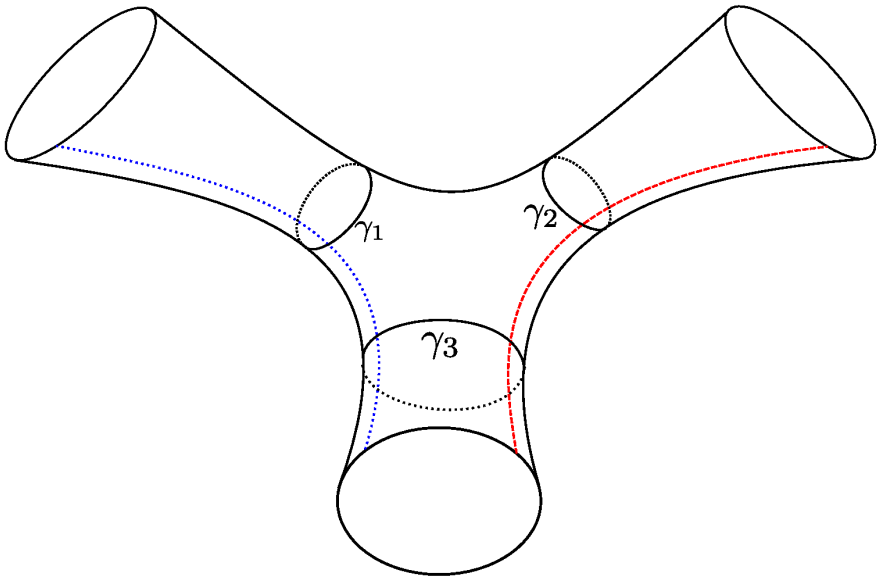

Figure 19.1: Visualization of a Schottky surface with 3-funnels. These surfaces are uniquely determined by the lengths l_1, l_2, l_3 of the three fundamental geodesics $\gamma_1, \gamma_2, \gamma_3$, that turn around each funnel. The surface can be obtained by gluing together the corresponding fundamental domain of the Schottky group (see Figure 19.2) along the dashed red and dotted blue lines.

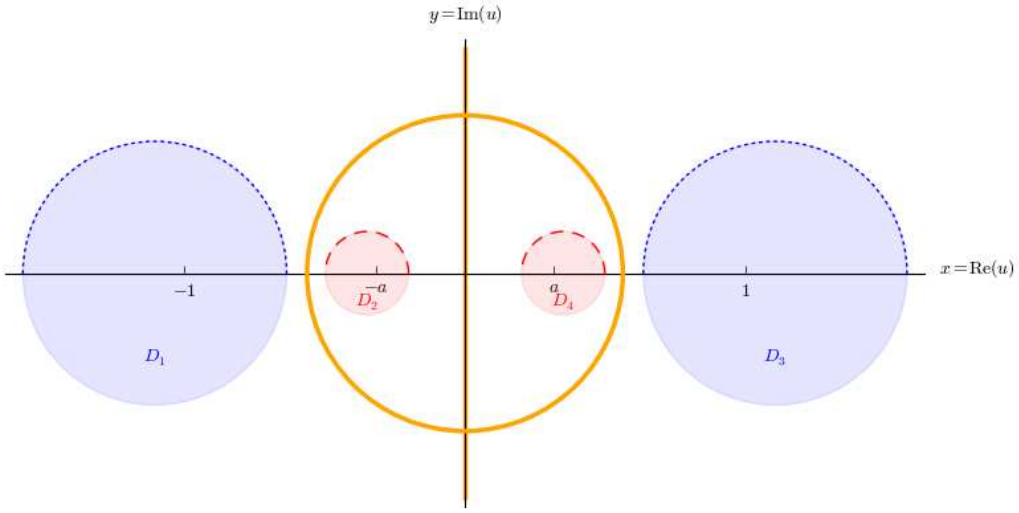

Figure 19.2: Illustration of the Symmetry of the Bowen-Series IFS for a 3-funneled Schottky surface with $l_1 = l_2$. Apart from the reflection along the imaginary axis, the IFS is also symmetric w.r.t. reflections along the yellow circle of radius $\sqrt{a}$.

and in order to prove that σ_1 is indeed a symmetry of the Bowen-Series IFS in the sense of Definition 19.1 we have to verify

$$\begin{aligned} \sigma_1\phi_{1,1}\sigma_1 = \phi_{3,3}, \quad \sigma_1\phi_{2,1}\sigma_1 = \phi_{4,3}, \quad \sigma_1\phi_{4,1}\sigma_1 = \phi_{2,3} \\ \sigma_1\phi_{1,2}\sigma_1 = \phi_{3,4}, \quad \sigma_1\phi_{2,2}\sigma_1 = \phi_{4,4}, \quad \sigma_1\phi_{3,2}\sigma_1 = \phi_{1,4}. \end{aligned}$$

The first line follows from the fact that

$$\sigma_1 S_1 \sigma_1 = \begin{pmatrix} \cosh(l_1/2) & -\sinh(l_1/2) \\ -\sinh(l_1/2) & \cosh(l_1/2) \end{pmatrix} = S_1^{-1} = S_3$$

and the second line analogously from $\sigma_1 S_2 \sigma_1 = S_4$.

If the Fenchel-Nielsen coordinates satisfy $l_1 = l_2$ then the Schottky surface X_{l_1,l_1,l_3} as well as the Bowen-Series IFS fulfill an additional symmetry. On the surface this symmetry would correspond to a rotation of 180° around the third funnel. For the IFS this symmetry is represented by a Moebius transformation of the matrix

$$\sigma_2 = \begin{pmatrix} 0 & \sqrt{a} \\ \frac{1}{\sqrt{a}} & 0 \end{pmatrix}.$$

This transformation represents a reflection at the orange circle in Figure 19.2 followed again by a complex conjugation to guarantee the holomorphicity. As

this transformation interchanges D_1 with D_2 and D_3 with D_4 we obtain the action on the symbols

$$\sigma_2(1) = 2, \sigma_2(2) = 1, \sigma_2(3) = 4, \sigma_2(4) = 3$$

and according to Definition 19.1 we have to check

$$\begin{aligned} \sigma_2\phi_{1,1}\sigma_2 = \phi_{2,2}, \quad \sigma_2\phi_{2,1}\sigma_2 = \phi_{1,2}, \quad \sigma_2\phi_{4,1}\sigma_2 = \phi_{3,2} \\ \sigma_2\phi_{2,3}\sigma_2 = \phi_{1,4}, \quad \sigma_2\phi_{3,3}\sigma_2 = \phi_{4,4}, \quad \sigma_2\phi_{4,3}\sigma_2 = \phi_{3,4}. \end{aligned}$$

This is again verified by a simple matrix calculation that shows that $\sigma_2 S_1 \sigma_2 = S_2$ and $\sigma_2 S_3 \sigma_2 = S_4$. In the case $l_1 = l_2$ the surface as well as the holomorphic IFS admit thus the Klein four-group as symmetry group.

If all three fundamental lengths are equal to each other $l_1 = l_2 = l_3$, then the Schottky surface $X_{l,l,l}$ has an even larger group as symmetry group which can be written as $D_3 \times \mathbb{Z}_2$, with D_3 being the symmetry group of the equilateral triangle (see Section 21.1 for more details). The Bowen-Series IFS shows however no further symmetry and has only the Klein four-group as symmetry group. The reason for this discrepancy lies in the construction of the Bowen-Series IFS. It morally corresponds to a Poincaré section which is defined by the blue dotted and red dashed cut-lines in Figure 19.1. This asymmetric choice of a Poincaré section is the reason why the holomorphic IFS has a weaker symmetry then the whole surface. In order to have the symmetry decomposition of the zeta function with respect to the whole symmetry group of the surface we will have to construct a holomorphic IFS whose dynamical zeta function corresponds also to the Selberg zeta function and which incorporate the whole symmetry group. This will be done for symmetric n-funneled surfaces in Section 21.1.

Given a symmetry group G of a holomorphic IFS we now want to define the symmetry decomposition of the function spaces $B(D)$. The symmetry group G acts from left on $B(D)$ by its left regular representation

$$(gf)(u) = f(g^{-1}u).$$

Note that in general this action is not unitary if the scalar product in $B(D)$ is taken with respect to the Lebesgue measure. However, by averaging the Lebesgue measure λ over G with the pushforward $g_*\lambda$ one obtains a G-invariant measure

$$\mu_G := \frac{1}{|G|} \sum_{g \in G} g_*\lambda = \frac{1}{|G|} \sum_{g \in G} |g'(u)|^{-1}\lambda$$

with positive, smooth density $\frac{1}{|G|}\sum_{g\in G}|g'(u)|^{-1}$. We denote the Bergman space with the scalar product defined by μ_G with $B_G(D)$. This space is identical to $B(D)$ and is only equipped with a different, however topologically equivalent scalar product.

On $B_G(D)$ the left regular action of G is unitary. By the Peter-Weyl theorem we thus get a decomposition

$$B_G(D) = \bigoplus_{\chi\in\hat{G}} B_\chi \tag{19.4}$$

where $\hat{G}$ is the set of equivalence classes of unitary representations of G and $B_\chi := P_\chi B_G(D)$ with the orthogonal projection operator

$$P_\chi := \frac{d_\chi}{|G|}\sum_{g\in G}\overline{\chi(g)}g.$$

Here $\chi(\bullet)$ is the character of the irreducible representation of dimension d_χ and g the operator defined by the left regular representation. Note that the definition of P_χ does not involve the scalar product, thus the operators P_χ are equally projectors on $B(D)$ and we also get the decomposition of $B(D)$ in closed linear subspaces

$$B(D) = \bigoplus_{\chi\in\hat{G}} B_\chi. \tag{19.5}$$

The only difference to (19.4) is that this decomposition is in general not orthogonal anymore.

If the potential V of the transfer operator is G-invariant, i.e. if it fulfills

$$V(gu) = V(u), \tag{19.6}$$

then $\mathcal{L}_V$ commutes with the left regular representation on $B(D)$ and accordingly also with the projectors P_χ. Consequently $\mathcal{L}_V$ leaves the spaces B^χ invariant and we define the symmetry reduced transfer operator to be

$$\mathcal{L}_V^\chi := \mathcal{L}_{V|B^\chi} : B^\chi \to B^\chi. \tag{19.7}$$

For this symmetry reduced operator we obtain the following formula for its trace.

Proposition 19.1. *Let G be the symmetry group of a holomorphic, eventually contracting IFS, $V : \phi(D) \to \mathbb{C}$ a holomorphic, bounded function which*

is symmetric with respect to the G-action and $\mathcal{L}_V$ the transfer operator associated to the IFS and V. Then for all $n \in \mathbb{N}$, $(\mathcal{L}_V^\chi)^n$ is trace class and its trace is given by:

$$\mathrm{Tr}_{B^\chi}\left[(\mathcal{L}_V^\chi)^n\right] = \frac{d_\chi}{|G|}\sum_{g\in G}\chi(g)\sum_{w\in\mathcal{W}_n^g}\frac{V_w(gu_{w,g})}{1-(\phi_w\circ g)'(u_{w,g})} \tag{19.8}$$

where $u_{w,g}$ is given by the unique fixed point fulfilling

$$u_{w,g} = \phi_w(gu_{w,g}) \tag{19.9}$$

and V_w by the iterated product

$$V_w(u) = \prod_{k=1}^{n} V(\phi_{w_{0,k}}(u)).$$

Proof. This proposition is a direct consequence of [5, Lemma 15.7]. First, we note that

$$\mathrm{Tr}_{B^\chi}[(\mathcal{L}_V^\chi)^n] = \mathrm{Tr}_{B(D)}[P_\chi(\mathcal{L}_V)^n]$$

and we calculate the action of this operator as

$$\begin{aligned}(P_\chi(\mathcal{L}_V)^n f)(u) &= \frac{d_\chi}{|G|}\sum_{g\in G}\overline{\chi(g)}\sum_{w\in\mathcal{W}_n \mathrm{s.t.} g^{-1}u\in D_{w_0}} V_w(g^{-1}u)f(\phi_w(g^{-1}u)) \\ &= \frac{d_\chi}{|G|}\sum_{g\in G}\chi(g)\sum_{w\in\mathcal{W}_n \mathrm{s.t.} gu\in D_{w_0}} V_w(gu)f(\phi_w(gu))\end{aligned}$$

where we substituted in the sum over G the elements g by g^{-1} for the last equality. This implies that

$$\mathrm{Tr}_{B^\chi}[(\mathcal{L}_V^\chi)^n] = \frac{d_\chi}{|G|}\sum_{g\in G}\chi(g)\sum_{w\in\mathcal{W}_n \mathrm{s.t.} gu\in D_{w_0}} \mathrm{Tr}_{B(D)}\left[T_{V,w,g}\right]$$

where $T_{V,w,g}$ is the following transfer operator

$$(T_{V,w,g}f)(u) := \begin{cases} V_w(gu)f(\phi_w\circ g(u)) & \text{if } u\in D_{g^{-1}w_0} \\ 0 & \text{else}\end{cases}$$

The map $\phi_w\circ g$ is a biholomorphic function $\phi_w\circ g : D_{g^{-1}w_0}\to D_w \Subset D_{w_n}$. If $w_n \neq g^{-1}w_0$, or in other words, if $w\notin\mathcal{W}_n^g$, then the operator has trace zero as it is an isomorphism between two orthogonal subsets of $B(D)$. Otherwise the eventually contracting property implies by the same arguments as in the

proof of Lemma 18.1 that the map $\phi_w \circ g$ has a unique fixed point which we call $u_{w,g}$. The operator $T_{V,w,g}$ then fulfills all the conditions of [5, Lemma 15.7] and we obtain

$$\mathrm{Tr}_{B(D)}(T_{V,w,g}) = \frac{V_w(gu_{w,g})}{1-(\phi_w \circ g)'(u_{w,g})}.$$

□

20 Factorization of the zeta function

Proposition 19.1 allows us to prove the following factorization of the dynamical zeta function.

Theorem 20.1. *Let G be the symmetry group of a holomorphic, eventually contracting IFS, let $V : \phi(D) \to \mathbb{C}$ be a holomorphic, bounded G-invariant potential and $d_V(z)$ the dynamical zeta function associated to the IFS and V. Then the dynamical zeta function can be written as the product*

$$d_V(z) = \prod_{\chi \in \hat{G}} d_V^\chi(z).$$

of the reduced zeta functions $d_V^\chi(z)$ which can be expressed for sufficiently small $|z|$ by

$$d_V^\chi(z) = \exp\left(-\sum_{n>0} \frac{z^n}{n} \frac{d_\chi}{|G|} \sum_{g\in G} \chi(g) \sum_{w \in \mathcal{W}_n^g} V_w(gu_{w,g}) \sum_{k\geq 0} [(\phi_w \circ g)'(u_{w,g})]^k\right) \tag{20.1}$$

and extend analytically to $\mathbb{C}$.

Proof. As Proposition 19.1 assures that $\mathcal{L}_V^\chi$ is trace class we can define the symmetry reduced zeta function

$$d_V^\chi(z) := \det_{B_\chi}(1 - z\mathcal{L}_V^\chi) \tag{20.2}$$

which is an analytic function on $\mathbb{C}$. From the symmetry decomposition (19.5) of $B(D)$ into invariant subspaces B_χ we furthermore directly obtain the following factorization of the dynamical zeta function

$$d_V(z) = \prod_{\chi \in \hat{G}} d_V^\chi(z).$$

Using the formula for the Fredholm determinant and the symmetry reduced trace formula we obtain

$$\begin{aligned} d_V^\chi(z) &= \exp\left(-\sum_{n>0}\frac{z^n}{n}\mathrm{Tr}_{B_\chi}\left[(\mathcal{L}_V^\chi)^n\right]\right) \\ &= \exp\left(-\sum_{n>0}\frac{z^n}{n}\frac{d_\chi}{|G|}\sum_{g\in G}\chi(g)\sum_{w\in\mathcal{W}_n^g}\frac{V_w(gu_{w,g})}{1-(\phi_w\circ g)'(u_{w,g})}\right) \end{aligned}$$

expanding the last fraction as a geometric series we obtain (20.1) which finishes the proof. □

From an abstract point of view this result is already completely satisfactory, as we have obtained a factorization of the zeta function into reduced zeta functions which themselves are again entire functions. This result is also sufficient to determine which zeros of the dynamical zeta function are related to eigenfunctions of $\mathcal{L}_V$ with a certain symmetry behavior. From a practical, computational point of view we will however see that (20.1) is not yet optimal. In fact we will show that the symmetry implies that many terms in the series appearing in (20.1) are equal and can be grouped together, which speeds up practical computations considerably. Thus the rest of this section will be devoted to simplify (20.1) and determine efficient formulas for $d_V^\chi(z)$.

In order to formulate them, we first have to study the symbolic dynamics more thoroughly and introduce some useful notation.

We first introduce the set of *words with arbitrary length*

$$\mathcal{W} := \bigcup_{n=1}^{\infty}\mathcal{W}_n$$

and denote for $w\in\mathcal{W}$ its *word length* by n_w such that $w\in\mathcal{W}_{n_w}$. Similarly, we want to define the set of all words closed under an arbitrary group element. However, in (20.1) the words appear always together with the group element which closes them. If one word admits several closing group elements, then the word will appear several times with all possible closing words. It will therefore turn out to be convenient to consider pairs of words and closing group elements and we define

$$\mathcal{W}^G := \{(w,g)\in\mathcal{W}\times G,\ \text{s.t. } gw_{n_w} = w_0\}\,.$$

In order to shorten the notation we will denote these pairs of words and group elements by a bold $\mathbf{w}$. The group element of the pair $\mathbf{w}$ will be written as

$g_{\mathbf{w}}$ and the word by a standard w such that $\mathbf{w} = (w, g_{\mathbf{w}})$.The wordlength of w will be written as $n_{\mathbf{w}}$..

As shown in the proof of Theorem 20.1 to any $\mathbf{w} \in \mathcal{W}^G$ there exists a unique $u_{\mathbf{w}}$ defined by

$$\phi_w(g_{\mathbf{w}} u_{\mathbf{w}}) = u_{\mathbf{w}}$$

and we will call these points *relative fixed points* in the sequel. The G-action on $\mathcal{W}_n$ can be extended to a G-action on $\mathcal{W}^G$ by taking the adjoint action on the G-part of $\mathcal{W}^G$ by setting for $h \in G$

$$g\mathbf{w} := (gw, gg_{\mathbf{w}}g^{-1}). \tag{20.3}$$

Beside the G-action on $\mathcal{W}^G$ we can also define the *shift action* by setting

$$\sigma_R\mathbf{w} := \big((g_{\mathbf{w}}w_{n-1}, w_0, \ldots, w_{n-1}), g_{\mathbf{w}}\big) \text{ and } \sigma_L w := \big((w_1, \ldots, w_n, g_{\mathbf{w}}^{-1}w_1), g_{\mathbf{w}}\big). \tag{20.4}$$

Note that it would not be possible to define this action on the g-closed words because the shift operation on the word depends explicitly on the choice of the closing group element. The importance of the shift action arises from the fact that it is conjugated to the action of the IFS on the relative fixed points $u_{\mathbf{w}}$. To be more precise we have for every $\mathbf{w} \in \mathcal{W}^G$ that $u_{\sigma_L\mathbf{w}} = \phi_{g_{\mathbf{w}}^{-1}w_{0,1}}(u_{\mathbf{w}})$ because

$$\begin{aligned}
\phi_{(w_1,\ldots,w_n,g_{\mathbf{w}}^{-1}w_1)}(g_{\sigma_L\mathbf{w}}\phi_{g_{\mathbf{w}}^{-1}w_{0,1}}(u_{\mathbf{w}})) &= \phi_{(w_1,\ldots,w_n,g_{\mathbf{w}}^{-1}w_1)}(g_{\mathbf{w}}\phi_{g_{\mathbf{w}}^{-1}w_{0,1}}(u_{\mathbf{w}})) \\
&= \phi_{(w_1,\ldots,w_n,g_{\mathbf{w}}^{-1}w_1)}\phi_{w_{0,1}}(g_{\mathbf{w}}u_{\mathbf{w}}) \\
&= \phi_{g_{\mathbf{w}}^{-1}w_{0,1}}(\phi_w(g_{\mathbf{w}}u_{\mathbf{w}})) \\
&= \phi_{g_{\mathbf{w}}^{-1}w_{0,1}}(u_{\mathbf{w}}).
\end{aligned}$$

Finally, as $\sigma_R = \sigma_L^{-1}$, the shift action generates a $\mathbb{Z}$-action on the set of words $\mathcal{W}$ and the set of G-closed words $\mathcal{W}^G$. As

$$\begin{aligned}
\sigma_L h\sigma_R\mathbf{w} &= \sigma_L h\big((g_{\mathbf{w}}w_{n-1}, w_0, \ldots, w_{n-1}), g_{\mathbf{w}}\big) \\
&= \sigma_L\big((hg_{\mathbf{w}}w_{n-1}, hw_0, \ldots, hw_{n-1}), hg_{\mathbf{w}}h^{-1}\big) \\
&= \big((hw_0, \ldots, hg_{\mathbf{w}}^{-1}h^{-1}hg_{\mathbf{w}}w_n), hg_{\mathbf{w}}h^{-1}\big) = h\mathbf{w}
\end{aligned}$$

holds, the G-action and the $\mathbb{Z}$-action commute and we can consider the group $G \times \mathbb{Z}$ acting on $\mathcal{W}^G$. Thus we can consider the space of $G \times \mathbb{Z}$-orbits $(G \times \mathbb{Z})\backslash\mathcal{W}^G$ and we will denote the orbit passing through w by

$$[\mathbf{w}] \in \big[\mathcal{W}^G\big] := (G \times \mathbb{Z})\backslash\mathcal{W}^G.$$

We next want to introduce the notion of *composite* and *prime* elements in $\mathcal{W}^G$. Given $\mathbf{w} \in \mathcal{W}^G$ we can define its *k-fold iteration* of by

$$\mathbf{w}^k := \big(g_{\mathbf{w}}^{k-1} w_0, \ldots, g_{\mathbf{w}}^{k-1} w_n, g_{\mathbf{w}}^{k-2} w_1, \ldots, g_{\mathbf{w}} w_1, \ldots, g_{\mathbf{w}} w_n, w_1, \ldots, w_n), g_{\mathbf{w}}^k\big). \tag{20.5}$$

By construction $\mathbf{w}^k \in \mathcal{W}^G$ and $n_{\mathbf{w}^k} = k n_{\mathbf{w}}$. Furthermore we calculate

$$\begin{aligned} \phi_{w^k}(g_{\mathbf{w}^k} u_{\mathbf{w}}) &= (\phi_w \circ \cdots \circ \phi_{g_{\mathbf{w}}^{k-1} w})(g_{\mathbf{w}}^k u_{\mathbf{w}}) \qquad (20.6) \\ &= [(\phi_w \circ g_{\mathbf{w}}) \circ (\phi_w \circ g_{\mathbf{w}}) \circ \ldots \circ (\phi_w \circ g_{\mathbf{w}})](u_{\mathbf{w}}) = u_{\mathbf{w}}, \end{aligned}$$

where the second last equality has been obtained by iteratively using the commutation rule (19.2), which implies that $u_{\mathbf{w}^k} = u_{\mathbf{w}}$.

Definition 20.1. All elements in $\mathcal{W}^G$ that are obtained by an iteration of a shorter word are called *composite*, all elements which can't be written as an iteration of shorter elements are called *prime*.

Lemma 20.2. *If $\mathbf{w} \in \mathcal{W}^G$ is a composite respectively prime element then all other elements in the $G \times \mathbb{Z}$-orbit are equally composite respectively prime.*

Proof. As an element is either prime or composite, it suffices to show the statement for one case. Thus assume that $\tilde{\mathbf{w}} = \mathbf{w}^k$ for $k \geq 2$ is composite and consider

$$\begin{aligned} h(\mathbf{w}^k) &= \big((h g_{\mathbf{w}}^{k-1} w_0, \ldots, h g_{\mathbf{w}}^{k-1} w_n, \ldots, h w_1, \ldots, h w_n), h g_{\mathbf{w}}^k h^{-1}\big) \\ &= \big(((h g_{\mathbf{w}} h^{-1})^{k-1} h w_0, \ldots, (h g_{\mathbf{w}} h^{-1})^{k-1} h w_n, \ldots, h w_1, \ldots, h w_n), (h g_{\mathbf{w}} h^{-1})^k\big) \\ &\underset{(20.3)}{=} \big((g_{h\mathbf{w}}^{k-1} h w_0, \ldots, g_{h\mathbf{w}}^{k-1} h w_n, \ldots, h w_1, \ldots, h w_n), g_{h\mathbf{w}}^k\big) \\ &= (h\mathbf{w})^k. \end{aligned}$$

Similarly one calculates $\sigma_{L/R}(\mathbf{w}^k) = (\sigma_{L/R}\mathbf{w})^k$. □

The preceding lemma allows us to define the set of *symmetry classes of G-closed prime orbits* as

$$\big[\mathcal{W}^G_{\text{prime}}\big] := \{[\mathbf{w}] \in (G \times \mathbb{Z}) \backslash \mathcal{W}^G, \mathbf{w} \text{ is prime } \}.$$

Having introduced all this notation we can go one step further towards the formulas for the symmetry reduced zeta functions by considering the terms $V_w(g_{\mathbf{w}} u_{\mathbf{w}})$ and $(\phi_w \circ g_{\mathbf{w}})'(u_{\mathbf{w}})$ appearing in the symmetry reduced trace formula

Proposition 20.3. *Let* $[\mathbf{w}] \in \left[\mathcal{W}^G\right]$ *be a* $G \times \mathbb{Z}$*-orbit. Then for all elements in the* $G \times \mathbb{Z}$*-orbit of* $\mathbf{w}^k$*, i.e. for all* $\mathbf{v} \in [\mathbf{w}^k]$ *we obtain*

$$V_v(g_{\mathbf{v}} u_{\mathbf{v}}) = [V_w(g_{\mathbf{w}} u_{\mathbf{w}})]^k \tag{20.7}$$

and

$$(\phi_v \circ g_{\mathbf{v}})'(u_{\mathbf{v}}) = [(\phi_w \circ g_{\mathbf{w}})'(u_{\mathbf{w}})]^k \tag{20.8}$$

Proof. All calculations for this proof are basically straight forward, we will nevertheless give them in detail.

For this proposition we have to prove two things: First, that the two quantities are independent on the choice of the element in the $G \times \mathbb{Z}$-orbit and second, that a k-fold iteration amounts simply to the k-th power of the quantities. Let's start with the first point and take an arbitrary element $\mathbf{w} \in \mathcal{W}^G$ and $h \in G$. Then

$$\begin{aligned}
V_{hw}(g_{h\mathbf{w}} u_{h\mathbf{w}}) &= \prod_{k=1}^{n} V(\phi_{(hw)_{0,k}}(g_{h\mathbf{w}} u_{h\mathbf{w}})) \\
&\underset{(20.3)}{=} \prod_{k=1}^{n} V(\phi_{(hw)_{0,k}}((hg_{\mathbf{w}}h^{-1})hu_{\mathbf{w}})) \\
&\underset{(19.2)}{=} \prod_{k=1}^{n} V(h\phi_{w_{0,k}}(g_{\mathbf{w}} u_{\mathbf{w}})) \\
&\underset{(19.6)}{=} \prod_{k=1}^{n} V(\phi_{w_{0,k}}(g_{\mathbf{w}} u_{\mathbf{w}})).
\end{aligned}$$

In order to see the invariance under σ_L we first recall that $u_{\sigma_L \mathbf{w}} = \phi_{g_{\mathbf{w}}^{-1} w_{0,1}}(u_{\mathbf{w}})$.

Consequently

$$\begin{aligned}
V_{\sigma_L w}(g_{\sigma_L \mathbf{w}} u_{\sigma_L \mathbf{w}}) &= \prod_{k=1}^{n} V[\phi_{(\sigma_L w)_{0,k}}(g_{\mathbf{w}} \phi_{g_{\mathbf{w}}^{-1} w_{0,1}}(u_{\mathbf{w}}))] \\
&= \prod_{k=1}^{n} V[\phi_{(\sigma_L w)_{0,k}}(\phi_{w_{0,1}}(g_{\mathbf{w}} u_{\mathbf{w}}))] \\
&= \left(\prod_{k=1}^{n-1} V[\phi_{w_{0,k+1}}(g_{\mathbf{w}} u_{\mathbf{w}})] \right) \cdot V(\phi_{(w_0,\ldots,w_n,g_{\mathbf{w}}^{-1} w_1)}(g_{\mathbf{w}} u_{\mathbf{w}})) \\
&= \left(\prod_{k=1}^{n-1} V[\phi_{w_{0,k+1}}(g_{\mathbf{w}} u_{\mathbf{w}})] \right) \cdot V(\phi_{(w_n,g_{\mathbf{w}}^{-1} w_1)}(\underbrace{\phi_w(g_{\mathbf{w}} u_{\mathbf{w}})}_{=u_{\mathbf{w}}})) \\
&\underset{(19.6)}{=} \left(\prod_{k=1}^{n-1} V[\phi_{w_{0,k+1}}(g_{\mathbf{w}} u_{\mathbf{w}})] \right) \cdot V(g_{\mathbf{w}} \phi_{(w_n,g_{\mathbf{w}}^{-1} w_1)}(u_{\mathbf{w}}) \\
&\underset{(19.2)}{=} \left(\prod_{k=2}^{n} V[\phi_{w_{0,k}}(g_{\mathbf{w}} u_{\mathbf{w}})] \right) \cdot V(\phi_{(w_0,w_1)}(g_{\mathbf{w}} u_{\mathbf{w}}) \\
&= \prod_{k=1}^{n} V[\phi_{w_{0,k}}(g_{\mathbf{w}} u_{\mathbf{w}})].
\end{aligned}$$

With an analogous calculation one obtains the invariance under σ_R.

In order to see the invariance of $(\phi_w \circ g_{\mathbf{w}})'(u_{\mathbf{w}})$ we first consider for arbitrary $u \in D_{g_{\mathbf{w}}^{-1} w_0}$ the equation

$$(\phi_{hw} \circ g_{h\mathbf{w}})(hu) \underset{(20.3)}{=} \phi_{hw}(h g_{\mathbf{w}} h^{-1} hu) \underset{(19.2)}{=} h \phi_w(g_{\mathbf{w}} u).$$

Differentiating both sides with respect to u yields

$$h'(u) \cdot (\phi_{hw} \circ g_{h\mathbf{w}})'(hu) = h'(\phi_w(g_{\mathbf{w}} u)) \cdot (\phi_w \circ g_{\mathbf{w}})'(u)$$

and plugging in $u_{\mathbf{w}}$ this shows the invariance as $\phi_w(g_{\mathbf{w}} u_{\mathbf{w}}) = u_{\mathbf{w}}$. The invariance under the shift can be derived similarly by starting from the equation

$$\begin{aligned}
(\phi_{\sigma_L w} \circ g_{\sigma_L \mathbf{w}})(\phi_{g_{\mathbf{w}}^{-1} w_{0,1}}(u)) &\underset{(20.4)}{=} \phi_{(w_1,\ldots,w_n,g_{\mathbf{w}}^{-1} w_1)}(g_{\mathbf{w}} \phi_{g_{\mathbf{w}}^{-1} w_{0,1}}(u)) \\
&\underset{(19.2)}{=} \phi_{(w_1,\ldots,w_n,g_{\mathbf{w}}^{-1} w_1)} \circ \phi_{w_0,w_1}(g_{\mathbf{w}} z) \\
&= \phi_{g_{\mathbf{w}}^{-1} w_{0,1}}((\phi_w \circ g_{\mathbf{w}})(u)).
\end{aligned}$$

Again differentiating both sides and plugging in $u_{\mathbf{w}}$ yields the desired result. The invariance under σ_R follows analogously.

Having proved the $G\times\mathbb{Z}$-invariance it finally remains to show the behavior under iterations. We calculate

$$\begin{aligned} V_{w^k}(g_{\mathbf{w}^k}u_{\mathbf{w}^k}) &= V_{w^k}(g_{\mathbf{w}}^k u_{\mathbf{w}}) \\ &= \prod_{l=1}^{kn_{\mathbf{w}}} V[\phi_{(w^k)_{0,l}}(g_{\mathbf{w}}^k u_{\mathbf{w}})] \\ &= \prod_{l=1}^{n_{\mathbf{w}}} V[\phi_{(g_{\mathbf{w}}^{k-1}w)_{0,l}}(g_{\mathbf{w}}^k u_{\mathbf{w}})] \cdot \prod_{l=1}^{n_{\mathbf{w}}} V[(\phi_{(g_{\mathbf{w}}^{k-2}w)_{0,l}} \circ \phi_{g_{\mathbf{w}}^{k-1}w})(g_{\mathbf{w}}^k u_{\mathbf{w}}))] \\ &\quad \cdot \ldots \cdot \prod_{l=1}^{n_{\mathbf{w}}} V[\phi_{w_{0,l}} \circ \phi_{g_{\mathbf{w}}w} \circ \ldots \circ \phi_{g_{\mathbf{w}}^{k-1}w}(g_{\mathbf{w}}^k u_{\mathbf{w}})]. \end{aligned}$$

However each of these products becomes equal to $V_w(g_{\mathbf{w}}u_{\mathbf{w}})$ after iteratively commuting the G-action with the IFS by (19.2). For example the second one becomes

$$\begin{aligned} \prod_{l=1}^{n_{\mathbf{w}}} V[(\phi_{(g_{\mathbf{w}}^{k-2}w)_{0,l}} \circ \phi_{g_{\mathbf{w}}^{k-1}w})(g_{\mathbf{w}}^k u_{\mathbf{w}}))] &\underset{(19.2)}{=} \prod_{l=1}^{n_{\mathbf{w}}} V[(\phi_{(g_{\mathbf{w}}^{k-2}w)_{0,l}} \circ g_{\mathbf{w}}^{k-1} \circ \phi_w)(g_{\mathbf{w}}u_{\mathbf{w}}))] \\ &\underset{(19.2)}{=} \prod_{l=1}^{n_{\mathbf{w}}} V[(g_{\mathbf{w}}^{k-2}\phi_{w_{0,l}} \circ g_{\mathbf{w}} \circ \phi_w)(g_{\mathbf{w}}u_{\mathbf{w}}))] \\ &= \prod_{l=1}^{n_{\mathbf{w}}} V[\phi_{w_{0,l}}(g_{\mathbf{w}}u_{\mathbf{w}})]. \end{aligned}$$

For the iteration behavior of $(\phi_w \circ g_{\mathbf{w}})'(u_{\mathbf{w}})$ we calculate as in (20.6)

$$(\phi_{w^k} \circ g_{\mathbf{w}^k})(u) = (\phi_w \circ g_{\mathbf{w}}) \circ \ldots \circ (\phi_w \circ g_{\mathbf{w}})(u).$$

Again differentiation of both sides w.r.t. u and insertion of $u_{\mathbf{w}^k} = u_{\mathbf{w}}$ shows that

$$(\phi_{w^k} \circ g_{\mathbf{w}^k})'(u_{\mathbf{w}^k}) = [(\phi_w \circ g_{\mathbf{w}})(u_{\mathbf{w}^k})]^k$$

which finishes the proof. □

The last result which we need for simplifying the symmetry reduced zeta function is the following

Lemma 20.4. *For $[\mathbf{w}] \in \left[\mathcal{W}^G_{\text{prime}}\right]$ we denote by $\#[\mathbf{w}]$ the number of elements of the $G \times \mathbb{Z}$-orbit in $\mathcal{W}^G$. If G acts freely on $\mathcal{W}^G$ then*

$$\#[\mathbf{w}] = |G| \cdot n_{\mathbf{w}}.$$

Proof. As the G-orbit $[\mathbf{w}]$ can be written as the quotient $[\mathbf{w}] = (G\times\mathbb{Z})/(G\times\mathbb{Z})_{\mathbf{w}}$ where $(G\times\mathbb{Z})_{\mathbf{w}}$ is the stabilizer of the element $\mathbf{w}\in\mathcal{W}^G$. So we can prove the lemma by studying the stabilizer $(G\times\mathbb{Z})_{\mathbf{w}}$. For any element $\mathbf{w}\in\mathcal{W}^G$ we have that $g_{\mathbf{w}}\sigma_L^{n_{\mathbf{w}}}\mathbf{w} = \mathbf{w}$, so the group generated by $(g_{\mathbf{w}}, n_{\mathbf{w}})$ is a subset of the stabilizer group, i.e.

$$\langle (g_{\mathbf{w}}, n_{\mathbf{w}})\rangle \subset (G\times\mathbb{Z})_{\mathbf{w}}. \tag{20.9}$$

Note that there are exactly $|G|\cdot n_{\mathbf{w}}$ orbits of the right group action of $\langle (g_{\mathbf{w}}, n_{\mathbf{w}})\rangle$ on $G\times\mathbb{Z}$ so if in (20.9) the equality holds, then $\#[\mathbf{w}] = |G|\cdot n_{\mathbf{w}}$. We have thus to show that for a prime elment $\mathbf{w}$, the stabilizer can't be bigger than $\langle (g_{\mathbf{w}}, n_{\mathbf{w}})\rangle$. So we first assume that there is $h\in G$ such that $(h, n_{\mathbf{w}})\in (G\times\mathbb{Z})_w$ which means

$$h\sigma_L^{n_{\mathbf{w}}}\mathbf{w} = \mathbf{w} = g_{\mathbf{w}}\sigma_L^{n_{\mathbf{w}}}\mathbf{w}.$$

But from the assumption that G acts freely on $\mathcal{W}^G$ we obtain $h = g_w$. Next we assume, hat there is a $k\notin n_{\mathbf{w}}\mathbb{Z}$ and $h\in G$ such that $(h,k)\in(G\times\mathbb{Z})_{\mathbf{w}}$. By adding or subtracting the elements $(g_{\mathbf{w}}, n_{\mathbf{w}})$ we can assume without loss of generality that $0<k<n_{\mathbf{w}}$. By basic number theoretic arguments there are integers $a,b\in\mathbb{N}$ such that $ak = bn_{\mathbf{w}} + c$ where c is the greatest common divisor of k and $n_{\mathbf{w}}$. Thus we can write

$$\begin{array}{rcl} h^a\sigma_L^{ak}\big((w_0,\dots w_{n_{\mathbf{w}}}), g_{\mathbf{w}}\big) & = & \big((w_0,\dots,w_{n_{\mathbf{w}}}), g_{\mathbf{w}}\big) \\ \big(h^a g_{\mathbf{w}}^{-b}(w_c,\dots,w_{n_{\mathbf{w}}-1}, g_{\mathbf{w}}^{-1}w_0,\dots,g_{\mathbf{w}}^{-1}w_c), h^a g_{\mathbf{w}} h^{-a}\big) & = & \big((w_0,\dots,w_{n_{\mathbf{w}}}), g_{\mathbf{w}}\big) \end{array} \quad \Leftrightarrow$$

Comparing the closing words we obtain

$$h^a g_{\mathbf{w}} = g_{\mathbf{w}} h^a. \tag{20.10}$$

Looking at the last c entries of the word we conclude that

$$(w_{n_{\mathbf{w}}-c},\dots,w_{n_{\mathbf{w}}}) = h^a g_{\mathbf{w}}^{-b-1}(w_0,\dots,w_c). \tag{20.11}$$

Inserting this back into the above equation we iteratively conclude that

$$(w_{n_{\mathbf{w}}-rc},\dots,w_{n_{\mathbf{w}}-(r-1)c}) = (h^a g_{\mathbf{w}}^{-b})^r g_{\mathbf{w}}^{-1}(w_0,\dots,w_c). \tag{20.12}$$

Additionally from (20.11) we obtain $h^a g_{\mathbf{w}}^{-b} g_{\mathbf{w}}^{-1} w_c = w_{n_{\mathbf{w}}} = g_{\mathbf{w}}^{-1} w_0$, so $h^a g_{\mathbf{w}}^{-b}$ is a closing group element of the word $g_{\mathbf{w}}^{-1}(w_0,\dots,w_c)$ and we can consider the pair

$$\tilde{\mathbf{w}} := \big(g_{\mathbf{w}}^{-1}(w_0,\dots,w_c), h^a g_{\mathbf{w}}^{-b}\big)\in\mathcal{W}^G.$$

We set $t := n_{\mathbf{w}}/c \in \mathbb{N}$ and calculate

$$\begin{aligned}(h^a g_{\mathbf{w}}^{-b})^t \tilde{\mathbf{w}} &= \big((h^a g_{\mathbf{w}}^{-1})^t (w_0, \ldots, w_c), h^a g_{\mathbf{w}}^{-b}\big) \\ &\underset{(20.12)}{=} \big((w_0, \ldots, w_c), h^a g_{\mathbf{w}}^{-b}\big) \\ &\underset{(20.10)}{=} g_{\mathbf{w}} \tilde{\mathbf{w}}.\end{aligned}$$

So from the assumption that G acts freely on G we obtain $(h^a g_{\mathbf{w}}^{-b})^t = g_{\mathbf{w}}$. Putting everything together we obtain

$$\mathbf{w} = \tilde{\mathbf{w}}^t$$

which is in contradiction to the assumption that $\mathbf{w}$ is prime. □

We can now come back to the formula for the symmetry reduced zeta function, and first consider the three sums

$$\sum_{n>0} \sum_{g \in G} \sum_{w \in \mathcal{W}_n^g}$$

which can be replaced by a sum over $\mathcal{W}^G$. In the domain of absolute convergence we get

$$d_V^\chi(z) = \exp\left(- \sum_{k \geq 0} \sum_{\mathbf{w} \in \mathcal{W}^G} \frac{z^{n_{\mathbf{w}}}}{n_{\mathbf{w}}} \frac{d_\chi}{|G|} \chi(g_{\mathbf{w}}) V_w(g_{\mathbf{w}} u_{\mathbf{w}}) \left[(\phi_w \circ g_{\mathbf{w}})'(u_{\mathbf{w}})\right]^k \right).$$

Note that $V_w(g_{\mathbf{w}} u_{\mathbf{w}}) \left[(\phi_w \circ g_{\mathbf{w}})'(u_{\mathbf{w}})\right]^k$ is independent under the $G \times \mathbb{Z}$-action from Proposition 20.3. Additionally for all $\mathbf{v} \in [\mathbf{w}]$ we have $g_{\mathbf{v}} = h g_{\mathbf{w}} h^{-1}$ so $\chi(g_{\mathbf{w}})$ is also invariant under this action. Furthermore we know how $V_w(g_{\mathbf{w}} u_{\mathbf{w}}) \left[(\phi_w \circ g_{\mathbf{w}})'(u_{\mathbf{w}})\right]^k$ and $g_{\mathbf{w}}$ behave under iteration so we can reduce the sum over $\mathcal{W}^G$ to $\left[\mathcal{W}^G_{\text{prime}}\right]$ and its iterates. We get

$$\begin{aligned} d_V^\chi(z) \;=\; \exp\Bigg(- \sum_{k \geq 0} \sum_{[\mathbf{w}] \in \left[\mathcal{W}^G_{\text{prime}}\right]} \sum_{l>0} \#[\mathbf{w}^l] \frac{z^{n_{\mathbf{w}} l}}{n_{\mathbf{w}} l} \frac{d_\chi}{|G|} \chi(g_{\mathbf{w}}^l) \\ \Big(V_w(g_{\mathbf{w}} u_{\mathbf{w}}) \left[(\phi_w \circ g_{\mathbf{w}})'(u_{\mathbf{w}})\right]^k \Big)^l \Bigg). \end{aligned} \tag{20.13}$$

The character χ belongs to an irreducible unitary representation ρ_χ on a finite dimensional vector space V_χ, and we can write $\chi(g) = \mathrm{Tr}_{V_\chi}[\rho(g)]$. Thus we

get

$$\begin{aligned} d_V^\chi(z) &= \exp\left(-d_\chi \sum_{k\geq 0} \sum_{[\mathbf{w}]\in\left[\mathcal{W}^G_{\text{prime}}\right]} \sum_{l>0} \frac{z^{n_{\mathbf{w}} l}}{l} \mathrm{Tr}_{V_\chi}\left[\rho_\chi(g_{\mathbf{w}})^l\right] \left(V_w(g_{\mathbf{w}}u_{\mathbf{w}})\left[(\phi_w\circ g_{\mathbf{w}})'(u_{\mathbf{w}})\right]^k\right)^l\right) \\ &= \prod_{k\geq 0}\prod_{[\mathbf{w}]\in\left[\mathcal{W}^G_{\text{prime}}\right]} \exp\left(-d_\chi \sum_{l>0} \frac{\left(z^{n_{\mathbf{w}}} V_w(g_{\mathbf{w}}u_{\mathbf{w}})\left[(\phi_w\circ g_{\mathbf{w}})'(u_{\mathbf{w}})\right]^k\right)^l}{l} \mathrm{Tr}_{V_\chi}\left[\rho_\chi(g_{\mathbf{w}})^l\right]\right) \\ &= \prod_{k\geq 0}\prod_{[\mathbf{w}]\in\left[\mathcal{W}^G_{\text{prime}}\right]} \left(\det_{V_\chi}\left[1-\left(z^{n_{\mathbf{w}}} V_w(g_{\mathbf{w}}u_{\mathbf{w}})\left[(\phi_w\circ g_{\mathbf{w}})'(u_{\mathbf{w}})\right]^k\right)\rho_\chi(g_{\mathbf{w}})\right]\right)^{d_\chi} \end{aligned}$$

and we have finally shown the following theorem.

Theorem 20.5. *Let G be the symmetry group of a holomorphic, eventually expanding IFS that acts freely on $\mathcal{W}^G$. Let $V : \phi(D) \to \mathbb{C}$ be a holomorphic, bounded function which is symmetric with respect to the G-action and $\mathcal{L}_V$ be the transfer operator associated to the holomorphic IFS and V. Let $\hat{G}$ be the set of all unitary irreducible representations of G and $\chi : G \to \mathbb{C}$ the character of an irreducible representation $\rho_\chi : G \to GL(V_\chi)$ on the d_χ-dimensional vector space V_χ.Then the dynamical zeta function $d_V(z) := \det(1 - z\mathcal{L}_V)$ factorizes according to*

$$d_V(z) = \prod_{\chi\in\hat{G}} d_V^\chi(z) \tag{20.14}$$

and the symmetry reduced zeta functions $d_V^\chi(z)$ are entire functions. If $\mathcal{L}_v^\chi : B_\chi \to B_\chi$ is the symmetry reduced transfer operator then they are defined by $d_V^\chi(z) := \det_{B_\chi}(1 - z\mathcal{L}_v^\chi)$ and for $|z|$ sufficiently small they are given by

$$d_V^\chi(z) = \prod_{k\geq 0}\prod_{[\mathbf{w}]\in\left[\mathcal{W}^G_{\text{prime}}\right]} \left(\det_{V_\chi}\left[1-\left(z^{n_{\mathbf{w}}} V_w(g_{\mathbf{w}}u_{\mathbf{w}})\left[(\phi_w\circ g_{\mathbf{w}})'(u_{\mathbf{w}})\right]^k\right)\rho_\chi(g_{\mathbf{w}})\right]\right)^{d_\chi}. \tag{20.15}$$

In (20.15) the action of the group elements on $D \subset \mathbb{C}$ still appear explicitly. Using the following Lemma this equation can, however, be reformulated such that the precise form of the G-action on D does not show up anymore and the symmetry reduction depends only on the G-action on the symbols.

Lemma 20.6. *Let $[\mathbf{w}] \in \left[\mathcal{W}^G_{\text{prime}}\right]$ and let $m_{\mathbf{w}} \in \mathbb{N}$ be such that $g_{\mathbf{w}}^{m_{\mathbf{w}}} = \mathrm{Id}$ and that $g^k \neq \mathrm{Id}$ for all $0 < k < m_w$. Then $w^{m_{\mathbf{w}}}$ is a closed word and we have*

$$(\phi_w \circ g_{\mathbf{w}})'(u_{\mathbf{w}}) = \left[(\phi_{w^{m_{\mathbf{w}}}})'(u_{w^{m_{\mathbf{w}}}})\right]^{\frac{1}{m_{\mathbf{w}}}} \tag{20.16}$$

$$V_w(g_{\mathbf{w}}u_{\mathbf{w}}) = \left[V_{w^m_{\mathbf{w}}}(u_{w^{m_{\mathbf{w}}}})\right]^{\frac{1}{m_{\mathbf{w}}}}. \tag{20.17}$$

Proof. The property that $w^{m_{\mathbf{w}}}$ is a closed word directly follows from the definition (20.5) of w^k and the definition of $m_{\mathbf{w}}$.

Lets continue with (20.16): As in (20.6) we calculate for $u \in D$

$$\phi_{w^{m_{\mathbf{w}}}}(u) = \phi_{w^{m_{\mathbf{w}}}}(g_{\mathbf{w}}^{m_{\mathbf{w}}} u) = [(\phi_w \circ g_{\mathbf{w}}) \circ (\phi_w \circ g_{\mathbf{w}}) \circ \ldots \circ (\phi_w \circ g_{\mathbf{w}})](u).$$

Differentiating both sides and using $\phi_w(g_{\mathbf{w}} u_{\mathbf{w}}) = u_w = u_{w^{m_{\mathbf{w}}}}$ we immediately get (20.16).

The second equality can be derived from the fact that for a G-invariant potential V we calculate

$$\begin{aligned} V_{w^{m_{\mathbf{w}}}}(u_{\mathbf{w}}) &= V_{w^{m_{\mathbf{w}}}}(g_{\mathbf{w}}^{m_{\mathbf{w}}} u_{\mathbf{w}}) \\ &= \prod_{k=1}^{m_{\mathbf{w}} n_{\mathbf{w}}} V(\phi_{(w^{m_{\mathbf{w}}})_{0,k}}(g_{\mathbf{w}}^{m_{\mathbf{w}}} u_{\mathbf{w}})) \\ &= \prod_{k=1}^{n_{\mathbf{w}}} V(\phi_{(g_{\mathbf{w}}^{m_{\mathbf{w}}-1} w)_{0,k}}(g_{\mathbf{w}}^{m_{\mathbf{w}}} u_{\mathbf{w}})) \cdot \prod_{k=1}^{n_{\mathbf{w}}} V(\phi_{(g_{\mathbf{w}}^{m_{\mathbf{w}}-2} w)_{0,k}}(\phi_{(w^{m_{\mathbf{w}}})_{0,n_{\mathbf{w}}}}(g_{\mathbf{w}}^{m_{\mathbf{w}}} u_{\mathbf{w}}))) \\ &\quad \ldots \cdot \prod_{k=1}^{n_{\mathbf{w}}} V(\phi_{w_{0,k}}(\phi_{(w^{m_{\mathbf{w}}})_{0,(m_{\mathbf{w}}-1)n_{\mathbf{w}}}}(g_{\mathbf{w}}^{m_{\mathbf{w}}} u_{\mathbf{w}}))) \end{aligned} \tag{20.18}$$

Using $\phi_{w^{m_{\mathbf{w}}}} = \phi_w \circ \ldots \circ \phi_{g_{\mathbf{w}}^{m_{\mathbf{w}}-1} w}$ we calculate for arbitrary $l = 0, \ldots, m_{\mathbf{w}}$

$$\begin{aligned} \phi_{(w^{m_{\mathbf{w}}})_{0,ln_{\mathbf{w}}}}(g_{\mathbf{w}}^{m_{\mathbf{w}}} u_{\mathbf{w}}) &= \phi_{g_{\mathbf{w}}^{m_{\mathbf{w}}-l} w} \circ \ldots \circ \phi_{g_{\mathbf{w}}^{m_{\mathbf{w}}-1} w}(g_{\mathbf{w}}^{m_{\mathbf{w}}} u_{\mathbf{w}}) \\ &= g_{\mathbf{w}}^{m_{\mathbf{w}}-l} \circ (\phi_w \circ g_{\mathbf{w}}) \circ \ldots \circ (\phi_w \circ g_{\mathbf{w}})(u_{\mathbf{w}}) \\ &= g_{\mathbf{w}}^{m_{\mathbf{w}}-l} u_{\mathbf{w}}. \end{aligned}$$

Thus

$$\begin{aligned} V(\phi_{(g_{\mathbf{w}}^{m_{\mathbf{w}}-l} w)_{0,k}}(\phi_{(w^{m_{\mathbf{w}}})_{0,(l-1)n_{\mathbf{w}}}}(g_{\mathbf{w}}^{m_{\mathbf{w}}} u_{\mathbf{w}}))) &= V(\phi_{(g_{\mathbf{w}}^{m_{\mathbf{w}}-l} w)_{0,k}}(g_{\mathbf{w}}^{m_{\mathbf{w}}-l} g_{\mathbf{w}} u_{\mathbf{w}}))) \\ &\underset{(19.2),(19.6)}{=} V(\phi_{w_{0,k}}(g_{\mathbf{w}} u_{\mathbf{w}})) \end{aligned}$$

Inserting this in (20.18) yields

$$V_{w^{m_{\mathbf{w}}}}(u_{\mathbf{w}}) = [V_w(g_{\mathbf{w}} u_{\mathbf{w}})]^{m_{\mathbf{w}}}.$$

□

Inserting (20.16) and (20.17) in (20.15) we get the following corollary.

Corrolary 20.7. *Under the same conditions as in Theorem 20.5 and with the same notation as in Theorem 20.5 and Lemma 20.6 we obtain*

$$d_V^{\chi}(z) = \prod_{k \geq 0} \prod_{[w] \in [\mathcal{W}_{\text{prime}}^G]} \left(\det_{V_\chi} \left[1 - z^{n_{\mathbf{w}}} \left[V_{w^{m_{\mathbf{w}}}}(u_{\mathbf{w}}) ((\phi_{w^{m_{\mathbf{w}}}})'(u_{\mathbf{w}}))^k \right]^{\frac{1}{m_{\mathbf{w}}}} \rho_\chi(g_{\mathbf{w}}) \right] \right)^{d_\chi} \tag{20.19}$$

21 Application to Selberg zeta functions

In this section we want to apply the results of the previous section in order to obtain factorizations of the Selberg zeta functions associated to Schottky surfaces. Our main interest is in the symmetric 3-funneled Schottky surfaces which were presented in Example 19.1. However, as pointed out in this example, the symmetry group of the standard Bowen-Series IFS is much smaller than the symmetry group of the surface, thus if one wants to obtain a full factorization of the Selberg zeta function one has to work with an alternative holomorphic IFS which incorporates the whole symmetry of the surface. Such an IFS has been introduced for 3-funneled surfaces in Part II under the name flow-adapted IFS. The idea behind these flow-adapted IFS, however, easily generalizes to certain n-funneled surfaces of genus zero. In Section 21.1 we will first introduce these symmetric n-funneled surfaces and their flow-adapted IFS. Then we will use Theorem 20.5 in order to obtain a factorization of the Selberg zeta function. In Section 21.2 and we will illustrate that this factorization yields an enormous speed-up in the calculation of the resonances of the Laplacian and allows for the first time to calculate the resonance structure on surfaces which were numerically not treatable such as 4-funneled surfaces.

21.1 Factorization of Selberg zeta functions for symmetric n-funneled Schottky surfaces

As mentioned in Example 19.1, the 3-funneled Schottky surfaces of genus zero are uniquely determined by the three funnel-widths l_1, l_2, l_3 i.e. by the lengths of the three geodesics $\gamma_1, \gamma_2, \gamma_3$ (see Figure 19.1) and the completely symmetric 3-funneled surfaces are uniquely determined by $l_1 = l_2 = l_3 = l$.[14] For n-funneled surfaces it is not true anymore that the surfaces are uniquely defined by the n funnel-widths. Due to their nontrivial pants decomposition also additional lengths along which the pants are glued together as well as the twist angles appear in their Fenchel-Nielsen coordinates and have to be taken into account in order to characterize them completely [5, Section 13.3] The symmetric n-funneled surfaces which we will consider in this section can, however, be easily defined as follows.

Definition 21.1. Let $n_f \geq 3$ and $0 < \psi < 2\pi/n_f$ then on the Poincaré disk-model $\mathbb{D}$ we can define n_f geodesics $\tilde{c}_1, \ldots, \tilde{c}_{n_f}$ by their start and end

[14] In Part II and III these surfaces were of special interest as they posses very strong resonance chains

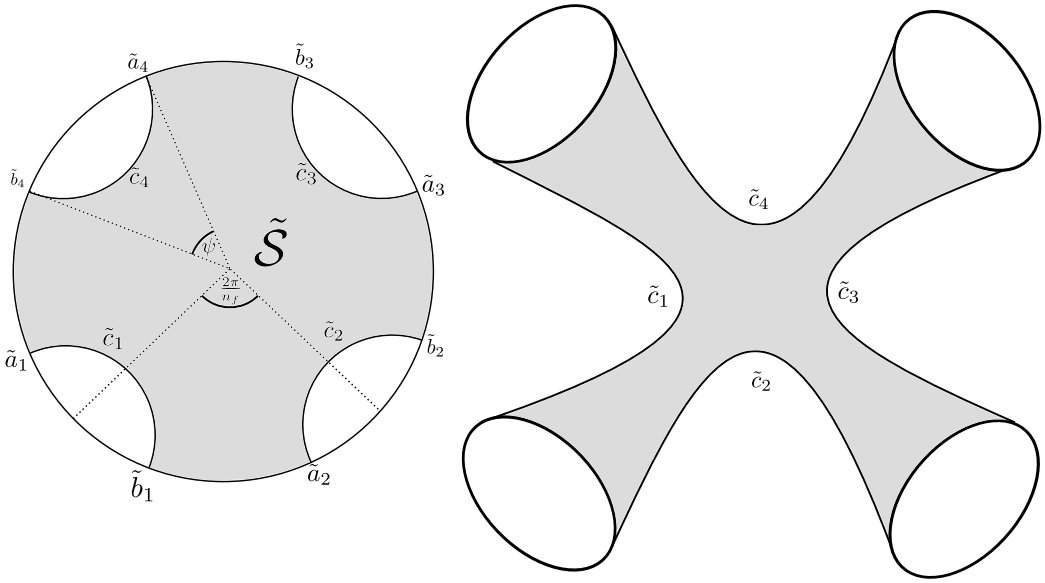

Figure 21.1: Sketch of the construction of a 4-funneled symmetric surface defined in Definition 21.1. On the left side one can see the definition of the domain *tildeS* in the Poincaré disk model. On the right side one can see a schematic sketch of the surface that consists of two copies of $\tilde{S}$ glued together at the geodesic boundaries $\tilde{c}_i$.

points (see Figure 21.1)

$$\tilde{a}_j = e^{i(\pi(2j+1+n_f)/n_f - \psi/2)} \in \partial\mathbb{D} \text{ and } \tilde{b}_j = e^{i(\pi(2j+1+n_f)/n_f + \psi/2)} \in \partial\mathbb{D}.$$

Each of these geodesics $\tilde{c}_j$ cuts $\mathbb{D}$ into two half spaces and we denote the intersection of all those j half spaces that contain $0 \in \mathbb{D}$ by $\tilde{\mathcal{S}}$. The surface $X_{n_f,\Psi}$ is then the hyperbolic surface obtained by gluing together two copies of $\tilde{\mathcal{S}}$ along the corresponding geodesic boundaries.

We will next explain, how the surfaces $X_{n_f,\psi}$ can be understood as Schottky surfaces in the sense of Example 18.1 and at the same time introduce the objects which are needed to define the flow-adapted IFS. We therefore transform the circles $\tilde{c}_i$ and the domain $\tilde{\mathcal{S}}$ to the upper half plane $\mathbb{H}$ by the Cayley transform

$$C : \left\{ \begin{array}{ccc} \mathbb{C} & \to & \mathbb{H} \\ u & \mapsto & -i\frac{u-1}{u+1} \end{array} \right.$$

and we obtain (see Figure 21.2) $\mathcal{S} := C(\tilde{\mathcal{S}}) \subset \mathbb{H}$, $c_j := C(\tilde{c}_j)$ as well as

$$a_j := C(\tilde{a}_j) = \frac{\sin\left((\pi(2j+1+n_f)/n_f - \psi/2)\right)}{1+\cos\left((\pi(2j+1+n_f)/n_f - \psi/2)\right)} \in \partial\mathbb{H}$$

and

$$b_j := C(\tilde{a}_j) = \frac{\sin\left((\pi(2j+1+n_f)/n_f - \psi/2)\right)}{1+\cos\left((\pi(2j+1+n_f)/n_f - \psi/2)\right)} \in \partial\mathbb{H}.$$

We will furthermore denote the Euclidean disks that are bounded by the geodesics c_j by D_j, their centers by $m_j := (b_j + a_j)/2$ and their radii by $r_j := (b_j - a_j)/2$. We can then define the matrices

$$R_j := \frac{1}{\sqrt{r_j}} \begin{pmatrix} m_j & r_j - m_j^2 \\ 1 & m_j \end{pmatrix}.$$

These matrices have determinant $\det(R_j) = -1$ and the Moebius transformations associated to these matrices

$$R_j u = \frac{m_j u - r_j - m_j^2}{u - m_j} = \frac{r_j}{u - m_j} + m_j$$

are holomorphic transformation on the Riemann sphere $\overline{\mathbb{C}}$ that correspond to a reflection at the circle boundary of D_j followed by a complex conjugation.

With these matrices we can now express the Schottky group associated to the surface $X_{n_f,\psi}$

Lemma 21.1. *With the notation from above let $n_f > 3$ and $0 < \psi < 2\pi/n_f$. Then the finitely generated group $\Gamma_{n_f,\psi} := \langle R_{n_f}R_1, \ldots, R_{n_f}R_{n_f-1}\rangle$ is a Schottky group and $X_{n_f,\psi} = \Gamma_{n_f,\psi}\backslash\mathbb{H}$.*

Proof. First we note that that for $j = 1, \ldots, n_f - 1$ we have $R_{n_f}R_j \in SL(2,\mathbb{R})$. If we define $D_{j+n_f-1} := R_{n_f}(D_j)$, then the transformation $R_{n_f}R_j$ maps the boundary of D_j to the boundary of D_{j+n_f-1} and the interior of D_j to the exterior of D_{j+n_f-1} and we have shown that $\Gamma_{n_f,\psi}$ is a Schottky group in the sense of Example 18.1. The fact that $X_{n_f,\psi}$ is the associated Schottky surface can be seen as follows: By definition of the disks D_j the fundamental domain of the Schottky group $\Gamma_{n_f,\psi}$ consists of two copies of the domain $\tilde{S}$ that are glued together along c_n. The Schottky surface $\Gamma_{n_f,\psi}\backslash\mathbb{H}$ is obtained by gluing together the fundamental domain along the geodesic boundaries of the disks that are identified by the generators of the Schottky group, so the $\Gamma_{n_f,\psi}\backslash\mathbb{H}$ consists of two copies of $\mathcal{S}$ that are glued together the same way as defined in Definition 21.1 (see Figure 21.2). □

We can now define the flow-adapted IFS and study its symmetry group. After this we will show that the dynamical zeta functions of these IFS coincides with the Selberg zeta function.

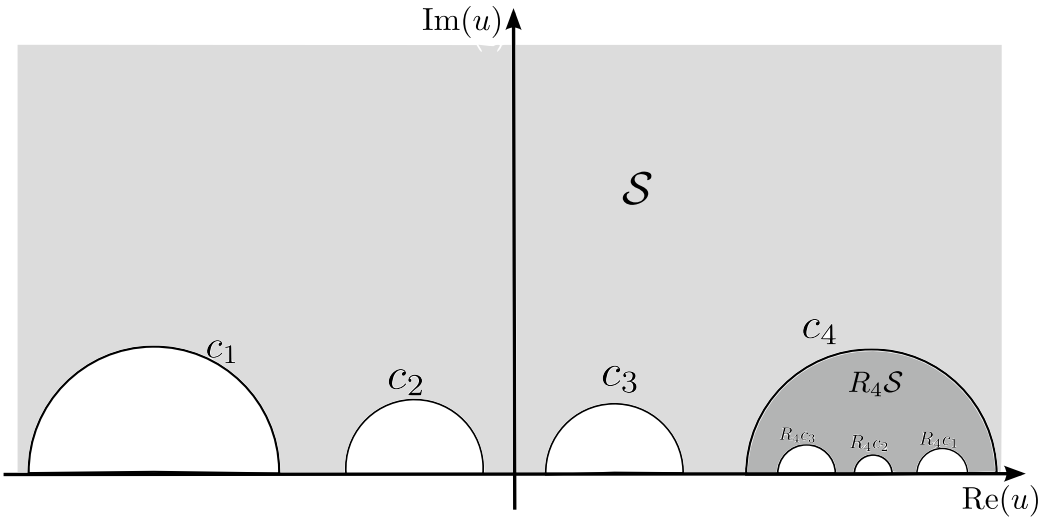

Figure 21.2: Sketch of the construction of the Schottky group associated to a 4-funneled symmetric surface. The fundamental domain consists of $\mathcal{S}$ and the reflection of this domain along the circle c_4. The Schottky surface is then obtained by gluing together the circles c_i and $R_4 c_i$ so finally one obtains the same surface as defined in Definition 21.1.

Definition 21.2 (Flow-adapted IFS)**.** Let $n_f \geq 3$ and $0 < \psi < 2\pi/n_f$. Let m_i, r_i and R_i be constructed as above. We define the offset variable

$$\delta_{\text{offset}} := b_{n_f} - a_1 + 1.$$

The *flow-adapted IFS* then is a holomorphic IFS with $N = 2n_f$ where the disks D_i are the Euclidean disks in $\mathbb{C}$ with centers m_i and radii r_i for $1 \leq i \leq n_f$ and with centers $m_{i-n_f} + \delta_{\text{offset}}$ and radii r_{i-n_f} for $n_f < i \leq 6$. The adjacency matrix A is given by $A_{i,j+n_f} = A_{j+n_f,i} = 1$ for all $1 \leq i, j \leq n_f$ with $i \neq j$ and $A_{i,j} = 0$ else. Finally for $i \rightsquigarrow j$ the maps $\phi_{i,j}$ are given by

$$\phi_{i,j}(u) := \begin{cases} R_{j-n_f}(u) + \delta_{\text{offset}} & \text{for } i \leq n_f \\ R_j(u - \delta_{\text{offset}}) & \text{for } i > n_f. \end{cases}$$

We now want to compare the symmetry group of the IFS with the symmetry group of the surface (for a sketch of the disk configuration of a 4-funneled surface see Figure 21.3). As the surfaces consists of two identical parts of $\tilde{\mathcal{S}} \subset \mathbb{D}$ we first note that the symmetry group of the domain $\tilde{\mathcal{S}}$ is given by D_{n_f}, the symmetry group of an n_f sided regular polygon of order $2n_f$. This symmetry group is generated by a rotation of $2\pi/n_f$ around $0 \in \mathbb{D}$

$$\tilde{g}_1(u) = e^{i2\pi/n_f} u$$

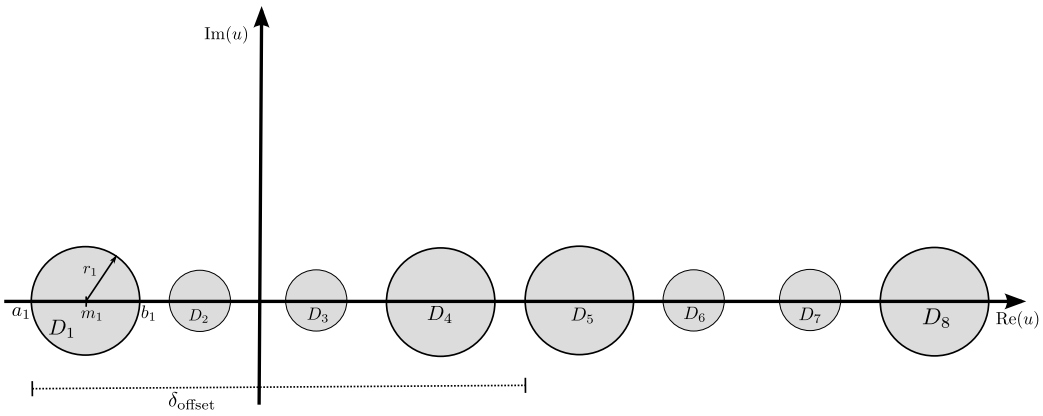

Figure 21.3: Illustration of the disk configuration of the flow-adapted IFS as defined in Definition 21.2 for a 4-funneled surface.

and by the reflection along the real axis

$$\tilde{g}_2(u) = \bar{u}.$$

Additionally the surface has a reflection symmetry along the plane, in which the two surfaces are glued together which identifies the two domains $\tilde{S}$. This reflection commutes with the action of D_{n_f} on the two copies of $\tilde{\mathcal{S}}$ so the whole symmetry group of $X_{n_f,\psi}$ is given by $D_{n_f} \times \mathbb{Z}_2$. As the flow-adapted IFS is directly constructed from the two parts $\tilde{\mathcal{S}}$ this symmetry action can directly be transferred via the Cayley transform to the IFS. Precisely the group action of the first generator is given by

$$g_1(u) := C \circ \tilde{g}_1 \circ C^{-1}(u) \text{ if } u \in \bigcup_{j=1}^{n_f} D_j$$

and

$$g_1(u) := \delta_{\text{offset}} + C \circ \tilde{g}_1 \circ C^{-1}(u - \delta_{\text{offset}}) \text{ if } u \in \bigcup_{j=n_f+1}^{2n_f} D_j.$$

For the definition of the second generator one has to pay a little bit more attention because, the reflection along the real axis is an antiholomorphic isometry of $\mathbb{D}$ and so is the transformation of this action to $\mathbb{H}$ which is given by $C \circ g_2 \circ C^{-1}(u) = -\bar{u}$. In order to make this action holomorphic, as required in Definition 19.1 we have to use the fact that the flow-adapted IFS naturally commutes with complex conjugation, so we can define

$$g_2(u) = \overline{C \circ g_2 \circ C^{-1}(u)} = -u \quad \text{if } u \in \bigcup_{j=1}^{n_f} D_j$$

and

$$g_2(u) = \delta_{\text{offset}} + \overline{C \circ g_2 \circ C^{-1}(u - \delta_{\text{offset}})} = \delta_{\text{offset}} - (u - \delta_{\text{offset}}) \quad \text{if } u \in \bigcup_{j=n_f+1}^{2n_f} D_j$$

The third group generator finally transforms to

$$g_3(u) = u + \delta_{\text{offset}} \text{ if } u \in \bigcup_{j=1}^{n_f} D_j \text{ and } g_3(u) = u - \delta_{\text{offset}} \text{ if } u \in \bigcup_{j=n_f+1}^{2n_f} D_j.$$

From the construction of the flow-adapted IFS it follows, directly, that the symmetry action commutes with the IFS and that $D_{n_f} \times \mathbb{Z}$ is really a symmetry group in the sense of Definition 19.1. The action on the symbols can be represented as a permutation group of the $2n_f$ symbols. In the cycle notation, the first and third generators can be written as

$$\begin{aligned} g_1 &= (1, 2, \ldots, n_f)(n_f + 1, n_f + 2, \ldots, 2n_f) \\ g_3 &= (1, n_f + 1)(2, n_f + 2) \ldots (n_f, 2n_f). \end{aligned}$$

For the second element we have to distinguish between the two cases of n_f being even or uneven. If n_f is even we have

$$\begin{aligned} g_2 &= (1, n_f)(2, n_f - 1) \ldots \left(\frac{n_f}{2}, \frac{n_f}{2} + 1\right) \\ &\quad (n_f + 1, 2n_f)(n_f + 2, 2n_f - 1) \ldots \left(\frac{3n_f}{2}, \frac{3n_f}{2} + 1\right) \end{aligned}$$

and else

$$\begin{aligned} g_2 &= (1, n_f)(2, n_f - 1) \ldots \left(\frac{n_f - 1}{2}, \frac{n_f + 3}{2}\right) \\ &\quad (n_f + 1, 2n_f)(n_f + 2, 2n_f - 1) \ldots \left(\frac{3n_f - 1}{2}, \frac{3n_f + 3}{2}\right). \end{aligned}$$

The flow-adapted IFS thus is an IFS, that incorporates the whole symmetry group $D_{n_f,\psi} \times \mathbb{Z}_2$ of the surface. As our aim is, however, to obtain a factorization of the Selberg zeta function $Z_{X_{n_f,\psi}}$ we additionally have to show that the dynamical zeta function of the flow-adapted IFS indeed contains the Selberg zeta function of the surface.

Proposition 21.2. *Let $n_f \geq 3$ and $0 < \psi < 2\pi/n_f$ and $\mathcal{L}_s$ be the Ruelle transfer operator of the flow-adapted IFS as defined in Definition 21.2 with potential $V_s(u) = [(\phi^{-1})'(u)]^{-s}$, then the dynamical zeta function coincides with the Selberg zeta function of $X_{n_f,\psi}$*

$$Z_{X_{n_f,\psi}}(s) = \det(1 - \mathcal{L}_s).$$

Proof. If we take the trivial group $G = \{\mathrm{Id}\}$ as a symmetry group, then as a special case of Theorem 20.5 we obtain

$$\det(1 - \mathcal{L}_s) = \prod_{[\mathbf{w}] \in \left[\mathcal{W}^{\{\mathrm{Id}\}}_{\mathrm{prime}}\right]} \prod_{k \geq 0} \left(1 - \phi'_w(u_{\mathbf{w}})^{k+s}\right).$$

Note that this formula is not at all related to a symmetry decomposition but can be obtained directly by a straight forward calculation (see e.g. [5, proof of Theorem 15.8] and c.f. Appendix A). Proposition 21.2 then follows from the following Proposition 21.3 which establishes a one-to-one correspondence between the prime words $\left[\mathcal{W}^{\mathrm{Id}}_{\mathrm{prime}}\right]$ of the flow-adapted IFS and the set of primitive closed geodesics on $X_{n_f,\psi}$. □

Proposition 21.3. [15] *Let $n_f \geq 3$ and $0 < \psi < 2\pi/n_f$ and consider the corresponding flow-adapted IFS from Definition 21.2. Then there exists a bijection between the classes of prime words in $\left[\mathcal{W}^{\{\mathrm{Id}\}}_{\mathrm{prime}}\right]$ and the primitive closed geodesics on $X_{n_f,\psi}$. Additionally the length of the geodesic associated to $[\mathbf{w}]$ is given by*

$$-\log(\phi'_w(u_{\mathbf{w}})). \tag{21.1}$$

Proof. Let R_j with $j = 1, \ldots, n_f$ be as in Definition 21.2 and $\Gamma_{n_f,\psi}$ the Schottky group from Lemma 21.1. It is known (see e.g. [5, Proposition 2.16]) that the set of primitive closed geodesics on $X_{n_f,\psi}$ is in bijection to the set of primitive conjugacy classes in $[T] \in \Gamma_{n_f,\psi}$ where primitive means that there is no $S \in [T]$ such that $S = R^k$ for some $R \in \Gamma_{n_f,\psi}$ and $k > 1$. Consequently our aim is to construct a bijection

$$T : \left[\mathcal{W}^{\{\mathrm{Id}\}}_{\mathrm{prime}}\right] \to \left\{\text{primitive conjugacy classes of } \Gamma_{n_f,\psi}\right\}.$$

In order to do so, we note that for $w \in \mathcal{W}_k$ from the form of the adjacency matrix in Definition 21.2 we have $w_i \leq n_f \Rightarrow w_{i+1} > n_f$. Thus, if w is a closed word, k has to be even. We first define the map

$$T : \left[\mathcal{W}^{\{\mathrm{Id}\}}\right] \to \left\{\text{conjugacy classes of } \Gamma_{n_f,\psi}\right\}.$$

on the closed words and will later show that we can easily restrict it to the prime words. For a closed word $w = (w_0, \ldots, w_{2r})$ we define the map T by

$$T(w) := \begin{cases} R_{w_{2r}} R_{w_{2r-1}-n_f} \ldots R_{w_2} R_{w_1-n_f} & \text{if } w_0 \leq n_f \\ R_{w_{2r-1}} R_{w_{2r-2}-n_f} \ldots R_{w_1} R_{w_0-n_f} & \text{if } w_0 > n_f \end{cases}. \tag{21.2}$$

[15] This proposition is very similar to Proposition 9.2. The difference is that here we allow an arbitrary number of funnels, while in Part II we could restrict ourselfs to 3 funnels but allowed different funnel width. Also the proofs work completely analogouse.

As closed words have to be of even length, $T(w)$ consists of a even number of reflections and is thus a positive isometry. We first show that T is well defined on $\left[\mathcal{W}^{\{\mathrm{Id}\}}_{\mathrm{prime}}\right]$, i.e. that it doesn't depend on the choice of the representative of $[\mathbf{w}]$. So let $\mathbf{v} \in [\mathbf{w}]$. Without loss of generality we can assume that $w_0 \leq n_f$ and $v_0 \leq n_f$ because otherwise we could simply apply the right-shift σ_R to obtain such an element in the same equivalence class that fulfills this condition and that is mapped to the identical element in $\Gamma_{n_f,\psi}$. Consequently there exists an integer $0 \leq t \leq r$ such that $v = (w_{2t}, \ldots, w_{2r}, w_1 \ldots, w_{2t})$ and we obtain

$$T(v) = R_{w_{2t}} \ldots R_{w_1 - n_f} R_{w_{2r}} \ldots R_{w_{2t+2}} R_{w_{2t+1} - n_f} = S^{-1} T(w) S$$

for $S = R_{w_{2r}} \ldots R_{w_{2t+1}-n_f}$. Thus $T(v)$ is in the same conjugacy class as $T(w)$.

In order to see the injectivity we take two words v and w that are mapped to the same conjugacy class. We assume first that

$$T(v) = R_a R_b T(w) R_b R_a.$$

However, from the form of the adjacency matrix it is not possible that an element in the image of T starts and ends with the same generator. Thus we have either

$$R_b R_a = R_{w_1 - n_f} R_{w_2}$$

or

$$R_a R_b = R_{w_{2r-1} - n_f} R_{w_{2r}}.$$

In the first case we have $v = \sigma_L^2 w$ in the latter case $v = \sigma_R^2 w$. By iterating this argument for arbitrary conjugations of $T(w)$ and $T(v)$ we have shown the injectivity of the map T.

In order to see the surjectivity we first note that for two arbitrary indices $1 \leq i, j \leq n_f$ the element $R_i R_j$ can be written as $(R_{n_f} R_i)^{-1} R_{n_f} R_j$, so $\Gamma_{n_f,\psi}$ contains all elements, that can be written as a composition of an even number of elements R_i. Let $S \in \Gamma_{n_f,\psi}$ be such an arbitrary element then we can write $S = R_{s_{2r}} \ldots R_{s_1}$ with $1 \leq s_i \leq n_f$. As two consecutive identical reflections cancel each other we can assume that $s_i \neq s_{i+1}$. Finally while $s_1 = s_{2_r}$ we can conjugate S by $R_{s_2} R_{s_1}$ which leads to an element composed from $2r - 2$ reflections. By iterative conjugation we can thus reduce the element to $\tilde{S} = R_{\tilde{s}_{2\tilde{r}}} \ldots R_{\tilde{s}_1}$ with $\tilde{s}_1 \neq \tilde{s}_{2\tilde{r}}$ and we obtain

$$\tilde{S} = T((s_{2\tilde{r}}, s_1 + n_f, s_2, \ldots, s_{2\tilde{r}-1} + n_f, s_{2\tilde{r}})).$$

We have thus constructed a bijective map between the classes of closed words and the conjugacy classes in $\Gamma_{n_f,\psi}$. We will now prove that this map

can be restricted to a bijection between the classes of prime words and the primitive conjugacy classes. As T is bijective and on both sides an element can either be primitive or composite it suffices to show that T maps composite closed words to composite conjugacy classes. This is, however, straight forward from the definition of T as obviously $T([w^k]) = T(w)^k$.

With this restriction we have constructed a bijection between the classes of closed, prime words and primitive conjugacy classes. Using the above mentioned result on the one-to-one correspondence between oriented primitive geodesics and primitive conjugacy classes, this is equivalently a bijection to the set of primitive, oriented, closed geodesics and it only remains to prove (21.1).

In order to achieve this, we first recall that the length of the primitive geodesic associated to a conjugacy class of an hyperbolic element $T \in \Gamma_{n_f,\psi}$ is equal to the displacement length of T (see e.g. [5, Proposition 2.16]) and it is also a well known fact that if $u_T \in \partial\mathbb{H}$ is the stable fixed point of T then $l(T) = -\log((T)'(u_T))$ (see e.g. [5, (15.2)]). Next we recall from the proof of Theorem 20.3 that $\phi'_w(u_w)$ is independent of the representative in $[\mathbf{w}]$. Assuming once more, that $w_0 \leq n_f$ we calculate that

$$\phi_w(u_{\mathbf{w}}) = R_{w_{2r}} \dots R_{w_1 - n_f} u_{\mathbf{w}}.$$

Thus $u_{\mathbf{w}}$ is the stable fixed point of the hyperbolic element $T(w)$ and for the displacement length of T we obtain $l(T(w)) = -\log((T(w))'(u_{\mathbf{w}}))$. As however the displacement length coincides with the length of the associated closed geodesic (see e.g. [5, Proposition 2.16]) we established (21.1) and finished the proof of Proposition 21.3. □

We have thus shown that the flow-adapted IFS incorporates the full symmetry group $G = D_{n_f} \times \mathbb{Z}_2$ of the surfaces $X_{n_f,\psi}$ and additionally leads to a transfer operator, whose dynamical zeta function incorporates the Selberg zeta function of the surface. Before we can however apply Theorem 20.5 in order to obtain a factorization of the Selberg zeta function we have to face a final remaining problem: The commutation of the group action with the IFS does not imply that the potentials

$$V_s(u) = [(\phi^{-1})'(u)]^s$$

that appear in the transfer operator $\mathcal{L}_s$ of Proposition 21.2 are G-invariant. This can be seen from the following calculations

$$\phi^{-1}(gu) = g(\phi^{-1}(u)) \quad \Rightarrow \quad (\phi^{-1})'(gu) = \frac{g'(\phi^{-1}(u))}{g'(u)} (\phi^{-1})'(u). \qquad (21.3)$$

Consequently the transfer operators $\mathcal{L}_s$ do not commute with the left regular G-action and they will in general not leave the symmetry reduced function spaces B_χ invariant. This problem can however be fixed by an averaging trick for the potential, i.e. by replacing the potential V_s by a family of G-invariant potentials V_s^G which leads to the same dynamical zeta functions.

Lemma 21.4. *There exists a family of potentials*

$$V_s^G(u) := \left(\prod_{g\in G} V_s(gu)\right)^{1/|G|} = \left(\prod_{g\in G} (\phi^{-1})'(gu)\right)^{s/|G|} \tag{21.4}$$

which is G-invariant.

Let furthermore $\mathcal{L}_s^G$ be the family of transfer operators obtained by the family of G-invariant potentials V_s^G defined in (21.4), then $\mathcal{L}_s^G$ commutes with the left regular G-action on $B(D)$ and

$$\det(1 - z\mathcal{L}_s^G) = \det(1 - z\mathcal{L}_s) = d(s, z) \tag{21.5}$$

Proof. The G-invariance is directly clear from the construction of V_s^G and it directly implies that $\mathcal{L}_s^G$ commutes with the left regular representation of the G-action.

In order to prove (21.5), we can use the fact that in (18.4) the potential appears only via the terms $V_w(u_w)$. Thus it suffices to show that for all $n \in \mathbb{N}$ and all closed words $w \in \mathcal{W}_n^{cl}$ we have

$$\left(V_s^G\right)_w (u_w) = (V_s)_w (u_w). \tag{21.6}$$

Thus we calculate for $u \in D$

$$\begin{aligned}
\left(V_s^G\right)_w (u) &= \prod_{k=1}^{n_w} V_s^G(\phi_{w_{0,k}}(u)) \\
&= \prod_{k=1}^{n_w} \left(\prod_{g\in G} (\phi^{-1})'(g\phi_{w_{0,k}}(u))\right)^{s/|G|} \\
&\underset{(21.3)}{=} \left(\prod_{g\in G}\prod_{k=1}^{n_w} \frac{g'(\phi^{-1}(\phi_{w_{0,k}}(u)))}{g'(\phi_{w_{0,k}}(u))} (\phi^{-1})'(\phi_{w_{0,k}}(u))\right)^{s/|G|}
\end{aligned}$$

As $\phi^{-1}(\phi_{w_{0,k}}(u)) = \phi_{w_{0,k-1}}(u)$ the terms in subsequent factors of the product over k cancel down and one obtains

$$\left(V_s^G\right)_w (u) = \left(\prod_{g\in G} \frac{g'(u)}{g'(\phi_{w_{0,n_w}}(u))} \prod_{k=1}^{n_w} (\phi^{-1})'(\phi_{w_{0,k}}(u))\right)^{s/|G|}.$$

Plugging in u_w and using $\phi_{w_{0,n_w}}(u_w) = u_w$ we finally obtain

$$\left(V_s^G\right)_w(u_w) = \left(\prod_{g\in G}\prod_{k=1}^{n_w}(\phi^{-1})'(\phi_{w_{0,k}}(u))\right)^{s/|G|} = \prod_{k=1}^{n_w}\left((\phi^{-1})'(\phi_{w_{0,k}}(u))\right)^s$$

which proves (21.6) and finishes the proof of Lemma 21.4. □

From Lemma 21.4 and Corollary 20.7 we conclude

$$\det(1 - z\mathcal{L}_s) = \prod_{\chi\in\hat{G}} d_\chi(s,z) \tag{21.7}$$

where

$$d_\chi(s,z) = \prod_{k\geq 0}\prod_{[\mathbf{w}]\in\left[\mathcal{W}^G_{\text{prime}}\right]}\left(\det_{V_\chi}\left[1 - \left(z^{n_\mathbf{w}}\left[(\phi_{w^{m_\mathbf{w}}})'(u_\mathbf{w})\right]^{\frac{s+k}{m_\mathbf{w}}}\right)\rho_\chi(g_\mathbf{w})\right]\right)^{d_\chi}. \tag{21.8}$$

Finally, this equation together with Proposition 21.2 yields a factorization of the Selberg zeta function

$$Z_{X_{n_f,\psi}}(s) = \prod_{\chi\in\hat{G}} Z^\chi_{X_{n_f,\psi}}(s) \tag{21.9}$$

with

$$Z^\chi_{X_{n_f,\psi}}(s) = d_\chi(s,1).$$

21.2 Numerical calculations of resonances on $X_{n_f,\psi}$

We now want to compute numerically the resonances on $X_{n_f,\psi}$ which coincide after the Patterson-Perry correspondence with the zeros of the Selberg zeta function $Z_{X_{n_f},\psi}$. $Z_{X_{n_f},\psi}$ factorizes according to (21.9) into a product of the analytic symmetry reduced zeta function $Z^\chi_{X_{n_f},\psi}$. So instead of calculating the zeros of $Z_{X_{n_f,\psi}}$ it suffices to calculate the zeros of $Z^\chi_{X_{n_f},\psi}$ which will turn out to be much easier because the computation of (21.8) requires much less fixed points than the full zeta function. A well known problem in the calculation of the zeros of dynamical zeta functions is that the standard product form (21.8) is only valid in the region of absolute convergence. All resonance lie, however, outside the region of absolute convergence so (21.8) is of no direct use for the numerical calculations of the zeros. The common trick to circumvent this problem, which was first used by Cvitanovic and Eckhardt in physics [25] and later by Jenkinson-Pollicott in mathematics

[56], is to use the analyticity of the dynamical zeta function in the z-variable. After performing a Taylor expansion in z one obtains an expression for the dynamical zeta function, that is everywhere absolutely convergent. For the symmetry reduced zeta function this is done in the following proposition which we will state for an arbitrary holomorphic IFS.

Proposition 21.5. *Let $d_V^\chi(s,z)$ be the symmetry reduced, dynamical zeta function from Theorem 20.5. The following expression is everywhere absolutely convergent*

$$d_V^\chi(z) = 1 + \sum_{N=1}^{\infty} z^N \sum_{r=1}^{N} \frac{(-1)^r}{r!} \sum_{\substack{[([\mathbf{w}_1],l_1),\ldots,([\mathbf{w}_r],l_r)] \\ l_1 n_{\mathbf{w}_1} + \ldots + l_r n_{\mathbf{w}_r} = N}} \prod_{k=1}^{r} T^\chi_{[\mathbf{w}_k],l_k} \tag{21.10}$$

where the third sum is over all r-tuples of pairs $([\mathbf{w}],l) \in \left[\mathcal{W}^G_{\text{prime}}\right] \times \mathbb{N}_{>0}$ such that $l_1 n_{\mathbf{w}_1} + \ldots + l_r n_{\mathbf{w}_r} = N$ and

$$T^\chi_{[\mathbf{w}],l} = \frac{d_\chi}{l} \frac{\chi(g_{\mathbf{w}}^l) V_{w^{m_{\mathbf{w}}}}(u_{\mathbf{w}})^{l/m_{\mathbf{w}}}}{1 - \phi'_{w^{m_{\mathbf{w}}}}(u_{\mathbf{w}})^{l/m_{\mathbf{w}}}}. \tag{21.11}$$

Remark 21.1. For the special case of the flow-adapted IFS of $X_{n_f,\psi}$ one simply has to replace (21.11) by

$$T^\chi_{[\mathbf{w}],l}(s) := \frac{d_\chi}{l} \frac{\chi(g_{\mathbf{w}}^l)(\phi'_{w^{m_{\mathbf{w}}}}(u_{\mathbf{w}}))^{sl/m_{\mathbf{w}}}}{1 - \phi'_{w^{m_{\mathbf{w}}}}(u_{\mathbf{w}})^{l/m_{\mathbf{w}}}}. \tag{21.12}$$

Proof. From (20.13) and Lemma 20.6 we obtain

$$d_V^\chi(z) = \exp\left(-d_\chi \sum_{[\mathbf{w}] \in \left[\mathcal{W}^G_{\text{prime}}\right]} \sum_{l>0} \frac{z^{n_{\mathbf{w}} l}}{l} \frac{\operatorname{Tr}_{V_\chi}\left[\rho_\chi(g_{\mathbf{w}})^l\right] \left(V_{w^{m_{\mathbf{w}}}}(u_{\mathbf{w}})\right)^{l/m_w}}{1 - \left(\phi'_{w^{m_w}}(u_{\mathbf{w}})\right)^{l/m_{\mathbf{w}}}} \right).$$

Using the series expression of the exponential function and reordering the terms with respect to powers of z leads to (21.10). As (20.13) is absolutely convergent in a neighborhood of zero and as $d_V^\chi(z)$ is analytic in z, the absolute convergence of its Taylor expansion (21.10) around zero follows immediately. □

Equation (21.10) can then be used for numerical calculations by truncating the series. We will denote the truncated Selberg zeta function of the surfaces $X_{n_f,\psi}$ by

$$Z^{(n)}_{X_{n_f,\psi}}(s) = \prod_{\chi \in \hat{G}} Z^{\chi,(n)}_{X_{n_f,\psi}}(s) \tag{21.13}$$

where

$$Z^{\chi,(n)}_{X_{n_f},\psi}(s) = 1 + \sum_{N=1}^{n}\sum_{r=1}^{N}\frac{(-1)^r}{r!}\sum_{\substack{[([\mathbf{w}_1],l_1),\ldots,([\mathbf{w}_r],l_r)]\\ l_1 n_{\mathbf{w}_1}+\ldots+l_r n_{\mathbf{w}_r}=N}}\prod_{k=1}^{r} T^{\chi}_{[\mathbf{w}_k],l_k}(s). \qquad (21.14)$$

This truncated zeta function has been implemented using Sage [86] which allows us to perform efficient numerical calculations using numpy and scipy [57] and also provides an interface to GAP [82] which allows an automated computation of the characters which appear in (21.11). The main problem of these Taylor expanded zeta functions is that the number of fixed points $u_{\mathbf{w}}$ required for the calculation of $Z^{\chi,(n)}_{X_{n_f},\psi}(s)$ grows exponentially with n. In order to have still a tractable numerical problem it is important that the convergence of $Z^{\chi,(n)}_{X_{n_f},\psi}(s)$ in n is rather fast. It has been observed that this convergence depends as well on the Schottky surface as on the complex parameter s [7, 56]. In [7] the relative error term

$$R_n(s) := \frac{|Z^{(n-1)}_X(s) - Z^{(n)}_X(s)|}{Z^{(n)}_X(s)}$$

has been used as a measure for the convergence. Figure 21.4 shows a comparison of the relative error term for the surface $X_{3,0.1723}$ which corresponds to a 3-funneled Schottky surface with funnel-width 12. We compared the error term obtained by the symmetry factorized zeta function (21.13) of order 6 (blue crosses) with the non-reduced zeta function as used in [7, 56] of order 11 (red dots). Even if the order of the symmetry factorized zeta function has been chosen much smaller, the relative error term is much smaller for the most s values. Especially for $\mathrm{Re}(s) < 0$ the advantage of the symmetry factorized zeta function becomes important. If one requires a relative accuracy of 10^2 the non-reduced zeta function of order 11 allows the calculation of the zeta function only up to Re(s) ≈ 0 while the symmetry factorized zeta function of order 6 already allows a calculation up to $\mathrm{Re}(s) \approx -0.2$. The benefit of the symmetry reduction becomes even clearer if one considers how many periodic orbits $u_{\mathbf{w}}$ have to be calculated in the two cases. For the non-reduced zeta function of order 11 one needs more than 170000 periodic orbits (c.f. [7, Table 1]) the symmetry reduced zeta function of order 6, however, requires only the calculation of 41 periodic orbits and still allows the calculation of resonances in a much larger domain.

This gain of efficiency can be used to calculate the resonances in a much larger domain. For example Figure 21.5 shows the resonance spectrum for

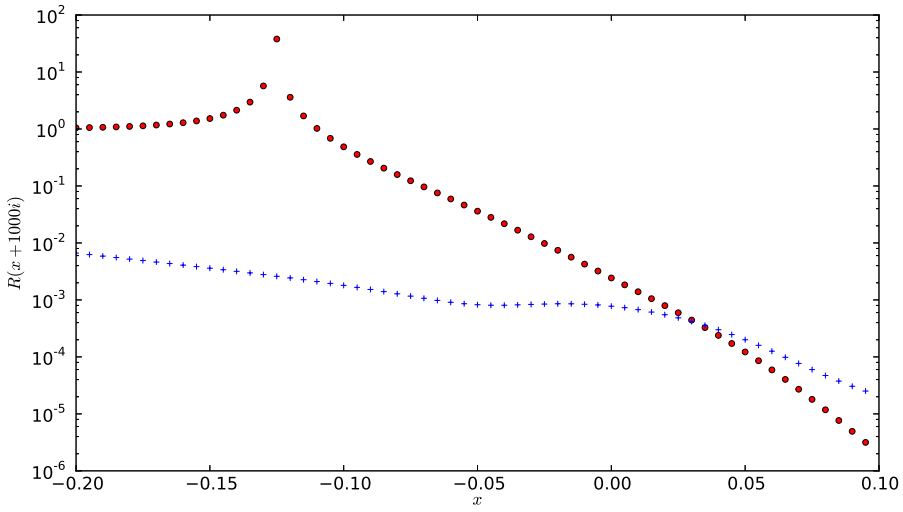

Figure 21.4: Relative error term. The blue crosses represent $R_6(x + 1000i)$ calculated with the truncated symmetry factorized zeta function (21.13). The red points represent $R_{11}(x + 1000i)$ for the truncated zeta function without symmetry reduction as used in [7].

the surface $X_{3,0.1723}$. While without symmetry reduction the numerical accessible resonance range was restricted [7] to $\mathrm{Re(s)} \gtrsim 0$ the symmetry reduction allows us to calculate the resonances easily up to $\mathrm{Re(s)} = -0.3$, which corresponds to an increase of the resonance strip by a factor of 4. The symmetry factorization, however, not only allows a much more efficient calculation but also provides additional information on the resonance spectrum. As (21.9) provides an factorization of the Selberg zeta function with explicitly known factors, we can associate the zeros of the Selberg zeta function to the different unitary irreducible representations. As discussed above the symmetry group of the symmetric 3-funneled surface is given by $D_3 \times \mathbb{Z}_2$ and via its action on the symbols, it can be realized as a permutation group on 6 elements. One calculates that this group has 6 conjugacy classes and thus 6 irreducible representations. The character table is given in Table 21.1. As it can be seen, the resonance chain-structure is compatible with the symmetry reductions. However, one chain does not only correspond to one representation, as one could have expected, but to a pair of representations. The resonances on one chain alternate between these two representations.

Finally the symmetry decomposition enables to study the resonance structure of surfaces which were numerically not treatable. As an example we

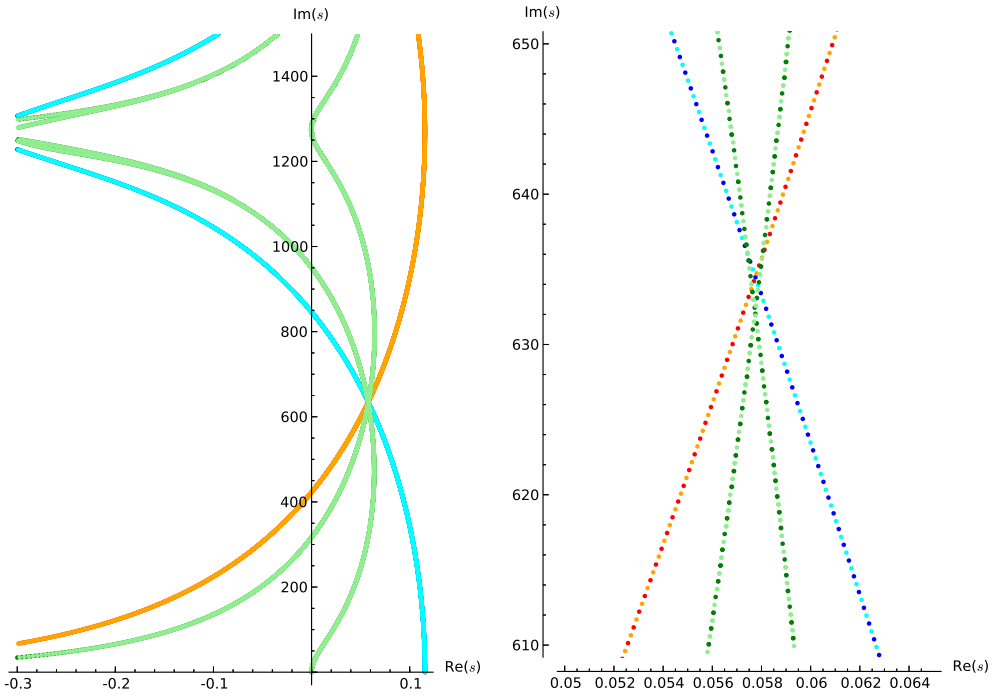

Figure 21.5: Resonance spectrum for the surface $X_{3,0.1723}$. The different colors correspond to the different representations I_1(dark blue) , I_2(light blue) , II_1(red) , II_2(orange), III_1(dark green) and III_2(light green). In the left plot the resonances are so dense that they can not be distinguished but appear as continuous line. The right plot shows a zoom into the region of the first crossing of the chains. Here one can distinguish the individual resonances and one observes that each chain is composed by resonances that alternately belong to two different representations.

	()	(2,3)(5,6)	(1,2,3)(4,5,6)	(1,4)(2,5)(3,6)	(1,4)(2,6)(3,5)	(1,5,3,4,2,6)
I_1	1	1	1	1	1	1
I_2	1	1	1	-1	-1	-1
II_1	1	-1	1	1	-1	1
II_2	1	-1	1	-1	1	-1
III_1	2	0	-1	-2	0	1
III_2	2	0	-1	2	0	-1

Table 21.1: Character table of the symmetry group $D_3 \times \mathbb{Z}_2$ of the symmetric 3-funneled surfaces $X_{3,\psi}$. In the first line the representatives of the conjugacy classes are given in cycle notation, where $D_3 \times \mathbb{Z}_2$ is realized as a permutation group on the symbols of the flow-adapted IFS. The following six lines represent the characters of the six unitary irreducible representations of this group.

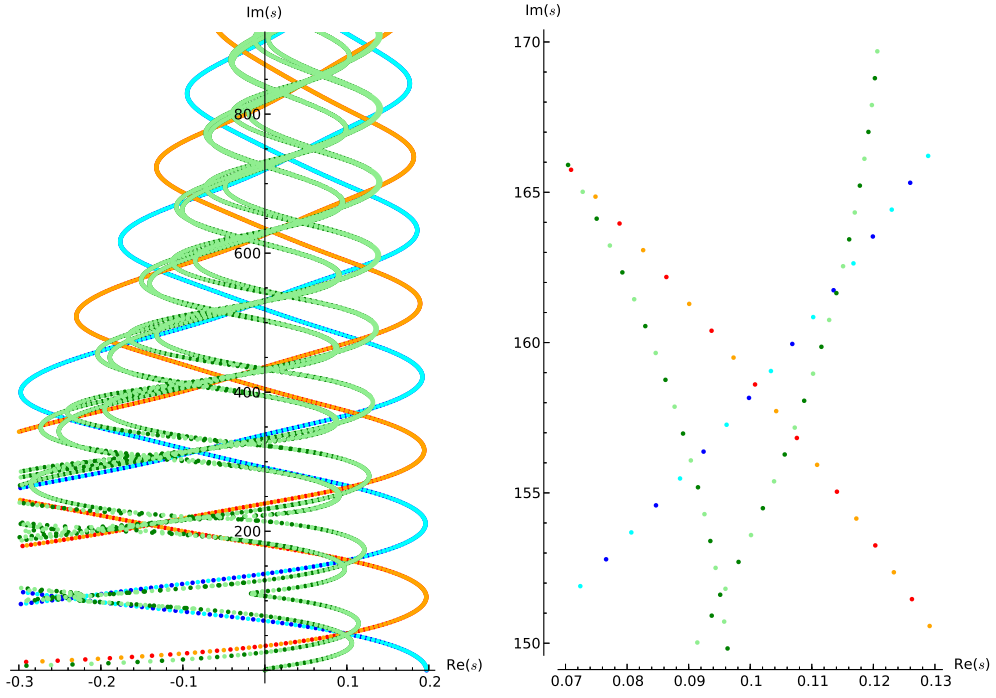

Figure 21.6: Resonance spectrum for the surface $X_{3,0.5930}$. The color code is the same as in Figure 21.5. The right plot is a zoom into the region of the second crossing of all three chain types. As the resonances on $X_{3,0.5930}$ are less dense than on $X_{3,0.1723}$ there are even regions in the left part of the plot, where the individual resonances can be distinguished.

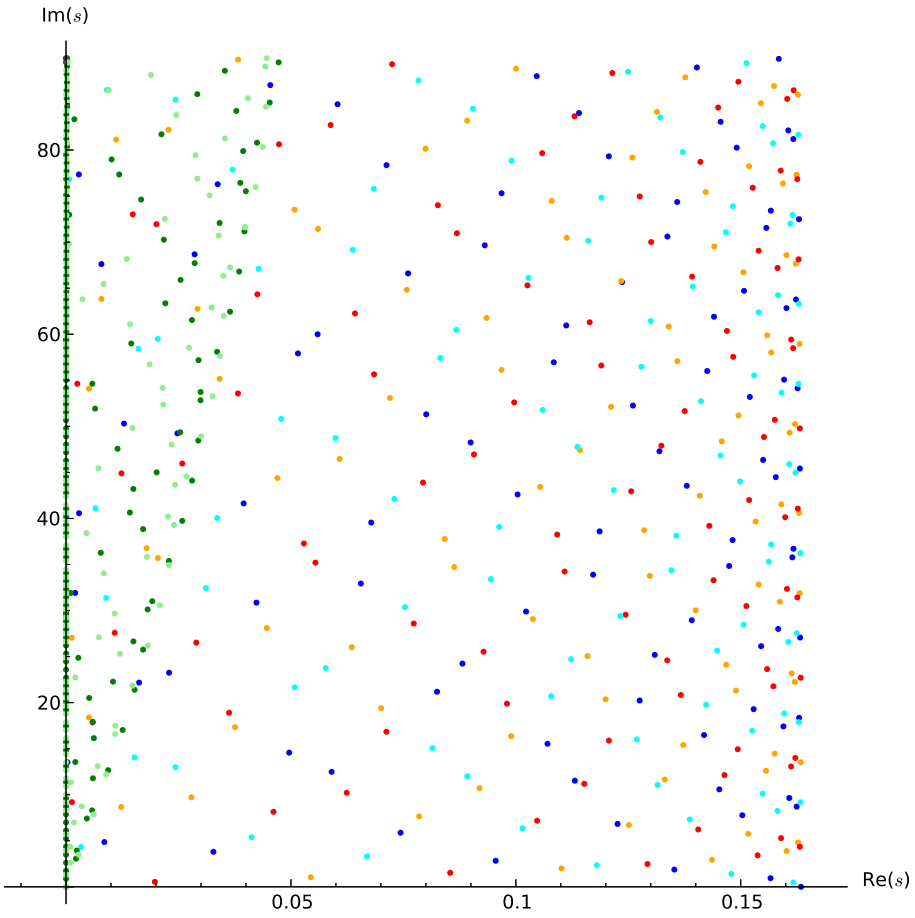

Figure 21.7: Resonance spectrum for the surface $X_{4,0.1010}$. Resonances of different unitary irreducible representations (cf. Table 21.2) are plotted in different colors: I_1(dark blue), I_2(light blue), II_1(red), II_2(orange), V_1(dark green) and V_2(light green). There were no resonances found in the plot regions, that belong to the representations III_1, III_2, IV_1 and IV_2.

	()	(2,4)(6,8)	(1,2)(3,4) (5,6)(7,8)	(1,2,3,4) (5,6,7,8)	(1,3)(2,4) (5,7)(6,8)	(1,5)(2,6) (3,7)(4,8)	(1,5)(2,8) (3,7)(4,6)	(1,6)(2,5) (3,8)(4,7)	(1,6,3,8) (2,7,4,5)	(1,7)(2,8) (3,5)(4,6)
I_1	1	1	1	1	1	1	1	1	1	1
I_2	1	1	1	1	1	-1	-1	-1	-1	-1
II_1	1	1	-1	-1	1	1	1	-1	-1	1
II_2	1	1	-1	-1	1	-1	-1	1	1	-1
III_1	1	-1	-1	1	1	-1	1	1	-1	-1
III_2	1	-1	-1	1	1	1	-1	-1	1	1
IV_1	1	-1	1	-1	1	-1	1	-1	1	-1
IV_2	1	-1	1	-1	1	1	-1	1	-1	1
V_1	2	0	0	0	-2	2	0	0	0	-2
V_2	2	0	0	0	-2	-2	0	0	0	2

Table 21.2: Character table of the symmetry group $D_4 \times \mathbb{Z}_2$ of the symmetric 4-funneled surfaces $X_{4,\psi}$. In the first line the representatives of the conjugacy classes are given in cycle notation, where $D_4 \times \mathbb{Z}_2$ is realized as a permutation group on the symbols of the flow-adapted IFS. The following six lines represent the characters of the ten unitary irreducible representations of this group.

show the resonance structure of the 3-funneled surface $X_{3,0.5930}$ (Figure 21.6) which corresponds to a funnel-width of 7 and the 4-funneled surface $X_{4,0.1010}$ (Figure 21.7) which corresponds to a funnel-width of 13. For the 3-funneled surface one observes again resonance chains on a large $\mathrm{Im}(s)$ range, where each chain is composed of resonances belonging to two representations. As expected from the observations in [3] these curves are, however, much stronger bent compared to the surface $X_{3,0.1723}$. For the 4-funneled surface there are no resonance chains visible on a comparable scale to the 3-funneled surfaces. Only if one zooms strongly into the $\mathrm{Im}(s)$-scale and colors the resonances according to the different representations one can see strongly bent chains that are again composed of two different representations. This different behavior between symmetric 3- and 4-funneled surfaces has been predicted in [3] because 4-funneled surface do not have naturally a strong clustering behavior in their primitive length spectrum. A surprising feature is, however, that there is one very stable resonance chain along the imaginary axis related to the two 2-dimensional representations V_1 and V_2.

A Derivation of the product form for dynamical zeta function

In this appendix we will recall the derivation of the product form (13.5) from the definition of the dynamical zeta function as it has been defined in (13.4) by the flat trace

$$d^\flat(z) := \exp\left(-\sum_{n>0}\frac{z^n}{n}\sum_{x\in\mathrm{Fix}(\phi^n)}\frac{V_n(x)}{|\det(1-(D\phi^n)(x))|}\right).$$

For each fixed point $\phi^n(x) = x$ the Jacobian is a hyperbolic, symplectic 2×2 matrix and it thus has two real eigenvalues Λ_n and $1/\Lambda_n$ with $|\Lambda_n| > 1$ and the determinant can be written as

$$\begin{aligned}\frac{1}{|\det(1-(D\phi^n)(x)|} &= \frac{1}{|1-\Lambda_n||1-1/\Lambda_n|}\\ &= |\Lambda_n|^{-1}\left(\sum_{r\geq 0}\Lambda_n^{-r}\right)\left(\sum_{s\geq 0}\Lambda_n^{-s}\right)\\ &= |\Lambda_n|^{-1}\sum_{k\geq 0}(k+1)\Lambda_n^{-k} \qquad (A.1)\end{aligned}$$

where for the last equality we used that a positive integer k can be written as $k+1$ different sums of two positive integers r and s.

As a next step we can treat the double sum $\sum_{n>0}\sum_{x\in\mathrm{Fix}(\phi^n)}$ which is simply the sum over all fixed points of ϕ^n for arbitrary length ϕ. First we note that as well the iterated product of the potential function $V_n(x)$ as the instable eigenvalue Λ_n do not depend on the choice of the fixed point in a fixed orbit $\{x, \phi(x), \ldots, \phi^{n-1}(x)\}$. Additionally we see that if an orbit of length $m\cdot n_p$ is a m-times iterate of a primitive orbit of length n_p, then the orbit contains n_p fixed points and as well the iterated product as the instable eigenvalue are the m-th power of the values from the primitive orbit

$$V_{m\cdot n_p}(x) = (V_{n_p}(x))^m \text{ and } \Lambda_{m\cdot n_p} = \Lambda_{n_p}^m.$$

This allows us to write the double sum $\sum_{n>0}\sum_{x\in\mathrm{Fix}(\phi^n)}$ as a double sum over

all primitive periodic orbits and their repetitions $\sum_{p\in P}\sum_{m>0}$ and we obtain

$$\begin{aligned} d^\flat(z) &= \exp\left(-\sum_{k\geq 0}(k+1)\sum_{n>0}\sum_{x\in \mathrm{Fix}(\phi^n)}\frac{z^n}{n}V_n(x)|\Lambda_n|^{-1}\Lambda_n^{-k}\right) \\ &= \exp\left(-\sum_{k\geq 0}(k+1)\sum_{p\in P}\sum_{m>0}\frac{z^{n_p\cdot m}}{m}(V_{n_p}(x))^m\left(|\Lambda_{n_p}|\Lambda_{n_p}^{-k}\right)^m\right) \\ &= \prod_{k\geq 0}\prod_{p\in P}\left[\exp\left(-\sum_{m>0}\frac{\left(z^{n_p}V_{n_p}(x)|\Lambda_{n_p}|^{-1}\Lambda_{n_p}^{-k}\right)^m}{m}\right)\right]^{k+1} \\ &= \prod_{k\geq 0}\prod_{p\in P}\left[1-z^{n_p}\frac{V_{n_p}(x)}{|\Lambda_{n_p}|\Lambda_{n_p}^k}\right]^{k+1} \end{aligned}$$

where we used the Taylor series of $\log(1-x)$ in the last equality.

B Numerical considerations for the calculation of the generalized spectrum $\sigma_s^{(\mathbf{n})}$

In this appendix we will shortly recall how the resonance spectrum on Schottky surfaces is usually calculated (see [56, 43, 7] for more details) and what modifications have to be performed for the calculation of the generalized zeta function and the generalized spectrum.

Usually the resonance spectrum is obtained by Taylor expanding (14.3) in z around zero

$$d_{BS}(s,z)=\sum_{k=0}^{\infty}z^k b_k(s).$$

The Taylor coefficients are then explicitly given by [56, Proposition 8]

$$b_k(s)=\sum_{r=1}^{k}\sum_{(n_1,\ldots,n_r)\in P(k,r)}\frac{(-1)^r}{r!}\prod_{l=1}^{r}\frac{1}{n_l}\sum_{u\in\mathrm{Fix}(B^{n_l})}\frac{((B^{n_l})'(u))^{-s}}{1-(B^{-n_l})'(u)} \tag{B.1}$$

where $P(k,r)$ are all r-partitions of k, i.e. all r-tuples of integers whose sum equals k. The numerical task in order to calculate these coefficients then consists in calculating the stabilities $(B^n)'(u)$ of sufficiently many fixed points. For a 3-funneled Schottky surface X_{l_1,l_2,l_3} this can efficiently be done using the generators of the corresponding Schottky group and a symbolic dynamic.

For X_{l_1,l_2,l_3} the generators can be written as

$$S_1 = \begin{pmatrix} \cosh(l_1/2) & \sinh(l_1/2) \\ \sinh(l_1/2) & \cosh(l_1/2) \end{pmatrix}, \quad S_2 = \begin{pmatrix} \cosh(l_2/2) & a\sinh(l_2/2) \\ a^{-1}\sinh(l_2/2) & \cosh(l_2/2) \end{pmatrix},$$

where the parameter a is chosen such that $\mathrm{Tr}(S_1 S_2^{-1}) = -2\cosh(l_3/2)$ and as usually one writes $S_3 = S_1^{-1}$ and $S_4 = S_2^{-1}$. If we then define the set of words of length n by

$$\mathcal{W}_n := \Big\{ w \in \{1,2,3,4\}^n,\ |w_{j+1} - w_j| \neq r \text{ for } j = 1,\ldots,n-1 \text{ and } |w_1 - w_m| \neq r \Big\}$$

then we can define for each $w \in \mathcal{W}_n$ the hyperbolic isometry

$$S_w := S_{w_1} S_{w_2} \ldots S_{w_n}.$$

One then can easily show from the definition of the Bowen-Series maps [5, Section 15.2] that for each $u \in \mathrm{Fix}(B^n)$ there is exactly one $w \in \mathcal{W}_n$ and

$$\Lambda(w) := 2\cosh^{-1}\left(\frac{|\mathrm{Tr}(S_w)|}{2}\right) = (B^n)'(u)$$

which allows an efficient calculation of (B.1) and thus of $d_{BS}(s,z)$.

For the calculation of $d_{\mathbf{n}}(s,z)$ one equally has to Taylor-expand the zeta function in z around zero

$$d_{\mathbf{n}}(s,z) = \sum_{k=0}^{\infty} z^k b_k^{(\mathbf{n})}(s).$$

Then one has to calculate the new Taylor coefficients $b_k^{(\mathbf{n})}(s)$. As we want to use the word coding to calculate the lengths of the geodesics or the stabilities $(B^n)'(u)$ respectively we fist have to transfer the order function $\mathbf{n} : P_{X_{l_1,l_2,l_3}} \to \mathbb{N}$ to an order function on $\mathcal{W} = \bigcup_{n>0} \mathcal{W}_n$. This transformation can be obtained via the correspondance between closed geodesics on X_{l_1,l_2,l_3} and fixed points of B [5, Proposition 15.5]. Using this identification one calculates that the order function as defined in (14.9) is then given by

$$\mathbf{n}(w) = n(w_1,w_2) + n(w_2,w_3) + \ldots + n(w_n,w_1) \tag{B.2}$$

where

$$\begin{aligned} n(1,1) &= n(3,3) = n_1, \quad n(2,2) = n(4,4) = n_2 \\ n(1,4) &= n(4,1) = n(2,3) = n(3,2) = n_3/2 \\ n(1,2) &= n(2,1) = n(3,4) = n(4,3) = (n_1+n_2)/2. \end{aligned}$$

The Bowen Series order function $\mathbf{n}_{BS}$ can much faster be translated. From its definition in Section 14.1 it immediately follows, that $\mathbf{n}_{BS}(w) = n$ for all $w \in \mathcal{W}_n$.

Using the order function on the words as well as the identification of fixed points and words, equation (14.3) can be written as

$$d_{BS}(s,z) = \exp\left(-\sum_{j>0}\frac{1}{j}\sum_{w\in\mathcal{W}_j} z^{\mathbf{n}_{BS}(w)}\frac{\Lambda(w)^{-s}}{1-\Lambda(w)^{-1}}\right).$$

Starting with (14.5) and reversing the argumentation of Appendix A the generalized zeta function $d_{\mathbf{n}}(s,z)$ can be written as

$$d_{\mathbf{n}}(s,z) = \exp\left(-\sum_{j>0}\frac{1}{j}\sum_{w\in\mathcal{W}_j} z^{\mathbf{n}(w)}\frac{\Lambda(w)^{-s}}{1-\Lambda(w)^{-1}}\right). \tag{B.3}$$

An analogous calculation to those in [56, Proposition 8] then gives us the formula for the Taylor coefficients

$$b_k^{(\mathbf{n})}(s) = \sum_{r=1}^{k}\sum_{(n_1,\ldots,n_r)\in P(k,r)}\frac{(-1)^r}{r!}\prod_{l=1}^{r}\sum_{j>0}\frac{1}{j}\sum_{w\in\mathcal{W}_j,\text{s.t. }\mathbf{n}(w)=n_l}\frac{\Lambda(w)^{-s}}{1-\Lambda(w)^{-1}}. \tag{B.4}$$

The stabilities $\Lambda(w)$ can be calculated by the generators S_i of the Schottky group as described above and in order to simplify the combinatorial task of building together the Taylor coefficients $b_k^{(\mathbf{n})}(s)$ from these stabilities we can use the same recurrence trick as presented in [43]. We therefore write

$$B_{k,r}^{(\mathbf{n})}(s) := \sum_{(n_1,\ldots,n_r)\in P(k,r)}\frac{(-1)^r}{r!}\prod_{l=1}^{r} a_{n_l}^{(\mathbf{n})}(s)$$

and

$$a_n^{(\mathbf{n})}(s) := \sum_{j>0}\frac{1}{j}\sum_{w\in\mathcal{W}_j,\text{s.t. }\mathbf{n}(w)=n}\frac{\Lambda(w)^{-s}}{1-\Lambda^{-1}}.$$

We can then use the recurrence relations

$$B_{k,r}^{(\mathbf{n})} = \frac{1}{r}\sum_{l=1}^{k-r+1} B_{k-l,r-1}^{(\mathbf{n})}(s)a_l^{(\mathbf{n})}(s).$$

The only difference in calculating the generalized zeta function compared to the dynamical zeta function of the Bowen-Series maps thus consists in the modified formula for the functions $a_n^{(\mathbf{n})}(s)$.

Note that as $d_{\mathbf{n}}(s,z)$ is analytic the Taylor coefficients $b_k^{(\mathbf{n})}(s)$ decay superexponentially in k and theoretically one can compute $d_{\mathbf{n}}(s,z)$ for arbitrary (s,z). Practically, however, the convergence becomes worse and worse the smaller $\mathrm{Re}(s)$ and the bigger $|z|$ become. Especially for order functions (14.9) with larger values of n_1, n_2, n_3 as they appeared for example for the surfaces $X_{12,13,14}$ the convergence depends very strongly on $|z|$. This implies that a reliable calculation of $d_{\mathbf{n}}$ is only possible for z values which are slightly larger then 1. In terms of the generalized spectrum this implies that the numerical calculation is only possible for z slightly smaller than 1. As the interesting region for the understanding of the resonance chains is however the unit circle, this is no severe problem for the numerical investigations presented in this article.

C Topological pressure and analyticity of $d^{(b)}(s,z)$

The topological pressure of a 3-disk system is a function $P(\beta)$ of a positive parameter $\beta > 0$ that describes the convergence behavior of certain zeta functions. Writing

$$V_s^\beta(x) := |\Lambda(x)|^{1-\beta} e^{-s\tau(x)}$$

the topological pressure of the 3-disk system can be defined [38] to be the real number $P(\beta)$ such that

$$d_\beta(s) := \det(1 - \mathcal{L}_{V_s^\beta}) = \exp\left(-\sum_{n>0} \frac{1}{n} \sum_{x \in \mathrm{Fix}(\phi^n)} \frac{(V_s^\beta)_n(x)}{|\det(1 - (D\phi^n)(x)|} \right)$$

is absolutely convergent for $\mathrm{Re}(s) > P(\beta)$. This directly implies that $d^{(a)}$ has no zeros for $\mathrm{Re}(s) > P(1/2)$ and that $d^{(b)}(s)$ has no zeros for $\mathrm{Re}(s) > P(3/2)$. For a symmetric 3-disk system with $R/a = 6$ this value of the topological pressure is given by

$$P(3/2) = -0.699.$$

Consequently all zeros of the Gutzwiller-Vorros zeta function $Z_{GV}(s,1)$ with $\mathrm{Re}(s) > -0.699$ are automatically zeros of the Fredholm determinant $d_{(a)}(s,1)$ and can thus be interpreted by the spectrum of the transfer operator $\mathcal{L}_{V_s^{(a)}}$. Note that all the numerical investigations presented in this article are within this s-range.

D Numerical implementation of symmetry reduced zeta functions for n-funneled Schottky surfaces

In this section we will discuss some practical aspects of the numerical implementation of the symmetry reduced Selberg zeta functions for symmetric n-funneled Schottky surfaces. For a given surface $X_{n_f,\psi}$, a given character χ and point $s \in \mathbb{C}$ the task consists in calculating the truncated Selberg zeta function (21.14) at a finite order n. This task basically splits into two subtasks: First one has to calculate $T^{\chi}_{[\mathbf{w}],l}(s)$ for every pair $([\mathbf{w}], l) \in \left[\mathcal{W}^G\right] \times \mathbb{N}$ that appears in the sum. Then one has to handle the combinatorial task of combining these $T^{\chi}_{[\mathbf{w}],l}$ to the products and sums according to (21.14).

By (21.12) the first task reduces for a given $(\mathbf{w}, l)$ to the calculation of $\phi'_{w^{m_{\mathbf{w}}}}(u_{\mathbf{w}})$. By the proof of Proposition 21.3 this quantity is directly related to the displacement length of the hyperbolic transformation $T(w^{m_{\mathbf{w}}})$ which was defined for a closed word in (21.2). Using the formula

$$\cosh(l(T)/2) = |\mathrm{Tr}(T)/2|$$

that relates the displacement length $l(T)$ to the trace of the hyperbolic element $T \in SL(2,\mathbb{R})$ we obtain

$$\phi'_{w^{m_{\mathbf{w}}}}(u_{\mathbf{w}}) = \exp\left(-2l(T(w^{m_{\mathbf{w}}}))\right) = \exp\left(-2\cosh^{-1}\left(\frac{|\mathrm{Tr}(T(w^{m_{\mathbf{w}}}))|}{2}\right)\right).$$

The second task can be significantly simplified by using a recurrence relation, which has been proposed in [43, Section 7]: We can write (21.14) in the form

$$Z^{\chi,(n)}_{X_{n_f,\psi}}(s) = 1 + \sum_{N=1}^{n}\sum_{r=1}^{N} B^{\chi}_{N,r}(s)$$

where

$$B^{\chi}_{N,r}(s) := \frac{1}{r!}\sum_{t\in P(N,r)}\prod_{k=1}^{r} a^{\chi}_{t_k}(s).$$

Here $P(N,r)$ is the set of all r-partitions of N, i.e. the set of all r-tuples $t = (t_1,\ldots,t_r) \in \mathbb{N}^r$ such that $t_1 + \ldots + t_r = N$ and

$$a^{\chi}_{t_k}(s) = -\sum_{\substack{([\mathbf{w}],l)\in\left[\mathcal{W}^G\right]\times\mathbb{N}_{>0}\\ n_{\mathbf{w}}\cdot l = t_k}} T^{\chi}_{[\mathbf{w}],l}(s).$$

With this notation it is sufficient to calculate $a_t(s)$ for all $t = 1, \ldots, n$. The coefficients $B_{N,r}(s)$ can then be obtained by the recurrence relation

$$B^{\chi}_{N,r}(s) = \frac{1}{r} \sum_{t=1}^{N-r+1} B^{\chi}_{N-t,r-1}(s) \cdot a^{\chi}_t(s)$$

with the start value $B_{N,1}(s) = a_N(s)$.

In order to calculate the coefficients $a_t(s)$ one has to find an efficient way to determine a representative for each class $[\mathbf{w}] \in \left[\mathcal{W}^G\right]$ for $0 < n_{\mathbf{w}} \leq n$. This task has to be performed only once for all surfaces $X_{n_f,\psi}$ with a fixed number of funnels n_f, so it is not of the uttermost importance to be very efficient at this point and a brute-force approach would also work. The numerically expansive task consists in calculating the values of $Z^{\chi,(n)}_{X_{n_f}}(s)$ several millions of times in order to determine its zeros at a good precision. Nevertheless we shortly want to describe an elegant and fast way to determine all representatives by a symmetry reduced symbolic dynamics. Therefore we define the symmetry reduced symbolic dynamics for a n_f-funneled surface to be the complete symbolic dynamics with the symbols

$$\left\{\frac{-n_f-1}{2}, \ldots, -1, 1, \ldots, \frac{n_f-1}{2}\right\} \text{ if } n_f \text{ uneven},$$

and

$$\left\{\frac{-n_f-2}{2}, \ldots, -1, 0, 1, \ldots, \frac{n_f-2}{2}\right\} \text{ if } n_f \text{ even}.$$

A complete symbolic dynamics means that all sequences of symbols are allowed, i.e. that the adjacency matrix has the value 1 in each entry and we call the set of words of the symmetry reduced symbolic dynamics $\mathcal{W}_{sr}$. The idea of this symmetry reduced coding has successfully been used in for 3- and 4-disk systems [26] as well as for 5-disk systems [2] and can be understood at the example of the 3-funneled surface as follows: A closed geodesic can be represented on two copies of $\tilde{S} \subset \mathbb{D}$. As the two copies are glued together along the circles c_i it alternates between these two copies, so if it hits one circle c_i it leaves again at the corresponding partner c_{i+3} or c_{i-3}, respectively. As there is no geodesic in $\tilde{S}$ entering and leaving the same boundary circle c_i, the geodesic has either to leave the region $\tilde{S}$ by the next circle in clockwise direction or by the next circle in counterclockwise direction. Given a word $w_{sr} \in \mathcal{W}_{sr}$ which consist of the symbols $\{1, -1\}$ we can construct the corresponding representative in $\mathcal{W}^G$ as follows. Start at an arbitrary circle c_{start} with an arbitrary orientation. As long as the letters of w_{sr} are equal to 1 go to the next circle in the current orientation. If the letter is

equal to -1, go to the next disk in the current orientation, but change the orientation for the next step. After going through all symbols of the word w_{sr} one ends at a circle c_{end} with a final orientation. Now there is a unique symmetry of the surface that maps c_{end} to c_{start} and the final orientation to the initial orientation. We define g to be the associated group element in $D_3 \times \mathbb{Z}_2$. Furthermore by collecting the indices of the circles from which the geodesic entered the domain $\mathcal{S}$ we get a word $w = (w_0, w_1, \ldots, w_n) \in \mathcal{W}$. The representative associated to w_{sr} is then exactly the pair $\mathbf{w} = (w, g)$.

For an uneven number of funnels $n_f > 3$ there is not only the possibility to leave $\tilde{S}$ through the next circle in clockwise or counterclockwise orientation, but also to leave it $2, 3, \ldots, (n_f - 1)/2$ circles in clockwise or counterclockwise direction. The symbols $1, \ldots, (n_f - 1)/2$ thus correspond to "go n steps into the current orientation and keep the orientation", and the symbols $-1, \ldots, -(n_f - 1)/2$ correspond to "go n steps into the current orientation and switch the orientation for the next step". In the even case one has also the possibility of stepping forward $n_f/2$ circles. Here it makes no difference in which orientation one goes. This possibility is encoded by the latter 0 and the current orientation for the further steps is not change by this letter.

Via this algorithm one can identify words in the reduced symbolic dynamics to elements $\mathbf{w} \in \mathcal{W}^G$. Note that the idea of the reduced symbolic dynamic is not to encode the absolute position of the closed geodesics, but to encode the relative changes as one moves along the geodesic. The reduced symbolic dynamic is thus by construction compatible with the action of the symmetry group in the following sense. If $\mathbf{w}$ and $\mathbf{w}'$ are two elements in $\mathcal{W}^G$ which were obtained from the same reduced word w_{sr} by starting from a different circle or orientation, then they are in the same G-orbit in $\mathcal{W}^G$ and vice versa. One can additionally convince oneself, that the shift action on $\mathcal{W}_{sr}$ corresponds to the shift action on $\mathcal{W}^G$ and that the same holds for the composition of words. Thus one has identified the orbits of prime words under the shift action in $\mathcal{W}$ with the prime elements in $\left[\mathcal{W}^G\right]$ which permits to easily generate a list of representatives of the elements in $\left[\mathcal{W}^G\right]$.

References

[1] R. Balian and C. Bloch. Distribution of eigenfrequencies for the wave equation in a finite domain: III. Eigenfrequency density oscillations. *Annals of physics*, 69(1):76–160, 1972.

[2] S. Barkhofen. *Microwave Measurements on n-Disk Systems and Investigation of Branching in correlated Potentials and turbulent Flows*. PhD thesis, Marburg, Philipps-Universität Marburg, Diss., 2013, 2013.

[3] S. Barkhofen, F. Faure, and T. Weich. Resonance chains in open systems, generalized zeta functions and clustering of the length spectrum. *arxiv:1403.7771*.

[4] S. Barkhofen, T. Weich, A. Potzuweit, H-J. Stöckmann, U. Kuhl, and M. Zworski. Experimental observation of the spectral gap in microwave n-disk systems. *Physical review letters*, 110(16):164102, 2013.

[5] D. Borthwick. *Spectral theory of infinite-area hyperbolic surfaces.* Basel: Birkhäuser, 2007.

[6] D. Borthwick. Sharp geometric upper bounds on resonances for surfaces with hyperbolic ends. *Analysis & PDE*, 5(3):513–552, 2012.

[7] D. Borthwick. Distribution of resonances for hyperbolic surfaces. *Experimental Mathematics*, 23:25–45, 2014.

[8] D. Borthwick, C. Judge, and P.A. Perry. Selberg's zeta function and the spectral geometry of geometrically finite hyperbolic surfaces. *Comment. Math.Helv.*, 80:483–515, 2005.

[9] J. Bourgain, A. Gamburd, and P. Sarnak. Generalization of Selberg's $\frac{3}{16}$ theorem and affine sieve. *Acta mathematica*, 207(2):255–290, 2011.

[10] G.E. Bredon. *Introduction to compact transformation groups*, volume 46. Academic Press, 1972.

[11] J. Brüning. Zur Eigenwertverteilung invarianter elliptischer Operatoren. *J. Reine Angew. Math.*, 339:82–96, 1983.

[12] J. Brüning and E. Heintze. Representations of compact Lie groups and elliptic operators. *Invent. Math.*, 50:169–203, 1979.

[13] U. Bunke and M. Olbrich. Group cohomology and the singularities of the Selberg zeta function associated to a kleinian group. *Annals of mathematics*, 149:627–689, 1999.

[14] R. Cassanas. *Hamiltoniens quantiques et symétries*. PhD thesis, Université de Nantes, 2005.

[15] R. Cassanas. Reduced Gutzwiller formula with symmetry: case of a finite group. *Journal of mathematical physics*, 47(4):042102–042102, 2006.

[16] R. Cassanas. Reduced Gutzwiller formula with symmetry: Case of a Lie group. *Journal de Mathématiques Pures et Appliqués*, 85(6):719–742, 2006.

[17] R. Cassanas and P. Ramacher. Reduced Weyl asymptotics for pseudodifferential operators on bounded domains. II: The compact group case. *J. Funct. Anal.*, 256(1):91–128, 2009.

[18] J. Chazarain. Formule de Poisson pour les variétés Riemanniennes. *Invent. Math.*, 24:65–82, 1974.

[19] Y. Colin de Verdière. Spectre du Laplacien et longueurs des géodésiques périodiques. I. *Compositio Mathematica*, 27(1):83–106, 1973.

[20] Y. Colin de Verdière. Spectre du Laplacien et longueurs des géodésiques périodiques. II. *Compositio Mathematica*, 27(2):159–184, 1973.

[21] Y. Colin de Verdière. Spectre conjoint d'opérateurs pseudo-différentiels qui commutent. I: Le cas non intégrable. *Duke Math. J.*, 46:169–182, 1979.

[22] Y. Colin de Verdière. Spectrum of the Laplace operator and periodic geodesics: thirty years after. In *ANNALES-INSTITUT FOURIER*, volume 57, page 2429. Association des Annales de l'Institute Fourier; 1999, 2007.

[23] M. Combescure, J. Ralston, and D. Robert. A proof of the Gutzwiller semiclassical trace formula using coherent states decomposition. *Communications in mathematical physics*, 202(2):463–480, 1999.

[24] M. Combescure and D. Robert. Semiclassical spreading of quantum wave packets and applications near unstable fixed points of the classical flow. *Asymptotic Anal.*, 14(4):377–404, 1997.

[25] P. Cvitanović and B. Eckhardt. Periodic-orbit quantization of chaotic systems. *Physical review letters*, 63(8):823–826, 1989.

[26] Predrag Cvitanovic and Bruno Eckhardt. Symmetry decomposition of chaotic dynamics. *Nonlinearity*, 6(2):277, 1993.

[27] H. Donnelly. G-spaces, the asymptotic splitting of $L^2(M)$ into irreducibles. *Mathematische Annalen*, 237(1):23–40, 1978.

[28] J.J. Duistermaat and V.W. Guillemin. The spectrum of positive elliptic operators and periodic bicharacteristics. *Inventiones mathematicae*, 29(1):39–79, 1975.

[29] J.J. Duistermaat and J.A.C. Kolk. *Lie groups*. Springer Verlag, 2000.

[30] A. Eberspächer. Fractal Weyl law for three-dimensional chaotic hard-sphere scattering systems. *Diplomarbeit Universität Stuttgart*, 2010.

[31] A. Eberspächer, J. Main, and G. Wunner. Fractal Weyl law for three-dimensional chaotic hard-sphere scattering systems. *Physical Review E*, 82(4):46201, 2010.

[32] Z. El Houakmi and B. Helffer. Comportement semi-classique en présence de symétries. Action d'un groupe de Lie compact. *Asymptotic analysis*, 5(2):91–113, 1991.

[33] F. Faure and N. Roy. Ruelle-Pollicott resonances for real analytic hyperbolic maps. *Nonlinearity*, 19(6):1233–1252, 2006.

[34] F. Faure and M. Tsujii. Prequantum transfer operator for symplectic anosov diffeomorphism. *arXiv preprint arXiv:1206.0282*, 2012.

[35] F. Faure and M. Tsujii. The semiclassical zeta function for geodesic flows on negatively curved manifolds. *arXiv preprint arXiv:1311.4932*, 2013.

[36] P. Gaspard and D. Alonso Ramirez. Ruelle classical resonances and dynamical chaos: The three- and four-disk scatterers. *Phys. Rev. A*, 45:8383, Jun 1992.

[37] P. Gaspard and S.A. Rice. Exact quantization of the scattering from a classically chaotic repellor. *The Journal of chemical physics*, 90:2255, 1989.

[38] P. Gaspard and S.A. Rice. Scattering from a classically chaotic repellor. *The Journal of chemical physics*, 90:2225, 1989.

[39] P. Gaspard and S.A. Rice. Semiclassical quantization of the scattering from a classically chaotic repellor. *The Journal of chemical physics*, 90:2242, 1989.

[40] A. Grothendieck. La théorie de fredholm. *Bulletin de la Société Mathématique de France*, 84:319–384, 1956.

[41] V. Guillemin and A. Uribe. Reduction and the trace formula. *J. Differential Geom*, 32(2):315–347, 1990.

[42] L. Guillopé. Fonctions zêta de selberg et surfaces de géométrie finie. *Adv. Stud. Pure Math*, 21:33–70, 1992.

[43] L. Guillopé, K.K. Lin, and M. Zworski. The Selberg zeta function for convex co-compact Schottky groups. *Communications in mathematical physics*, 245(1):149–176, 2004.

[44] L. Guillopé and M. Zworski. Upper bounds on the number of resonances for non-compact Riemann surfaces. *J. Funct. Anal.*, 129(2):364–389, 1995.

[45] L. Guillopé and M. Zworski. Scattering asymptotics for riemann surfaces. *Annals of mathematics*, 145(3):597–660, 1997.

[46] L. Guillopé and M. Zworski. The wave trace for riemann surfaces. *Geometric & Functional Analysis GAFA*, 9(6):1156–1168, 1999.

[47] M.C. Gutzwiller. Periodic orbits and classical quantization conditions. *Journal of Mathematical Physics*, 12:343, 1971.

[48] B. Helffer and D. Robert. Calcul fonctionnel par la transformation de Mellin et opérateurs admissibles. *Journal of Functional Analysis*, 53(3):246–268, 1983.

[49] B. Helffer and D. Robert. Étude du spectre pour un operateur globalement elliptique dont le symbole de Weyl presente des symetries: I. Action des groupes finis. *American Journal of Mathematics*, 106(5):1199–1236, 1984.

[50] B. Helffer and D. Robert. Étude du spectre pour un opérateur globalement elliptique dont le symbole de Weyl présente des symétries II. Action des groupes de Lie compacts. *American Journal of Mathematics*, 108(4):973–1000, 1986.

[51] L. Hörmander. The spectral function of an elliptic operator. *Acta mathematica*, 121(1):193–218, 1968.

[52] L. Hörmander. *The analysis of linear partial differential operators. I. Distribution theory and Fourier analysis. Reprint of the second (1990) edition.* Springer, Berlin, 2003.

[53] Mitsuru Ikawa. Decay of solutions of the wave equation in the exterior of several convex bodies. *Ann. Inst. Fourier*, 38(2):113–146, 1988.

[54] D. Jakobson and F. Naud. On the critical line of convex co-compact hyperbolic surfaces. *Geometric and Functional Analysis*, 22(2):352–368, 2012.

[55] Dmitry Jakobson and Frédéric Naud. On the resonances of convex co-compact subgroups of arithmetic groups. *arXiv preprint arXiv:1011.6264*, 2010.

[56] O. Jenkinson and M. Pollicott. Calculating Hausdorff dimension of Julia sets and Kleinian limit sets. *American Journal of Mathematics*, 124(3):495–545, 2002.

[57] E. Jones, T. Oliphant, P. Peterson, et al. SciPy: Open source scientific tools for Python, 2001–.

[58] W. Lu, M. Rose, K. Pance, and S. Sridhar. Quantum resonances and decay of a chaotic fractal repeller observed using microwaves. *Physical Review Letters*, 82(26):5233–5236, 1999.

[59] W. Lu, S. Sridhar, and M. Zworski. Fractal Weyl laws for chaotic open systems. *Physical review letters*, 91(15):154101, 2003.

[60] R.R. Mazzeo and R.B. Melrose. Meromorphic extension of the resolvent on complete spaces with asymptotically constant negative curvature. *Journal of Functional analysis*, 75(2):260–310, 1987.

[61] C.T. McMullen. Hausdorff dimension and conformal dynamics, III: Computation of dimension. *American journal of mathematics*, pages 691–721, 1998.

[62] E. Meinrenken. Semiclassical principal symbols and Gutzwiller's trace formula. *Rep. Math. Phys.*, 31(3):279–295, 1992.

[63] F. Naud. Expanding maps on Cantor sets and analytic continuation of zeta functions. *Ann. Sci. Éc. Norm. Supér. (4)*, 38(1):116–153, 2005.

[64] F. Naud. Density and location of resonances for convex co-compact hyperbolic surfaces. *Inventiones mathematicae*, (3):723–750, 2014.

[65] S. Nonnenmacher. Spectral problems in open quantum chaos. *Nonlinearity*, 24(12):R123, 2011.

[66] S. Nonnenmacher, J. Sjöstrand, and M. Zworski. Fractal weyl law for open quantum chaotic maps. *Annals of Math.*, 179(1):179–251, 2014.

[67] S. Nonnenmacher and M. Zworski. Distribution of resonances for open quantum maps. *Commun. Math. Phys.*, 269(2):311–365, 2007.

[68] S. Nonnenmacher and M. Zworski. Quantum decay rates in chaotic scattering. *Acta mathematica*, 203(2):149–233, 2009.

[69] J.P. Ortega and T.S. Ratiu. *Momentum maps and Hamiltonian reduction*, volume 222. Birkhauser, 2004.

[70] S.J. Patterson. The limit set of a Fuchsian group. *Acta mathematica*, 136(1):241–273, 1976.

[71] S.J. Patterson. On a lattice-point problem in hyperbolic space and related questions in spectral theory. *Arkiv för Matematik*, 26(1):167–172, 1988.

[72] S.J. Patterson and P.A. Perry. The divisor of Selberg's zeta function for Kleinian groups. Appendix A by Charles Epstein. *Duke Math. J.*, 106(2):321–390, 2001.

[73] T. Paul and A. Uribe. Sur la formule semi-classique des traces. (On the semi-classical trace formula). *C. R. Acad. Sci., Paris, Sér. I*, 313(5):217–222, 1991.

[74] T. Paul and A. Uribe. The semi-classical trace formula and propagation of wave packets. *J. Funct. Anal.*, 132(1):192–249, 1995.

[75] P. Perry. A poisson summation formula and lower bounds for resonances in hyperbolic manifolds. *International Mathematics Research Notices*, 2003(34):1837–1851, 2003.

[76] V. Petkov and L. Stoyanov. Analytic continuation of the resolvent of the Laplacian and the dynamical zeta function. *Anal. PDE*, 3:427, 2010.

[77] A. Potzuweit, T. Weich, S. Barkhofen, U. Kuhl, H.-J. Stöckmann, and M. Zworski. Weyl asymptotics: From closed to open systems. *Physical Review E*, 86(6):066205, 2012.

[78] P. Ramacher. Singular equivariant asymptotics and Weyl's law. *Arxiv preprint arXiv:1001.1515*, 2010.

[79] D. Robert and B. Helffer. Comportement semi-classique du spectre des hamiltoniens quantiques elliptiques. *Ann. Inst. Fourier*, 31(3):169–223, 1981.

[80] D. Ruelle. Zeta-functions for expanding maps and Anosov flows. *Inventiones mathematicae*, 34(3):231–242, 1976.

[81] H.H. Rugh. The correlation spectrum for hyperbolic analytic maps. *Nonlinearity*, 5(6):1237, 1992.

[82] Martin Schönert et al. *GAP – Groups, Algorithms, and Programming – version 3 release 4 patchlevel 4*. Rheinisch Westfälische Technische Hochschule, 1997.

[83] H. Schanze. Realisierung von nichteuklidischen Billiards durch Wellenwannen. *Diplomarbeit Universität Marburg*.

[84] H. Schomerus and J. Tworzydło. Quantum-to-classical crossover of quasibound states in open quantum systems. *Physical review letters*, 93(15):154102, 2004.

[85] J. Sjöstrand. Geometric bounds on the density of resonances for semiclassical problems. *Duke Math. J*, 60(1):1–57, 1990.

[86] W. A. Stein et al. *Sage Mathematics Software (Version 6.1.1)*. The Sage Development Team, 2014. `http://www.sagemath.org`.

[87] H.J. Stöckmann. *Quantum Chaos: An Introduction*. Cambridge Univ Press, 1999.

[88] W.P. Thurston. *The Geometry and Topology of Three-Manifolds*. http://www.msri.org/publications/books/gt3m/, electronic version 1.1 edition, 2002.

[89] B.R. Vainberg. On the analytical properties of the resolvent for a certain class of operator-pencils. *Sbornik: Mathematics*, 6(2):241–273, 1968.

[90] A. Voros. Unstable periodic orbits and semiclassical quantisation. *J. Phys. A*, 21(3):685, 1988.

[91] T. Weich, S. Barkhofen, U. Kuhl, C. Poli, and H. Schomerus. Formation and interaction of resonance chains in the open 3-disk system. *New Journal of Physics*, 16:033029, 2014.

[92] H. Weyl. Das asymptotische Verteilungsgesetz der Eigenwerte linearer partieller Differentialgleichungen (mit einer Anwendung auf die Theorie der Hohlraumstrahlung). *Mathematische Annalen*, 71(4):441–479, 1912.

[93] J. Wiersig and J. Main. Fractal Weyl law for chaotic microcavities: Fresnel's laws imply multifractal scattering. *Physical Review E*, 77(3):36205, 2008.

[94] A. Wirzba. Quantum mechanics and semiclassics of hyperbolic n-disk scattering systems. *Physics Reports*, 309(1-2):1–116, 1999.

[95] M. Zworski. Dimension of the limit set and the density of resonances for convex co-compact hyperbolic surfaces. *Inventiones mathematicae*, 136(2):353–409, 1999.

[96] M. Zworski. Resonances in physics and geometry. *Notices of the AMS*, 46(3):319–328, 1999.

[97] M. Zworski. *Semiclassical analysis*, volume 138. American Mathematical Society, 2012.

Acknowledgments

I thank everybody who contributed to the success of this thesis. My special thanks goes to the following persons:

Pablo Ramacher for giving me the opportunity to write my thesis in his group, for proposing interesting projects, the encouraging discussions and especially for giving me a great freedom to follow own ideas.

Frédéric Faure who has all the time been a great source of inspiration and motivation. I am especially thankful for his input about the resonance chains and his encouragement to follow this project.

David Borthwick for motivating discussions and his feedback on the symmetry factorization of zeta functions.

Ulrich Kuhl for many interesting discussion about the physics-side of the resonance chains

Joachim Hilgert for agreeing as a second referee for this thesis and his interest in my work.

Jos Höll, Ilka Agricola, Octavio Paniagua, Aprameyan Parthasarathy and everybody else on the A8 floor. It was because of you that I always enjoyed making my way up to the Lahnberge.

Thomas Friedrich for many fascinating graduate courses and a lot of mathematical inspiration.

All my friends in Marburg. You made my time in Marburg to a great period of my life.

My parents for supporting me all my life and enabling me to come to this point.

And finally to Sonja, not only for the collaboration on the resonance chains but first and foremost for seven great years.